Ephrin-B1 Regulation of Cell Positioning in Craniofacial Development and Congenital Disease

by

Terren Kathryn Niethamer

DISSERTATION

Submitted in partial satisfaction of the requirements for the degree of

DOCTOR OF PHILOSOPHY

in

Biomedical Sciences

in the

GRADUATE DIVISION

of the

UNIVERSITY OF CALIFORNIA, SAN FRANCISCO

Approved:

[redacted]

Committee in Charge

CONTRIBUTIONS TO PUBLISHED WORK

The work presented in this dissertation was done under the direct supervision and guidance of Dr. Jeffrey Bush.

Chapters 1 and 2. Some of the text and figures in Chapters 1 and 2 are modified and reproduced from the following review article: Niethamer, T.K. and Bush, J.O. (2018). Getting direction(s): The Eph/ephrin signaling system in cell positioning. *Developmental Biology* [ePub ahead of print]. https://doi.org/10.1016/j.ydbio.2018.01.012

This manuscript is reproduced in accordance with the policies of Elsevier. I created the figures and initially drafted all sections of the manuscript. Jeffrey Bush added additional writing and edited all sections of the manuscript.

Chapter 3. Text and figures in Chapter 3 are modified and reproduced from the following publication: Niethamer, T.K., Larson, A.R., O'Neill, A.K., Bershteyn, M., Hsiao, E.C., Klein, O.D., Pomerantz, J.H., and Bush, J.O. (2017). EPHRIN-B1 Mosaicism Drives Cell Segregation in Craniofrontonasal Syndrome hiPSC-Derived Neuroepithelial Cells. *Stem Cell Reports* 8(3), 529-537. https://doi.org/10.1016/j.stemcr.2017.01.017

This manuscript is reproduced in accordance with the policies of Elsevier under a Creative Commons License: https://creativecommons.org/licenses/by-nc-nd/4.0/

I created the figures and initially drafted all sections of the manuscript. Jeffrey Bush added additional writing. Andrew Larson generated data included in Figure 7 and Figures S1-S3, and I am incredibly grateful to him for his diligent work generating the CFNS hiPSC lines. This manuscript also depended on the previous work of Audrey O'Neill and Jeffrey Bush investigating ephrin-B1-mediated cell segregation in the developing mouse embryo. Marina Bershteyn and Ed Hsiao played a critical role in assisting us to establish hiPSC culture and differentiation protocols, and Ophir Klein and Jason Pomerantz made it possible for us to obtain

CFNS patient and family dermal tissue to generate the hiPSC lines. All authors contributed to the editing process.

Chapter 4. This chapter is a work in progress based on a collaboration with Christopher Percival, an assistant professor in the Department of Anthropology at Stony Brook University. The text and figures included herein, along with additional data currently being produced by Christopher Percival, will be compiled into a manuscript for later submission.

I generated, dissected, and processed all mouse embryos for analysis of tissue sections and performed cryosectioning and immunofluorescence experiments. Yu Xin (Victoria) Du assisted me with cryosectioning and immunofluorescence as she learned these techniques during her work as an undergraduate volunteer in the lab. I am grateful for her willingness to learn and enthusiasm for experimentation. With the help of Jeffrey Bush and Melanie Franco, I generated and dissected mouse embryo heads for micro-CT scanning. Christopher Percival performed micro-CT scanning on embryo heads and all landmark-based morphometrics analysis, generated the data included in Figure 10 and Tables 3-5, and initially wrote the corresponding sections of the manuscript. I generated all other figures and wrote the sections of the manuscript pertaining to ephrin-B1 expression and cell segregation. Jeffrey Bush added additional writing and edited all sections of the text.

Chapter 5. This chapter is a work in progress based on data I collected to investigate the possibility of *cis* interactions between ephrin-B1 and its signaling partners EphB2 and EphB3. I did not find evidence for such interactions, but instead, I discovered evidence that ephrin-B1 can modulate EphB2 and EphB3 expression in tissues in which they are coexpressed through signaling *in trans*. This data is an important advance for the field, as it was not known whether ephrin-Bs could interact with EphB receptors *in cis* as ephrin-As interact with EphA receptors, and it inspired us to make two novel mouse lines that allow for the expression of wild type and

trans-mutant ephrin-B1 under the control of Cre recombinase. The design and targeting of these mouse lines are described herein, and this data will contribute to a manuscript to be compiled and published at a later date upon receipt and analysis of these mice.

I would like to acknowledge the following sources of support and funding:

UCSF Department of Cell and Tissue Biology

UCSF Program in Craniofacial Biology

UCSF Biomedical Sciences Graduate Program

NSF Graduate Research Fellowship 2013157314

NIH/NIDCR F31DE026059 (Ruth L. Kirschstein Predoctoral National Research Service Award)

NIH/NIDCR R01DE0233375 (to Jeffrey Bush)

NIH/NIDCR R21DE025923 (to Jeffrey Bush)

This work is dedicated to the people who believed in me, even when I did not believe in myself.

For Momma:

Thank you for teaching me to be an independent woman and for insisting that I should be more assertive. I had a great role model for both in you.

For Dad:

Thank you for always encouraging me to spread my wings and fly, even though it meant leaving the nest.

For Chris, my beloved husband:

Thank you for your kind words, never-ending support, and tough love when I needed it. I could not have done this without you, and I certainly would not have wanted to. I love you.

“Nothing in the world can take the place of persistence. Talent will not; nothing is more common than unsuccessful men with talent. Genius will not; unrewarded genius is almost a proverb. Education will not; the world is full of educated derelicts. Persistence and determination alone are omnipotent. The slogan ‘Press On’ has solved and always will solve the problems of the human race.”

- attributed to Calvin Coolidge

ACKNOWLEDGMENTS

This dissertation would not exist without the assistance, knowledge, and patience of a group of people that I am fortunate to have worked with while in graduate school. First, I would like to thank my advisor, Dr. Jeffrey Bush, for his wonderful and insightful mentorship over my years in his lab. He has taught me so much about experimental protocol, grantsmanship, writing, presenting, and career planning. He has also given me the chance to develop these skills by encouraging me to present my work, attend conferences, and apply for fellowships. I am his first graduate student, and it has been an honor and a privilege to work with him as he started his lab. I cannot wait to see the great heights the lab will undoubtedly obtain and hear about the fascinating research that will be ongoing over the years to come. Most of all, I would like to thank Jeff and the rest of the Bush lab for their hard work and enthusiasm. The environment they have fostered made working in the lab a pleasure and has helped make the stresses of graduate school seem lighter.

I would also like to thank the other UCSF faculty who have given me the benefit of their wealth of expertise over the years. My thesis committee, Dr. Ophir Klein, Dr. Bruce Conklin, and Dr. Zev Gartner, have given me the benefit of their time and feedback, have helped me set up collaborations, and have given me reagents and tools to facilitate my experiments. Their thoughtfulness in assisting me to set up my project and carry it forward has made this work what it is today. I would like to thank Dr. Douglas Gould for his experimental advice and his lessons on grantsmanship, as well as for his encouragement in a time of professional crisis. I would also like to thank Dr. Ed Hsiao and Dr. Marina Bershteyn for their assistance in learning hiPSC culture and differentiation; without them, Chapter 3 of this thesis would not exist. Dr. Jason Pomerantz, Dr. Sarah Knox, and Dr. Licia Selleri of the Program in Craniofacial Biology have also given their time and feedback generously in listening to me present my project, and I am very grateful to them as well as to the other trainees of the PCB and HSE15. Thank you also to

the additional UCSF faculty members who have given me feedback through research in progress seminars, joint lab meetings, and informal talks.

The administrative staff of the Biomedical Sciences graduate program at UCSF have made getting a Ph.D. as easy as it probably could be and have saved me many headaches over the years with their expert handling of every possible situation that arises. Especial thanks go to Lisa Magargal, Demian Sainz, Ned Molyneaux, and Monique Piazza for all of their assistance. Thank you also to the administrators of the PCB, the Department of Cell and Tissue Biology, and the UCSF grants management office for helping me with all the logistical matters I encountered during my work here.

In addition to those at UCSF, I have benefited from the advice, expertise, and enthusiasm of a number of scientific mentors who encouraged me along the path to becoming a graduate student. Susan Fourness-Ewell recognized my interest in chemistry as a freshman in high school and gently pushed me towards her AP Chemistry course, where I discovered a love for experimentation that persists today. Dr. Richard Higby took a chance on me as a high school student and brought me into his analytical chemistry lab for an internship, where I got my first taste of working in industry. He and the rest of my mentors at Arista Laboratories taught me everything I have learned (and since forgotten) about gas and liquid chromatography. Dr. Gary Molander at the University of Pennsylvania and his former postdoctoral fellow Dr. Floriane Beaumard welcomed me into the world of organometallic synthesis as an undergraduate researcher and taught me and trusted me to work with pyrophoric materials on a daily basis. Dr. Molander treated undergraduates like graduate students, gave me my own project to work on and present, and continues to promote my career today through advice and recommendations. Floriane was the most patient and kind mentor at the bench that I could have asked for. Dr. William Gahl of the National Human Genome Research Institute and NIH Undiagnosed Diseases Program, his staff scientist Dr. Marjan Huizing, and his former graduate student Dr. Tal Yardeni, were all instrumental in my decision to apply to graduate school in the biomedical

sciences. Going on clinical rounds with Dr. Gahl and seeing patients gave a “face” to science that I had never seen before. Marjan is one of the most supportive and encouraging people I have ever met, and she trusted me to run a mouse project on my own. Tal taught me everything she knew about working in a biology lab and beyond. My work has benefited from her expertise, and my life has been richer because of her friendship.

Finally, I am so grateful for my family and friends, without whom my sanity would be even more questionable than it is now. My mother and father are my best friends, and I thank them for raising me, for driving me crazy, and for loving me through it all. Their encouragement and belief in my dreams has allowed me to believe in myself, too. Thank you also to my in-laws, the Micklitsch family, who have accepted me into their tight-knit group and have also been so supportive and encouraging from afar. Thank you to my friends from Richmond, Virginia; Philadelphia and the University of Pennsylvania; and Washington, D.C. for sticking by me as I flew across the country and then proceeded to hibernate in the lab for six years. Our moments together have not been as numerous or as long as I would have liked, but keeping in touch and visiting each other has been wonderful. It has been an incredible blessing to have some of my best friends from the East Coast join me in California, and their companionship has made me feel like I am not so far from home. Thank you also to my newfound California friends, those in the BMS program and those whom I have met through ultimate frisbee. You all have been like family to me during my time here. I will give the biggest thanks of all to my husband, Chris Micklitsch, who has stood steadfast by my side throughout this whole endeavor. Thank you for joining me in California, for your patience as you had to experience all of the emotions of graduate school again through me, and for continuing to encourage and challenge me daily. I cannot wait to start our next adventure hand in hand.

Ephrin-B1 Regulation of Cell Positioning in Craniofacial Development and Congenital Disease

Terren Kathryn Niethamer

Congenital craniofacial anomalies represent one-third of all structural birth defects, but although the genetic causes of many syndromes are known, the molecular and cellular mechanisms often remain poorly understood. This is the case for craniofrontonasal syndrome (CFNS), an X-linked syndrome caused by mutations in *EFNB1* and characterized by craniofacial, skeletal, and neurological anomalies. *EFNB1* encodes ephrin-B1, a member of the Eph/ephrin family of signaling molecules that regulate cell positioning and tissue morphology during embryonic development. Unlike most X-linked diseases, CFNS manifests very mildly in hemizygous males with no functional ephrin-B1, whereas females heterozygous for ephrin-B1 mutations are severely affected. The increased severity that occurs in the presence of mosaicism of ephrin-B1 expressing and non-expressing cells after random X chromosome inactivation has been named "cellular interference." In *Efnb1*$^{+/-}$ mice, ephrin-B1 expressing and non-expressing cells aberrantly segregate from one another in the neural plate neuroepithelium, providing a general potential mechanism for cellular interference; however, whether and how ephrin-B1-mediated cell segregation contributes to craniofacial phenotypes in human patients was not known. Using mouse models and the first human induced pluripotent stem cell model of a human craniofacial disease, we established that ephrin-B1 mosaicism drives pathogenic cell segregation in human cell types relevant to CFNS and that ephrin-B1 is a potent regulator of segregation not only in the early neuroepithelium, but also in the craniofacial mesenchyme, correlating with dysmorphology of facial structures. Ephrin-B1 also regulates EphB receptor levels when these molecules are coexpressed, and aberrant EphB receptor accumulation in ephrin-B1 mosaic cell populations may influence segregation or phenotypic outcome and disease severity. These discoveries contribute to a greater understanding of the role of ephrin-

B1 in regulating cell positioning during development, as well as how disruption of its function can result in congenital craniofacial disease.

TABLE OF CONTENTS

LIST OF TABLES

LIST OF FIGURES

LIST OF SUPPLEMENTAL FIGURES

CHAPTER 1. Introduction to craniofacial development and congenital disease

Summary

Development of the face during early embryogenesis is a complex series of events requiring not only cell proliferation, apoptosis, and differentiation, but also changes to cell positioning. These events contribute to morphogenesis, the process by which these tissues begin to develop their shape. Many transcription factor networks and signaling pathways contribute to the morphogenesis of the face, and disruption to any of these networks and pathways results in congenital disease. This work concentrates on one such signaling pathway, the Eph family of receptor tyrosine kinases and their membrane-bound signaling partners, the ephrins. Eph/ephrin signaling directs cell positioning during morphogenesis in many different embryonic contexts (for a full review of this topic, please see **Chapter 2**), including the development of craniofacial structures. Mutations in Eph/ephrin signaling family members result in a number of different developmental phenotypes in mice. In humans, the congenital craniofacial disease craniofrontonasal syndrome (CFNS) is caused by mutations to ephrin-B1, which is the focus of this work. To understand the developmental etiology of CFNS, the contributions of ephrin-B1 to different morphogenetic processes in the development of the face, and the possibility of developing novel molecular therapeutics for this disorder, it is first necessary to appreciate the events that take place during development of the craniofacial complex as well as what remains unknown about these processes.

Development and morphogenesis of the midface

The face forms from neural crest cells, a multipotent stem cell population

Neural crest cells (NCCs) are a specialized, highly migratory population of multipotent stem cells that arise at the neural plate border, delaminate, and travel in discrete streams through the developing embryo to contribute to skeletal, connective, vascular, and nervous system tissues, including the craniofacial primordia (LaBonne and Bronner-Fraser, 1998; Le Douarin and Dupin, 2003). The face begins to form with the induction of NCCs at the border

between the neural and non-neural ectoderm of the neural plate prior to neural tube closure (LaBonne and Bronner-Fraser, 1998). This occurs early in embryonic development, from week 3 in humans (40 week total gestation period) and from embryonic day (E) 8 in mouse (21 day total gestation period) (Moore et al., 2007). NCCs then delaminate from this position and migrate ventrolaterally in defined paths, differentiating to form neurons and glia of the peripheral nervous system, melanocytes, smooth muscle, and craniofacial mesenchyme from which bone and cartilage of the face and some structures of the skull will be derived (Le Douarin and Dupin, 2003). Many transcription factor networks and signaling pathways coordinate to regulate NCCs during these early developmental events (Betancur et al., 2010), and the cellular and molecular processes they direct must function and coordinate properly to correctly form the face. Defects in any stage of NCC development from induction to migration to differentiation result in disorders known as neurocristopathies (Etchevers et al., 2006). Because neurocristopathies affect NCCs and their derivatives, they have a wide variety of symptoms ranging from craniofacial dysmorphology to peripheral nervous system deficiencies to pigmentation defects, among others. Other precursor cells at the neural plate, the neuroepithelial cells, have also been proposed to contribute to neurocristopathies when damage to these cells occurs prior to neural crest induction (Jones et al., 2008; Sakai et al., 2016). The broad scope of craniofacial and other phenotypes evident in neurocristopathy patients demonstrates the incredible range and importance of NCCs to proper development of many tissues in the forming embryo, including the craniofacial complex.

The face forms from five initial prominences composed of NCC-derived mesenchyme, which is enclosed by a thin layer of epithelial cells. At E9.5 in mouse (22 days in humans), the frontonasal prominence (FNP), two maxillary prominences (MXP), and two mandibular prominences (MDP) frame the primitive mouth, the stomodeum; by E10.5 (28 days in humans), the two mandibular prominences have fused at the midline (**Figure 1A**). As development of these structures progresses, additional complexity is introduced as the lateral portion of the FNP

divides into lateral and medial nasal prominences (LNP and MNP) surrounding the forming nasal pits by E11.5 in mouse (33 days in humans) (**Figure 1B**). The LNP, MNP, and MXP will fuse surrounding the nasal pit on each side of the face at the lambdoid (λ) junction to form the upper lip by E12.0 (35 days in humans) (**Figure 1C**) (Depew and Compagnucci; Jiang et al., 2006). The secondary palatal shelves extend from the maxillary prominences at E12.0-12.5 (35-40 days in humans) and will later elevate above the tongue, grow out towards the midline, and fuse to form the secondary palate (Bush and Jiang, 2012; Kim et al., 2015). Following the formation and fusion of these structures, craniofacial cartilage and bone will differentiate from NCC-derived mesenchyme as more mature facial structures develop; these are evident by E17.0 in mouse (10 weeks in humans) (**Figure 1D**). Formation of normal facial structures is an intricate process that involves both proliferation and differentiation of cells as different cell types are specified, as well as apoptosis as structures are refined and fuse with one another.

Development of the face also requires the formation and maintenance of developmental boundaries that prevent the intermingling of cells between different structures. Although boundary formation is essential for proper craniofacial development, boundaries are also removed as different craniofacial prominences, such as the upper lip and secondary palate, fuse to generate mature structures with continuous tissue. The fusion process may occur by apoptosis, epithelial-to-mesenchymal transition, cell extrusion, or some combination thereof (Kim et al., 2015; Losa et al., 2018). Disruption of any of the components that direct boundary formation and maintenance or tissue fusion can result in congenital craniofacial disease. Although many studies of craniofacial development and disease focus on early stages involving NCCs, or specific events such as lip or palate fusion, these events cannot be studied in isolation. Other tissues in close proximity to the facial prominences contribute to growth and expansion of the midface and to its normal morphogenesis, and disruption of any of these tissues may lead to craniofacial dysmorphology.

Influences on growth and expansion of the midface

The five facial prominences actively grow during development of the face, but how growth of NC-derived craniofacial structures and expansion of the midface are regulated to contribute to proper craniofacial development remains incompletely understood. This regulation is mediated not only by events that occur within NCC-derived mesenchymal tissues, but also by events in other tissues (Cox, 2004), as well as by later differentiation of cells to form cartilage and bone.

One essential factor to consider in the growth and expansion of the midface is the growth of the brain, which can impact facial size in two important ways. First, the neural tube, and later the more developed brain, serve as a scaffold on which the facial prominences form and may exert physical forces on the facial prominences that affect their positioning or directional growth (Marcucio et al., 2015). Slower brain growth in comparison to growth of the facial prominences can lead to more prognathic facial structures, whereas increased growth of the brain relative to the facial prominences can lead to a wider, flatter face (Boughner et al., 2008). Second, neural tissue and surface ectoderm also represent sources of signaling that affect growth and development of the facial prominences and assist in patterning neural crest-derived mesenchyme (Marcucio et al., 2011). In the developing chicken embryo, for example, reducing sonic hedgehog signaling in the brain causes facial narrowing, whereas increasing it causes midfacial widening and even bifurcation of the frontonasal prominence (Young et al., 2010). As the early development of the brain and face are closely related both in space and in time (Richtsmeier et al., 2006), the positional and signaling influences of the brain represent important factors contributing to early midfacial expansion.

Later events, such as differentiation of NCC-derived mesenchyme to form cartilage and bone, may also contribute to the final size and shape of the midface. Between 35 days and 12 weeks of development in humans, it has been hypothesized that directional growth of

craniofacial cartilages prior to craniofacial bone formation is essential for the formation of the face; in rats whose primary cartilages were altered due to teratogens, the size and shape of later bone formation was affected (Diewert, 1985). More recent studies also suggest that the chondrocranium can affect craniofacial growth, with structures such as the nasal septum acting as growth centers or supports for midface expansion (Marulanda and Murshed, 2018; Marulanda et al., 2017). In addition, the facial structures of different species are similar at early stages, such as the time prior to midline fusion, possibly to minimize the possibility of clefting. However, divergence to create many different facial shapes from chickens to mice to alligators to humans occurs after this time point (Young et al., 2014), suggesting that post-fusion events contribute significantly to facial shapes. Syndromes such as craniosynostosis, or premature fusion of one or more sutures of the skull, create imbalances in growth in different parts of the skull and are often accompanied by craniofacial dysmorphology (Johnson and Wilkie, 2011), indicating that in some cases, changes to the skull correlate with changes to the shape of the face.

In considering the growth of the midface, and congenital diseases that result in its dysmorphology, it is essential to consider that the facial prominences have many different components influencing their overall structures, and therefore their function. These components cannot be studied in isolation (Aldridge et al., 2005), as they all contribute to the development and proper function of the face. Disruption of early events, such as the induction of NCCs at the neural plate, or migration of these NCCs, can have far-reaching effects that cause dysmorphology in spite of normal proceeding of following events. Similarly, defects in later processes, such as the development and morphogenesis of the skeletal elements of the face, can cause changes in facial shape even if all preceding events have occurred correctly. The interaction of many cell types, including the neural plate neuroepithelial cells, the non-neural ectoderm, NCCs, mesoderm, and later mesenchymal cell types and their derivatives, is required for craniofacial development, and the necessary interaction between many different molecules

and signaling pathways to facilitate proper morphogenesis only adds to this complexity (Chai and Maxson, 2006; Helms et al., 2005; Suzuki et al., 2016). These complex cellular and tissue-level interactions require in-depth study to discover the etiology of any particular defect that involves expansion of the midface.

Disruptions to craniofacial morphogenesis result in congenital disease

Congenital craniofacial disease

In the series of complex developmental events comprising craniofacial development, if any of the necessary processes are disrupted, the result is congenital craniofacial disease. This type of disruption occurs often enough that congenital craniofacial disorders make up over one-third of all congenital birth defects ("Global Strategies to Reduce the Health Care Burden of Craniofacial Anomalies," 2004). These disorders are associated with significant morbidity and burdens not only to patients and families, but also on the healthcare system (Wehby and Cassell, 2010). Failure of early events in craniofacial development, such as fusion of the LNP, MNP, and MXP to form the lip, or midline fusion of the palatal shelves, results in cleft lip, cleft palate, or both (CL/P). Infants with these disorders have difficulty feeding and may be undernourished; they may also have difficulty with hearing and speaking and thus with social interaction (Dixon et al., 2011). CL/P can present as part of a wider syndromic diagnosis, or in isolation (non-syndromic). Although many genetic causes of CL/P have been identified, the causes of non-syndromic CL/P are only now beginning to be discovered, and the molecular events resulting in clefts are still under study (Dixon et al., 2011). Failure of later events that occur after craniofacial bone formation can also result in craniofacial disorders, such as craniosynostosis, or premature fusion of one or multiple sutures of the skull (loss of suture patency). Suture patency is thought to be important for passage through the birth canal and for accommodating growth of the brain; fusion of one or more sutures in the skull can constrain brain growth and result in changes to the shape of the skull and face. Children with

craniosynostosis often undergo multiple surgeries before the age of 2 (Johnson and Wilkie, 2011). Indeed, for congenital craniofacial anomalies, surgery represents the only treatment option available for patients, and although surgical techniques are advanced and bring increased quality of life to these patients, the ability to detect congenital craniofacial disorders *in utero* and treat them at the cellular or molecular level remains an elusive goal.

Craniofrontonasal syndrome

Clinical and genetic features of craniofrontonasal syndrome

One such congenital craniofacial disorder is craniofrontonasal syndrome (CFNS), an X-linked disorder caused by mutations in *EFNB1*, which encodes EPHRIN-B1, a member of the Eph/ephrin family of signaling molecules. CFNS occurs in 1 in 120,000 individuals and is characterized by craniofacial phenotypes including hypertelorism, unilateral or bilateral coronal craniosynostosis, frontonasal dysplasia, and bifid nasal tip; patients occasionally present with cleft lip and palate (Cohen, 1979; Twigg et al., 2004; Wieland et al., 2004). CFNS patients may also have skeletal phenotypes, such as longitudinal splitting of the nails, diaphragmatic hernia, and occasionally, syndactyly or polydactyly; they may also present with neurological phenotypes, such as agenesis of the corpus callosum (Twigg et al., 2004). Unlike many X-linked diseases that affect male patients, CFNS is most severe in female patients heterozygous for mutations in *EFNB1*. These females are mosaic for EPHRIN-B1 expression after random X chromosome inactivation, a method for preserving gene dosage between the sexes. This mosaicism leads to aberrant segregation of ephrin-B1 expressing and non-expressing cells in a mouse model for CFNS, visible as large patches in the limb bud and secondary palate (Bush and Soriano, 2010; Compagni et al., 2003; Davy et al., 2004) of $Efnb1^{+/\Delta}$ mouse embryos. Male patients with no functional EPHRIN-B1 are less severely affected, often presenting only with hypertelorism and occasionally with cleft lip (Twigg et al., 2004). The range of mutations in *EFNB1* seen in CFNS patients is wide, from missense mutations to deletions to frameshift

mutations. There are also noncoding mutations in *EFNB1* that cause CFNS; although the large number of observed mutations has thus far precluded an in-depth study of the individual consequences of each one, they are all thought to result in loss of function of EPHRIN-B1 (Twigg et al., 2004; Twigg et al., 2006; Wieland et al., 2004).

The discovery that mutations in *EFNB1* were causative for CFNS solved a genetic conundrum that had long puzzled clinicians, who noted that transmission of the disease from a father to his daughters but not to his sons suggested X-linked inheritance, but that paradoxically, males were never as severely affected as females (Twigg et al., 2004; Wieland et al., 2004). Confirming the importance of EPHRIN-B1 mosaicism to disease pathology, rare male patients with severe CFNS phenotypes were found to have somatic mosaicism for *EFNB1* mutation (Twigg et al., 2013). However, the answer to this puzzle only created more questions, as researchers strove to determine how mosaicism for EPHRIN-B1 expression might lead to increased severity in craniofacial phenotypes. The connection between EPHRIN-B1 mosaicism and craniofacial phenotypes in female CFNS patients has remained elusive, with many hypotheses proposed since the genetic cause of the syndrome was discovered; although there is agreement that “cellular interference” occurs between ephrin-B1 expressing and non-expressing cells (Wieacker and Wieland, 2005), the nature of this interaction remains incompletely understood.

Cellular mechanisms of CFNS

CFNS likely results from disrupted Eph/ephrin signaling due to mosaic loss of EPHRIN-B1 in severely affected female heterozygotes or total loss of EPHRIN-B1 in mildly affected male hemizygotes. Eph/ephrin signaling and its many pathway members play important roles in cell positioning during embryonic development, often acting in the translation of patterning information into the formation and maintenance of embryonic boundaries (see **Chapter 2**). It is likely that heterozygous female patients are severely affected not only due to loss of

endogenous boundaries created or maintained by EPHRIN-B1, which must also be lost in hemizygous males, but also due to creation of ectopic EPHRIN-B1-generated boundaries through pathogenic cell segregation. Ectopic ephrin-B1 expression boundaries may restrict normal cell migration, intermingling, or orientation in mesenchymal structures during embryonic development to result in the wide range of CFNS phenotypes. The disruption of normal expression of ephrin-B1 also results in cell segregation in ephrin-B1 heterozygous mice. Although ectopic ephrin-B1 expression patches were initially noted in more fully developed structures, such as the palate (Bush and Soriano, 2010; Davy et al., 2006) and limb mesenchyme (Compagni et al., 2003), this process occurs much earlier, in the neural plate neuroepithelial cells of *Efnb1*$^{+/-}$ mice (O'Neill et al., 2016). The resulting patches of ephrin-B1 expression and non-expression may contribute to later craniofacial and limb phenotypes in *Efnb1*$^{+/-}$ mice, and possibly in human CFNS patients as well. In *Efnb1*$^{+/-}$ mice, ephrin-B1-mediated cell segregation requires kinase signaling through the EphB2 and EphB3 receptors (O'Neill et al., 2016). In mosaic cell mixtures, ephrin-B1 non-expressing cells upregulate actin, generating a cortical actin differential between ephrin-B1 expressing and non-expressing cells that results in segregation, with actin cables forming around aberrant patches of ephrin-B1 non-expressing cells (O'Neill et al., 2016). This process requires the small GTPase RhoA and Rho kinase (ROCK); genetic disruption or pharmacological inhibition of ROCK dramatically decreases pathogenic cell segregation in *Efnb1*$^{+/-}$ embryos (O'Neill et al., 2016). Interestingly, genetic interaction studies also indicated that loss of Cdc42 or Rac1 function did not reduce segregation, consistent with the possibility that actomyosin contractility *per se*, and not cell migratory capacity more generally, may drive segregation. Further studies will elucidate the signaling partners downstream of Eph/ephrin activation that contribute to modulation of the cytoskeleton, as well as the biophysical differences leading to segregation of ephrin-B1 expressing and non-expressing cells.

Understanding the contribution of Eph/ephrin signaling and cell segregation to CFNS

To better understand how mosaic loss of EPHRIN-B1 leads to craniofacial phenotypes in CFNS patients, it is first critical to understand the role of Eph/ephrin signaling in cell positioning and tissue separation as a whole (for full consideration of this topic, refer to **Chapter 2**). Studies of cellular mechanisms of CFNS are also important to contribute to the search for possible treatments or cures for this congenital craniofacial disease. To determine whether cell segregation holds the key to craniofacial phenotypes in CFNS, this work will investigate three essential questions (**Figure 2**). First, does cell segregation occur in human cell types relevant to craniofacial development? Second, when and where does ephrin-B1 force the segregation of wild type and mutant cells during development of mosaic embryos, and is it a potent regulator of cell positioning throughout the developing embryo? Third, how do specialized Eph/ephrin signaling modes contribute to ephrin-B1 mediated cell segregation? The answers to these questions have not been previously studied and will advance our knowledge of molecular, cellular, and tissue-level mechanisms of CFNS pathology as well as the role of ephrin-B1 in cell positioning in the developing embryo as a whole.

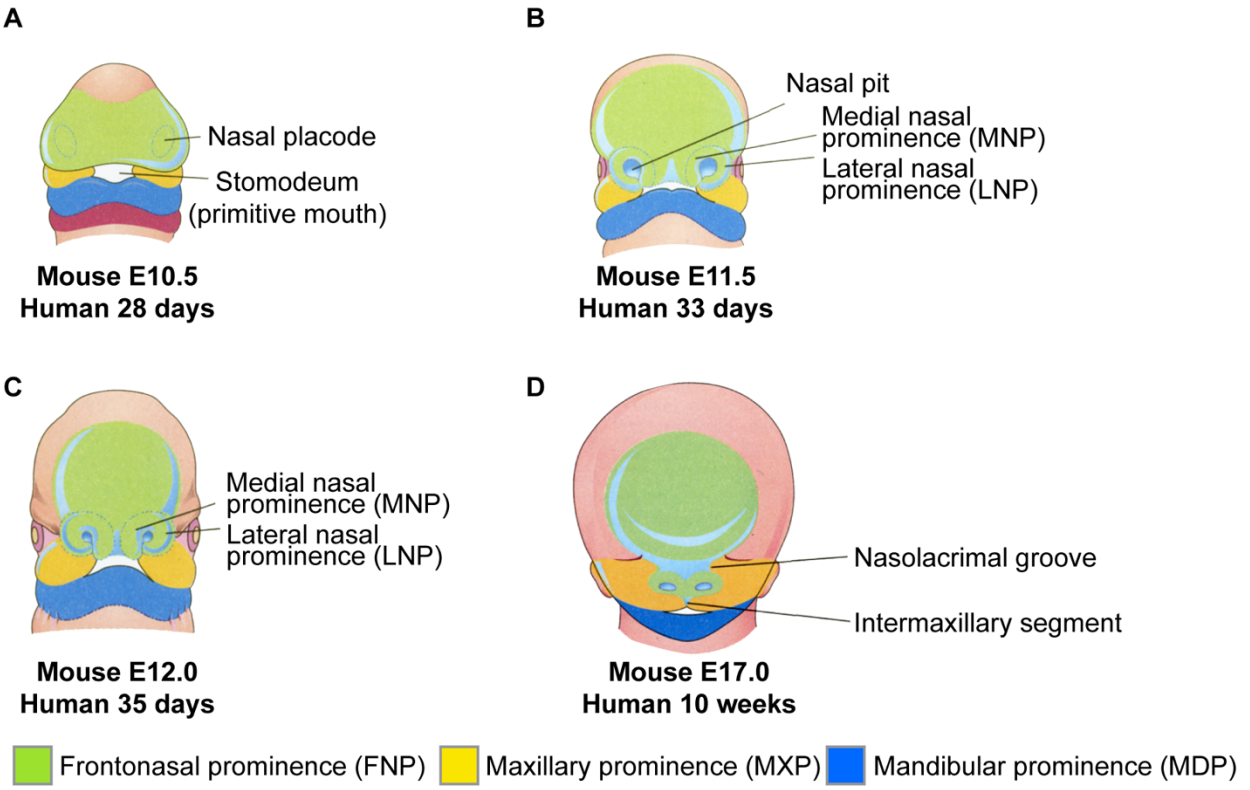

Figure 1. An overview of the development of the midface. (A) The midface develops from five embryonic prominences surrounding the stomodeum, or primitive mouth. The frontonasal prominence (FNP) is depicted in green. The two maxillary prominences (MXP) are depicted in yellow. By embryonic day 10.5 in mouse (equivalent to 28 days gestation in humans), the two mandibular prominences (MDP; depicted in blue) have fused at the midline. **(B)** At E11.5 in mouse (equivalent to 33 days gestation in humans), the lateral nasal prominence and medial nasal prominence surround the nasal pit, which will become the nostril. **(C)** Fusion of the MNP and LNP with the MXP at the lambdoid junction forms the upper lip between E11.5 and E12.0 in mouse (equivalent to 33-35 days gestation in humans). The secondary palatal shelves will extend from the MXP at E12.0-E12.5 in mouse (equivalent to 35-40 days gestation in humans). **(D)** Cartilage and bone differentiate from craniofacial mesenchyme to form more mature facial structures from E15.0-E18.0 in mouse. This figure is adapted from Moore et al., 2007.

A Does ephrin-B1-mediated segregation occur in human CFNS patient cells?

mouse embryos ✓ human patients?

B When and where does ephrin-B1 drive cell segregation during craniofacial development?

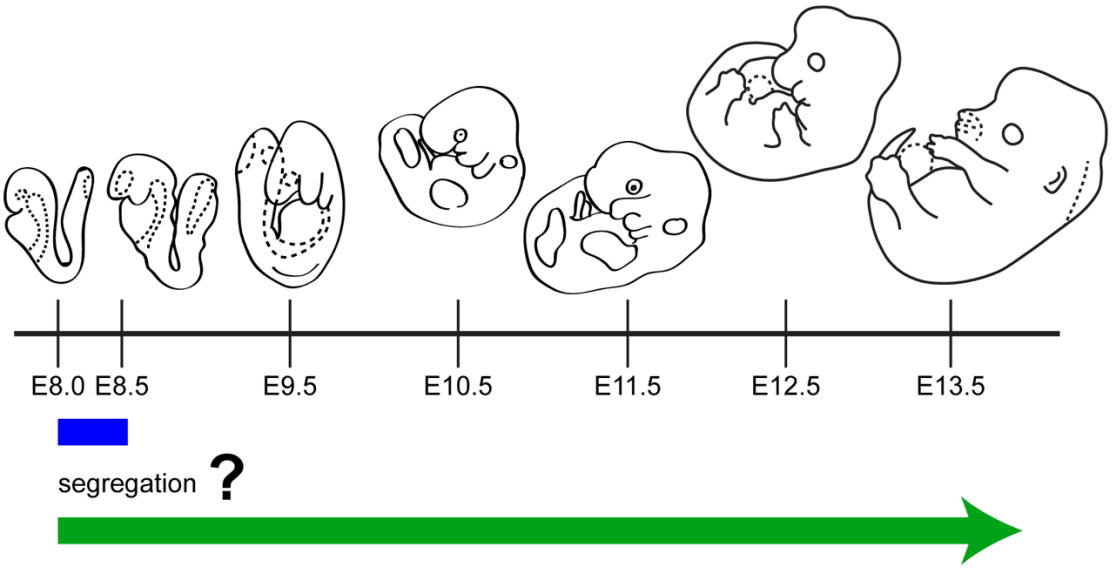

C How does coexpression of ephrin-B1 with EphB receptors regulate signaling and segregation?

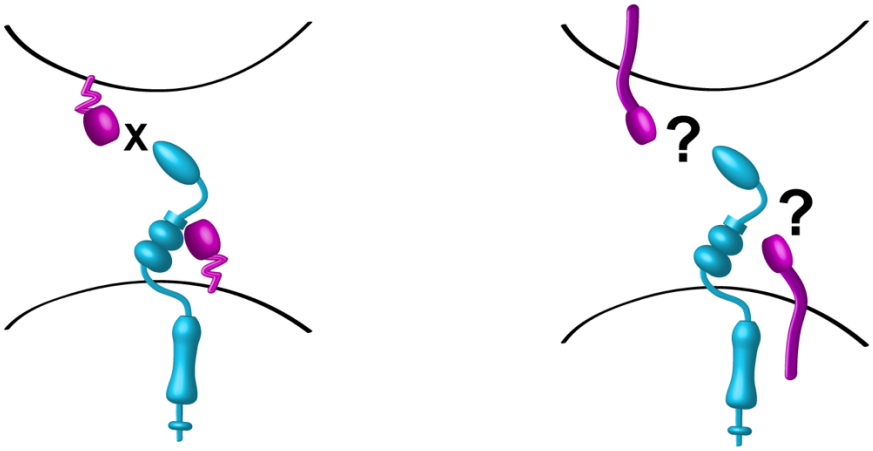

ephrin-A *cis* inhibition of EphA receptor ephrin-B *cis* interactions with EphB receptors?

Figure 2. Essential questions in the study of CFNS. (A) Does ephrin-B1-mediated segregation occur in human CFNS patient cells to contribute to disease pathology? **(B)** When and where does ephrin-B1 drive cell segregation during craniofacial development? Does segregation occur at a fixed point in development, at the neural plate between E8.0 and E8.5 (blue bar), or does it continue in other tissues throughout development of the face (green arrow)? Embryo staging images adapted from eMouseAtlas, http://www.emouseatlas.org/emap/ema/home.html **(C)** Ephrin-As inhibit EphA receptors *in cis*; how might ephrin-B1 interact with EphB receptors *in cis* to affect receptor signaling and cell segregation?

CHAPTER 2. Introduction to Eph/ephrin signaling in cell positioning during embryonic development

Eph/ephrin signaling is critical for embryonic development

The Eph receptor tyrosine kinases were first identified based on their overexpression in human carcinoma (Hirai et al., 1987) and were later found to be expressed on initial outgrowths of neuronal axons, suggesting a role in axon guidance (Henkemeyer et al., 1994). Though their role in these contexts has been studied in great depth, Ephs and their signaling partners, the ephrins, are also expressed in most tissues during embryonic development and are essential to a wide variety of developmental processes (Batlle and Wilkinson, 2012; Bush and Soriano, 2012; Egea and Klein, 2007; Kania and Klein, 2016; Klein and Kania, 2014; Kullander and Klein, 2002; Merlos-Suárez and Batlle, 2008; Pasquale, 2008; Wilkinson, 2001). This is perhaps unsurprising, as the Eph receptors are the largest family of receptor tyrosine kinases found in mammals (Gale et al., 1996; Henkemeyer et al., 1994; Kullander and Klein, 2002).

Ephrins, the signaling partners of the Eph receptors, are also membrane-bound, allowing Eph/ephrin signaling to utilize several unique signaling modes. Ephrins are separated into two classes: ephrin-As are membrane-bound through a GPI anchor, and ephrin-Bs are transmembrane molecules with a cytoplasmic domain (Gale et al., 1996). Eph receptors have also been separated into A and B classes based on sequence similarity and whether they bind to ephrin-A or ephrin-B signaling partners (Gale et al., 1996), although there is some overlap in binding affinity between the two classes (Himanen et al., 2004). Eph receptor oligomerization is necessary for propagation of a forward signal, with the size of the Eph receptor cluster determining the strength of the signal, such that trimers and tetramers signal maximally (Himanen et al., 2010; Schaupp et al., 2014; Seiradake et al., 2010). The membrane-bound nature of Ephs and ephrins dictates that cell-cell contact is an important part of their signal transduction (Davis et al., 1994; Henkemeyer et al., 1994), and in many developmental contexts, Eph/ephrin signaling between adjacent cells is critical. However, Eph/ephrin signaling via cellular protrusions may be capable of mediating signaling between nonadjacent cells (Cayuso et al., 2016), and release of Ephs and ephrins by exosomes also allows for the

possibility of signaling at greater distances (Gong et al., 2016). Whereas Eph and ephrin ectodomains can be proteolytically cleaved (Georgakopoulos et al., 2006; Hattori et al., 2000), the ectodomain alone is incapable of initiating oligomerization and is therefore unlikely to activate signaling; indeed, the unclustered ectodomain is often used as a competitive antagonist (Daar, 2012; Pegg et al., 2017), suggesting that antagonistic modulation of signaling at a distance by soluble Eph/ephrin ectodomains may be possible.

Eph/ephrin signaling affects not only axon guidance, as originally hypothesized, but also cell proliferation, apoptosis, and cell positioning, often driving cell migration and tissue separation (Bush and Soriano, 2012; Kania and Klein, 2016; Laussu et al., 2014; Merlos-Suárez and Batlle, 2008; Pasquale, 2008; Xu and Henkemeyer, 2012). In this variety of developmental roles, Eph/ephrin signaling often acts as a middleman between patterning information that defines cell and tissue fate and the cellular movement necessary for the morphological changes that define the shape of these tissues.

Eph/ephrin signaling modes

Biochemically, Eph/ephrin interactions have bidirectional signaling capacity (Brückner et al., 1997; Holland et al., 1996; Lin et al., 1999; Torres et al., 1998). Upon binding of an ephrin to an Eph receptor, signaling may be transduced into the receptor-expressing cell; this classical forward signaling (**Figure 3A**) is mediated by Eph tyrosine phosphorylation followed by binding of partners that mediate downstream signaling, though the *in vivo* utilization of these binding partners in distinct developmental contexts is largely unknown (Bush and Soriano, 2012). An Eph/ephrin binding event can also result in transduction of a signal into the ephrin-expressing cell, known as reverse signaling (**Figure 3B**) (Henkemeyer et al., 1996; Holland et al., 1996). Therefore, in addition to Eph and ephrin expression levels and degree of oligomerization, the extent to which forward, reverse, and bidirectional signaling modes are utilized represents another layer of regulation that contributes to modulating downstream signaling.

Since the discovery that Eph receptor-ephrin interactions could result in signal transduction not only in the receptor-expressing cell, but also in the ephrin-expressing cell (Henkemeyer et al., 1996; Holland et al., 1996), many studies have delved into the possible mechanisms of ephrin reverse signaling. In biochemical studies, ephrin-Bs were found to use their cytoplasmic domains to mediate reverse signaling through phosphorylation of highly conserved tyrosines (Brückner et al., 1997) and interaction with PDZ-domain-containing proteins (Lin et al., 1999; Lu et al., 2001). Although ephrin-Bs themselves do not possess intrinsic kinase activity, therefore, they may mediate downstream signaling by recruitment of other signaling molecules. Ephrin-B reverse signaling may also occur by non-SH2/PDZ mechanisms, such as by interactions with scaffold proteins to regulate tight junctions or interactions with connexin-43 to regulate gap junctions (Daar, 2012; Davy et al., 2006). Although ephrin-As possess no intracellular domain, there is biochemical and genetic evidence for ephrin-A reverse signaling (Dudanova et al., 2012). The precise mechanisms of this remain unclear, but cell culture studies indicate that ephrin-As may mediate reverse signaling through interaction with Src family kinases in membrane microdomains (Davy et al., 1999) and interaction with integrins to promote adhesion (Davy and Robbins, 2000; Huai and Drescher, 2001). In addition, EphA3-dependent activation of the ADAM10 metalloprotease to cleave ephrin-As allows a switch from adhesion to repulsion, in essence modulating the cellular response of the ephrin-expressing cell (Hattori et al., 2000; Janes et al., 2005). Thus, upon the binding of an Eph to an ephrin on an adjacent cell and subsequent oligomerization, a signal can be transduced into the Eph-expressing cell, the ephrin-expressing cell, or into both cells simultaneously, generating a bidirectional signaling cascade. Which of these events is crucial to achieve the appropriate downstream signaling outcome seems to depend heavily on cellular context, and therefore has required direct evaluation *in vivo* in distinct cell and tissue types.

Adding an additional layer of complexity to the regulation of Eph/ephrin signaling, there is evidence that expression of Eph receptors and ephrins in the same cell (*in cis*) can negatively

regulate Eph receptor signaling through ephrins in an adjacent cell (*in trans*) (**Figure 3C**) (Hornberger et al., 1999). Eph receptors have been proposed to interact with ephrins *in cis* using their canonical ligand-binding domain (Yin et al., 2004) as well as their membrane-proximal fibronectin type III domain (Carvalho et al., 2006). Expression of ephrin-As *in cis* with EphA receptors in neuronal growth cones can fine-tune control of EphA receptor activation to accurately define the correct axon termination zone, and changing the *cis*-expression of ephrin-As alters EphA phosphorylation and signaling as well as termination of axons as measured by growth cone collapse, demonstrating that the biochemical changes caused by *cis*-expression of ephrin-As with EphAs have a functional effect (Carvalho et al., 2006; Hornberger et al., 1999). *Cis* inhibition has been proposed to play a role in retinotectal topographic mapping and spinal motor axon guidance, at the synapse, and in cancer cell lines (Carvalho et al., 2006; Falivelli et al., 2013; Gatto et al., 2014; Hornberger et al., 1999; Kao and Kania, 2011; Marquardt et al., 2005). The breadth of functional relevance of *cis*-expression of Ephs and ephrins remains unknown, and this has not been investigated in the context of craniofacial development. Moreover, *cis* interactions between Eph receptors and ephrins have thus far been demonstrated only for the A subclass; whether EphBs and ephrin-Bs interact *in cis* remains unknown.

In vivo *evidence for bidirectional signaling in the developing embryo*

The study of *in vivo* Eph/ephrin signaling mechanisms has been consistently active from the earliest studies of this signaling pathway. Our understanding of the broadly-used genetic tools, as well as the general principles derived from these studies, continue to evolve, providing us with a more nuanced understanding of *in vivo* signaling directionality.

The prototypical *in vivo* roles for reverse signaling were first suggested by studying axon guidance phenotypes in mice lacking EphB receptor signaling capacity. Three receptors (EphB1, EphB2, EphB3), with similar affinity for B-type ephrins, and presumably similar intracellular signaling capabilities, are each involved in the patterning of two major

interhemispheric commissural axon tracts, the anterior commissure (AC) and corpus callosum (CC) (**Figure 4A, B**) (Henkemeyer et al., 1996; Mendes, 2006; Orioli et al., 1996; Robichaux et al., 2016). Initial genetic evidence for the existence of reverse signaling was based on discrepant phenotypic outcomes upon complete loss of EphB2 compared with mutants in which most of the intracellular domain was replaced with β-galactosidase, while maintaining the extracellular, transmembrane, and juxtamembrane domains (Henkemeyer et al., 1996). Whereas all *Ephb2*$^{-/-}$ mutant embryos exhibited defects in the posterior projection of the AC (ACp) and 61% exhibited defects in the CC, *Ephb2*$^{LacZ/LacZ}$ mutant embryos did not exhibit either of these phenotypes, leading to the conclusion that they were attributable to loss of reverse and not forward signaling (Henkemeyer et al., 1996; Mendes, 2006). A recent study reexamining these mutant alleles in guidance of the AC confirmed that null loss of EphB2 led to a higher penetrance of ACp phenotypes than intracellular truncation of EphB2 in *Ephb2*$^{LacZ/LacZ}$ mutant embryos (**Figure 4D, F**). Further, while complete loss of EphB1 resulted in an abnormal ACp approximately 30% of the time (**Figure 4E**), EphB1 mutants in which the intracellular domain of EphB1 was replaced with LacZ (EphB1$^{T\text{-}LacZ}$) did not exhibit defects in ACp development (**Figure 4C**) (Chenaux and Henkemeyer, 2011; Robichaux et al., 2016). Surprisingly, however, loss of forward signaling through EphB1 and EphB2 together resulted in ACp defects in 80% of *Ephb1*$^{T\text{-}LacZ/T\text{-}LacZ}$*; Ephb2*$^{LacZ/LacZ}$ compound mutants, demonstrating that the intracellular domains of EphB1 and EphB2 have redundant function. An almost identical scenario was borne out for the CC; loss of forward signaling through EphB1 resulted in defects in the CC in 27% of *Ephb1*$^{T\text{-}LacZ/T\text{-}LacZ}$ mutants (**Figure 4C**) and 43% of *Ephb2*$^{LacZ/LacZ}$ mutants (**Figure 4D**), but loss of forward signaling through EphB1 and EphB2 resulted in CC defects in 91% of *Ephb1*$^{T\text{-}LacZ/T\text{-}LacZ}$*; Ephb2*$^{LacZ/LacZ}$ compound mutants (**Figure 4H**). In both contexts, the penetrance upon loss of the intracellular domain was not as high as complete compound loss of EphB1 and EphB2 (100%) (**Figure 4G**), a discrepancy that was attributed to reverse signaling (Robichaux et al., 2016). However, this difference could instead be due to the retained presence of EphB3 forward

signaling. Indeed, the penetrance of ACp or CC phenotypes in *Ephb2*$^{-/-}$; *Ephb3*$^{-/-}$ compound mutants is 100%, and higher than in either homozygous mutant alone, demonstrating their redundancy (Mendes, 2006; Orioli et al., 1996). Based on these studies, we conclude that in the case of *Ephb1*$^{T\text{-}LacZ/T\text{-}LacZ}$; *Ephb2*$^{LacZ/LacZ}$ mutants, reverse signaling activation should still be retained, but these mutants still exhibit high penetrance of AC and CC defects, arguing that it is not necessary to evoke the existence of a reverse signal to explain differences between EphB null and intracellular mutant phenotypic penetrance.

If redundant receptor forward signaling function is responsible for the bulk of ACp and CC phenotypes, why is complete loss of EphB1 or EphB2 receptor more severe than loss of only the intracellular domain? In both cases, the C-terminally truncated fusion protein retains the extracellular and transmembrane domains; the EphB2^{LacZ} mutant protein also still retains the juxtamembrane region. Notably, Eph receptors can cocluster, or heterooligomerize, both within and beyond subclass, and Eph-Eph receptor interaction domains reside within the extracellular region and can mediate lateral propagation of signaling, independent of ephrin ligation (Freywald et al., 2002; Janes et al., 2011; Lackmann et al., 1998; Marquardt et al., 2005; Wimmer-Kleikamp et al., 2004). This raises the question of whether these intracellular mutants may still retain some forward signaling function, possibly as a scaffold to the larger signaling complex when coexpressed with other active receptors possessing redundant intracellular signal transduction capabilities. If so, receptor heterooligomerization and retention of some forward signaling capacity is a plausible explanation for the decreased phenotypic severity of intracellular EphB receptor mutants compared to complete receptor knockouts. To distinguish between this possibility and that of a reverse signaling contribution, further *in vivo* exploration of both hypotheses will be required.

What, then, are the genetic data in support of reverse signaling in these contexts? Studies complementary to the above have created mouse mutants with changes to the intracellular domain of ephrin-Bs, either by replacing the entire domain with β-galactosidase

(ephrin-B2^{LacZ}) (Cowan et al., 2004; Dravis and Henkemeyer, 2011; Dravis et al., 2004; Yokoyama et al., 2001), or by making specific point mutations to the phosphorylatable tyrosines or the PDZ binding domain in the highly-conserved region of the cytoplasmic domain. The latter allows more specific assessment of phosphorylation or PDZ-dependent reverse signaling but does not test other potential modes of reverse signaling (Bush and Soriano, 2009; Davy and Soriano, 2007; Dravis and Henkemeyer, 2011; Makinen, 2005; Xu and Henkemeyer, 2009; Xu et al., 2011). Null loss of function of ephrin-B1, or point mutations abrogating its ability to bind to PDZ-domain containing proteins, results in normal ACp development, but agenesis of the CC (aCC), in a 129S4 genetic background (Bush and Soriano, 2009). Though a recent study reported that *Efnb1* null mutant embryos did not exhibit CC defects in a CD1 genetic background, human craniofrontonasal syndrome patients harboring mutations in *EFNB1* also exhibit aCC, indicating that although the involvement of *Efnb1* is genetic background-dependent in mice, its requirement is conserved across species (Twigg et al., 2004). *Efnb2*$^{LacZ/LacZ}$ mutant mice exhibited severe defects in the formation of the ACp axon tract, suggesting that ephrin-B2 reverse signaling is important in this context (Cowan et al., 2004). However, this allele has since been demonstrated to result in a gain of function of ephrin-B2 signaling in some contexts (described below), casting some uncertainty on the interpretation of phenotypes observed in these mutants (Zhang et al., 2015). Ephrin-B3 apparently regulates formation of the CC entirely *via* forward signaling, because complete loss of ephrin-B3 results in severe defects of the CC, whereas loss of the intracellular domain does not (Mendes, 2006). Null loss of ephrin-B3 does not disrupt formation of the AC, on the other hand, indicating it likely does not play a role in this context (Kullander et al., 2001). Together, these results support a major role for EphB forward signaling in formation of the AC and CC, with some reverse signaling contribution from the intracellular domain of B-type ephrins as well.

In some cases, examination of ephrin-B cytoplasmic signaling mutants has made direct attribution of signaling directionality possible. For example, ephrin-B1$^{6F\Delta V}$ mutant embryos do

not have the craniofacial or skeletal defects seen in ephrin-B1^{null} embryos, indicating that reverse signaling by PDZ- or phosphorylation-dependent mechanisms is not necessary for craniofacial and skeletal development (Bush and Soriano, 2009); instead, forward signaling has been implicated in these processes (Bush and Soriano, 2010; Risley et al., 2009). Mice expressing one copy of ephrin-B2^{F5}, in which each of the five phosphorylatable tyrosines in the cytoplasmic tail of ephrin-B2 is mutated to phenylalanine, on a null background (*Efnb2*$^{-/F5}$ mice) do not exhibit the early embryonic phenotypes exhibited by *Efnb2*$^{-/-}$ embryos, indicating that these defects are not caused by lack of ephrin-B2 tyrosine phosphorylation (Davy and Soriano, 2007). *Efnb3*$^{\Delta C/\Delta C}$ mice lacking the entire cytoplasmic domain of ephrin-B3 do not have the same corticospinal tract defects as *Efnb3*$^{-/-}$ mice, indicating that it is the forward signaling aspects of ephrin-B3 signaling that prevents EphA4-expressing axons from crossing the spinal cord midline (Yokoyama et al., 2001).

In a study of Eph/ephrin-mediated cell segregation in CFNS, our laboratory has implicated unidirectional signaling in tissue separation (O'Neill et al., 2016). We showed that in the developing *Efnb1*$^{+/-}$ mouse embryo, a model for CFNS, ephrin-B1-mediated segregation first occurs in the neural plate neuroepithelium at E8.5, prior to neural tube closure. Through a series of genetic mouse mutants, we demonstrated that mosaic loss of reverse signaling (in *Efnb1*$^{+/6F\Delta V}$ embryos) does not result in cell segregation, indicating that mosaicism for ephrin-B1 reverse signaling alone is not sufficient to induce segregation. Mosaicism for loss of reverse signaling in an ephrin-B1 null embryo (in *Efnb1*$^{\Delta/6F\Delta V}$ embryos), however, results in cell segregation indistinguishable from that seen in ephrin-B1 heterozygous embryos, indicating that the SH2/PDZ-dependent reverse signaling modes of ephrin-B1 are not required for segregation. Consistent with cell segregation being driven by forward signaling alone, ephrin-B1 heterozygous embryos lacking forward signaling through EphB2 (*Efnb1*$^{+/\Delta}$; *Ephb2*$^{LacZ/LacZ}$) or through both EphB2 and EphB3 (*Efnb1*$^{+/\Delta}$; *Ephb2*$^{LacZ/LacZ}$; *Ephb3*$^{-/-}$) lose segregation. This forward signal requires EphB kinase activity, as demonstrated by a chemical genetic approach

using *Efnb1*$^{+/\Delta}$ mice also expressing mutant forms of EphB1, EphB2, and EphB3 engineered to be kinase-inhibited by the inhibitor 1-NA-PP1; these embryos exhibited robust segregation in the absence of 1-NA-PP1, but reduced segregation upon 1-NA-PP1 inhibition of kinase signaling. Therefore, reverse signaling through phosphorylation or PDZ mechanisms is neither necessary nor sufficient for cell segregation, whereas forward signaling is required.

Based on mutations to ephrin-B cytoplasmic domains in mice, reverse signaling by B-type ephrins has also been proposed in a variety of additional developmental contexts, including cardiac valve formation (Cowan et al., 2004), secondary palate development, foregut and urorectal morphogenesis (Dravis and Henkemeyer, 2011; Dravis et al., 2004), lymphangiogenesis (Makinen, 2005), axon pruning (Xu and Henkemeyer, 2009), and postsynaptic neuron maturation (Xu et al., 2011). Studies using these mutant proteins to interrogate reverse signaling functionality, however, have sometimes resulted in confusing conclusions about the role of the ephrin-B cytoplasmic domain. Ephrin-B2$^{LacZ/LacZ}$ embryos have urorectal and hindgut defects (Dravis et al., 2004), defects in cardiac development (Cowan et al., 2004), tracheoesophageal fistula (TEF), and cleft palate (Dravis and Henkemeyer, 2011). Ephrin-B2$^{\Delta V/\Delta V}$ embryos (lacking PDZ interactions) and homozygous Ephrin-B2$^{6YF\Delta V/6YF\Delta V}$ embryos (lacking PDZ interactions and tyrosine phosphorylation), however, have no urorectal, tracheoesophageal, or palatal defects, whereas ephrin-B2$^{LacZ/\Delta V}$ and ephrin-B2$^{LacZ/6YF\Delta V}$ embryos have hypospadias (Dravis and Henkemeyer, 2011). This led to the conclusion that PDZ-dependent reverse signaling functions of ephrin-B2, in addition to a not-yet identified function of the intracellular domain, are important for midline closure of the embryo.

Further investigation of the effects of ephrin-B2 cytoplasmic mutants in the context of lymphatic valve development resulted in the surprising discovery that these mutants may affect not only reverse signaling, but also forward signaling. EphB4/ephrin-B2 signaling is critical for lymphatic valve development, which in turn is important for maintaining tissue fluid homeostasis by allowing drainage of interstitial fluid and preventing backflow of lymph (Zhang et al., 2015).

Treating early neonatal mice (P1-P2) with antibodies that block ephrin-B2 or EphB4 function results in dilation of lymphatic vessels and defects in lymphatic valve structure soon thereafter, with complete absence of valves and death by postnatal day 8 (P8). However, Zhang and colleagues showed that co-administration of anti-ephrin-B2 with an antibody that is agonistic to EphB4 function, increasing its tyrosine phosphorylation, rescued these defects, suggesting that forward signaling may be sufficient in this context. These defects are similar to those seen in mice expressing a mutant ephrin-B2 lacking its PDZ domain interaction site (ephrin-B2$^{\Delta V}$) (Makinen, 2005) or in ephrin-B2$^{6YF\Delta V/6YF\Delta V}$ mice that lack PDZ- and phosphorylation-dependent reverse signaling (Zhang et al., 2015), but EphB4 tyrosine phosphorylation is also significantly reduced, at least in *Efnb2*$^{6YF\Delta V/6YF\Delta V}$ embryos, indicating that this ephrin-B2 mutant also affects forward signaling. Treatment with the EphB4 agonist antibody also rescues the lymphatic valve defects in *Efnb2*$^{6YF\Delta V/6YF\Delta V}$ mutants, strongly suggesting that it is ephrin-B2-driven EphB4 forward signaling that is required for lymphatic valve development (Zhang et al., 2015). Although the mechanism by which mutating the cytoplasmic domain of ephrin-B2 could lead to defects in EphB4 forward signaling is not yet known, it has been shown that the intracellular region of ephrin-Bs can affect how a signal is processed in EphB expressing cells (Jorgensen et al., 2009). Further, *Efnb2*$^{LacZ/LacZ}$ mutant mice, with the entire cytoplasmic domain of ephrin-B2 replaced with LacZ, do not have lymphatic valve defects, and in fact have increased EphB4 tyrosine phosphorylation, probably due to tetramerization driven by the β-galactosidase (Zhang et al., 2015). This suggests that the ephrin-B2^{LacZ} allele is hypermorphic for forward signaling rather than a reverse signaling mutant. Zhang and colleagues inhibited EphB4 kinase signaling using either a small molecule inhibitor or mice expressing an analog-sensitive EphB4 kinase mutant and showed that inhibiting EphB4 kinase signaling results in a severe lymphatic valve phenotype, without any manipulation of ephrin-B2 (Zhang et al., 2015). The results from the above experiments suggest that a variety of cytoplasmic mutations in ephrin-B2 disrupt forward signaling; in combination with the data that interruption of forward signaling alone is sufficient to

recapitulate the lymphatic valve phenotypes under study, this work calls into question whether or not reverse signaling is involved in this developmental event.

The extent to which studies using mutations of the ephrin-B cytoplasmic domain could lead to incorrect conclusions about the respective roles of forward and reverse signaling in contexts outside of lymphatic development is unclear. It is unlikely that gain-of-function activity of the ephrin-B2^{LacZ} allele is responsible for all of the exhibited phenotypes, because *Efnb2*$^{LacZ/6F\Delta V}$ and *Efnb2*$^{LacZ/\Delta V}$ mutants still exhibit urorectal malformations with a penetrance significantly higher than *Efnb2*$^{LacZ/+}$ embryos (Dravis and Henkemeyer, 2011). Further, the *Efnb2*^{CR} conditional loss of function model also exhibits urorectal malformations and TEF, indicating that these phenotypes are loss of function phenotypes that may be caused by loss of reverse signaling (Lewis et al., 2015). Cleft palate, on the other hand, does not occur in these *Efnb2*^{CR} mice, suggesting that this phenotype in *Efnb2*$^{LacZ/LacZ}$ mice could be caused by hyperactivation of forward signaling.

The data that have emerged regarding the effects of ephrin-B reverse-signaling mutants on Eph receptor forward signaling suggests that the interplay between forward and reverse signaling will prove to be an even more complicated subject than was previously thought. In determining the contributions of forward and reverse signaling to *in vivo* phenotypes, it will be essential to examine forward signaling activation in reverse signaling mutants to rule out contributions of cytoplasmic ephrin-B mutants to hyper- or hypo-activation of forward signaling. It should also be noted that very similar mutants to those described in the above section are frequently re-expressed, over-expressed, or mis-expressed to evaluate signaling function in other model systems where knock-ins are not technically straightforward. Nearly all of the potential caveats and complications considered above are also possible in these systems, which additionally must account for the consequences of exogenous expression. Thus, these studies highlight that our understanding of *in vivo* Eph/ephrin signaling mechanism is still evolving and will benefit from additional approaches. For example, mutations that selectively

block Eph receptor kinase signaling, such as those that use kinase-dead or analog-sensitive kinase mutant Eph receptors, have been recently used to study kinase signaling mechanisms in a number of contexts (O'Neill et al., 2016; Robichaux et al., 2014; Robichaux et al., 2016; Soskis et al., 2012). In the future, it will be valuable to identify effectors downstream of forward and reverse signaling activation relevant to specific contexts and demonstrate that loss of function of these downstream processes contributes to the observed phenotype.

Eph/ephrin signaling directs cell positioning during embryonic development

Eph/ephrin signaling is essential to axon guidance, with repulsive interactions between Ephs and ephrins expressed in axons and in their target zone cells mediating correct formation of synapses in many different areas of the developing nervous system (Egea and Klein, 2007). Analogous to this role in axonal pathfinding, Ephs and ephrins have also been described as guidance cues that mediate migration of cells over long distances by repeated short-range interactions. Although from a cellular perspective, Eph/ephrin signaling has been widely implicated in regulating cell migration, the specific functions differ somewhat across different developmental contexts such as neural crest migration, neuronal migration guidance pathways in the brain, and the migration of cells to establish left-right asymmetry.

Neural crest cell migration

Eph/ephrin signaling has repeatedly been shown to be critical for development of neural crest cells (NCCs). From the earliest stages, Eph/ephrin signaling regulates NCC development in *Xenopus*. Forward signaling from ephrin-B1 and ephrin-B2 in the dorsal mesoderm inhibits Wnt signaling required to induce NCCs; the Adam13 metalloprotease cleaves ephrin-B1 and ephrin-B2 to relieve this inhibition and allow NCC induction (Wei et al., 2010). Studies in chick and *Xenopus* have proposed a repulsive mode of neural crest guidance, wherein disruption of Eph/ephrin signaling results in invasion of NCCs into ectopic territories. Using *in vitro* stripe

assays in which soluble ephrin ligand is immobilized in narrow stripes on cover slips, cultured chick or rat NCCs, which express EphB receptors, avoid stripes of ephrin-B protein, instead preferring to migrate alongside (Krull et al., 1997; Wang and Anderson, 1997). In rat and mouse embryos, ephrin-B2 expression is restricted to the caudal half of the somite, whereas in chick embryos ephrin-B1 exhibits this pattern of expression, leading to the idea that caudally-expressed ephrin-B guides EphB-expressing trunk NCC migration to the rostral half of the somite (**Figure 5A**). Eph/ephrin signaling has been implicated in cranial neural crest guidance as well. In *Xenopus*, rhombomeric boundaries set up by expression of EphA4 and ephrin-B2 expression in r5 and r4, respectively, extend to migratory NCC populations derived from those rhombomeres, whereas EphB1 is expressed in NCCs destined for branchial arches (BA) 3 and 4. Disruption of EphA4/EphB1 function by overexpression of truncated receptors, or by blinding the NCCs to the position of ephrin-B2 signal by overexpression of ephrin-B2, results in NCC intermingling during migration (Smith et al., 1997). In addition to a role in segmental guidance, Eph/ephrin signaling in *Xenopus* has also been demonstrated to regulate migration of NCCs along the ventral or dorsolateral pathways. Expression of multiple ephrins along the dorsolateral pathway repels and guides early-migrating NCCs expressing EphB receptors along the ventral pathway. Interestingly, migration of melanoblast NCCs, which also express EphB receptors, is promoted along the dorsoventral pathway by increasing adhesion (Santiago and Erickson, 2002).

In mouse, genetic disruption of ephrin-B2 also perturbs normal NCC development, with *Efnb2*^{null} mouse embryos exhibiting both angiogenic remodeling defects and NCC defects that result in abnormal BA development and trunk NCC segmentation (Davy and Soriano, 2007). It has been difficult to assess the exact role of ephrin-B2 in NCC development *in vivo*, as angiogenic defects lead to early embryonic lethality of *Efnb2*^{null} embryos. An attempt to separate the role of ephrin-B2 in the vasculature from its contributions to NCC migration resulted in the surprising discovery that rescuing expression of ephrin-B2 only in the vascular endothelium (VE)

is sufficient to obtain normal NCC migration and BA development (Lewis et al., 2015). In mice with a conditional rescue of ephrin-B2 in the vasculature in an otherwise ephrin-B2 null embryo (*Tie2-Cre; Efnb2*^{CR}), not only angiogenesis defects, but also BA morphogenesis and cranial and trunk NCC defects, are rescued. Further, loss of ephrin-B2 specifically in the vasculature, again mediated by Tie2-Cre, resulted in angiogenic and neural crest phenotypes, as well as increased cell death in migrating cranial and trunk NCCs, suggesting that without proper vascular development, NCC survival is compromised. From these studies, it is apparent that in mouse, proper ephrin-B2 expression, or angiogenesis regulated by ephrin-B2, is a requirement for NCC development, and that ephrin-B2 may not have a role in repulsive NCC guidance as previously proposed. The role of the VE in regulating NCC migration, however, remains unclear. EphB4 plays an important role in ephrin-B2 signaling in the context of angiogenesis: *Ephb4*$^{-/-}$ mice have similar angiogenic remodeling defects to *Efnb2*^{null} mice, as well as similar NCC and BA morphogenesis phenotypes. However, because EphB4 is not expressed in NCCs, it seems unlikely that signaling to NCCs from ephrin-B2 in the VE is required (Lewis et al., 2015). Even without pinpointing the exact mechanism by which angiogenic remodeling contributes to NCC migration, it seems likely that the role of ephrin-B2 in the process is a secondary one in allowing the vasculature to develop and function normally, which in turn provides an as yet unknown, but essential, support to NCCs. It is possible that ephrin-B2 signaling from the VE may provide a guidance role for NCCs; further studies will be needed to determine whether this is the case, or whether angiogenesis plays a more permissive role in NCC survival. For example, normal angiogenesis may be required for delivery of oxygen, nutrients, or other signaling molecules required for NCC survival (**Figure 5A**) (Lewis et al., 2015). Interestingly, Eph/ephrin signaling may also have a more direct role in NCC survival. Ectopic expression of ephrin-A5-Fc in mouse dorsal neuroectoderm and NCCs, mediated by Wnt1-Cre, led to decreased NCC survival and diminished NCCs of the frontonasal prominence and BA1 and BA2 (Noh et al., 2014).

Like the trunk NCCs from which they are derived, the sympathetic ganglia (SG) are also segregated to the rostral half of each somite. This organization, however, is not the consequence of early migratory guidance of NCCs, which lose their segregated pattern and intermix along the anteroposterior axis upon arrival at the site of SG formation, but of later re-sorting of NCCs into discrete ganglia following their arrival at sympathetic ganglia target sites (Kasemeier-Kulesa et al., 2005). Live imaging studies in chick have demonstrated that the segregation of NCCs into SG involves repulsive Eph/ephrin signaling wherein expression of ephrin-B1 in the rostral half of the somite expands to the mesoderm, signaling to NCCs expressing EphB2 to drive their condensation into discrete SG (Kasemeier-Kulesa et al., 2006). Disruption of this late repulsive cue disrupts SG formation even when early segmental NCC guidance is maintained due to loss of directionality in their repulsion.

Neuronal migration

Eph/ephrin signaling plays important roles in development of the mammalian neocortex and hippocampus by regulating radial and tangential neuronal migration. In the cortex, tightly controlled migration of neurons born at the ventricular zone leads to formation of a highly organized, layered structure. As the location of different excitatory neurons with different functions in each layer is essential to the future function of the cortex, newly born neurons at the proliferative ventricular zone of the cortex must migrate radially to a distinct position, with each successive generation of neurons migrating past older-born neurons. In the hippocampus, migration of neuronal precursors is also essential for the differentiation of these neurons to form mature structures. Interestingly, several studies have indicated that Eph/ephrin signaling functions together with Reelin signaling in neuronal guidance in the cortex and hippocampus (Bouché et al., 2013; Catchpole and Henkemeyer, 2011; Sentürk et al., 2011). Reelin is a secreted glycoprotein that regulates neuronal migration and cortical layering, and *reeler* (*Reln*$^{-/-}$) mice have cortical phenotypes including “inside-out” layering, with late-born neurons aberrantly

located in deeper layers of the cortex and earlier-born neurons in upper layers. *Efnb1/b2/b3* compound knockout mice mimic *reeler* cortical phenotypes, and loss of one copy of Reelin on an *Efnb2*$^{-/-}$ or *Efnb3*$^{-/-}$ background leads to alterations in cortical layering and hippocampal structures similar to those seen in *reeler* mice, though *Reln*$^{+/-}$ mice alone are unaffected (Sentürk et al., 2011). Although this suggests that Reelin and ephrin-Bs interact to facilitate correct radial migration of neurons to form the laminated cortex (**Figure 5B**), these phenotypes seem to depend on the *Efnb3* knockout strategy used, as well as the genetic background of the mouse strain (Pohlkamp et al., 2016).

In the hippocampus, loss of forward signaling from ephrin-B1 to EphB2 leads to a reduction in granule cell neurons in the lateral suprapyramidal blade (LSB) of the dentate gyrus, resulting from decreased migration of precursor cells into this area (Catchpole and Henkemeyer, 2011). Notably, EphB2 and ephrin-B1 mutant mice demonstrate a decrease in Reelin expression adjacent to the LSB, suggesting that forward signaling through EphB2 is necessary for Reelin expression to promote migration of precursor cells into the LSB (Catchpole and Henkemeyer, 2011). However, the direct mechanisms by which EphB2 and ephrin-B1 influence the expression and secretion of Reelin in the hippocampus are unknown.

Canonical Reelin signaling involves Reelin binding to lipoprotein receptors VLDLR and ApoER2, leading to tyrosine phosphorylation of Dab1, but VLDLR/ApoER2 have no intrinsic kinase activity, which is instead fulfilled by the recruitment of Src-family kinases (D'Arcangelo et al., 1999; Howell et al., 1999). Physical interactions between Reelin, EphB, and ephrin-B proteins have been demonstrated in both the cortex and the hippocampus, suggesting that EphB/ephrin-B signaling may synergize with Reelin signaling to affect neuronal migration. Specifically, Reelin interacts with ephrin-B2 and ephrin-B3 proteins, and stimulation of cultured cortical neurons with Reelin results in clustering of ephrin-Bs (Sentürk et al., 2011). Sentürk and colleagues point to reverse signaling through ephrin-Bs as a "missing link" that recruits Src family kinases to phosphorylate Dab1. Stimulation of cortical neurons with EphB3-Fc results in

tyrosine phosphorylation of Dab1, and *Efnb1/b2/b3* knockout mice have decreased Dab1 phosphorylation (Sentürk et al., 2011), though genetic evidence supporting the involvement of the ephrin-B cytoplasmic domain in Dab1 phosphorylation has not yet been shown. Reelin also coimmunoprecipitates with recombinant EphB1, EphB2, and EphB3 in cultured neurons and induces EphB tyrosine phosphorylation, proteolytic processing, and cytoskeletal responses in Cos1 cells (Bouché et al., 2013). These effects are independent of the canonical Reelin receptors (Bouché et al., 2013). However, the *in vivo* relevance of these biochemical interactions to cortical lamination, and the mechanisms of synergy between Eph/ephrin signaling and Reelin signaling, remain uncertain. Loss of EphB2 kinase signaling results in aberrant cell dispersal in the CA3 region of the hippocampus (**Figure 5B**), demonstrating that EphB forward signaling is required for this *in vivo* event. However, these studies face a challenge in distinguishing Reelin-to-Eph signaling from ephrin-to-Eph signaling. Bouché and colleagues argue that the hippocampal CA3 defects in compound *Ephb1; Ephb2* mutant mice are a result of Reelin-mediated forward signaling, not ephrin-B1-mediated forward signaling, because ephrin-B1 knockout mice have a much milder CA3 phenotype than the *Ephb1; Ephb2* mutants, whereas the *reeler* mouse phenotype is similar to the *Ephb1; Ephb2* mutant phenotype (Bouché et al., 2013). However, although neither ephrin-B2 nor ephrin-B3 were found to be expressed in the CA3 region during hippocampal neuronal migration, it is impossible to rule out the contribution of ephrin-B1 or as yet unknown contributions from other ephrins that may bind to and activate EphB1/EphB2. In the future, studies that examine compound EphB receptor/Reelin mutant mice, probe EphB receptor signaling changes in *reeler* mice, or differentiate the downstream signaling pathways of EphB receptors activated by ephrins vs. activated by Reelin, may shed further light on the *in vivo* relevance of these interactions. Although the mechanism of Reelin interactions with EphBs or ephrinBs to facilitate neuronal migration remains unclear, it is apparent that Reelin can interact genetically and biochemically with several members of this pathway, demonstrating that Eph/ephrin signaling molecules are

able to integrate with Reelin signaling to assist in mediating signaling outcomes that lead to correct positioning of neurons.

Ephrin-B1 also plays an early role in maintenance of the structural integrity of the apical surface of the developing cortex, which is necessary for correct cortical lamination. Maintenance of apical attachment of neural progenitors at the ventricular zone and attachment of neighboring apical progenitors to each other *via* adherens junctions are regulated by ephrin-B1 signaling, and *Efnb1*$^{+/-}$ and *Efnb1*$^{-/-}$ embryos demonstrate abnormal folding of the apical surface of the neuroepithelium (Arvanitis et al., 2013). *Efnb1* mutant embryos demonstrate changes in cell-ECM adhesion at the apical surface, with decreases in apical localization, but not mRNA or protein expression of integrin-β1. Notably, cell-cell adhesion, examined *via* N-cadherin expression, and cell polarity, marked by the apical distribution of β-catenin, are unaffected in these mutants. In *ex vivo* cortical slices, acute loss of ephrin-B1 results in loss of elongated cell morphology and detachment of cells from the apical surface of the ventricular zone. Ephrin-B1 tyrosine phosphorylation and the PDZ interaction domain of the ephrin-B1 intracellular domain are not necessary for maintenance of apical adhesion, as expression of ephrin-B1 lacking its cytoplasmic domain rescues the cell-ECM adhesion defects (Arvanitis et al., 2013). By synergizing with integrin-β1 signaling to maintain the integrity of the apical surface of the ventricular zone of the cortex, therefore, ephrin-B1 signaling plays a critical role in coordinating the development of the cortex. Here, ephrin-B1 does not serve directly as a guidance cue, but rather plays an indirect role, serving as a structural support system for neural progenitors to allow maintenance of apical adhesion during the early development of the cortex. Future studies defining the mechanisms of Eph/ephrin support of neuronal migration, through Reelin signaling or other pathways, will provide more insight into the roles of this pathway in defining correct cell positioning in the developing brain.

Guidance of cell migration to establish left-right asymmetry

Eph/ephrin signaling has recently been implicated in establishing left-right asymmetry in the developing zebrafish embryo. The dorsal forerunner cells (DFCs), precursor cells to the Kupffer's vesicle (KV), the left-right organizer in zebrafish, express EphB4b, while the surrounding mesendodermal cells express ephrin-B2b, and signaling between them maintains DFC cluster integrity as the cells migrate past each other (Zhang et al., 2016). These interactions are mediated by extension of protrusions from DFCs that are then repulsed by the neighboring cells, and loss of EphB4b leads to loss of RhoA and pMLC expression at the DFC-mesendoderm boundary, slowing of this repulsive response, and subsequent dispersal of DFCs, ultimately resulting in a smaller or absent KV and defects in later asymmetric positioning of organs (Zhang et al., 2016). Eph/ephrin signaling is also involved in epithelial-mesenchymal interactions that control asymmetrical positioning of the liver (Cayuso et al., 2016). Cayuso and colleagues demonstrate that EphB3b/ephrin-B1 signaling between the lateral plate mesoderm (LPM) and the hepatoblasts of the forming liver results in hepatoblast repulsion that is critical for correct asymmetric positioning of the liver (**Figure 5C**), challenging the existing model that the LPM actively pushes hepatoblasts, which are passively corralled into place. Hepatoblasts form long cellular protrusions that are lost in *ephrin-B1* morpholino-treated embryos but increased with loss of direction in *ephb3b* morphants (Cayuso et al., 2016). Expressing reverse signaling mutant ephrin-B1 proteins in an ephrin-B1-deficient background has varying effects on protrusion formation. Adding ephrin-B1^{6F} rescues hepatoblast protrusion formation, whereas adding ephrin-B1$^{\Delta V}$ does not. The authors conclude that PDZ-dependent reverse signaling mediates protrusion formation, independent of tyrosine phosphorylation of the cytoplasmic domain of ephrin-B1, to permit hepatoblast movement away from the midline and facilitate asymmetric positioning of the liver. Though no examination of possible changes to forward signaling in EphB3b-expressing LPM cells was made, ectopic expression of EphB3b$^{\Delta ICD}$ (lacking the intracellular domain) in the left LPM, where there is little endogenous EphB3b, resulted in

movement of the hepatoblasts to the right side, consistent with a role of reverse signaling in repulsion of hepatoblasts from the LPM and establishing the asymmetric positioning of the liver. Further studies of the role of Eph/ephrin signaling in liver positioning, as well as in the establishment of asymmetry in other organ systems, will elucidate the signaling mechanisms involved in these processes.

Eph/ephrin signaling translates patterning cues to separation between embryonic tissues

Establishing and maintaining separation between tissues during development is a multifaceted process requiring patterning to establish cell fate, segregation of different cell types to form boundaries, and prevention of cell migration and intermingling across these boundaries. A classical view of Eph/ephrin-mediated tissue separation involves reciprocal expression of Ephs and ephrins in separate compartments, with bidirectional signaling across the Eph/ephrin expression boundary preventing intermingling (Kania and Klein, 2016). This model stems from studies of Eph receptors and ephrins in the organization of the developing embryo: in the brain, spinal cord, branchial arches, limb buds, and somites, Eph receptor and ephrin expression appeared mutually exclusive and restricted to defined domains, leading to the proposal that Ephs may encounter ephrins only at the boundaries between these domains (Gale et al., 1996). Further study suggested that reciprocal expression can contribute to tissue separation and maintenance of boundaries between morphologically defined compartments, such as the rhombomeres of the zebrafish hindbrain (Xu et al., 1999). More recent evidence demonstrates the existence of more complex patterns of Eph/ephrin expression and signaling during development (Barrios et al., 2003; O'Neill et al., 2016; Rohani et al., 2014). Eph/ephrin signaling has long been studied as a mediator of boundary formation and maintenance in early neural development, gastrulation, and somitogenesis. Recently, increased complexity of Eph/ephrin expression patterns and signaling has been demonstrated in each of these contexts, providing evidence for a more nuanced role of Eph/ephrin signaling at tissue boundaries that depends

both on context and on the combinatorial expression of Eph receptors and ephrins in the tissue in question. In each of these situations, Eph/ephrin signaling is a downstream effector of boundary formation and maintenance, translating patterning information to physical separation. The mechanisms by which tissue separation is achieved are still under study, but include changes to adhesion, cytoskeletal dynamics, cellular repulsion, and cell migration.

Eph/ephrin-mediated boundary formation during early neural development

The first discovery of Eph/ephrin signaling in cell segregation and boundary formation was in the developing nervous system. Segmentation of the vertebrate hindbrain during development leads to the formation of compartments termed rhombomeres, which demarcate boundaries between different areas of the hindbrain that will eventually develop into different adult structures. Importantly, the organization of the rhombomere separates precursor cells of different neuronal subtypes and contributes to the later organization of hindbrain neurons (Moens and Prince, 2002); inappropriate cell mixing must therefore be prevented to preserve normal adult hindbrain function. Eph receptors are expressed in odd-numbered rhombomeres, and ephrins are expressed in even-numbered rhombomeres, leading to the proposal that signaling mediates repulsive interactions at rhombomere boundaries (**Figure 6A**) (Xu et al., 1999) or differential adhesion between cells of different rhombomeres (Cooke et al., 2005; Kemp et al., 2009).

In the developing zebrafish hindbrain, gene expression boundaries become morphological boundaries, which manifest as shallow indentations between rhombomeres by 15h post fertilization. Morpholino knockdown of EphA4a, which is usually expressed in rhombomeres r3 and r5, resulted in jagged edges to rhombomere boundaries, with *krx20*-expressing cells from r3 and r5 invading into the adjacent even-numbered rhombomeres (Calzolari et al., 2014). Invading cells do not immediately change their fate, suggesting that Eph/ephrin signaling acts downstream of patterning cues, and indeed, Eph/ephrin expression

patterns in rhombomeres are established in part through the transcription factors Krox20 and HoxB4. In zebrafish, Krox20 binds and drives expression from an r3/r5 enhancer element harbored by *EphA4* and deletion of this binding site leads to loss of r3/r5 enhancer activity, suggesting that *EphA4* is directly regulated by Krox20 (Theil et al., 1998). Krox20 also directly regulates the expression of multiple *Hox* genes, suggesting a means of coupling downstream A-P cell fate specification with physical separation of rhombomeres (Theil et al., 1998). More recently, it has been suggested that coupling cell fate with tissue separation in the hindbrain may entail a more complicated hierarchy that also depends on A-P specification; indeed, loss of *Hox* genes disrupts not only A-P identity, but also rhombomere boundaries (Prin et al., 2014). In mouse and chick, *Hoxb4* and *Hoxd4* share their anterior expression border at the r6/r7 boundary, and loss of both resulted in loss of the r6/r7 boundary. In addition, widespread misexpression of *Hoxb4* also disrupted rhombomere boundaries, and mosaic misexpression of Hoxb4 or any of several other Hox genes caused aberrant segregation within a rhombomere, indicating that a differential in Hoxb4 (and its targets) drives rhombomere formation. One such target may be EphA7: upon loss of Hoxb4 and Hoxd4, EphA7 was upregulated caudal to the site of the r6/r7 border, while ectopic expression of Hoxb4 resulted in EphA7 repression rostral to this border. Functional evidence for a requirement of EphA7 in r6/r7 boundary formation is so far lacking, however, and complementary ephrin expression at this boundary has not been identified. Mosaic expression of several different Hox proteins induced cell segregation, but the segregating effect of Krox20 expression predominated, suggesting that a hierarchy of combinatorial regulation of Eph/ephrin genes by multiple transcription factors couples A-P cell fate specification to tissue separation.

As the morphological changes that define rhombomere boundaries take place, actin and myosin II accumulate to form a cable between rhombomeres (Calzolari et al., 2014), suggesting a mechanism by which Eph/ephrin signaling may direct both cell segregation and the formation of a physical barrier to cell intermingling. Work in *Drosophila*, *Xenopus*, and mouse, as well as

in human cell culture, similarly support the broad idea that regulation of actomyosin contractility contributes to Eph/ephrin-mediated segregation (Aliee et al., 2012; Monier et al., 2010; O'Neill et al., 2016; Rohani et al., 2011; Umetsu et al., 2014). In the rhombomere, cells can move past a boundary *via* cell division but are rapidly pushed back into their proper position, perhaps by the elastic boundary formed by the actomyosin cable (Calzolari et al., 2014). The actomyosin cables appear to colocalize with EphA4a in r3/r5, and disrupting actin or myosin II using ROCK inhibitors or Blebbistatin results in dismantling of the cables and invasion of r3/r5 cells into even-numbered rhombomeres, creating jagged rhombomere boundaries. Conversely, stabilizing phosphorylated myosin by treatment with calyculin A results in even more pronounced rhombomere boundaries. Importantly, morpholino knockdown of EphA4a disrupts actomyosin cable formation in a similar manner to ROCK inhibition or Blebbistatin treatment, and the jagged boundaries that form can be rescued by treatment with calyculin A (Calzolari et al., 2014), indicating that EphA4a acts upstream of myosin to modulate formation of this physical boundary. Further, ectopic activation of EphA4a in even-numbered rhombomeres results in accumulation of actomyosin in EphA4a-expressing cells only if they are surrounded by ephrin-expressing cells, suggesting that Eph/ephrin signaling acts to upregulate actomyosin. Boundary sharpening appeared to begin before actomyosin enrichment could be observed, however (Calzolari et al., 2014), suggesting that additional mechanisms may be at play in initial rhombomere boundary sharpening.

Eph/ephrin signaling also acts downstream of patterning cues during forebrain development in zebrafish. During neurulation, the cells of the prospective eye field evaginate to form the optic vesicles, which must remain separated from the cells of the prospective telencephalon and diencephalon for proper eye development. Eph receptor expression in the telencephalon and ephrin expression in the eye field are essential to this process, as morpholino knockdown or misexpression of these molecules results in delayed optic vesicle evagination and aberrant localization of eye field cells within the telencephalon (Cavodeassi et

al., 2013). In addition, misexpression of the normally telencephalon-restricted EphB4a in eye field cells causes them to segregate into the telencephalon while retaining eye field markers, indicating that Eph/ephrin expression determines their movement regardless of fate (Cavodeassi et al., 2013). In zebrafish mutants that have lost expression of the eye field transcription factor Rx3, Eph receptor expression expands into the eye field while ephrin expression remains normal, placing Eph/ephrin signaling downstream of patterning (Cavodeassi et al., 2013). Although the boundary between the eye field and the telencephalon is enriched in both F-actin and pMLCII, this study does not investigate whether Eph/ephrin signaling directly regulates the cytoskeleton in this context.

Pathogenic cell segregation in the neural plate neuroepithelium in the mouse model for CFNS also depends on modulation of the cytoskeleton (**Figure 6B**). Genetic disruption of ROCK using a dominant-negative allele in *Efnb1*$^{+/-}$ mice or pharmacological inhibition using the ROCK inhibitor Y-27632 in a cell culture model for segregation dramatically decreased the size of aberrant ephrin-B1 expression patches in each context (O'Neill et al., 2016). Interestingly, genetic interaction studies indicated that loss of Cdc42 or Rac1 function did not reduce segregation in *Efnb1*$^{+/-}$ embryos, consistent with the possibility that actomyosin contractility *per se*, and not cell migratory capacity more generally, may drive segregation in CFNS.

Eph/ephrin signaling in germ layer separation during gastrulation

Gastrulation represents one of the earliest tissue separation events in the embryo. The propensity for separation between cells of the germ layers is so strong that in the classic experiments of Townes and Holtfreter, even when cells of the amphibian germ layers were dissociated into single cells and forcibly mixed, they segregated from one another in culture to re-aggregate in groups of like cells (Townes and Holtfreter, 1955). Eph/ephrin signaling is required to maintain the boundary between the ectoderm and mesoderm during *Xenopus* gastrulation. Recent studies of the formation and maintenance of these boundaries have added

a layer of complexity to our understanding of Eph/ephrin regulation of these early tissue separation processes.

In the *Xenopus* gastrula, the mesoderm translocates across the ectodermal blastocoel roof (BCR), producing a paradox whereby mesoderm cells must be prevented from integrating into the ectoderm as they adhere to it while migrating. This process can be reconstituted *in vitro* using explant culture experiments, and live imaging of the mesoderm-ectoderm explant boundary reveals fast cell detachment and reattachment events, which may enable the adhesive contacts that mediate the collective migration of the mesoderm along the BCR, while preventing intermingling (Rohani et al., 2011). Multiple EphB and ephrin-B proteins are expressed in both the mesoderm and the ectoderm, and morpholino knockdown of ephrin-B1, ephrin-B2, or EphB4 in either the mesoderm or the ectoderm leads to increased integration of mesoderm cells into the BCR, suggesting a more complex situation than in the classical complementary expression model. Competitive inhibition of forward signaling by overexpression of truncated EphB4 resulted in diminished separation, and while combinatorial morpholino knockdown of ephrin-B expression in one explant and EphB expression in the opposing explant did not further decrease segregation, loss of both ephrin-B and EphB expression in the same explant does. These data have led to the conclusion that ectoderm-mesoderm separation is likely governed by multiple antiparallel forward signaling pathways across the boundary (**Figure 6C**) (Rohani et al., 2011; Rohani et al., 2014). Addition of preclustered ephrin-B-Fc fusion proteins to activate forward signaling can rescue attachment-detachment cell behaviors and separation from ephrin-B knockdown mesoderm or endoderm, further indicating that activation of Eph receptors in both tissues mediates segregation. This result is surprising in that it suggests that positional information conferred by cellular ephrin signaling in each cell population may not be important; activation of Eph receptor signaling in all cells in the explant results in tissue separation only at the explant boundaries. It seems, therefore, that activation of Eph receptor signaling in either population renders the populations somehow less miscible. The

outcome of Eph/ephrin signaling across the ectoderm-mesoderm boundary is at least partly mediated by activation of RhoA and Rac and results in enrichment of F-actin at the boundary (Rohani et al., 2011). In contrast to reciprocal Eph/ephrin expression, these data demonstrate that more complex mechanisms involving multiple coexpressed Ephs and ephrins may be required to localize cytoskeletal and cell behavioral changes to a boundary. These results also indicate that unidirectional signaling is sufficient to produce separation, although in this case it is required in both tissues (Rohani et al., 2011).

If Ephs and ephrins are expressed throughout both the ectoderm and mesoderm, how is tissue separation restricted only to their interface? Whereas complete specificity of Eph/ephrin pair binding, with signaling only at the boundary, is unlikely based on known receptor-ligand affinities, completely promiscuous binding would result in repulsion within both the ectoderm and mesoderm, leading to complete dissolution of the tissue. Instead, work by Rohani and colleagues suggests that an intermediate situation exists, in which antiparallel signaling between complementary pairs of Ephs and ephrins creates the strongest signaling interface at the heterotypic mesoderm-ectoderm boundary (Rohani et al., 2014). Importantly, although complete specificity is not necessary for separation in this model (both ephrin-B2 and ephrin-B3 can signal through EphA4, for example), neither are the Ephs and ephrins functionally redundant. Only ephrin-B2 signals through EphB4, and the phenotypes of morpholino knockdown of one Eph/ephrin family member are not rescued by expression of another. Further, chimeric Eph receptors composed of the extracellular domain of one receptor and the intracellular domain of another can only rescue depletion of the Eph whose extracellular domain they possess, indicating that specificity depends on differential Eph/ephrin binding occurring at the boundary, which may activate different downstream signaling cascades. A baseline level of adhesion between homotypic cell pairs of the ectoderm and mesoderm, provided by cadherin expression, is required to maintain the homotypic tissue cohesivity required for border sharpening (Rohani et al., 2014; Taylor et al., 2017). Whether homotypic repulsion is simply

overcome by differential adhesive forces provided by cadherins, or whether other mechanisms, such as *cis* inhibition of signaling, also contribute to blunting homotypic signaling outcomes, is not yet known.

An important remaining question involves the mechanisms that establish the differential expression of Eph and ephrin proteins in different germ layers. It is possible that transcription factor patterning alone maintains Eph/ephrin expression domains, but transcription factors that affect Eph/ephrin expression in the *Xenopus* ectoderm and mesoderm are not yet known. However, during gastrulation, Eph/ephrin protein stability is regulated through degradation of ephrin-B1 by ubiquitination, which is mediated by Smad ubiquitin regulatory factors (Smurfs). Interactions between ephrin-B1 and Smurf2 lead to ephrin-B1 ubiquitination and degradation, whereas interactions between ephrin-B1 and Smurf1 prevent its interaction with Smurf2, forestalling degradation (Hwang et al., 2013). Smurf2-mediated degradation of ephrin-B1 prevented separation between the endoderm and mesoderm, but Smurf1 binding to ephrin-B1 inhibits this interaction to allow separation. Loss of separation upon loss of Smurf1 can be rescued by subsequent knockdown of Smurf2 (Hwang et al., 2013). This reveals that modulating protein stability is one mechanism by which ephrin-B1 can be regulated to eventuate tissue separation during gastrulation.

Eph/ephrin signaling in the separation between forming somites

The formation of somites is a key step in the axis elongation and segmentation of the vertebrate embryo. The cells of the somites are precursors to vertebral and rib structures, as well as to skeletal muscle and dermis of the skin. Segmentation must be tightly regulated to ensure that segment number is strictly maintained, which is essential to further normal development; although the number of somites may vary between species, it is generally fixed within a species (Bénazéraf and Pourquié, 2013). Somites form with a defined period, the length of which is dependent on the species (Bénazéraf and Pourquié, 2013). To achieve this, Wnt,

FGF, and Notch signaling pathways are activated in pulses in the presomitic mesoderm (PSM), leading to a “traveling wave” of mRNA expression of their transcriptional targets. Many of these targets encode negative-feedback inhibitors of Wnt, FGF, and Notch signaling, which may explain the periodic control of signaling through these pathways (Bénazéraf and Pourquié, 2013). Downstream of this feedback loop, expression of segmentation genes such as *Mesp2* is seen in the PSM of the future somite, preceding the morphological changes that mediate somite boundary formation.

After the future somite is defined by patterning of segmentation genes, intercellular signaling is required to translate these cues into the morphogenetic processes that result in boundary formation and separation. Several Eph receptors and ephrins are expressed in the somites in developing mouse embryos (Gale et al., 1996), and expression of ephrin-A1, ephrin-B2, and EphA4 in segmented patterns in the zebrafish PSM suggested that these signaling molecules may play a role in somite formation (Durbin et al., 1998). Indeed, overexpression of truncated Eph or ephrin proteins, which serve a dominant-negative function by binding their cognate ephrin or Eph and blocking downstream signaling, disrupted somite boundary formation, resulting in absent or abnormally-shaped somites (Durbin et al., 1998). Perturbation of Eph/ephrin signaling did not affect segmental prepatterning, but downstream markers of somite differentiation reflected the organization of the ectopic somite, indicating that Eph/ephrin signaling mediates the translation of segmental prepattern into physical somite separation. Activation of Eph/ephrin signaling is sufficient for boundary formation, because exogenous expression of EphA4 in zebrafish *fss*$^{-}$ mutants, which lack segmental expression of several Eph/ephrins and fail to form somites, was sufficient to induce somite boundary formation at the interface between clusters of EphA4-expressing and -nonexpressing cells (Barrios et al., 2003; Durbin et al., 2000). Separation was also induced when cells expressed a truncated EphA4 that lacks the intracellular tyrosine kinase domain, indicating that tissue separation can be induced in the absence of kinase signaling in this context (Barrios et al., 2003). These data suggest that

Eph/ephrin signaling may be directly involved in the morphogenetic processes that occur at the somite boundary, which include the formation of an indentation or furrow between adjacent somites; mesenchymal-to-epithelial transition of cells at either side of the boundary, which assume a columnar shape; accumulation of adhesion complex components, such as beta-catenin, at the apical pole of the cell; basal movement of cell nuclei towards the somite boundary; and apical movement of centrosomes. Whereas initial gap formation requires reverse signaling, several of the subsequent epithelialization changes require forward signaling through either direct or non-cell-autonomous means (Barrios et al., 2003).

Later work in chicken embryos suggests that both forward and reverse Eph/ephrin signaling may act in initial formation of the somite gap (Watanabe et al., 2009). In a gap-inducing assay, transplantation of a cMeso-1-expressing explant into the PSM of a host chick embryo results in upregulation of EphA4 and formation of a gap at the cMeso-1 expression boundary (Watanabe et al., 2009). Likewise, overexpression of EphA4 or ephrin-B2 is sufficient to induce an ectopic gap. Overexpression of EphA4 lacking its intracellular domain also creates an ectopic gap, indicating that the intracellular domain of EphA4 is dispensable for somitic gap formation. Consistent with this, overexpression of ephrin-B2 lacking its intracellular domain or ephrin-B2^{YF} (lacking three phosphorylatable tyrosines) does not induce an ectopic gap, indicating that phosphorylation-dependent ephrin-B2 reverse signaling is necessary for gap formation (Watanabe et al., 2009). Overexpression of constitutively active Cdc42 with ephrin-B2 negates the ability of ectopic ephrin-B2 expression to induce an ectopic somite gap, but suppression of Cdc42 alone is not sufficient to induce the gap, though it is sufficient to rescue cell epithelialization. Inhibition of Cdc42 in conjunction with overexpression of ephrin-B2^{YF} rescues both gap formation and cell epithelialization (Watanabe et al., 2009). The authors conclude that tyrosine phosphorylation of ephrin-B2 likely regulates Cdc42 to enable somite gap formation. Although it is clear that some portion of the cytoplasmic domains of both Ephs and ephrins are required for various aspects of the somite gap formation and cell epithelialization

process, the consequences of these mutations must be considered in light of new knowledge of the effects of ephrin cytoplasmic mutants on forward signaling, and much remains to be learned about the underlying mechanism. In particular, it remains to be determined whether somites, like the ectoderm and mesoderm in *Xenopus* gastrulation, require antiparallel forward signaling in addition to bidirectional signaling across a boundary.

Changes in adhesion molecules and extracellular matrix interactions are key outcomes of Eph/ephrin signaling to promote somite separation (**Figure 6D**). As somites form and boundary cells undergo MET, a fibronectin (FN) matrix is assembled along the somite boundary. Both FN and its receptor, the heterodimer Integrinα5β1, are required for somite formation (Koshida et al., 2005). Live imaging and genetic studies in transgenic zebrafish expressing the Itgα5-GFP fusion protein show that Itgα5 clustering occurs along the basal side of cells during formation of the somite border followed by the emergence of a FN matrix (Jülich et al., 2009). "Inside-out" signaling (that is, cellular signaling to integrins resulting in clustering and crosslinking of FN to form a matrix), rather than "outside-in" signaling (signaling from accumulated FN to the integrins inducing integrin clustering) is therefore likely required for somite separation (Jülich et al., 2009). Forward signaling through EphA4/ephrin-B2a induced Itgα5 clustering, FN matrix assembly, and the formation of "actin belts" in mosaic experiments, implicating Eph/ephrin signaling as a candidate regulator for inside-out activation of Itgα5 in somite separation (Jülich et al., 2009). However, the signaling mechanisms by which ephrin-B2 reverse signaling might drive Itgα5 clustering remain unknown.

Cellular mechanisms of Eph/ephrin-mediated segregation

In each of these systems, a common underlying question exists regarding the cellular mechanisms of segregation mediated by Eph/ephrin signaling. Generally, cell segregation was originally hypothesized to result from differences in affinities between two cell types that could

be driven by quantitative or qualitative differences in adhesiveness conferred by distinct constellations or levels of adhesion molecule expression (Nose et al., 1988; Steinberg, 1970; Townes and Holtfreter, 1955). The differential adhesion hypothesis (DAH) proposes the specific case in which a quantitative difference in cell adhesion between two cell populations drives the segregation of randomly-migrating cells (Steinberg, 1970). Indeed, multiple studies have implicated direct regulation of cell adhesion by Eph/ephrin signaling as a driver of cell segregation. In the intestinal epithelium, EphB activation by ephrin-B1 results in the recruitment of the ADAM10 metalloproteinase, which cleaves E-cadherin and therefore presumably results in differential adhesion at the Eph/ephrin signaling interface (Cortina et al., 2007; Solanas et al., 2011).

As opposed to differential adhesion, Eph/ephrin-mediated segregation is more widely attributed to a “repulsive” mechanism, though the cell biological definition and biophysical consequences of repulsive Eph/ephrin cellular interactions are varied. In many contexts, Eph/ephrin signaling guides cell migration by a repulsion mechanism analogous to axon guidance in which cellular collapse and disengagement of Eph- and ephrin-expressing cells is followed by directional migration, as in contact inhibition of locomotion (Astin et al., 2010; Pasquale, 2005; Poliakov et al., 2004). In cell segregation, this guidance activity would result in a repeated redirection of cells away from their heterotypic partners, resulting in segregation of the heterotypic populations by a trial and error process that would be predicted to result in a greater distance traveled over the course of segregation compared to other models of segregation. Indeed, in cell segregation assays in low density HEK293 cell culture, EphB2 expressing cells exhibit collapse and directional migration away with an increased migration speed and travel a greater total distance than cells not undergoing segregation (O’Neill et al., 2016; Poliakov et al., 2008; Taylor et al., 2017). However, at high density, EphB2 cells undergoing segregation do not exhibit an increased distance travelled, probably due to constraints imposed by the confluent culture conditions (O’Neill et al., 2016). Nevertheless, cells

segregate robustly at high density, consistent with the fact that cell segregation in the embryo is a behavior that occurs at high cell densities, which leads to the question of whether directional migratory guidance is required for Eph/ephrin cell segregation in the embryo (O'Neill et al., 2016; Taylor et al., 2017).

A separate model, the differential interfacial tension hypothesis (DITH), has proposed that differences in cortical tension, driven primarily by actomyosin contractility, oppose cell adhesion and drive differences in the ability of cells to establish and maintain stable contacts (Brodland, 2002; Krieg et al., 2008). Based on elevated Lifeact-RFP signals in EphB2 cells during live imaging of cell segregation, and on the apparently highly conserved involvement of actomyosin contractility in cell segregation, we previously proposed that cellular collapse upon ephrin-B activation of Eph receptor signaling may result in a change in cortical tension, leading to minimization of heterotypic contacts in favor of homotypic contacts (O'Neill et al., 2016). In cases where Eph and ephrin populations begin fully intermixed, as in cell mixing assays or in CFNS, the "signaling interface" initially includes all EphB2 cells. In other situations, such as *Xenopus* gastrulation, however, the signaling interface is limited to a patterned interface where Eph/ephrin signaling sharpens and maintains the existing boundary. A recently proposed heterotypic interfacial tension (HIT) model that relates to this specific case observes that there need not be differences in cortical tension or homotypic adhesion between the entirety of two populations if local differences in these properties occur specifically at heterotypic cell contacts (Canty et al., 2017). Such a local difference would, of course, be the case in boundaries generated by Eph/ephrin signaling, which relies on cell contact for signaling. Interestingly, atomic force microscopy to infer cortical tension showed that in fact ectoderm cells were stiffer than mesoderm cells, but levelling these differences by myosin depletion in the ectoderm or overexpression of constitutively active Rho in the mesoderm had no effect on separation. Similarly, a dissociation assay indicated that ectoderm cells were more adherent than mesoderm cells, and in this case, levelling these differences decreased separation only

modestly. These data led to the conclusion that tissue separation in *Xenopus* gastrulation is governed by local Eph/ephrin-mediated repulsion leading to reduced contact at the heterotypic interface, though whether cortical tension is changed specifically at that interface remains untested (Canty et al., 2017).

In contrast, at the *Xenopus* notochord-PSM boundary, Eph/ephrin signaling may regulate both adhesion and cortical tension (Fagotto et al., 2013). Cadherin clustering at interfaces between heterotypic notochord-PSM cell pairs at the boundary is less pronounced than that at interfaces between homotypic cell pairs, which possess larger cadherin clusters. Smaller or absent cadherin clusters at the heterotypic interface allow for cell protrusions and blebbing at the boundary. This cadherin pattern is dependent on myosin, which in turn depends on Eph/ephrin signaling between notochord and PSM cells at the boundary (Fagotto et al., 2013). This suggests that separation at this boundary does not depend on differing *levels* of expression of cadherin complexes between cells of the different tissue types, but rather on differences in *recruitment* at different cell interfaces. Differences in heterotypic and homotypic Eph/ephrin signaling therefore result in differential cell contractility at the notochord-PSM boundary, with protrusions and blebbing of the boundary cells, which then inhibits cadherin clustering between heterotypic cell pairs.

Importantly, these studies reinforce the idea that a boundary cannot be defined simply by examining the adhesive or contractile properties of each individual tissue. Instead, the interaction between heterotypic cell pairs at the boundary must somehow differ from that of homotypic cell pairs within each individual tissue. This requires an intricately regulated interface with many small interactions between cells of each tissue, resulting in dynamic changes to the cytoskeleton and to adhesion complexes that mediate boundary maintenance. The Eph/ephrin signaling family, with its large variety of molecules and complex regulatory abilities, is a perfect fit for this role. Further investigation of this complex interplay at other embryonic boundaries will

reveal the mechanisms by which Eph/ephrin signaling mediates tissue separation in different contexts.

Evolving perspectives on Eph/ephrin signaling mechanism and directionality

It is readily apparent that Eph/ephrin signaling acts to regulate cell movement and positioning to effect tissue morphogenesis in a wide variety of developmental processes (**Table 1**), perhaps unsurprising considering the expression of pathway members in almost every tissue during development. Eph/ephrin signaling is unique among major signaling pathways that direct developmental processes on a large scale, in that it generally appears to have relatively little influence on establishing transcription of downstream target genes in the contexts studied so far. Instead, the members of this pathway act more directly to define tissue architecture by acting as a "middleman" between upstream transcription factor patterning and the cell physical and behavioral changes required to direct cells to their correct positions. Specifically, a major role for this pathway has been identified in regulation of cytoskeletal changes. This mediation of cellular changes downstream of transcription factor expression can be aided by the ability of Ephs and ephrins to signal in both the receptor and ephrin-expressing cells and is essential for Eph/ephrin signaling to mediate cell migration and tissue separation. Here, we have summarized a number of challenges addressed by recent developments in the field: these include analysis of the complexity of signaling directionality and signaling mechanisms *in vivo*, identification of new contexts for Eph/ephrin regulation of cell migration, the role of combinatorial expression of Ephs and ephrins in tissue separation, and the role for differing cellular mechanisms of segregation to effect tissue separation in a variety of contexts. The results of these recent studies have deepened our understanding of how Eph/ephrin signaling regulates cell position and have made clear the need for continuing studies in these areas to fully understand how this complex pathway regulates developmental morphogenesis.

The complexity of Eph/ephrin signaling has led to longstanding challenges in understanding signaling mechanisms *in vivo*; these challenges may also impact our consideration of cellular mechanisms. Whereas genetic evidence for bidirectional signaling in development remains, refinement of this understanding continues, causing us to reevaluate the relevance of this paradigm in specific situations. While Eph/ephrin signaling mutants are tremendously valuable for determining signaling mechanisms involved in the formation and maintenance of boundaries, they must also be interpreted with care, especially when overexpression is employed. It has become clear that a simple complementary expression model, with bidirectional signaling across the expression divide, will no longer be sufficient in most developmental scenarios. First and foremost, in many developing tissues, both Eph receptors and ephrins are co-expressed. For example, both EphB receptors and ephrin-Bs are expressed in the early mouse neural plate neuroepithelium prior to induction of the neural crest (O'Neill et al., 2016), as well as in mouse palatal shelves later in development (Bush and Soriano, 2010). It is also clear that co-expression of EphAs and ephrin-As, such as in the developing chick retina (Hornberger et al., 1999), can play critical roles in axon guidance. In addition, recent evidence indicates that unidirectional Eph/ephrin signaling is sufficient to drive the formation of boundaries during development, calling into question the idea that bidirectional signaling is necessary for Eph/ephrin signaling-mediated processes. Rather, parallel or anti-parallel combinations of Eph- and ephrin-expression may work together to drive separation of tissues.

Studies of tissue separation in disparate contexts often seem to converge on Eph/ephrin regulation of the cytoskeleton, firmly establishing the paradigm of this signaling pathway as a "middleman" between transcription factor patterning and the cellular changes necessary for morphogenetic processes to occur. What then are the upstream mechanisms by which differential Eph/ephrin expression is determined? Often, it seems that expression patterns of these signaling molecules are determined in parallel to the definition of cell fate by upstream

transcription factors. For example, *tbx24 (fss)* in the zebrafish PSM, *cMeso-1* in forming chick somites, *Krox20* in rhombomeres 3 and 5 in the mouse (Theil et al., 1998), *val* in rhombomeres 5/6 in zebrafish (Cooke et al., 2001), and *rx3* in the zebrafish eye field (Cavodeassi et al., 2013) can all affect the proper expression of Ephs and ephrins that is necessary for later boundary formation. Loss of Eph/ephrin expression does not seem to affect expression of these transcription factors, suggesting that gene expression patterning is not generally an important outcome of Eph/ephrin signaling. In considering complementary expression domains, we must also consider the effect of post-transcriptional mechanisms. In some cases, what appears as reciprocal expression of Eph and ephrin proteins could be caused by signaling leading to cleavage or endocytosis of receptor-ligand complexes, this high signaling turnover appearing as a reduction in Eph receptor expression in populations of cells with high ephrin expression, or *vice versa*.

How Eph/ephrin signaling leads to cell segregation and boundary formation has long been under debate, with differential adhesion, repulsive migration, and differential cortical tension all accumulating evidence to support these various hypotheses. Whether the outcome of Eph/ephrin signaling is tissue-specific, or whether one of these hypotheses will dominate in all contexts in which Eph/ephrin-mediated tissue separation occurs, remains to be determined by future careful studies of these processes.

Table 1. Eph/ephrin relationships and roles in cell positioning in the developing embryo
Page 1 of 2

	Signaling partner(s)	Role in cell positioning	Signaling directionality	References
ephrin-B1	EphB1, EphB2, EphB3	Axon guidance of the corpus callosum	Forward Reverse - ?	(Henkemeyer et al., 1996; Mendes, 2006; Orioli et al., 1996; Robichaux et al., 2016)
	EphB2, EphB3	Craniofacial and skeletal development	Forward	(Bush and Soriano, 2010; O'Neill et al., 2016) (see **Chapter 3**)
	EphB2, EphB3	Cell segregation	Forward	(O'Neill et al., 2016)
	EphB2	Sorting of neural crest cells into sympathetic ganglia	Forward	(Kasemeier-Kulesa et al., 2005)
	EphB2	Apical attachment of neural progenitor cells	Forward	(Arvanitis et al., 2013)
	EphB1, EphB2	Migration of precursor cells in the hippocampus	Forward*	(Bouché et al., 2013; Catchpole and Henkemeyer, 2011)
	EphB3	Cortical neuronal migration	Reverse	(Sentürk et al., 2011)
	EphB3	Asymmetric liver positioning	Bidirectional	(Cayuso et al., 2016)
	EphA4, EphB2	*Xenopus* ectoderm-mesoderm separation during gastrulation	Forward	(Rohani et al., 2014)
ephrin-B2	EphB1, EphB2, EphB3	Axon guidance of the anterior commissure	Reverse - ?	(Cowan et al., 2004; Robichaux et al., 2016)
	EphB2, EphB3, EphB4	Midline closure of the embryo	Reverse - ?	(Cowan et al., 2004; Dravis et al., 2004; Dravis and Henkemeyer, 2011)
	EphB3	Cortical neuronal migration	Reverse	(Sentürk et al., 2011)
	EphB4	Lymphatic valve development	Forward Reverse - ?	(Makinen, 2005; Zhang et al., 2015)
	EphB4	Neural crest migration (indirect); angiogenic remodeling	Forward	(Davy and Soriano, 2007; Lewis et al., 2015)
	EphB4	Dorsal forerunner cell migration to form the Kupffer's vesicle	Bidirectional - ?	(Zhang et al., 2016)
	EphB2, EphB4	Xenopus ectoderm-mesoderm separation during gastrulation	Forward	(Rohani et al., 2011, 2014)
	EphA4	Somite formation	Reverse	(Jülich et al., 2009; Watanabe et al., 2009)

Table 1. Eph/ephrin relationships and roles in cell positioning in the developing embryo

	Signaling partner(s)	Role in cell positioning	Signaling directionality	References
ephrin-B3	EphB1, EphB2, EphB3	Axon guidance of the corpus callosum	Forward	(Kullander et al., 2001; Mendes, 2006)
	EphB3	Cortical neuronal migration	Reverse	(Sentürk et al., 2011)
	EphA4	Axon guidance in the spinal cord	Forward	(Yokoyama et al., 2001)
	EphA4	*Xenopus* ectoderm-mesoderm separation during gastrulation	Forward	(Rohani et al., 2014)

*Bouché et al. also propose a role for Reelin-to-Eph forward signaling in hippocampal progenitor migration in the CA3 region.

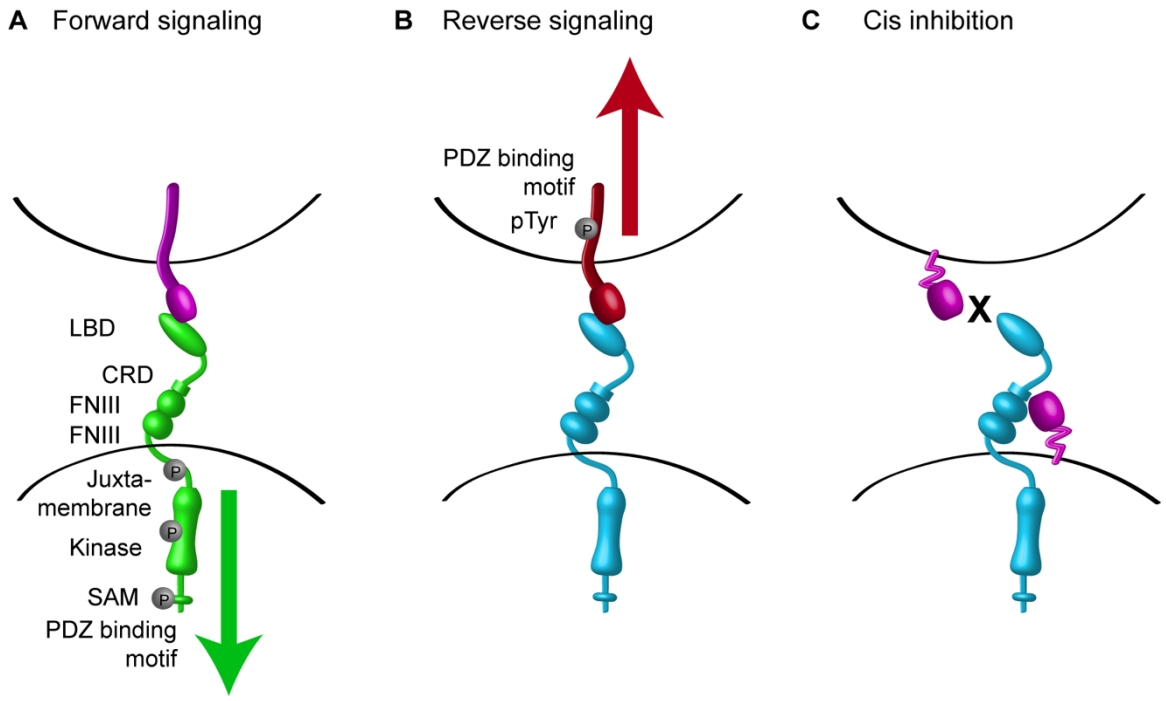

Figure 3. Eph/ephrin signaling modes. Binding of an Eph receptor to an ephrin in an adjacent cell can initiate **(A)** forward signaling through receptor tyrosine phosphorylation in the Eph-expressing cell, **(B)** reverse signaling through ephrin tyrosine phosphorylation or binding to PDZ domain-containing proteins in the ephrin-expressing cell, or both (bidirectional signaling). Some forms of Eph/ephrin forward signaling do not require the kinase domain of the Eph receptor (kinase-independent signaling). **(C)** Coexpression of an EphA receptor and an ephrin-A in the same cell has been shown to attenuate receipt of signals from adjacent cells, a process that has been termed *cis* inhibition. The mechanism of signal attenuation is unknown. Green color of the Eph receptor indicates activation of forward signaling, whereas blue color of the Eph receptor indicates no activation. Red color of the ephrin indicates activation of reverse signaling, whereas purple color indicates no activation. Ephrin-Bs are transmembrane proteins (shown in **A, B**); ephrin-As are membrane-linked through a GPI anchor (shown in **C**).

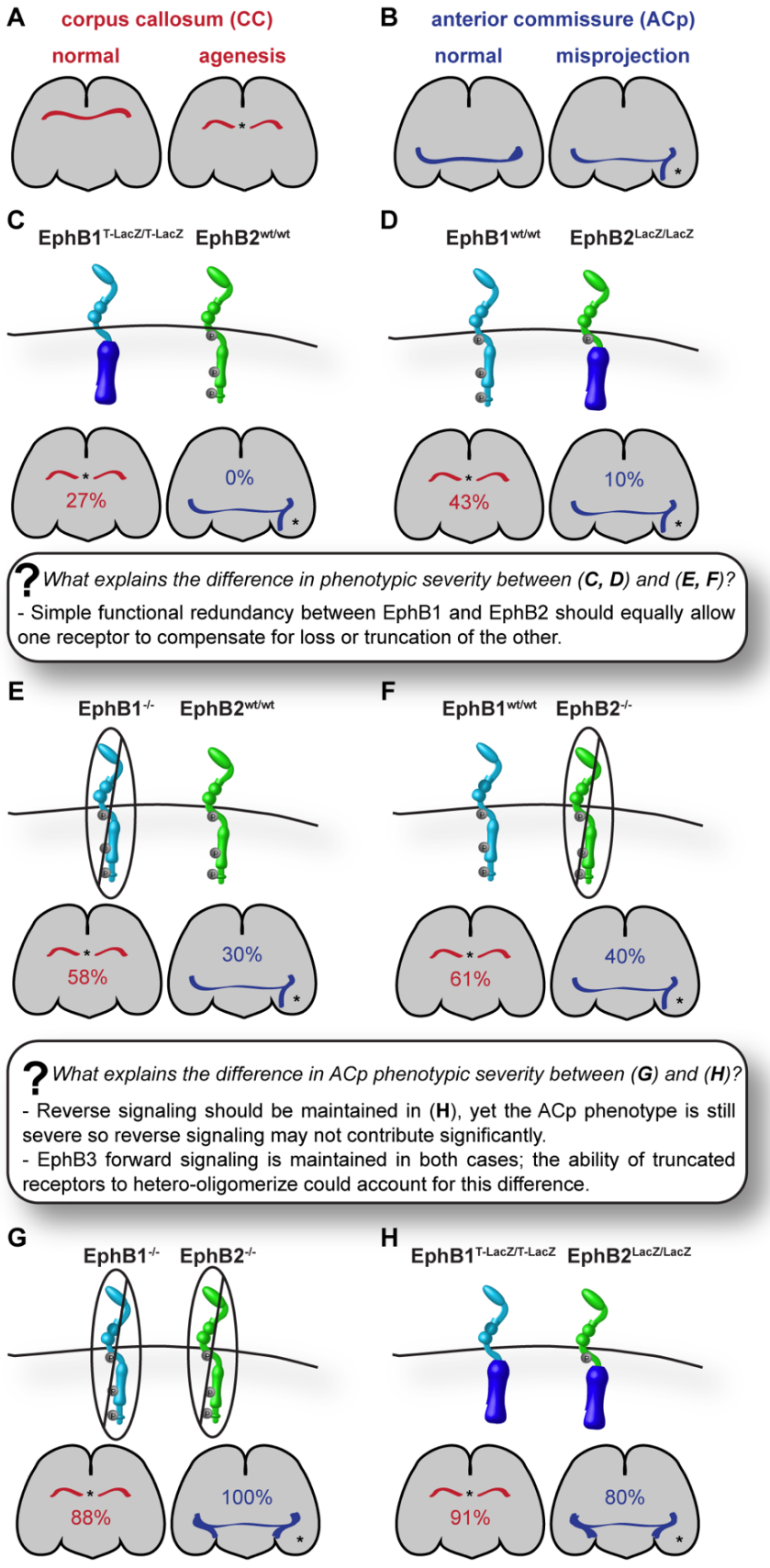
A
corpus callosum (CC)
normal
agenesis
B
anterior commissure (ACp)
normal
misprojection
C
EphB1T-LacZ/T-LacZ
EphB2wt/wt
27%
0%
D
EphB1wt/wt
EphB2LacZ/LacZ
43%
10%
?What explains the difference in phenotypic severity between (C, D) and (E, F)?
- Simple functional redundancy between EphB1 and EphB2 should equally allow one receptor to compensate for loss or truncation of the other.
E
EphB1-/-
EphB2wt/wt
58%
30%
F
EphB1wt/wt
EphB2-/-
61%
40%
?What explains the difference in ACp phenotypic severity between (G) and (H)?
- Reverse signaling should be maintained in (H), yet the ACp phenotype is still severe so reverse signaling may not contribute significantly.
- EphB3 forward signaling is maintained in both cases; the ability of truncated receptors to hetero-oligomerize could account for this difference.
G
EphB1-/-
EphB2-/-
88%
100%
H
EphB1T-LacZ/T-LacZ
EphB2LacZ/LacZ
91%
80%

Figure 4. Differentiating Eph/ephrin forward and reverse signaling in the development of two axon tracts, the corpus callosum and the anterior commissure. (A) Key to representations of a normal corpus callosum (CC) and agenesis of the corpus callosum (aCC). **(B)** Key to representations of a normal posterior branch of the anterior commissure (ACp) and of ACp misprojections. **(C–F)** Mice expressing a truncated version of EphB1 in which the intracellular domain is replaced with LacZ ($EphB1^{T\text{-}LacZ}$) **(C)** have a 20% penetrance of aCC and no ACp defects. Similarly, mice expressing $EphB2^{LacZ}$ **(D)** have a 43% penetrance of aCC and a 10% penetrance of ACp defects. However, mice with total loss of EphB1 **(E)** or EphB2 **(F)** have a higher incidence of CC and ACp defects, raising the question of whether functional redundancy can truly explain the low penetrance of phenotypes in the truncated mutants. Functional redundancy should allow one receptor to compensate for both loss and truncation of the other. **(G–H)** EphB1; EphB2 double knockout mice have 100% penetrance of severe ACp misprojection defects **(G)**, while mice in which the intracellular domain of both receptors has been replaced with LacZ **(H)** have only 80% incidence of moderate-to-severe phenotypes. How can the difference between these cases be explained? It is possible that the maintenance of reverse signaling *via* receptor extracellular domains in **(H)** allows preservation of some function, though it is unlikely that reverse signaling plays a dominant role in CC or ACp formation, as the phenotype in **(H)** is still quite severe. Although EphB3 forward signaling may compensate somewhat, this should be the case in both mutants, and is unlikely to explain the difference. The most likely explanation is the possibility that truncated EphB1 and EphB2 receptors maintain the capacity to hetero-oligomerize with full-length Eph receptors, such as EphB3, to contribute to forward signaling and preserve a small amount of function.

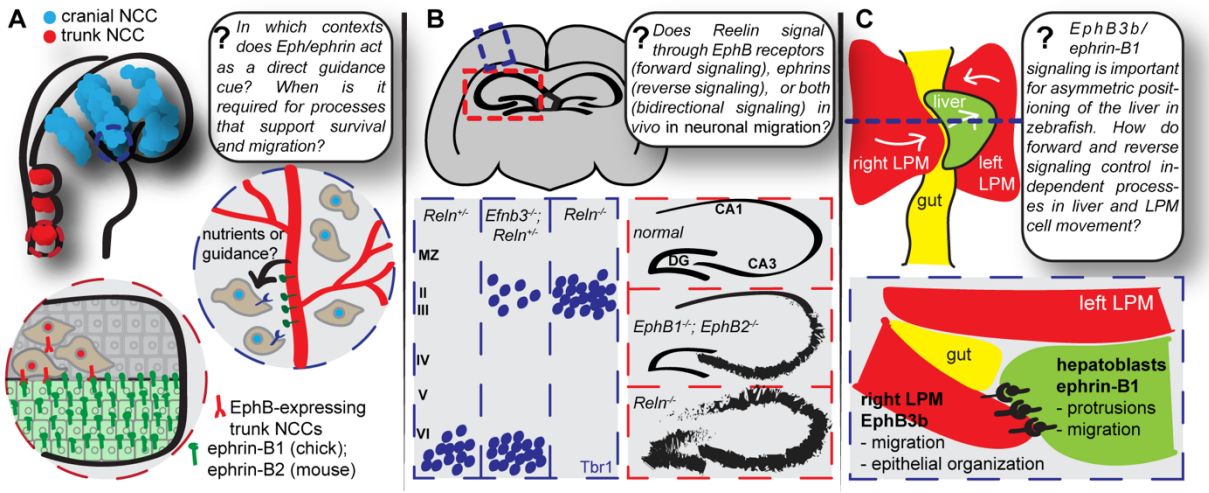

Figure 5. Eph/ephrin signaling provides support and guidance for migrating cells during development. (A) Ephrin-Bs have been implicated in both cranial and trunk neural crest cell (NCC) migration. Recent genetic evidence in mice suggests that the role of ephrin-B2 in cranial NCC migration is secondary to its role in the vasculature, and therefore that ephrin-B2 signaling in this context acts not as a guidance cue, but rather as a supplier of support and nutrients critical to NCC survival. During trunk NCC migration, ephrin-B1 (in chick) or ephrin-B2 (in mouse) is thought to act as a guidance cue for migrating cells, with their expression in the posterior half of the somite restricting migration of EphB-expressing NCCs to the anterior half of the somite. **(B)** The secreted neuronal guidance cue Reelin interacts biochemically with Eph receptors, and compound EphB receptor mutant mice as well as compound ephrin-B mutant mice have *reeler* (*Reln*$^{-/-}$)-like neuronal migration phenotypes in both the cortex and hippocampus. Although many Eph or ephrin compound mutant phenotypes are not as severe as *Reln*$^{-/-}$ phenotypes, this raises the intriguing possibility that Eph/ephrin signaling and Reelin signaling may synergize to promote neuronal migration in the cortex and hippocampus. **(C)** EphB/ephrin-B signaling, with EphB3b expressed in the lateral plate mesoderm (LPM) and ephrin-B1 expressed in the hepatoblasts, is essential for correct asymmetric positioning of the liver during zebrafish development. *NCC, neural crest cell; LPM, lateral plate mesoderm.*

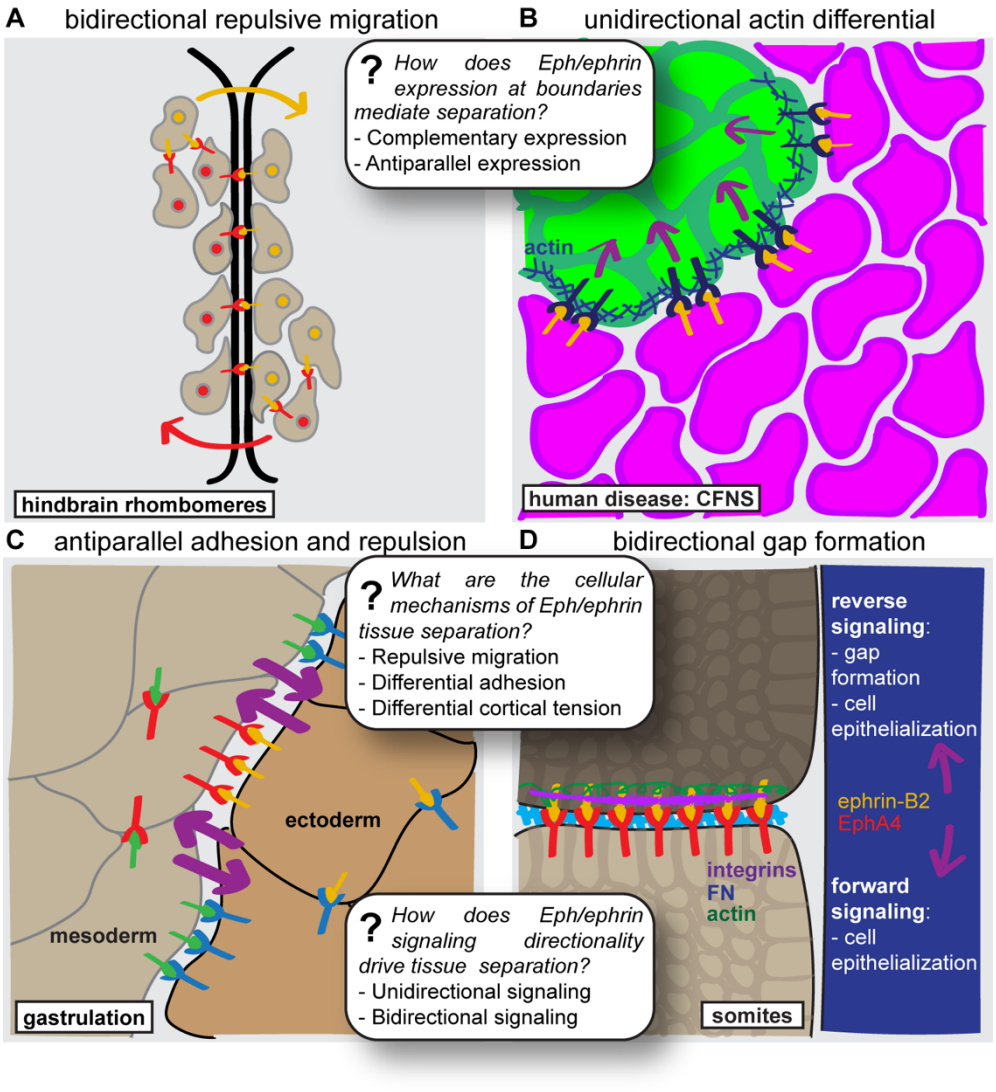

Figure 6. Eph/ephrin signaling mechanisms in developmental tissue separation. (A) A classical view of Eph/ephrin signaling mechanisms in the rhombomeres of the zebrafish hindbrain involves complementary expression of Eph receptors and ephrins in adjacent rhombomere compartments, with bidirectional signaling mediating repulsive migration of Eph-expressing cells away from the ephrin-expressing compartment and *vice versa*. **(B)** Mosaicism for ephrin-B1 expression in the congenital craniofacial disease craniofrontonasal syndrome (CFNS) leads to aberrant cell segregation, which is characterized by unidirectional signaling from ephrin-B1 expressing cells (magenta) to ephrin-B1 non-expressing (EphB-expressing) cells (green), leading to upregulation of actin and formation of an actin cable in the EphB-expressing cells. **(C)** In the *Xenopus* gastrula, the mesoderm migrates along the ectodermal blastocoel roof without integrating into the ectoderm. This simultaneous migration and separation is mediated by antiparallel Eph/ephrin forward signaling across the ectoderm-mesoderm boundary, leading to repeated attachment and detachment of the migrating mesoderm cells. **(D)** Bidirectional signaling between ephrin-B2 in the posterior region of a newly formed somite and EphA4 in the anterior region of a forming somite contributes to somite gap formation and subsequent cell epithelialization at the somite border. While gap formation requires reverse signaling but not forward signaling, cell epithelialization requires both reverse signaling and forward signaling

through direct or cell-non-autonomous mechanisms. *CFNS, craniofrontonasal syndrome; FN, fibronectin.*

CHAPTER 3. EPHRIN-B1 mosaicism drives cell segregation in craniofrontonasal syndrome hiPSC-derived neuroepithelial cells

Summary

Although human induced pluripotent stem cells (hiPSCs) hold great potential for the study of human diseases affecting disparate cell types, they have been underutilized in seeking mechanistic insights into the pathogenesis of congenital craniofacial disorders. Craniofrontonasal syndrome (CFNS) is a rare X-linked disorder caused by mutations in *EFNB1* and characterized by craniofacial, skeletal, and neurological anomalies. Heterozygous females are more severely affected than hemizygous males, a phenomenon termed cellular interference that involves mosaicism for EPHRIN-B1 function. Although the mechanistic basis for cellular interference in CFNS has been hypothesized to involve Eph/ephrin-mediated cell segregation, no direct evidence for this has been demonstrated. Here, by generating hiPSCs from CFNS patients, we demonstrate that mosaicism for EPHRIN-B1 expression induced by random X inactivation in heterozygous females results in robust cell segregation in human neuroepithelial cells, thus supplying experimental evidence that Eph/ephrin-mediated cell segregation is relevant to pathogenesis in human CFNS patients.

Introduction

Congenital craniofacial disorders represent over one-third of all birth defects ("Global strategies..." 2004). While the genetic causes of many syndromes are known, how these mutations lead to abnormal cellular mechanisms underlying these disorders is incompletely understood. A better understanding of the underlying etiology of these disorders is needed to develop new treatment strategies targeted to the cellular and molecular basis of disease. The emergence of hiPSCs as a tool for human disease modeling (Takahashi and Yamanaka, 2006; Takahashi et al., 2007; Tiscornia et al., 2011; Yu et al., 2007) holds great promise for improving our cellular understanding of craniofacial diseases, as hiPSCs can be differentiated into patient-specific, disease-relevant cell types. However, perhaps due to the challenge of modeling

structural aspects of craniofacial disease in two dimensions in cell culture, hiPSC models for these disorders are not yet widely used.

Craniofrontonasal syndrome (CFNS; OMIM #304110) is an X-linked disorder caused by mutations in *EFNB1* and characterized by craniofacial, skeletal, and neurological anomalies (Twigg et al., 2004; Wieland et al., 2004). The most common clinical findings include hypertelorism, frontonasal dysplasia, coronal synostosis, bifid nasal tip, longitudinal splitting of the nails, and wiry or frizzy hair; other less frequent symptoms include cleft lip and palate, diaphragmatic hernia, agenesis of the corpus callosum, syndactyly, and polydactyly (Twigg et al., 2004; Twigg et al., 2006; Twigg et al., 2013; Wieacker and Wieland, 2005; Wieland et al., 2004). CFNS is an unusual X-linked disorder in that heterozygous females are more severely affected than hemizygous male patients, who are usually unaffected or mildly affected and often present only with hypertelorism (Wieacker and Wieland, 2005). This counterintuitive inversion of severity has been termed cellular interference, a phenomenon whereby random X chromosome inactivation (XCI) in heterozygous female CFNS patients results in mosaicism for *EFNB1* expression, leading to abnormal cellular interactions (Twigg et al., 2013; Wieacker and Wieland, 2005). Consistent with this notion, rare severely-affected male CFNS patients have somatic mosaic mutations in *EFNB1* (Twigg et al., 2013), reinforcing mosaicism as an important aspect of CFNS pathogenesis.

EFNB1 encodes EPHRIN-B1, a member of the Eph/ephrin family of membrane-linked signaling molecules, and abnormal signaling between cells expressing wild-type EPHRIN-B1 and cells that are functionally EPHRIN-B1-null may occur in the mosaic state (Compagni et al., 2003; Wieacker and Wieland, 2005). During development, Eph/ephrin signaling plays an important role in boundary formation, an essential process that requires signaling between adjacent cells and often involves segregation between different cell types (Batlle and Wilkinson, 2012; Cayuso et al., 2015; Fagotto, 2014; Fagotto et al., 2014). Differential expression of Eph receptors and ephrins *in vivo* can restrict cell intermingling in the vertebrate hindbrain (Xu et al.,

1999), limb bud (Compagni et al., 2003; Davy et al., 2004), eye (Cavodeassi et al., 2013), somites (Barrios et al., 2003; Durbin et al., 1998; Durbin et al., 2000), cranial sutures (Merrill et al., 2006; Ting et al., 2009), and intestinal crypts (Holmberg et al., 2006), as well as in the *Drosophila* wing disc (Umetsu et al., 2014). In culture, expressing an Eph receptor in one population of cells and an ephrin in another restricts intermingling of cells from the two populations (Jorgensen et al., 2009; Mellitzer et al., 1999; Poliakov et al., 2008). Further, cell segregation occurs in developing *Efnb1*$^{+/-}$ mouse limb (Compagni et al., 2003) and secondary palate (Bush and Soriano, 2010), supporting the idea that XCI-induced mosaicism leads to segregation of Ephrin-B1 expressing and non-expressing cells.

The role of Eph/ephrin signaling in boundary formation and supporting data from mouse models suggest that mosaicism for EPHRIN-B1 expression may lead to aberrant cell segregation in human CFNS patients (Compagni et al., 2003; Twigg et al., 2004; Twigg et al., 2006; Twigg et al., 2013; Wieacker and Wieland, 2005; Wieland et al., 2004). However, it has proven difficult to determine the mechanism of cellular interference, and EPHRIN-B1-mediated cell segregation has not been demonstrated in CFNS patients. Here, we report the generation of an hiPSC model to study defects in morphogenesis in a congenital craniofacial disorder. We demonstrate that cell segregation is a consequence of EPHRIN-B1 mosaicism in CFNS, providing evidence that this cell behavior is relevant to CFNS pathogenesis in humans. The CFNS hiPSC model provides proof of principle that hiPSC-derived cell types can be used both to model structural anomalies and to gain valuable insights into fundamental cellular mechanisms of morphogenesis in patient cells.

Results

Isolation of CFNS human dermal fibroblasts and reprogramming to hiPSCs

To investigate cellular mechanisms of CFNS, we established human dermal fibroblast (HDF) cultures from a 10-month-old female CFNS patient with a heterozygous mutation in exon

5 of *EFNB1* (*EFNB1*$^{+/c.712delG}$) (Byrne et al., 2009; Hogue et al., 2010). We also established HDF cultures from skin biopsies of the patient's father, a hemizygous carrier of the mutation (*EFNB1*$^{Y/c.712delG}$), and her unaffected mother (*EFNB1*$^{+/+}$). We generated hiPSC lines from low-passage HDFs of each individual using non-integrating episomal vectors (Bershteyn et al., 2014; Okita et al., 2011) and selected three hiPSC lines from each individual for further analysis and experimentation (from the patient, lines CFNShet-1, -2, and -3; from the patient's father, lines CFNShemi-1, -2, and -3; and from the patient's mother, lines wt-1, -2, and -3). Sequencing of exon 5 of *EFNB1* confirmed the expected genotypes (**Figures 7A and S1**). All nine hiPSC lines were free of reprogramming plasmid integration by PCR (data not shown) and had normal G-banded karyotypes (**Figure S1**).

Characterization of CFNS hiPSC pluripotency and differentiation potential

CFNShet and CFNShemi HDFs were reprogrammed to generate hiPSCs, which possessed embryonic stem cell-like morphology similar to that of wild-type hiPSCs. All lines, regardless of genotype, possessed differentiation potential to ectoderm (βIII tubulin), endoderm (α-fetoprotein), and mesoderm (muscle actin) in an embryoid body protocol (**Figures 7B and S2**) and expressed the endogenous pluripotency markers OCT4, SOX2, NANOG, TRA-1-60 and TRA-1-81 (**Figures 7C and S3**).

XCI-induced mosaicism in females plays a central role in CFNS (Twigg et al., 2004; Twigg et al., 2006; Twigg et al., 2013; Wieacker and Wieland, 2005; Wieland et al., 2004). However, XCI status of female hiPSCs can vary across different lines (Lessing and Lee, 2013), depending on conditions used for reprogramming (Tchieu et al., 2010; Tomoda et al., 2012; Wutz, 2012). To model CFNS, we used reprogramming conditions that favor maintenance of XCI rather than X reactivation (Wutz, 2012) and characterized XCI status of CFNShet HDFs and each CFNShet hiPSC line using the human androgen receptor assay (HUMARA) (Kiedrowski et

al., 2011). CFNShet HDFs showed an expected XCI ratio close to 50%, as in earlier studies that indicated no skewed X inactivation in female CFNS patients (**Table 2**) (Twigg et al., 2004; Wieland et al., 2004; Wieland et al., 2007). All three CFNShet hiPSC lines showed complete inactivation of the maternal, wild-type X chromosome, consistent with the clonal XCI expected from female hiPSC lines derived from a single fibroblast under conditions that favor XCI maintenance (Tchieu et al., 2010). Therefore, only the paternal, mutant copy of *EFNB1* is expressed in these lines (**Table 2**), and they are not expected to express functional EPHRIN-B1.

Differentiation and characterization of CFNS neuroepithelial cells

CFNS affects multiple structures derived from neural crest cells (NCCs), a multipotent population of stem cells that are induced at the neural plate border, delaminate, and migrate ventrolaterally to populate the craniofacial structures and contribute to skeletal, connective, neural, and vascular tissues. In mice, Ephrin-B1-mediated cell segregation occurs in the NE prior to NCC emigration (O'Neill et al., 2016). We therefore reasoned that NE cells are a good model for testing whether cell segregation occurs in CFNS, and we began by differentiating CFNS and control hiPSCs to human neuroepithelial cells (hNE). We adapted a monolayer protocol that uses dual-SMAD inhibition to improve neural differentiation efficiency through inhibition of activin and nodal signaling (Chambers et al., 2009). All hNE cells, regardless of genotype, had neuroepithelial morphology and expressed the neural progenitor cell markers PAX6, SOX1, and OTX2 (**Figure 8A**). These data indicate that CFNS patient hiPSCs are able to differentiate into hNE cells independently of EPHRIN-B1 expression. hNE cells of all genotypes, but not hiPSCs, expressed *EFNB1* mRNA (**Figure 8B**), and over the course of differentiation to hNE cells, expression of mRNA transcripts of both *EFNB1* and *PAX6* increased in a similar manner in cells of each genotype (**Figure 8C**). hNE cells of all three genotypes expressed *EFNB2*, a closely related B-type ephrin, as well as *EPHB2* and *EPHB3*, signaling

partners of EPHRIN-B1 that are involved in craniofacial development (Orioli et al., 1996) (**Figure S4A-S4C**). Wild-type hNE cells expressed EPHRIN-B1 protein, whereas CFNShet and CFNShemi *EFNB1* mutant hNE cells did not (**Figure 8D**).

EPHRIN-B1 mosaicism results in cell segregation in CFNS hNE cells

To model *EFNB1* mosaicism and determine whether it results in segregation, we generated mixed cultures of fluorescently labeled hNE cells of different genotypes at a 1:1 ratio. Control mixed cultures in which all cells expressed EPHRIN-B1 (wt-3 + wt-3, N=11/11 trials) or in which no cells expressed EPHRIN-B1 (CFNShet-3 + CFNShet-3, N=7/7 trials; CFNShemi-1 + CFNShemi-1, N=4/4 trials) resulted in hNE cells commingling freely, with no notable segregation after 48 hr (**Figures 9A-9C**). However, in hNE cell populations mosaic for EPHRIN-B1 expression, EPHRIN-B1-expressing cells segregated dramatically from EPHRIN-B1 non-expressing cells, forming distinct boundaries between the two different cell types by 48 hr (**Figures 9D and 9E**) (wt-3 + CFNShet-3, N=10/10 trials; wt-3 + CFNShemi-1, N=4/4 trials). To ensure that this segregation depended on EPHRIN-B1 expression and not on differences between independent hNE cell lines, we mixed hNE lines derived from different hiPSC lines of the same genotype and also observed intermixing of cells (wt-3 + wt-2, **Figure 9F**; CFNShet-3 + CFNShet-1, **Figure 9G**) (N=3/3 trials, each condition). Further, mixing hNE lines derived from different genotypes lacking EPHRIN-B1 expression (CFNShet-3 + CFNShemi-1, N=3/3 trials) did not result in cell segregation (**Figure 9H**), demonstrating that hNE cells segregate based on the presence or absence of EPHRIN-B1 expression and not some other factor associated with individual variability.

To observe the process of cell segregation over time, we used live cell imaging to capture the first 25 hr after cell mixing in both mosaic and EPHRIN-B1 non-expressing cell mixtures. Both cell mixtures were intermingled at time of mixing (t=0, **Figures S5A and S5G**). Cells in both mixtures continued to interact with each other over time, and EPHRIN-B1 non-

expressing mixtures remained freely commingled at each time point (**Figures S5B-S5E**). However, the EPHRIN-B1 mosaic population of cells segregated progressively over 25 hr (**Figures S5H-S5L**), indicating that segregation is a continuous process that occurs over time. These data provide evidence that EPHRIN-B1-mediated cell segregation can occur in human CFNS.

Discussion

Here, we have generated an hiPSC model of a human craniofacial condition and have used it to address an outstanding question: does mosaicism for *EFNB1* expression result in cell segregation in human CFNS? The c.712delG mutation found in this CFNS family occurred 5' to the transmembrane domain-encoding region of *EFNB1*, and we found that *EFNB1* mutant hNE cells did not express EPHRIN-B1, indicating that this mutation results in an unstable EPHRIN-B1 protein and most likely null loss of function. To enable us to model CFNS, it was essential that loss of *EFNB1* function not prevent CFNS patient-derived HDFs from undergoing reprogramming to hiPSCs. We did not observe differences in reprogramming ability between *EFNB1* mutant and control HDFs, leading us to conclude that EPHRIN-B1 expression is not necessary for reprogramming. Further, we found that both control and CFNS hiPSCs possessed differentiation potential to all three germ layers; loss of EPHRIN-B1 expression does not apparently prevent differentiation. This is consistent with our qRT-PCR data demonstrating that transcripts of *EFNB1* and several other Eph/ephrin signaling family members are expressed at very low levels in hiPSCs relative to hNE cells, suggesting that these signaling molecules may not play critical roles in hiPSCs.

Previous human genetic studies have indicated that mosaicism for *EFNB1* mutation is central to CFNS pathology, a phenomenon termed cellular interference suggested to result in cell segregation based on evidence from model organisms (Compagni et al., 2003; Twigg et al., 2004; Twigg et al., 2006; Twigg et al., 2013; Wieacker and Wieland, 2005; Wieland et al., 2004).

Whether cell segregation occurs in CFNS, however, and in what cell types, was not known. Based on evidence of cell segregation in the neural plate NE in *Efnb1*$^{+/-}$ mice (O'Neill et al., 2016), we differentiated hiPSCs to hNE cells to address this question.

Both wild-type and CFNS patient-derived hNE cells expressed neural stem cell markers and several members of the Eph/ephrin gene family, including *EFNB1*. Expression of *EFNB1* varied between hNE lines, as well as between independent differentiations of the same hiPSC line, indicating that there was inherent variability in the differentiations. Consistently, however, hNE cells expressed higher levels of *EFNB1* than hiPSCs, indicating that increased *EFNB1* expression is a characteristic of the hNE cell type. In addition, *EFNB1* expression decreased as hNE cells were maintained over time, suggesting that higher levels of *EFNB1* expression may mark a progenitor stage in the differentiation program.

As hiPSCs are clonally derived cell lines, CFNShet hNE lines are not mosaic for *EFNB1* expression, necessitating a different approach to model cellular interference. Upon mixing wild-type and EPHRIN-B1 non-expressing hNE cells to generate EPHRIN-B1 mosaicism, the EPHRIN-B1 expressing and non-expressing cells segregated to form ectopic boundaries in culture. This robust segregation occurred in mosaic mixtures of wild-type + CFNShet cells and wild-type + CFNShemi cells, but not in mixtures of two different populations of EPHRIN-B1 expressing cells, or two different populations of EPHRIN-B1 non-expressing cells, even if these two populations were derived from different hiPSC lines. We therefore conclude that segregation is not an effect of mixing different hNE lines, but rather an effect of mosaicism for EPHRIN-B1 expression, and that cellular interference through EPHRIN-B1-mediated cell segregation occurs in CFNS cells. This finding informs our understanding of the etiology of CFNS and indicates that cell segregation contributes to cellular interference. How cell segregation leads to more severe disease phenotypes is not yet clear; the hiPSC model we have developed is a highly relevant system in which to answer remaining questions about CFNS pathology.

An hiPSC model is an important resource because patient cells can be differentiated into multiple disease-relevant cell types, overcoming the challenge of isolating primary cells from patients. It is notable that cell segregation occurs in the neuroepithelium in models of CFNS; recent studies have indicated that Treacher Collins syndrome, another neurocristopathy, also exhibits cellular defects originating in the neuroepithelium and ongoing in the NCC (Jones et al., 2008). Our hiPSC model of CFNS will facilitate further studies of cell segregation, such as investigating whether it occurs in hNCCs and their descendants. This will contribute to a better understanding of the developmental timing of CFNS etiology and will provide the ability to study aspects of the disease that are less well understood. For example, mutations in *EFNB1* that cause CFNS are responsible for approximately 7% of cases of craniosynostosis in which a genetic cause is known (Johnson and Wilkie, 2011), and studies in mice have demonstrated that suture boundary formation is regulated by A-type Eph/ephrin signaling (Merrill et al., 2006; Ting et al., 2009). However, how EPHRIN-B1 affects boundary formation and maintenance at the suture is unknown, because *EFNB1* mutant mice do not exhibit craniosynostosis. Further, in CFNS, other organ systems not derived from NCCs are also affected; patients exhibit limb anomalies and defects of the axial skeleton that may be attributable to cell segregation (Compagni et al., 2003; Davy et al., 2004; Davy et al., 2006). Differentiation of hiPSCs into these various cell types is a method for testing the importance of EPH/EPHRIN-mediated cell segregation in various tissues.

hiPSC models of congenital craniofacial disease will also facilitate targeted molecular therapies for these disorders. As we have shown that cell segregation resulting from EPHRIN-B1 mosaicism occurs in human CFNS cells, therapeutic benefits may be derived from preventing segregation. Additional research to determine the mechanism by which hNE cell segregation leads to craniofacial phenotypes in CFNS patients is likely to identify molecular candidates that could be targeted to achieve this goal. A human model system of EPHRIN-B1-mediated cell segregation could then serve as a high-throughput system for testing candidate

therapeutic molecules. Finally, this CFNS hiPSC model system may encourage the use of hiPSC-based systems to model structural aspects of other congenital craniofacial anomalies in which self-organization of cells may play a role. Such studies have the potential to inform therapeutic approaches for congenital craniofacial anomalies, as well as to increase our understanding of cell self-organizing properties to facilitate tissue engineering and cell replacement therapies for patients with these disorders.

Materials and Methods

hiPSC generation and culture. All human tissue collection, stem cell studies, procedures, and written consents were approved by the UCSF Committee on Human Research and the UCSF Gamete, Embryo, and Stem Cell Research Committee. Prior to their inclusion in this study, written informed consent was obtained from all participants or from their parents. A small dermal tissue sample was collected from an excess specimen at the time of a surgical procedure of the 10-month-old female CFNS proband. Punch biopsies were obtained from the proband's father and mother. Primary human fibroblast cultures were established and cultured on plastic culture dishes in DMEM high glucose (Life Technologies) containing 10% FBS (HyClone), 2 mM L-glutamine, 1 mM sodium pyruvate, 0.1 mM MEM non-essential amino acids, and penicillin-streptomycin-fungizone. Human iPSCs were generated using episomal reprogramming (Bershteyn et al., 2014; Okita et al., 2011). Briefly, one microgram of each of the Y4 combination of episomal reprogramming factors (Addgene 27078, 27080, 27082) was electroporated into 3 x 10^5 fibroblasts (passage 5-6) with the Neon Electroporation Device (Invitrogen) using the 100-uL kit and conditions of 1650 V, 10 ms, and three pulses. Cells were detached 6 days after electroporation and seeded at 1.5 x 10^5 cells per 10-cm dish onto irradiated mouse embryonic fibroblasts (Globalstem). On day 7, media was changed from fibroblast media to KnockOut^{TM} ESC/hiPSC culture media containing 4 ng/mL bFGF (Life Technologies), and cells were cultured for a further 18-25 days. Colonies with hiPSC-like

morphology were manually selected under a dissecting microscope and subcultured on irradiated MEFs. By passage four, hiPSCs were transferred to feeder-free conditions and cultured in mTeSR1 medium (STEMCELL Technologies) on dishes coated with hESC-qualified Matrigel (Corning).

hiPSC characterization. G-banded karyotype analysis of hiPSC lines was performed after passage 9 by WiCell Research Institute (Madison, WI). To confirm *EFNB1* genotypes, DNA samples were isolated from both HDF and hiPSC lines with a DNeasy Blood and Tissue Kit (Qiagen) and sequenced by SeqWright, Inc. (Houston, TX). To assay for plasmid integration, DNA samples were amplified by PCR with *EBNA-1* plasmid backbone-specific primers and normalized to *GAPDH* as a loading control (**Table 7**). PCR products were resolved against a positive control plasmid diluted to the equivalent of 1 and 0.2 copies plasmid/diploid genome. Female HDF and hiPSC cultures were assayed for relative inactivation of each X-chromosome with the HUMAR assay (Kiedrowski et al., 2011). Briefly, capillary electrophoresis was performed on genomic DNA samples both digested and undigested with the methylation-sensitive restriction enzyme HpaII, which selectively digests the active X chromosome. Each allele is represented as a separate peak in the capillary electrophoresis trace based on the differential number of CAG repeats at the human androgen receptor locus on each X-chromosome. Areas under the peak for each allele were measured on Peak Scanner™ (Applied Biosystems) for both undigested and digested samples, and these peak areas were used to calculate X_A (fraction of expression from a given X chromosome).

hNE cell differentiation and culture. hNE cell differentiations from hiPSCs were performed using a monolayer dual-SMAD inhibition protocol (Chambers et al., 2009), with some modifications. hiPSCs were plated on hESC-qualified Matrigel (Corning)-coated dishes at a density of 2.5 x 10^5 cells/cm^2 (day 0) in STEMdiff Neural Induction Medium (NIM; STEMCELL Technologies)

supplemented with penicillin-streptomycin (P/S) and 10 μM Y-27632 (Santa Cruz Biotechnology) to increase cell survival as single cells (Watanabe et al., 2007). Daily media changes were made with NIM supplemented with P/S, 10 μM SB-431542 (Santa Cruz Biotechnology), and 5 μM DMH1 (Sigma) (Neely et al., 2012) on days 1-3 and NIM + P/S alone on days 4 onward. After 8-10 days in culture, cells were dissociated to a single-cell suspension in Accutase and replated on Matrigel-coated dishes at a 1:1 dilution in NIM supplemented with P/S and 10 μM Y-27632. hNE cell cultures were maintained in NIM with or without SB-431542 and DMH1 and split at ratios of 1:1 to 1:3 until experimentation.

hNE cell segregation assays. EPHRIN-B1-expressing and EPHRIN-B1-non-expressing hNE cells were either labeled with CellTracker dye CMFDA (Molecular Probes) for 45 minutes at a concentration of 5 μM in NIM supplemented with penicillin-streptomycin (P/S) or infected with adenovirus Ad-CMV-eGFP or Ad-CMV-mCherry (Vector Biolabs) overnight at a concentration of 1-5 x 10^6 IFU/cm^2 in NIM + P/S, followed by incubation in NIM + P/S for 2 additional days. hNE cells from differentially labeled lines were mixed at a concentration of 5 x 10^5 cells/line and plated on Matrigel-coated 24-well glass-bottom dishes (MatTek), for a total of 1 x 10^6 cells per well. Cells were imaged at 48 hours after mixing on a Zeiss Cell Observer spinning disc confocal microscope to assess cell segregation. For live imaging of cell segregation, cell mixing experiments were set up as described above and plated in 4-chamber glass-bottom dishes (Greiner Bio-One), with cell number adjusted to achieve the same density. 15 mM HEPES (UCSF Cell Culture Facility) was added to cell media to facilitate buffering outside the CO_2 incubator during the imaging process. Cell mixtures were imaged at twenty-minute intervals over 25 hours after mixing using a Zeiss Cell Observer spinning disc confocal microscope.

Immunocytochemistry. Cells were plated on Matrigel-coated glass coverslips and fixed in 2% paraformaldehyde in PBS at room temperature. The cells were washed with PBS, blocked in

5% normal donkey serum (Jackson ImmunoResearch) and 0.1% Triton-X-100 in PBS, incubated in primary antibody (**Table 6**) for 1 hour at room temperature or overnight at 4°C, washed with PBS, and incubated in secondary antibody (**Table 6**) at room temperature. Cells were counterstained in 0.1 µg/mL DAPI (Millipore) in PBS for 20 minutes at room temperature and mounted on slides using Aquamount (Thermo Scientific) for imaging.

Immunoblotting. Cells were lysed in NP-40 lysis buffer (20 mM Tris-HCl, 137 mM NaCl, 10% glycerol, 1% NP-40, 2 mM EDTA) supplemented with 1 mM dithiothreitol (Sigma) and the following protease and phosphatase inhibitors: aprotinin, 2 µg/mL; leupeptin, 5 µg/mL; pepstatin, 1 µg/mL; PMSF, 1 mM; NaF, 10 mM; and $NaVO_4$, 1 mM. Protein quantification was performed using the Pierce BCA Protein Assay Kit (Thermo Fisher Scientific). Immunoblotting was performed according to standard procedures using Odyssey® TBS blocking buffer (LI-COR) for blocking and dilution of antibodies (**Table 6**) and TBS with 0.1% Tween-20 for washing. Imaging of immunoblots was performed using an Odyssey® Infrared Imaging System (LI-COR), and analysis was carried out using Image Studio™ software (LI-COR).

qRT-PCR of hiPSCs and neuroepithelial cells. Total RNA was extracted from cells using TRIzol (Life Technologies). RNA was reverse transcribed using a SuperScript™ II First-Strand Synthesis System for RT-PCR (Life Technologies). qRT-PCR was performed using iTaq Universal SYBR Green and a CFX96 Real Time System (Bio-Rad), with primer pairs that span exon-intron boundaries (**Table 7**).

Statistics. For analysis of qRT-PCR data, GraphPad Prism 6 was used to plot mean expression ± standard deviation of technical replicate reactions, indicated by error bars. Biological replicates (different hiPSC lines or different hNE differentiations), if applicable, are shown as separate bars on the graph.

Author Contributions

T.K.N., A.R.L., and J.O.B. designed experiments and analyzed data. O.D.K. and J.H.P. obtained patient material for generation of hiPSCs. A.R.L. and J.O.B. made and characterized hiPSC lines with technical expertise from E.C.H. T.K.N. differentiated, characterized, and performed experiments on hiPSC-derived neuroepithelial cells with technical expertise from M.B. and A.K.O. T.K.N. and J.O.B. wrote the text, with editing by all authors.

Acknowledgments

This study was supported by a Graduate Research Fellowship (2013157314) to T.K.N. from the National Science Foundation, and by grant F31DE026059 to T.K.N. and grant R01DE02337 to J.O.B., both from the National Institute of Dental and Craniofacial Research. A.R.L. was a Howard Hughes Medical Institute Medical Research Fellow and completed this work as partial fulfillment of the requirements for an M.D. with Distinction in the UCSF Molecular Medicine Pathway to Discovery. Any opinions, findings, or conclusions in this work are those of the authors and do not necessarily reflect the views of the Howard Hughes Medical Institute, National Science Foundation or National Institutes of Health.

Table 2. HUMARA demonstrates clonal inactivation of maternal (wild type) X chromosome in each CFNShet hiPSC line

	Peak Areas Undigested Samples		**Peak Areas** Digested Samples		**Possible Values of X_A** (Fraction of X activation)		**Ratio of X_A^{wt} to X_A^{mut}** (Average % X activation)	
	Maternal	Paternal	Maternal	Paternal	X_A, maternal	X_A, paternal	X_A, maternal	X_A, paternal
CFNS het HDF	64276	61770	9880	19316	0.65	0.35	61	39
	51069	43431	16592	24562	0.56	0.44		
					0.63	0.37		
					0.58	0.42		
CFNS het-1 hiPSCs	59768	205805	28403	0	0.00	1.00	0	100
	17428	57018	4606	0	0.00	1.00		
					0.00	1.00		
					0.00	1.00		
CFNS het-2 hiPSCs	69895	230728	183006	0	0.00	1.00	0	100
	41823	157233	173086	0	0.00	1.00		
					0.00	1.00		
					0.00	1.00		
CFNS het-3 hiPSCs	50731	158352	42899	0	0.00	1.00	0	100
	53890	163248	94864	0	0.00	1.00		
					0.00	1.00		
					0.00	1.00		

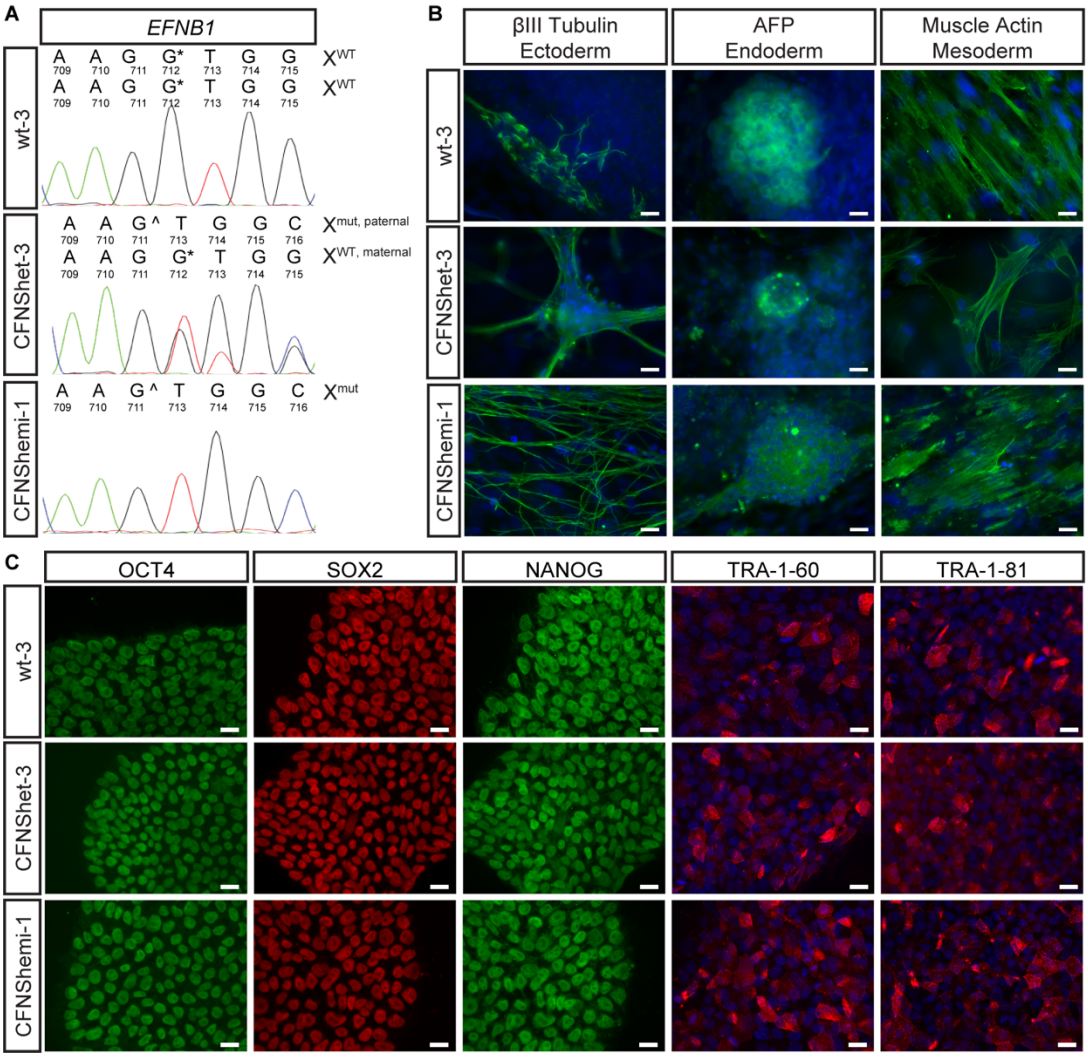

Figure 7. Reprogramming of wild-type, CFNShet, and CFNShemi HDFs to hiPSCs. (A) CFNShet-3 and CFNShemi-1 hiPSCs possess the *EFNB1*$^{c.712delG}$ mutation compared with wt-3 hiPSCs. See also **Figure S1**. **(B)** wt-3, CFNShet-3, and CFNShemi-1 hiPSCs possess differentiation potential to ectoderm (βIII-tubulin), endoderm (alpha-fetoprotein, AFP), and mesoderm (muscle actin). Samples were counterstained with DAPI (blue). *Scale bars, 20 μm*. See also **Figure S2**. **(C)** wt-3, CFNShet-3, and CFNShemi-1 hiPSCs express the endogenous pluripotency markers OCT4, SOX2, and NANOG, as well as the surface markers TRA-1-60 and TRA-1-81 (counterstained with DAPI (blue)). *Scale bars, 20 μm*. See also **Figure S3**.

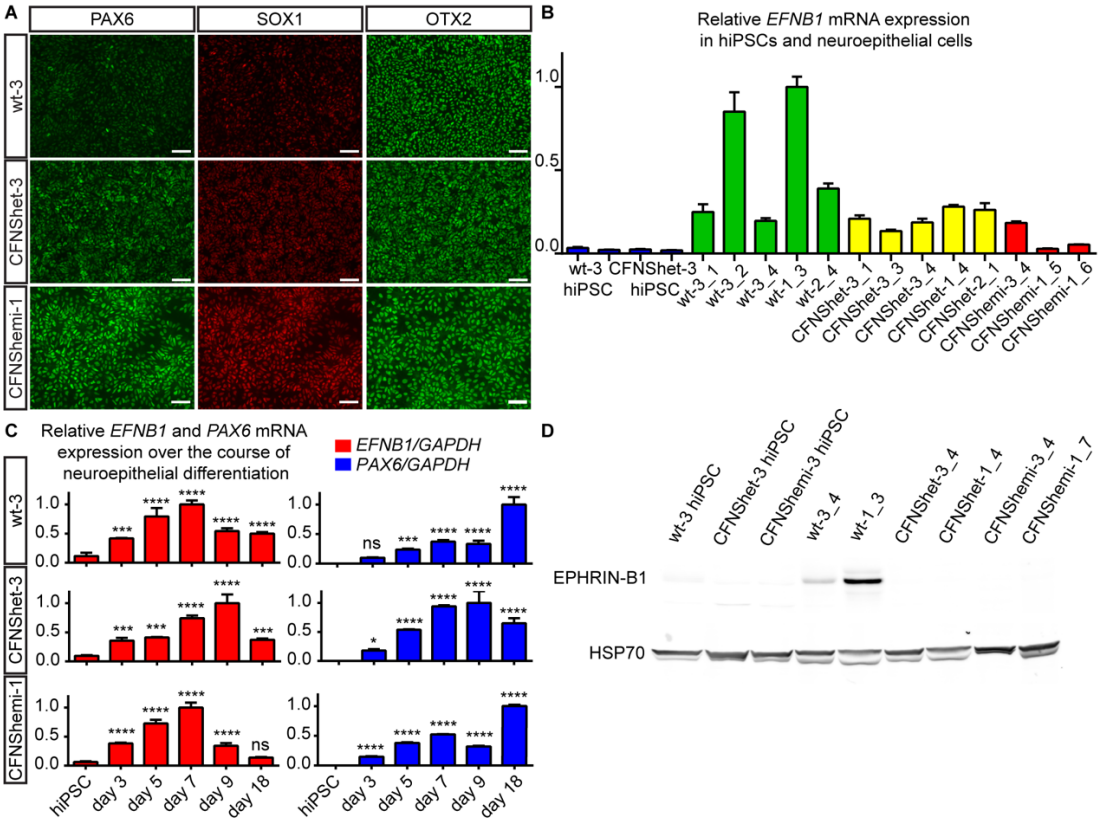

Figure 8. Differentiation and characterization of hNE cells from hiPSCs. (A) Immunostaining reveals that wt-3, CFNShet-3, and CFNShemi-1 hNE cells express the hNE cell markers PAX6, SOX1, and OTX2. *Scale bars, 50 μm*. **(B)** *EFNB1* mRNA expression (normalized to *GAPDH* mRNA expression) in hiPSCs and wild-type, CFNShet, and CFNShemi hNE cells. Numbers following underscores represent separate hNE differentiations. Error bars represent the standard deviation of n = 3 technical replicate qRT-PCR reactions per hiPSC or hNE line. See also **Figure S4**. **(C)** Relative *EFNB1* and *PAX6* expression (normalized to *GAPDH* expression) increase over the course of hNE cell differentiation of wt-3, CFNShet-3, and CFNShemi-1 hiPSCs. Error bars represent the standard deviation of n = 3 technical replicate qRT-PCR reactions per condition. Data shown are one of n = 2 biological replicates of each wt-3 and CFNShet-3 or one of n = 3 biological replicates of CFNShemi-1 (n = 2) and CFNShemi-3 (n = 1). **(D)** Immunoblotting reveals expression of EPHRIN-B1 protein in wild-type but not CFNShet or CFNShemi hNE cells or in hiPSCs of any genotype.

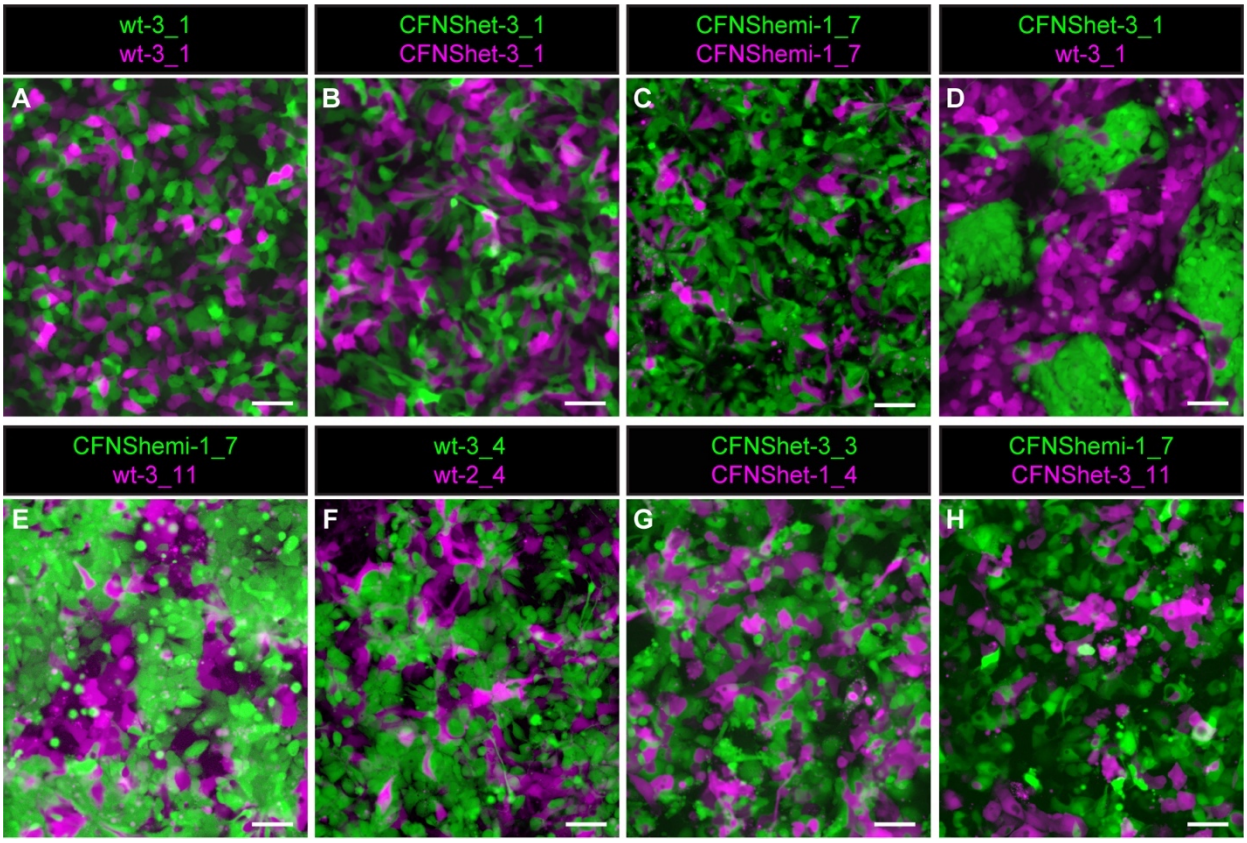

Figure 9. Robust cell segregation in neuroepithelial cells mosaic for EPHRIN-B1 expression. (A–C) Mixing two populations of wild-type EPHRIN-B1 expressing hNE cells **(A)**, two populations of CFNShet hNE cells not expressing EPHRIN-B1 **(B)**, or two populations of CFNShemi hNE cells not expressing EPHRIN-B1 **(C)** results in cell intermingling over 48 hours. **(D and E)** Cell mixing to generate cultures mosaic for EPHRIN-B1 expression (wt-3 + CFNShet-3 **(D)**; wt-3 + CFNShemi-1 **(E)**) results in robust segregation of EPHRIN-B1 expressing and non-expressing hNE cells over 48 hours. See also **Figure S5**. **(F–H)** Mixing two different wild-type (EPHRIN-B1 expressing) hNE cell lines (wt-3 + wt-2) **(F)**, two different CFNShet (EPHRIN-B1 non-expressing) hNE cell lines (CFNShet-3 + CFNShet-1) **(G)**, or two EPHRIN-B1 non-expressing hNE cell lines of different genotypes (CFNShet-3 + CFNShemi-1) **(H)** results in cell intermingling without cell segregation. Adjustments to gamma were made to better visualize independent cell populations. *Scale bars, 50 μm.*

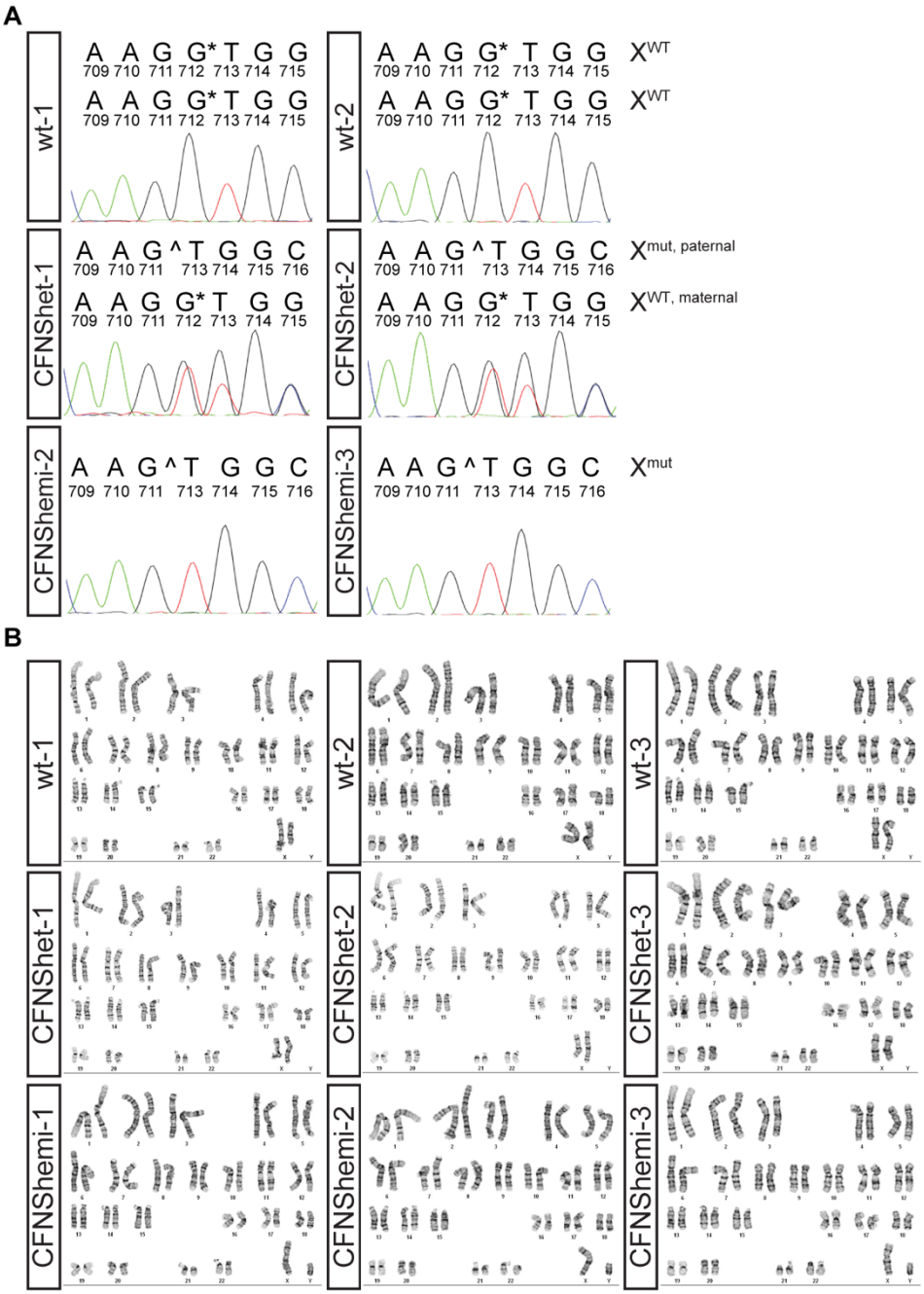

Figure S1. Genetic characterization of CFNS patient-derived hiPSCs. (A) Sequencing chromatograms show retention of G712 in wt hiPSC lines, heterozygous deletion of G712 in CFNShet lines, and deletion of G712 in CFNShemi lines. **(B)** G-banded karyotype analysis shows that all nine hiPSC lines have normal karyotypes (46, XX for female wild-type and CFNS heterozygous lines and 46, XY for male CFNS hemizygous lines).

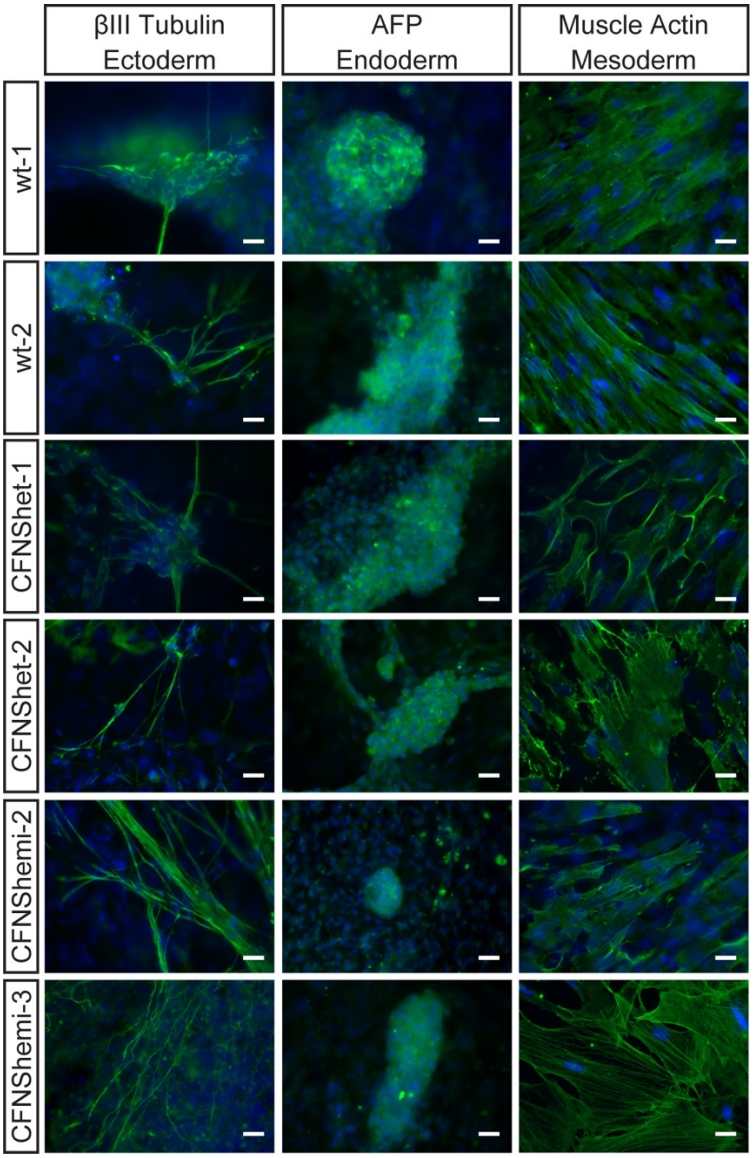

Figure S2. CFNS patient-derived hiPSCs possess differentiation potential to all three germ layers. Upon *in vitro* embryoid body differentiation, *EFNB1*$^{+/+}$ lines (wt-1, -2), *EFNB1*$^{+/c.712delG}$ lines (CFNShet-1, -2), and *EFNB1*$^{Y/c.712delG}$ lines (CFNShemi-2, -3) demonstrated differentiation potential to ectoderm (βIII tubulin), endoderm (alpha-fetoprotein, AFP), and mesoderm (muscle actin). Samples were counterstained with DAPI (blue). *Scale bars, 20 μm*.

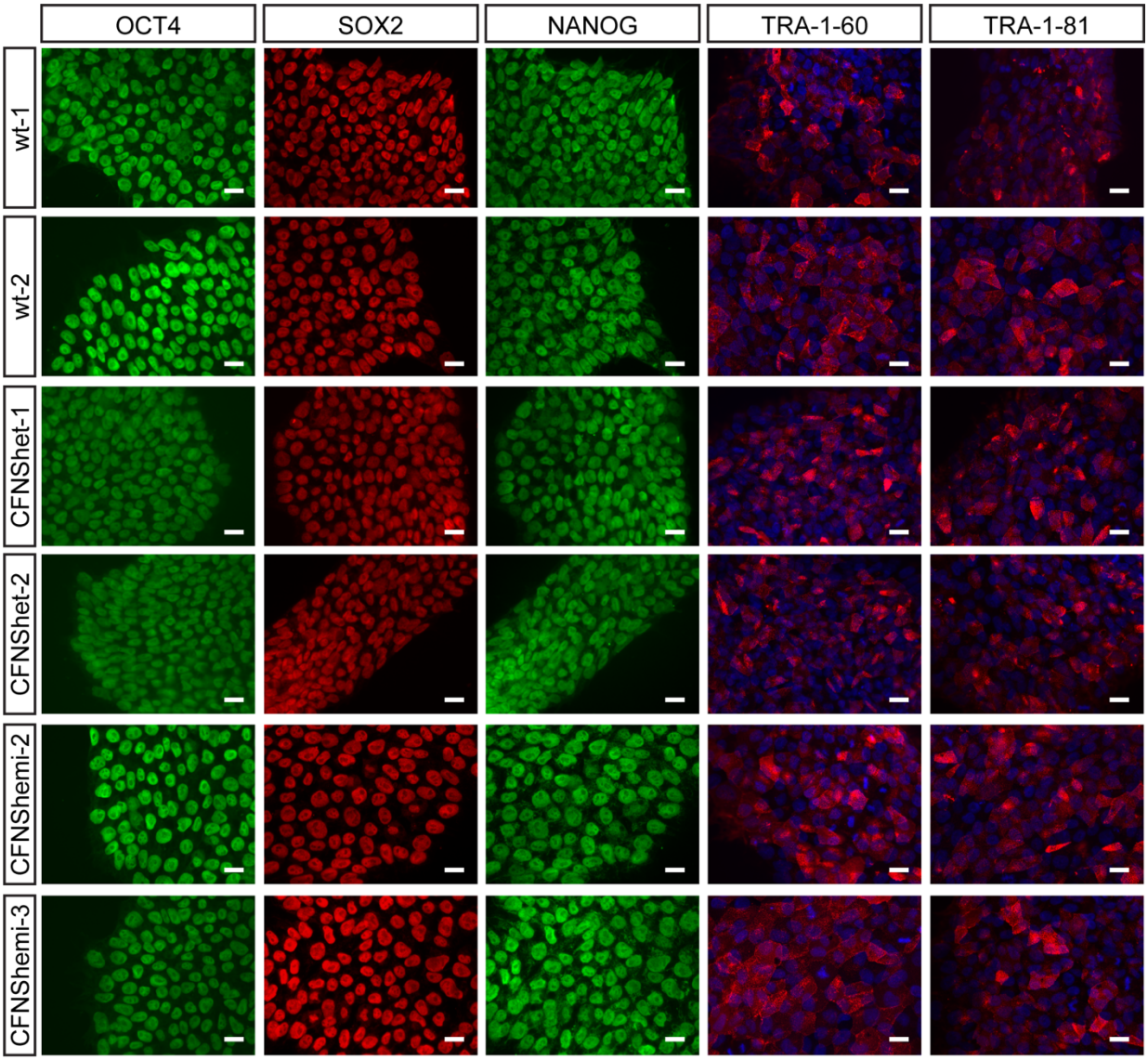

Figure S3. CFNS patient-derived hiPSCs express pluripotency markers. Immunocytochemical characterization of *EFNB1*$^{+/+}$ lines (wt-1, -2), *EFNB1*$^{+/c.712delG}$ lines (CFNShet-1, -2), and *EFNB1*$^{Y/c.712delG}$ lines (CFNShemi-2, -3) reveals positive staining for the nuclear factors OCT4, SOX2, and NANOG, as well as the surface antigens TRA-1-60 and TRA-1-81 (counterstained with DAPI (blue)). *Scale bars, 20 µm*.

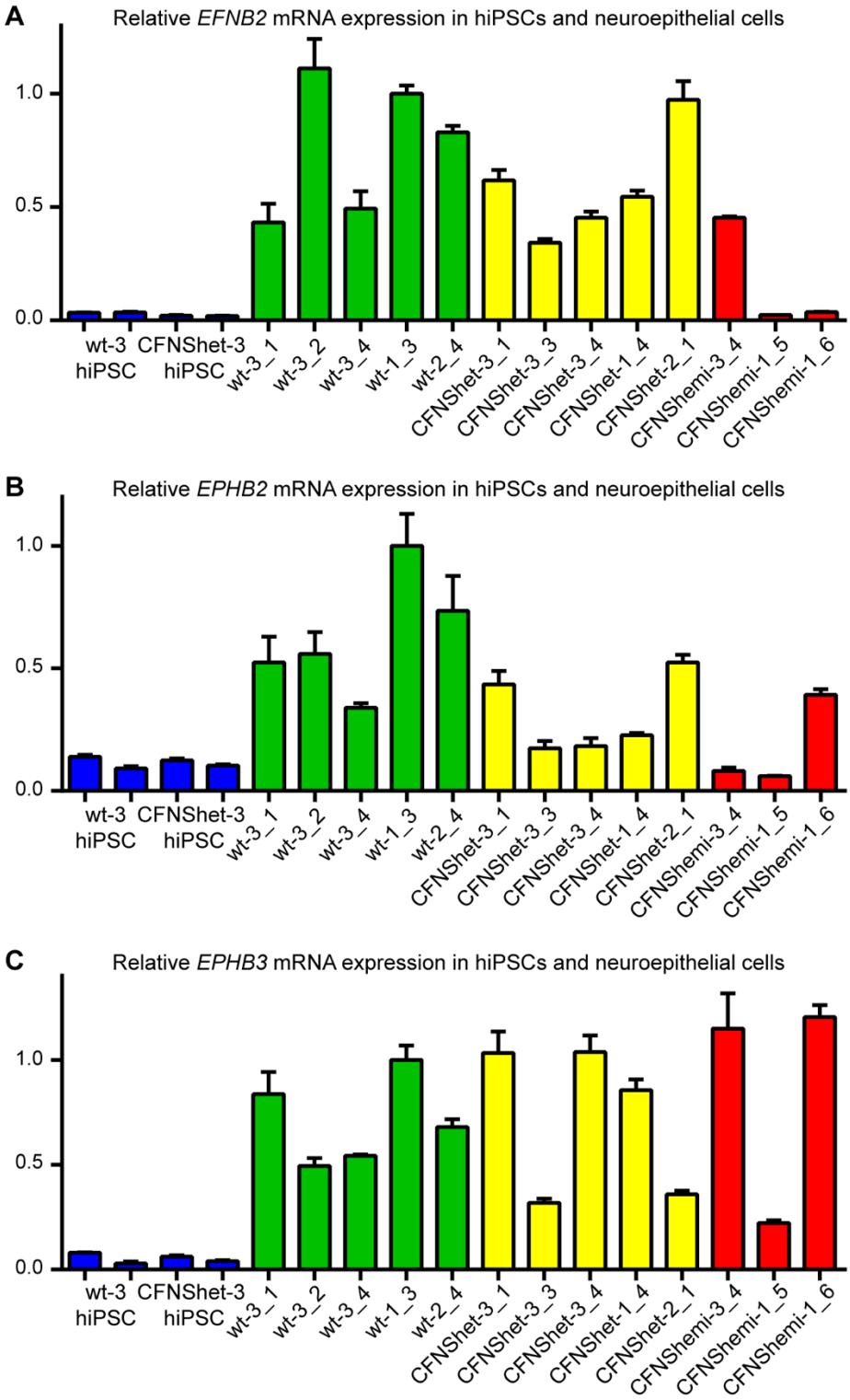
A
Relative EFNB2 mRNA expression in hiPSCs and neuroepithelial cells
1.0
0.5
0.0
wt-3 hiPSC
CFNShet-3 hiPSC
wt-3_1
wt-3_2
wt-3_4
wt-1_3
wt-2_4
CFNShet-3_1
CFNShet-3_3
CFNShet-3_4
CFNShet-1_4
CFNShet-2_1
CFNShemi-3_4
CFNShemi-1_5
CFNShemi-1_6
B
Relative EPHB2 mRNA expression in hiPSCs and neuroepithelial cells
1.0
0.5
0.0
wt-3 hiPSC
CFNShet-3 hiPSC
wt-3_1
wt-3_2
wt-3_4
wt-1_3
wt-2_4
CFNShet-3_1
CFNShet-3_3
CFNShet-3_4
CFNShet-1_4
CFNShet-2_1
CFNShemi-3_4
CFNShemi-1_5
CFNShemi-1_6
C
Relative EPHB3 mRNA expression in hiPSCs and neuroepithelial cells
1.0
0.5
0.0
wt-3 hiPSC
CFNShet-3 hiPSC
wt-3_1
wt-3_2
wt-3_4
wt-1_3
wt-2_4
CFNShet-3_1
CFNShet-3_3
CFNShet-3_4
CFNShet-1_4
CFNShet-2_1
CFNShemi-3_4
CFNShemi-1_5
CFNShemi-1_6

Figure S4. Expression of additional EphB/ephrin-B signaling family members in hiPSCs and hNE. qRT-PCR demonstrates relative expression levels of **(A)** *EFNB2*, **(B)** *EPHB2*, and **(C)** *EPHB3* in hNE cells of all three genotypes. Very low expression of each of these Eph/ephrin signaling family members is seen in hiPSCs. Expression of each Eph/ephrin signaling family member in each sample was normalized to expression of *GAPDH*. Error bars represent the standard deviation of three technical replicates per hiPSC or hNE line.

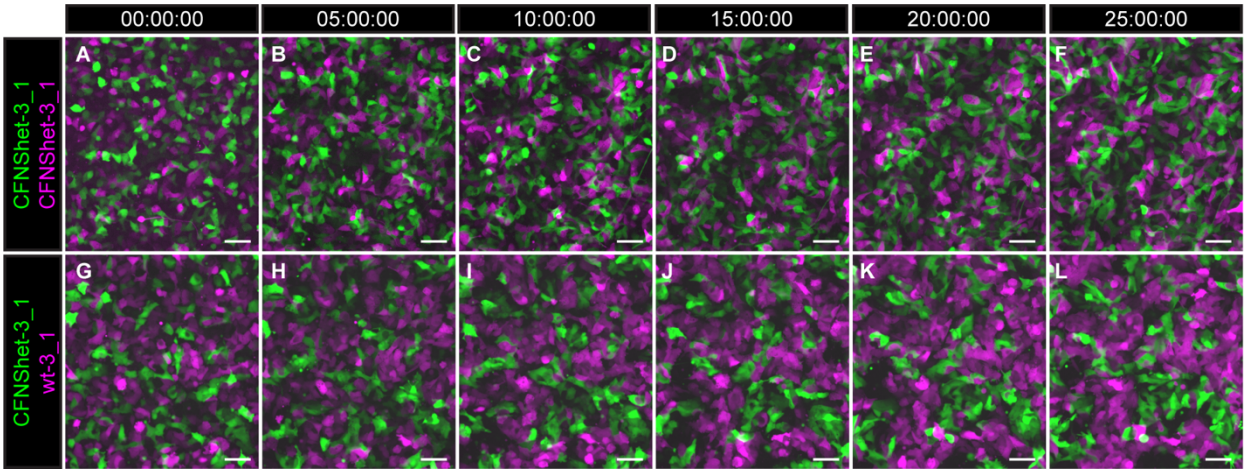

Figure S5. Time lapse imaging of hNE cell mixing experiments. (A-F) Live imaging of a mixture of EPHRIN-B1 non-expressing cells (CFNShet-3 + CFNShet-3) over 25 hours demonstrates that EPHRIN-B1 non-expressing cells remain intermixed as they continue to interact with each other and are not segregating at 25 hours **(F)**. **(G-L)** Live imaging of a cell mixture mosaic for EPHRIN-B1 expression (CFNShet-3 + wt-3) shows that cells are intermixed at the beginning of the experiment **(G)**, but segregate from each other over time, and are already forming patches of EPHRIN-B1 expressing and non-expressing cells at 25 hours **(L)**. Adjustments to gamma were made to better visualize independent cell populations. *Scale bars, 50 μm*.

CHAPTER 4. Aberrant cell segregation in craniofacial primordia and the emergence of facial dysmorphology in craniofrontonasal syndrome

Summary

Craniofrontonasal syndrome (CFNS) is a rare X-linked disorder characterized by craniofacial, skeletal, and neurological anomalies and caused by mutations in *EFNB1*. Heterozygous females are observed to be more severely affected than hemizygous male patients, a phenomenon called cellular interference that has been attributed to cell segregation resulting from EPHRIN-B1 mosaicism and that can be recapitulated in *Efnb1* mutant mice. However, the developmental origin of craniofacial dysmorphology and its spatiotemporal relationship with cell segregation is unknown, and the role of cell segregation in CFNS etiology therefore remains poorly understood. Here, we couple geometric morphometric techniques with interrogation of cell segregation to quantitatively relate facial shape to cell segregation in an *Efnb1* mutant mouse model of CFNS. We show that differences in the development of the face emerge early but continue to become more dramatic during critical stages of craniofacial morphogenesis, correlating with the progression of cell segregation. Whereas craniofacial shape changes are qualitatively similar in *Efnb1* heterozygous and hemizygous mutant embryos, heterozygous embryos are more severely affected, indicating that *Efnb1* mosaicism exacerbates phenotypes rather than having a neomorphic affect. Further, by generating ephrin-B1 mosaicism in specific cell populations, we find that ephrin-B1 is a potent regulator of cell segregation throughout craniofacial development and that emergence of differences in face shape between control and ephrin-B1 mutant embryos correlates with occurrence of segregation in craniofacial primordia. Together, these data suggest that cell segregation in post-migratory neural crest-derived mesenchyme progressively drives dysmorphology in CFNS.

Introduction

Congenital craniofacial anomalies account for one third of all birth defects (“Global Strategies to Reduce the Health Care Burden of Craniofacial Anomalies,” 2004). Advances in craniofacial genetics have identified many genes involved in craniofacial syndromes (Twigg and

Wilkie, 2015), but an understanding of the underlying etiology and progression over developmental time for each condition will be necessary for improved therapies for this large group of disorders. Craniofrontonasal syndrome (CFNS, OMIM #304110) is a subgroup of frontonasal dysplasia that is caused by mutations in EPHRIN-B1 (*EFNB1*), which is located on the X chromosome (Cohen, 1979; Twigg et al., 2004; Wieland et al., 2004). Paradoxically, this X-linked syndrome is associated with more severe disease phenotypes in heterozygous females than hemizygous males, a phenomenon termed "cellular interference" (Twigg et al., 2004; Wieacker and Wieland, 2005; Wieland et al., 2004). Whether this "increased severity" represents increased disease severity (additional phenotypes in female patients) or an increased degree of severity of the same disease, or both, has not been rigorously examined. Heterozygous female patients frequently display a combination of orbital hypertelorism (based on measurements of inner canthal and interpupillary distances or on computed tomography (CT) scans), a short and wide upper face, facial asymmetry, unilateral or bilateral coronal craniosynostosis, a short nose, bifid nasal tip, and a broad nasal bridge (Twigg et al., 2004; van den Elzen et al., 2014; Wieland et al., 2004). In a subset of cases, cleft lip and palate, agenesis of the corpus callosum (Twigg et al., 2004), and maxillary hypoplasia (van den Elzen et al., 2014) have also been noted. In addition to craniofacial defects, patients present with axial skeletal defects including syndactyly and polydactyly.

CFNS has been termed a neurocristopathy, and it has been hypothesized that CFNS phenotypes may be partly attributable to impacts on early neural crest cell (NCC) migration or to later bone differentiation defects (Davy et al., 2004; Davy et al., 2006; Nguyen et al., 2016; Twigg et al., 2004); however, the precise developmental etiology of this disorder remains unknown. Because CFNS patients are clinically evaluated postnatally but craniofacial development occurs very early during embryogenesis, it is difficult to pinpoint the developmental timing and tissue origin of the craniofacial phenotypes, and therefore this remains a subject of debate. Hypertelorism, a key defining phenotype of female CFNS patients that is also seen at a

milder level in males with hemizygous mutations in *EFNB1*, as well as frontonasal dysplasia and widened midface, are phenotypes that may have a variety of tissue origins. It is possible that these changes are due to defects in NCCs or their derivatives, but they may also be secondary to changes in brain shape, or to craniosynostosis that restricts the growth of the skull vault. Changes to the shape of the brain can cause changes to facial shape by several described mechanisms (Marcucio et al., 2011; Marcucio et al., 2015); for example, reduction of brain size in Crf4 mutant mice is associated with more advanced fusion in the developing face, leading to a narrower and more prognathic face (Boughner et al., 2008). There is also some evidence for the idea that increases in brain size may underlie clefting phenotypes by increasing separation of the facial prominences to an extent that they can no longer make contact, even if their outgrowth is normal (Parsons et al., 2011; Young et al., 2007). Changes in brain morphology have also been proposed to contribute to hypertelorism (Young et al., 2010), but hypertelorism could also be secondary to expansion of the midface in CFNS patients. Previous data has shown that cell segregation between ephrin-B1 expressing and non-expressing cells occurs in the early neural plate (O'Neill et al., 2016), but it is unknown whether this phenomenon contributes to changes in the brain that may affect the face, or whether segregation or other changes to different tissues underlie these phenotypes. A detailed quantification of CFNS phenotypes and assessment of their developmental etiology will be required to determine when and where changes in the shape of the face arise in these patients.

Ephrin-B1 is a member of the Eph/ephrin family of membrane-linked signaling molecules; signaling between Eph receptors and ephrins is important for boundary formation, cell migration, axon guidance, vascular development, and neurogenesis (Batlle and Wilkinson, 2012; Fagotto et al., 2014; Kania and Klein, 2016; Klein and Kania, 2014; Kullander and Klein, 2002; Pasquale, 2005; Pasquale, 2008; Wilkinson, 2001) (see **Chapter 2**). Ephrins are classified into two types: ephrin-As, which are anchored to the cell membrane, and ephrin-Bs, which are transmembrane proteins, while Eph-A and Eph-B receptors are classified by their

binding affinity to ephrin-As or ephrin-Bs. No specific mutations in *EFNB1* or aberrant patterns of X-inactivation have been associated with variation in severity or type of dysmorphology, though mutations in the region of the fifth exon encoding the intracellular domain have been identified less frequently (Twigg et al., 2004; van den Elzen et al., 2014). Analysis of several tissue types indicate that X-inactivation is not biased by presence of an *EFNB1* mutation (Twigg et al., 2004; Wieland et al., 2008), suggesting that loss of gene function does not impact cell survival. Supporting the idea that mosaicism for ephrin-B1 expression results in more severe dysmorphogenesis, rare male patients with severe CFNS phenotypes exhibit somatic mosaicism for *EFNB1* mutations (Twigg et al., 2006; Twigg et al., 2013; Wieland et al., 2008). Studies of the role of ephrin-B1 in development and the mechanism by which ephrin-B1 mosaicism results in more severe developmental phenotypes have often been carried out using *Efnb1* mutant mice as a model for CFNS.

The *Efnb1* mutant mouse has largely been accepted as a good model for CFNS, as $Efnb1^{+/\Delta}$ mice share many of the same phenotypic characteristics as human $EFNB1^{+/-}$ CFNS patients. $Efnb1^{+/\Delta}$ embryos are overall less affected than hemizygous ($Efnb1^{\Delta/Y}$) or homozygous ($Efnb1^{\Delta/\Delta}$) embryos (Bush and Soriano, 2010; Compagni et al., 2003; Davy et al., 2004), mirroring the situation seen in female heterozygous CFNS patients. Although this mouse model has been widely used to study CFNS, the craniofacial phenotypes associated with heterozygous or hemizygous loss of *Efnb1* have not been characterized beyond the report of relatively high frequency of cleft palate and shorter skulls with altered bone formation (Compagni et al., 2003; Davy et al., 2004; Davy et al., 2006; Nguyen et al., 2016), and it remains unknown to what extent face shape changes in $Efnb1^{+/\Delta}$ embryos mirror those of CFNS patients. The mild phenotypes seen in $Efnb1^{\Delta/Y}$ mice also inspire the question of whether *Efnb1* heterozygosity represents a neomorphic state, or a more severe version of the hemizygous state. If mouse phenotypes can be shown to quantitatively mirror human phenotypes, the $Efnb1^{+/\Delta}$ model will be a valuable tool for determining the developmental etiology of CFNS phenotypes; the timing and

tissues in which facial shape changes first become apparent in *Efnb1*$^{+/\Delta}$ embryos will shed light on the important question of when and where these phenotypes may arise in human patients.

Increased severity in heterozygous females has been proposed to stem from "cellular interference" between cells that express a mutant allele and cells that do not after random X inactivation (Wieacker and Wieland, 2005). Cellular interference has been shown to involve cell segregation in the developing limb buds of heterozygous female mice, where ectopic borders between ephrin-B1 expression and non-expression coincide with the development of additional digits (Compagni et al., 2003; Davy et al., 2004), and in the developing craniofacial complex (Bush and Soriano, 2010; Davy et al., 2006; O'Neill et al., 2016). Ephrin-B1-mediated cell segregation in *Efnb1*$^{+/-}$ mice can be seen as early as E8.5 in neural plate neuroepithelial cells (O'Neill et al., 2016), and this aberrant cellular behavior also occurs in CFNS patient hiPSC-derived neuroepithelial cells (see **Chapter 3**), indicating that cell segregation is likely to occur in human CFNS patients. How ephrin-B1-mediated segregation contributes to facial dysmorphogenesis remains mysterious, however, as the timing and tissue specificity of cell segregation and phenotypic progression of CFNS craniofacial phenotypes have not been documented. For example, it is unknown whether segregation in precursor cells at the neural plate stage is ultimately responsible for the large ephrin-B1 expression patches visible later in development in craniofacial structures, or whether ephrin-B1 mosaicism continues to drive segregation in multiple cell types throughout the development of these structures. It is also unknown whether dysmorphogenesis is directly driven by segregation or is a secondary consequence of the inappropriate Eph/ephrin boundaries that are established. Further, though ephrin-B1 mosaicism and cell segregation likely play a pivotal role in the cellular etiology of CFNS, it remains unclear whether and how aberrant ephrin-B1 expression domains contribute to dysmorphic facial shape.

Here, we use mouse models of CFNS to understand the cellular and developmental etiology of craniofacial phenotypes. First, we compare the facial form of *Efnb1* heterozygous

female and hemizygous male embryos with control embryos to quantify the specific effects of *Efnb1* loss on facial growth and development to better understand how CFNS dysmorphology develops. Next, we demonstrate that ephrin-B1 is a potent regulator of cell segregation in multiple cell types across craniofacial development and that the timing of segregation in craniofacial primordia correlates with the onset and progression of facial phenotypes in developing embryos. These results indicate that cell segregation occurring in the craniofacial primordia may be the principal driver of cellular interference and severe facial dysmorphogenesis in CFNS.

Results

Ephrin-B1 has a significant effect on embryonic facial shape from E11.5 to E14.5 that mirrors CFNS

Robust quantitative methods will be required to investigate how early the effects of mosaic expression of ephrin-B1 on facial morphology appear, whether the earliest facial shape effects parallel later facial shape effects and how these change in severity over time, and whether phenotypic severity varies between heterozygous females and hemizygous males. We therefore quantified mouse embryo facial shape between E11.5 and E14.5 using geometric landmark-based morphometrics analysis based on micro-computed tomography (μCT) scans of heads of $Efnb1^{+/\Delta}$ and $Efnb1^{\Delta/Y}$ embryos as well as a pooled control sample of $Efnb1^{+/lox}$ and $Efnb1^{lox/Y}$ embryos. To determine the significance and relative contribution of facial size (estimated as centroid size) and *Efnb1* genotype in determining facial shape, we carried out a Procrustes ANOVA analysis on E11.5 embryos using a published landmark set (Percival et al., 2014). The shape change vectors of each landmark were illustrated separately for each genotype and plotted alongside μCT surfaces of specimens that are representative of mean genotype facial shapes (**Figure 10A**). Within the E11.5 analysis, facial size and *Efnb1* genotype both contribute significantly to facial shape (**Table 3**), explaining approximately 23% and 11% of

the variation, respectively. Genotype effect comparisons based on the E11.5 Procrustes ANOVA model can be analyzed to pinpoint specific differences between genotypes. Nasal and mouth landmarks between facial prominences illustrate increased relative width and decreased relative height of the face. A relatively wide face is noted, and the eye and facial prominences appear to be relatively posterior, while the anterior vault landmarks are relatively anterior, suggesting a lack of facial prominence outgrowth. Overall, the faces of affected specimens show a lack of anterior outgrowth, combined increased relative width, and decreased relative height. The significant genotype effect indicates that ephrin-B1 mosaicism or loss influences facial shape as early as E11.5. With a few exceptions, including at the mandibular prominence, the facial effects noted in *Efnb1*$^{\Delta/Y}$ males are largely less severe versions of *Efnb1*$^{+/\Delta}$ dysmorphology at E11.5.

To determine the significance and relative contribution of facial size (estimated as centroid size), embryonic age, and *Efnb1* genotype in determining facial shape from E12.5-E14.5, we completed a Procrustes ANOVA analysis using a novel landmark set defined for the E12.5-E14.5 age group. Each factor within the E12.5-E14.5 analysis, in addition to the interaction between age and genotype, had significant effects on facial shape (**Table 4**). Variation in *Efnb1* genotype explained almost 7% of facial shape variation, indicating that ephrin-B1 has a significant effect on facial morphology. As expected for a sample covering multiple embryonic days, size explained a very large percentage of facial shape variation (77%, based on Rsq; see **Table 4**). The much higher percentage of variation explained by size in comparison with the E11.5 analysis occurs because the E11.5 analysis includes samples from a much shorter range of developmental time than the E12.5-E14.5 analysis. This is driven by the correlation of facial size and shape across development, also known as allometry. Even after size is accounted for, embryonic age and the interaction of age and genotype factors are significantly associated with a small amount of facial variation (<1% each).

The first principal component (PC) of a principal components analysis (PCA) of facial shape across E12.5-E14.5 largely clusters specimens by embryonic age, which is strongly correlated with size; this is expected from the large percentage of variation explained by size. A multivariate linear model was used to estimate the allometric component that is common across the sample regardless of genotype. The residuals of this regression are interpreted as facial shape after accounting for allometry. The first PC of a PCA of these facial shape residuals largely separates genotypes, regardless of age (**Figure 10B**). Control shapes are found on the positive end, *Efnb1*$^{\Delta/Y}$ males are found in the middle, and *Efnb1*$^{+/\Delta}$ females are found at the negative end. This PC represents a common axis of facial shape covariation that separates the genotypes, suggesting major similarities in a genotype's effect on facial shape at E12.5, E13.5, and E14.5. It also suggests that hemizygous male embryos have less severe, but qualitatively similar, facial dysmorphology to heterozygous female embryos.

Although individual PCs illustrate broad patterns of facial shape covariation, they each represent only part of overall covariation. Therefore, we calculated Procrustes distances between mean control and affected genotype facial shapes to confirm the significance of facial shape differences between genotypes and estimate the relative severity of affected facial shape dysmorphology. There were significant differences in mean facial shape between control and each affected genotype at each embryonic age (**Table 5**). In addition, the mean facial shapes of *Efnb1*$^{+/\Delta}$ embryos were always more different from controls than were *Efnb1*$^{\Delta/Y}$ facial shapes, confirming that female heterozygotes display more severe dysmorphology. Comparisons of typical E14.5 genotype-specific facial shapes, estimated from the E12.5-E14.5 Procrustes ANOVA analysis multivariate linear model, indicate overall similarities in the effects of *Efnb1*$^{\Delta/Y}$ and *Efnb1*$^{+/\Delta}$ genotypes on facial shape, but also a few differences. Shape change vectors for each landmark at E14.5 can be illustrated for each genotype and plotted alongside representative μCT surfaces indicating mean genotype facial shape (**Figure 10C**). These genotype effect comparisons are similar to those used with the E11.5 model and indicate that

parallel genotype effects present at E11.5 are still present at E14.5. Both affected genotypes display hypertelorism, represented by an increased relative width between anterior eye landmarks. They also have a relatively inferior-posterior nose, anterior ear, and superior-lateral-posterior lip corners. Altogether, these shared patterns of dysmorphology indicate hypertelorism and facial shortening in both male hemizygotes and female heterozygotes.

There are also some noted differences in the effect of each genotype on facial shape. Although both males and females display increased relative width at the eyes, only *Efnb1*$^{+/\Delta}$ embryos display increased relative width of the posterior whisker margins and a posterior inferior corner of the whisker region. This suggests a larger increase in relative width of the midfacial region in the female heterozygotes that is not matched by the male hemizygotes. In addition, the degree of facial shortening in the females is more extreme, as seen by longer vectors at the ear and nose landmarks. Finally, the female heterozygotes display a much higher point of maxillary prominence fusion at each embryonic age, suggesting reduced midline lip fusion. These results quantitatively demonstrate that in the mouse, as in human CFNS patients, female heterozygotes possess more severe facial dysmorphology than hemizygous male patients; they also suggest that increased midface expansion underlies more severe phenotypes in female heterozygotes.

Our shape analysis indicates that the anterior canthus of the eye is relatively lateral in *Efnb1*$^{+/\Delta}$ embryos compared to control mice (**Figure 10C**), with *Efnb1*$^{\Delta/Y}$ mice in between. This suggests that our affected mice display hypertelorism, as is seen in humans with CFNS. However, because overall scale and size-correlated shape variation was removed prior to the final PCA analysis, the same result might be achieved with an absolutely shorter snout or an absolutely wider biorbital breadth. A comparison of bicanthic breadth was completed to confirm whether our affected embryos display hypertelorism. Kruskal-Wallis tests indicate that there are significant differences in relative bicanthic breadth (bicanthic breadth/whisker region length) between genotypes at each age. Pairwise Wilcoxan tests were completed to determine how

they differed. At E11.5 and E12.5, *Efnb1*$^{+/\Delta}$ mice have significantly wider relative bicanthal breadth than control mice, but *Efnb1*$^{\Delta/Y}$ mice do not. At E13.5 and E14.5, both *Efnb1*$^{+/\Delta}$ and *Efnb1*$^{\Delta/Y}$ mice have significantly wider relative bicanthal breadth than control mice. These results confirm that *Efnb1*$^{+/\Delta}$ mice display hypertelorism at all ages tested, and *Efnb1*$^{\Delta/Y}$ mice display hypertelorism at E13.5 and E14.5; this earlier difference may contribute to the increased severity in heterozygous embryos. Overall, our analyses of facial shape indicated the presence of CFNS-like facial dysmorphology as early as E11.5 in *Efnb1*$^{+/\Delta}$ and *Efnb1*$^{\Delta/Y}$ embryos.

Sox1^{Cre} *mediates cell segregation independently in the brain, but this does not affect NCC-derived craniofacial mesenchyme or facial shape*

Cell segregation has been proposed to underlie increased severity in heterozygous female CFNS patients with ephrin-B1 mosaicism (Bush and Soriano, 2010; Compagni et al., 2003; O'Neill et al., 2016; Wieacker and Wieland, 2005) (see **Chapter 3**). We have previously shown that ephrin-B1 mediates segregation in the neural plate neuroepithelium (O'Neill et al., 2016), but it was not known whether this segregation in neural progenitors, leading to large patches of ephrin-B1 expression and non-expression later in the brain, can mediate changes in facial shape. There is some evidence that disruption of neuroepithelial cells can negatively affect NCCs, resulting in abnormal craniofacial development in Treacher-Collins syndrome patients (Jones et al., 2008; Sakai et al., 2016), and changes to the shape of the brain can cause changes to facial shape (Marcucio et al., 2011; Marcucio et al., 2015). We therefore wondered whether ephrin-B1 mosaicism in neural progenitor cells alone could result in ephrin-B1-mediated changes to facial shape later in development.

To determine whether early neural progenitor segregation contributes to later segregation in the brain and craniofacial structures, we generated neural progenitor-specific ephrin-B1 mosaic *Sox1*$^{Cre/+}$*; Efnb1*$^{+XGFP/\Delta}$ embryos and compared frontal sections through the brain, FNP, and palatal shelves to matched control *Efnb1*$^{+XGFP/lox}$ sections at E13.5. These

embryos express a GFP transgene from one (wild-type) X chromosome (Hadjantonakis et al., 1998; Hadjantonakis et al., 2001), which we use to monitor X chromosome inactivation (XCI). Control embryos demonstrate high ephrin-B1 expression in the brain and a fine-grained mosaic pattern of XGFP expression, as expected after random XCI (**Figure 11A, A'**). Full heterozygous *Efnb1*$^{+XGFP/\Delta}$ embryos (mediated by β-actin-Cre) have robust segregation in the brain at E13.5, visible as large ephrin-B1/GFP positive and negative patches (**Figure 11B, B'**). Likewise, the brains of *Sox1*$^{Cre/+}$*; Efnb1*$^{+XGFP/\Delta}$ embryos show large patches of ephrin-B1/GFP positive and negative cells (**Figure 11C, C'**), indicating that ephrin-B1 mosaicism restricted to neural progenitor cells leads to robust segregation in the brain.

We next wished to determine whether neural progenitor cell segregation has any effect on craniofacial structures later in development. Sox1^{Cre}-mediated recombination of the *ROSA26* locus in *Sox1*$^{Cre/+}$*; ROSA26*$^{mTmG/+}$ reporter embryos leads to widespread membrane GFP expression throughout the brain at E13.5 (**Figure 12A, A'**) without expression in craniofacial structures such as the palatal shelves (**Figure 12B, B'**) and FNP (**Figure 12C, C'**). We therefore did not expect to see segregation in these structures, and indeed, XGFP expression patterns in *Sox1*$^{Cre/+}$*; Efnb1*$^{+XGFP/\Delta}$ palatal shelves (**Figure 12D, D'**) and FNP (**Figure 12E, E'**) appeared evenly distributed throughout the craniofacial mesenchyme, with ephrin-B1 expression indistinguishable from that seen in control *Efnb1*$^{+XGFP/lox}$ embryos (**Figures 16-17**). Facial shape comparison between *Sox1*$^{Cre/+}$*; Efnb1*$^{+/\Delta}$ and control embryos using μCT scans of E14.5 embryo heads, followed by a Procrustes ANOVA analysis using the landmark set developed for E12.5-E14.5 embryos, indicated that there was no overall effect of genotype between the two groups. Calculation of Procrustes distances between mean control and affected genotype facial shapes also showed no significant difference in mean shape between *Sox1*$^{Cre/+}$*; Efnb1*$^{+/\Delta}$ and control embryos (data not shown). From these data, we can conclude that ephrin-B1 mosaicism in neural progenitor cells does drive segregation that is later visible in the brain, but this process is independent from facial shape changes seen in full *Efnb1*$^{+/\Delta}$ mouse

embryos. Instead, it is possible that early neural plate segregation is maintained through NCC induction and migration, or that later stages of cell segregation occur in NCCs and their derivatives. Either mechanism could result in changes to craniofacial structures; if ephrin-B1 mosaicism in NCCs and their derivatives leads to segregation in these cell types, these later segregation events may contribute to the facial shape changes we have demonstrated.

Ephrin-B1-mediated cell segregation occurs in post-migratory neural crest cells correlating with upregulation of ephrin-B1 expression in craniofacial primordia

To better understand how cell segregation contributes to facial shape changes, we sought to determine where and when ephrin-B1 mediates segregation throughout developmental time. Because NCCs are migratory stem cells that populate the structures of the face (Bhatt et al., 2013; LaBonne and Bronner-Fraser, 1998), we first tested the ability of ephrin-B1 mosaicism in NCCs to induce cell segregation in these cells. We generated NCC-specific ephrin-B1 mosaic *Sox10-Cre$^{Tg/o}$; Efnb1$^{+XGFP/\Delta}$* embryos and examined them for NCC segregation. At E10.5, Sox10-Cre-mediated recombination of the *ROSA26* locus in *Sox10-Cre$^{Tg/o}$; ROSA26$^{mTmG/+}$* reporter embryos was robust in the post-migratory NCCs of the maxillae and FNP (**Figure 13A-B**). Like control *Efnb1$^{+XGFP/lox}$* embryos (**Figure 13C-D**), however, neither NCC-specific *Sox10-Cre$^{Tg/o}$; Efnb1$^{+XGFP/\Delta}$* embryos nor full *Efnb1$^{+XGFP/\Delta}$* (mediated by β-actin-Cre) embryos exhibited cell segregation in the maxillae at this stage (**Figure 13E, G**), suggesting that if cell segregation occurs in migratory NCCs, it does not carry through to post-migratory NCC-derived mesenchyme of the maxillary prominences. Ephrin-B1 expression was low in the maxillae at this stage (**Figure 13C, E, G**), indicating that perhaps its upregulation in post-migratory craniofacial mesenchyme is required for segregation. Very small groups of ephrin-B1/XGFP expressing and non-expressing cells could be seen in the LNP of each group of mosaic embryos at E10.5 (**Figure 13F, H**), indicating either that cell segregation in pre-

migratory NCCs can carry through to the LNP, or (more likely) that segregation occurs in the LNP earlier than in the MXP due to earlier upregulation of ephrin-B1 in this structure.

To test whether an increase in ephrin-B1 expression in post-migratory NCC-derived mesenchyme leads to cell segregation at later stages, we next examined NCC-specific ephrin-B1 mosaic *Sox10-Cre*$^{Tg/o}$*; Efnb1*$^{+XGFP/\Delta}$ embryos at E11.5, an embryonic stage at which phenotypic differences in *Efnb1*$^{+/\Delta}$ embryos are first apparent (**Figure 10A**) and ephrin-B1 begins to exhibit robust expression in the maxillary prominences (MXP) and lateral nasal prominences (LNP). In control *Efnb1*$^{+XGFP/lox}$ embryos, ephrin-B1 expression and a fine-grained mosaic pattern of XGFP expression are visible in the MXP and LNP at this stage (**Figure 14A-B**). However, in *Sox10-Cre*$^{Tg/o}$*; Efnb1*$^{+XGFP/\Delta}$ NCC mosaic embryos, distinct patches of ephrin-B1/XGFP expression and non-expression are visible in both structures (**Figure 14C-D**), indicating both that ephrin-B1 drives segregation in the neural crest and that segregation occurs in the maxilla after migration of NCCs to populate the craniofacial prominences. Notably, the upregulation of ephrin-B1 expression in the FNP prior to the maxilla may provide a plausible explanation for why segregation may be seen earlier in the FNP, but we cannot rule out the possible contribution of pre-migratory NCC segregation. Together, these data indicate that multiple distinct phases of cell segregation occur; in addition to early cell segregation in the headfold, a second phase of cell segregation begins in the post-migratory NCC-derived craniofacial mesenchyme upon upregulation of ephrin-B1 expression in this population.

Post-migratory neural crest cell segregation results in local dysmorphogenesis in craniofacial structures

The finding that segregation occurs in post-migratory NCCs demonstrates that ephrin-B1 mediates this process after the headfold stage; we next wished to determine whether segregation continues in later post-migratory NCC-derived craniofacial mesenchyme. Ephrin-B1 has strong expression in the anterior secondary palate (Bush and Soriano, 2010), the study of

which has implications for cleft palate in CFNS patients. We therefore asked whether cells of the palate mesenchyme mosaic for ephrin-B1 expression can undergo segregation mediated by ephrin-B1. We generated palate mesenchyme-specific ephrin-B1 mosaic *Shox2*$^{IresCre/+}$; *Efnb1*$^{+XGFP/\Delta}$ embryos and compared them to control *Efnb1*$^{+XGFP/lox}$ embryos at E11.5, before palatal shelf extension, and at E12.5, a stage at which the palatal shelves are extending from the maxillary prominences. As expected, prior to the onset of Shox2-mediated recombination in the secondary palate mesenchyme, no cell segregation was observed in *Shox2*$^{IresCre/+}$; *Efnb1*$^{+XGFP/\Delta}$ embryos, which instead resembled controls (**Figure 15A-B**). Although Shox2^{IresCre} mediated some recombination of the *ROSA26* locus in *Shox2*$^{IresCre/+}$; *ROSA26*$^{mTmG/+}$ reporter embryos in the maxilla at E11.5, almost all membrane GFP-positive cells (**Figure 15C, C'**) coexpressed neurofilament (2H3) (**Figure 15D, D'**), indicating that these are likely nerve cells of the maxillary trigeminal ganglion. By embryonic day 12.5, however, palate-specific ephrin-B1 mosaic *Shox2*$^{IresCre/+}$; *Efnb1*$^{+XGFP/\Delta}$ embryos exhibited small patches of ephrin-B1/GFP expression and non-expression that were not observed in control embryos (**Figure 15E-F**), indicating that segregation is beginning to take place in this tissue. By this embryonic timepoint, Shox2^{IresCre} recombination of the *ROSA26* locus in *Shox2*$^{IresCre/+}$; *ROSA26*$^{mTmG/+}$ reporter embryos led to mesenchyme-specific membrane GFP expression (**Figure 15G, G'**) that does not overlap with 2H3 expression (**Figure 15H, H'**). Ephrin-B1 is therefore a powerful driver of segregation not only in progenitor cells, such as neuroepithelial cells or NCCs, but also in more differentiated cell types of the craniofacial mesenchyme. These data also demonstrate that ephrin-B1-mediated cell segregation is not a single event in developmental time; rather, it likely continues through development of craniofacial structures.

We have demonstrated that differences in facial shape are evident in female heterozygous embryos as early as E11.5, but these shape changes continue to develop over time and increase in severity through E14.5. To investigate the extent of segregation later in development and to determine whether there are visible changes to craniofacial tissue

morphology at later stages, we examined embryos with ephrin-B1 mosaicism in specific cell types at E13.5. In addition to the anterior secondary palate, the developing frontonasal prominence (FNP) also has strong *Efnb1* expression and may contribute to CFNS phenotypes such as midface expansion and frontonasal dysplasia. We therefore focused on the effects of segregation within these two embryonic structures. We examined full *Efnb1*$^{+XGFP/\Delta}$ embryos (mediated by β-actin-Cre) as well as NCC-specific ephrin-B1 mosaic *Sox10-Cre*$^{Tg/o}$*; Efnb1*$^{+XGFP/\Delta}$ embryos and palate mesenchyme-specific ephrin-B1 mosaic *Shox2*$^{IresCre/+}$*; Efnb1*$^{+XGFP/\Delta}$ embryos and compared both palatal shelves and FNP to control *Efnb1*$^{+XGFP/lox}$ embryos at E13.5. Control embryos have strong ephrin-B1 expression in the tips of the anterior palatal shelves and lateral FNP, while XGFP is visible in a fine-grained mosaic pattern in each structure (**Figure 16A, A'**; **Figure 17A, A'**). In full *Efnb1*$^{+XGFP/\Delta}$ heterozygotes, large ephrin-B1/GFP expressing and non-expressing patches are apparent in the palatal shelves (**Figure 16B, B'**) and FNP (**Figure 17B, B'**). In these embryos, regions of local dysmorphogenesis correlate with aberrant ephrin-B1 expression boundaries, including smaller and abnormally shaped palatal shelves and bifurcation of the nasal concha.

Neural crest specific mosaic *Sox10-Cre*$^{Tg/o}$*; Efnb1*$^{+XGFP/\Delta}$ embryos also have visible ephrin-B1/GFP positive and negative patches in the palate, which correspond with local dysmorphology of shelf structure including less extension of the palatal shelves (**Figure 16C, C'**). Comparable to full heterozygotes, these embryos also exhibit segregation in the FNP and often have bifurcations of the nasal conchae (**Figure 17C, C'**). This indicates that restricting ephrin-B1-mediated segregation to the NCCs is sufficient to create dysmorphology similar to that seen in full ephrin-B1 heterozygotes and further highlights the importance of segregation in the neural crest.

In palate mesenchyme-specific *Shox2*$^{IresCre/+}$*; Efnb1*$^{+XGFP/\Delta}$ heterozygotes, small ephrin-B1/GFP expressing and non-expressing patches are apparent in the palate mesenchyme (**Figure 16D, D'**). These patches appear smaller than those in full or NCC-specific mosaic

embryos, and the palatal shelves appear normally sized and not as dramatically dysmorphic. However, there is still some local dysmorphogenesis correlating with aberrant ephrin-B1 expression boundaries. No segregation is present in the lateral FNP of these embryos (**Figure 17D, D'**), although some segregation can be seen in the nasal septum and upper lip mesenchyme, where Shox2^{IresCre}-mediated recombination and ephrin-B1 expression overlap. As expected, upon examining the brains of these embryos with Cre-restricted ephrin-B1 heterozygosity, ephrin-B1 mosaicism in NCCs or secondary palate mesenchyme alone does not result in cell segregation in the brain at E13.5 (**Figure 11D-E**). In total, these data demonstrate that ephrin-B1 mediates segregation within the post-migratory NCC-derived mesenchyme in structures key to CFNS pathology and suggest that aberrant ephrin-B1 expression patches may contribute to craniofacial dysmorphology by mediating tissue structure changes at their ectopic boundaries.

Discussion

The results of our analyses illuminate the developmental basis for craniofacial dysmorphogenesis in craniofrontonasal syndrome (CFNS). Using landmark analysis, we have determined the exact locations of facial changes across *Efnb1* mutations from the heterozygous to null state and defined the timing of onset of these changes during embryonic development; the critical period is from E11.5-E14.5, which approximately corresponds to weeks 5-8 in human embryonic development. During this period, both ephrin-B1 null hemizygote and ephrin-B1 mosaic heterozygous embryos demonstrate changes in facial shape relative to control embryos, but the changes are more pronounced in mosaic heterozygous embryos, suggesting that the increased severity seen in heterozygous female CFNS patients is a quantitatively more severe version of the hemizygous phenotype. In addition, we have shown that cell segregation occurs in the post-migratory NCCs that populate the craniofacial mesenchyme at E11.5, which correlates both with the onset of ephrin-B1 expression in these tissues and with the first

changes we observe in facial shape. When restricted to the NCCs or the secondary palate mesenchyme, ephrin-B1 mosaicism drives segregation to generate ectopic expression borders that correlate with local dysmorphology in craniofacial structures. When restricted to neural progenitor cells, ephrin-B1 mosaicism drives segregation independently in the brain, but this does not cause changes in facial shape, indicating that it is ephrin-B1 mosaicism in a different tissue that predominantly drives dysmorphology in CFNS. Future studies will determine the contribution of ephrin-B1 mosaicism and segregation in other tissues to changes in facial shape and the requirement for individual EphB receptors to mediate these changes. To work towards therapeutic strategies for these patients, it will also be essential to investigate whether or not cell segregation can be blocked or reversed, as it appears to hold the key to increased severity in female CFNS patients.

Using *Efnb1*$^{+/\Delta}$ mice, a model for heterozygous CFNS patients, as well as *Efnb1*$^{\Delta/Y}$ mice, their ephrin-B1 null counterparts, we have quantified the nature, severity, and progress of facial dysmorphogenesis during the embryonic days subsequent to NCC migration to populate the facial prominences. Significantly wider and shorter faces in *Efnb1* null mice were noted as early as E11.5 and maintained through E14.5, even as the face continues to develop. Additionally, female heterozygotes displayed more severe dysmorphology than hemizygous males throughout this period. The quantitative characterization of phenotypic changes in these embryos revealed that dysmorphology analogous to CFNS phenotypes seen in humans with *EFNB1* mutations arose very early during facial morphogenesis, including hypertelorism and midfacial hypoplasia, and these phenotypes were more severe in heterozygous females from the earliest stages. This further establishes *Efnb1*$^{+/\Delta}$ mice as a useful system for modeling facial dysmorphogenesis in CFNS and allows for direct connection between *Efnb1* mutation on an inbred background and changes to face shape.

Aberrant ephrin-B1-mediated cell segregation, or “cellular interference,” has long been posited as the causative mechanism for producing craniofacial and skeletal phenotypes in

CFNS patients (Compagni et al., 2003; O'Neill et al., 2016; Twigg et al., 2013; Wieland et al., 2008) (see **Chapter 3**). It has remained difficult, however, to definitively demonstrate the connection between cell segregation and craniofacial dysmorphogenesis. To begin to address this question, it is necessary to understand both when (in developmental time) and where (in relevant tissues to CFNS) cell segregation occurs. We have shown that in addition to an early wave of segregation in the neural plate neuroepithelium, where ephrin-B1 expression is high, a second wave of segregation occurs upon upregulation of ephrin-B1 in NCC-derived craniofacial mesenchyme of the MXP and LNP at E11.5. As dramatic segregation is not apparent in these structures at E10.5, we propose that this segregation is not maintained or established throughout NCC migration, but rather represents a separate segregation event occurring after migration is complete. Furthermore, if ephrin-B1 mosaicism is restricted to postmigratory NCCs of the palate mesenchyme, segregation still occurs in these cells, indicating that later derivatives of NCCs are also subject to ephrin-B1-mediated segregation and suggesting that even more differentiated cell types might possess the potential to undergo this process. Future studies will determine whether aberrant ephrin-B1 expression boundaries, or failure of endogenous boundary maintenance, caused by ephrin-B1 mosaicism contribute to CFNS phenotypes that arise later in development, such as craniosynostosis.

The combination of careful histological and morphometric analyses suggests that the etiology of craniofacial phenotypes in CFNS patients occurs early in development of the face, as aberrant ephrin-B1-mediated segregation begins in post-migratory neural crest cells of the MXP and LNP. Our data represent a first step towards establishing a connection between cell segregation and craniofacial dysmorphogenesis; local changes in craniofacial structures are evident even when ephrin-B1 mosaicism is restricted to NCCs or to the palate mesenchyme, suggesting that later segregation in these cell types contributes to craniofacial phenotypes. We have also shown that although segregation occurs dramatically in neural precursor cells at the neural plate and is present in the brains of *Efnb1*$^{+/\Delta}$ embryos, restriction of ephrin-B1 mosaicism

to neural progenitor cells in *Sox1*$^{Cre/+}$*; Efnb1*$^{+/\Delta}$ embryos does not result in changes to craniofacial structures or changes to face shape, although segregation in the brain remains equally robust in these embryos. Although previous studies have shown that changes to the structure of the brain can alter the shape of the face (Marcucio et al., 2011; Marcucio et al., 2015), we demonstrate that this is not the case for the developmental etiology of craniofacial dysmorphology in CFNS. Further studies will be required to continue investigating the connection between ephrin-B1 mosaicism, cell segregation, and changes in facial shape; in particular, it will be important to determine whether ephrin-B1 mosaicism in NCCs causes differences in facial shape between *Sox10-Cre*$^{Tg/o}$*; Efnb1*$^{+/\Delta}$ and control embryos.

Future experiments will use geometric morphometrics-based analysis to determine whether ephrin-B1 mosaicism specifically in neural crest cells in *Sox10-Cre*$^{Tg/o}$*; Efnb1*$^{+/\Delta}$ embryos creates significant changes in facial shape, thereby shedding light on the tissue origins of craniofacial dysmorphology. In addition, it will be important to determine which EphB receptors are required for signaling that results in both segregation and changes to facial shape. For a better understanding of how cell segregation creates craniofacial dysmorphology, it will also be essential to identify the cellular mechanisms that drive changes in craniofacial structures in response to the presence of aberrant ephrin-B1 boundaries. Finally, given the importance of cell segregation to CFNS and the fact that it is not a fixed event early in development of the neural plate, we are actively working on experiments to block or genetically reverse cell segregation *in vivo*. If this is feasible, these experiments will serve as proof of principle that this cell behavior is dynamic and reversible, and CFNS patients may benefit from molecular therapies to reduce or eliminate segregation in the future.

Materials and Methods

Mouse lines. All animal experiments were performed in accordance with the protocols of the University of California, San Francisco Institutional Animal Care and Use Committee. Mice were

socially housed under a twelve-hour light-dark cycle with food and water *ad libitum*. If single housing was required for breeding purposes, additional enrichment was provided. All alleles used for the experiments herein have been previously described. All mice were backcrossed and maintained on a congenic C57Bl/6J genetic background. *Efnb1^{lox}*, MGI: 3039289 (Davy et al., 2004); *X^{GFP}*, MGI: 3055027 (Hadjantonakis et al., 1998); *β-actin-Cre*, MGI: 2176050 (Lewandoski et al., 1997); *Sox10-Cre*, MGI: 3586900 (Matsuoka et al., 2005); *Shox2^{IresCre}*, MGI: 5567920 (Dougherty et al., 2013); *Sox1^{Cre}*, MGI: 3807952 (Takashima et al., 2007); *ROSA26^{mTmG}*, MGI: 3716464 (Muzumdar et al., 2007). For a full description of genetic crosses used to generate embryos; strain background, sex, and stage of embryos; and numbers of embryos analyzed, please refer to **Table 8**.

Generation of embryos for immunofluorescence analysis of cell segregation. An X-linked beta-actin GFP transgene (XGFP) that demonstrates a fine-grained mosaic pattern of GFP expression after random X chromosome inactivation (XCI) in female embryos (Compagni et al., 2003; Hadjantonakis et al., 1998; Hadjantonakis et al., 2001) was used to visualize XCI as well as cell segregation in all mosaic embryos. Full ephrin-B1 heterozygotes were generated using β-actin-Cre mice. *β-actin-Cre$^{Tg/o}$; X^{GFP}/Y* male mice were crossed to *Efnb1$^{lox/lox}$* female mice to generate both *β-actin-Cre$^{Tg/o}$; Efnb1$^{+XGFP/Δ}$* and *Efnb1$^{+XGFP/lox}$* control embryos. Embryos mosaic for ephrin-B1 expression specifically in the neural crest cell (NCC) lineage were generated using Sox10-Cre mice (Matsuoka et al., 2005), which were crossed to *Efnb1$^{lox/lox}$* female mice to generate both *Sox10-Cre$^{Tg/o}$; Efnb1$^{+XGFP/Δ}$* heterozygous mutant and *Efnb1$^{+XGFP/lox}$* control embryos. Embryos mosaic for ephrin-B1 expression specifically in the palate and limb mesenchyme were generated using Shox2^{IresCre} (Dougherty et al., 2013). *Shox2$^{IresCre/+}$; X^{GFP}/Y* male mice were crossed to *Efnb1$^{lox/lox}$* female mice to generate both *Shox2$^{IresCre/+}$; Efnb1$^{+XGFP/Δ}$* heterozygous mutant and *Efnb1$^{+XGFP/lox}$* control embryos. Embryos mosaic for ephrin-B1

expression in early neural progenitor cells were generated using $Sox1^{Cre}$, which drives recombination in neural plate neuroepithelial cells at E8.5 (Takashima et al., 2007). *$Sox1^{Cre/+}$; X^{GFP}/Y* male mice were crossed to *$Efnb1^{lox/lox}$* female mice to generate both *$Sox1^{Cre/+}$; $Efnb1^{+XGFP/\Delta}$* heterozygous mutant and *$Efnb1^{+XGFP/lox}$* control embryos.

Morphometrics specimen and data acquisition. Embryos mosaic for ephrin-B1 expression in all tissues (full heterozygotes) were collected at embryonic days E11.5, E12.5, E13.5, and E14.5 from crosses of *$Efnb1^{lox/lox}$* mice and *β-actin-Cre* mice. This sample includes hemizygote males (*$Efnb1^{\Delta/y}$*), heterozygote females (*$Efnb1^{+/\Delta}$*), and control specimens that were sometimes littermates of affected specimens and sometimes came from separate crosses of *β-actin-Cre* and C57BL/6J mice to control for possible effects of Cre transgene insertion. Embryos were fixed in a mixture of 4% PFA and 5% glutaraldehyde in PBS. After approximately an hour soaking in Cysto-Conray II (Liebel-Flarsheim Canada), micro-computed tomography (μCT) images of embryo heads were acquired with a Scanco μ35 at the University of Calgary with 45kV/177μA for images of 0.012 mm^3 voxel size. All facial landmarks were collected on minimum threshold based ectodermal surfaces (downsampled x2) from the μCT images in Amira (FEI). Because of striking changes in the morphology of the face between E11.5 and E14.5, two different landmark sets were required to quantify facial shape across this period. Previously defined ectodermal landmarks (Percival et al., 2014), minus those previously identified as problematic (i.e. landmarks 2, 7(24), 10(27), 13(30), 17(34), 18(35), 21(38), 22), were used to quantify facial form of E11.5 embryos. A modified and reduced version of this published landmark set was developed to allow for comparison of ectodermal facial form between E12.5 and E17.5, which we used to quantify facial form of our E12.5, E13.5, and E14.5 embryos.

Morphometric analysis E12.5-E14.5. Procrustes superimposition was performed on landmarks collected from E12.5, E13.5, and E14.5 specimens to align each specimen and remove scale from analysis. Superimposition and subsequent geometric morphometric analysis was completed using geomorph (Adams and Otárola-Castillo, 2013) in R Statistical Software (R Developmental Core Team, 2008). Procrustes ANOVA analysis, with permutation-based tests for significance, was used to determine whether size (numeric; centroid size), genotype (factor; *+/Δ*, *Δ/y*, *control*), age (numeric; 12.5, 13.5, 14.5) and their interactions have a significant influence on facial shape (α=0.05). We visualized the effects of $Efnb1^{+/\Delta}$ and $Efnb1^{\Delta/y}$ genotypes on facial shape by plotting differences between genotype specific shapes estimated from the Procrustes ANOVA multivariate linear model (assuming E14.5 age and average E14.5 centroid size). Given the strong changes in facial shape that normally occur between E12.5 and 14.5, we completed a multivariate regression of facial shape on centroid size to estimate allometry and used the rescaled residuals of that regression as "allometry corrected" coordinates for further analysis. Principal components analyses of coordinate values were completed both before and after "allometry correction" to visualize patterns of specimen clustering along major axes of facial shape covariation within the sample. Procrustes distances between mean control and affected facial shapes were calculated from residual landmark coordinates at each age to determine whether genotypes displayed significantly different facial shapes. Significance was determined by comparing Procrustes distances to 95% age-specific confidence intervals that were estimated with 1000 permutations of distances between two randomly selected control groups of 15 specimens.

Morphometrics analysis E11.5. Procrustes coordinate based analyses were completed for E11.5 facial landmarks in much the same way they were performed for the E12.5-14.5 sample. The major difference is that all analyses were completed without allometry correction, because only one age was under analysis. The Procrustes distance values, Procrustes ANOVA output

values, and other values are not directly comparable between the E11.5 and the E12.5-E14.5 analysis, because a different set of landmarks undergoing independent Procrustes superimpositions were completed for each age group. However, comparisons of the type of facial shape changes associated with genotype within each age group are valuable to determine if affected phenotypes like those noted in older specimens exist as early as E11.5.

Immunofluorescence. Embryos were fixed in 4% PFA in PBS, dehydrated through sucrose, embedded in OCT, and frozen in dry ice/ethanol. 12 μm sections were cut using an HM550 (Thermo Scientific) or a CM1900 (Leica) cryostat. Slides were washed with PBS, blocked in 5% normal donkey serum (Jackson ImmunoResearch) and 0.1% Triton-X-100 in PBS, incubated in primary antibody overnight at 4°C, washed with PBS, and incubated in secondary antibody at room temperature (for antibody information, please refer to **Table 6**). Slides were counterstained in DAPI (Millipore) in PBS and coverslips were mounted on slides using Aquamount (Thermo Scientific) for imaging. Images were obtained on an Axio Imager.Z2 upright microscope using an AxioCamMR3 camera and AxioVision Rel.4.8 software (Zeiss).

Table 3. Significant influences on facial shape at E11.5

	Df	SS	MS	Rsq[c]	F	Z	Pr(>F)
Size[a]	1	0.141	0.141	0.229	24.719	6.274	0.001*
Genotype[b]	2	0.069	0.034	0.111	6.005	5.970	0.001*
Residuals	74	0.406	0.006				
Total	77	0.615					

[a]Output of a multivariate linear ANOVA to estimate the influence of overall size (estimated as centroid size) on facial shape.
[b]Output of a multivariate linear ANOVA to estimate the influence of genotype (as a factor) on facial shape.
[c]Rsq provides an estimate of how much facial shape variance a given covariate explains.
* indicates a significant effect on facial shape, as calculated using a permutation test.

Table 4. Significant influences on facial shape from E12.5-E14.5

	Df	SS	MS	Rsq[e]	F	Z	Pr(>F)
Size[a]	1	1.706	1.706	0.772	1083.475	7.158	0.001*
Genotype[b]	2	0.145	0.072	0.066	46.005	13.728	0.001*
Age[c]	1	0.011	0.011	0.005	7.287	9.243	0.001*
Genotype:Age[d]	2	0.016	0.008	0.007	5.207	10.914	0.001*
Residuals	210	0.331	0.002				
Total	216	2.210					

[a]Output of a multivariate linear ANOVA to estimate the influence of overall size (estimated as centroid size) on facial shape.
[b]Output of a multivariate linear ANOVA to estimate the influence of genotype (as a factor) on facial shape.
[c]Output of a multivariate linear ANOVA to estimate the influence of age (as continuous) on facial shape across E12.5-E14.5 specimens.
[d]Genotype:Age is the interaction effect of genotype and age.
[e]Rsq provides an estimate of how much facial shape variance a given covariate explains.
* indicates a significant effect on facial shape, as calculated using a permutation test.

Table 5. Age-specific comparisons of the Procrustes distances between the mean shape of affected and control genotypes, after accounting for allometry

		Efnb1 genotype	
	Control (95% CI)	***Δ/y*[a]**	***+/Δ*[a]**
E11.5^	0.07-0.18^	0.22*^	0.32*^
E12.5	0.04-0.09	0.15*	0.23*
E13.5	0.03-0.06	0.19*	0.28*
E14.5	0.03-0.06	0.18*	0.29*

[a]Higher values represent a greater difference in facial shape, a proxy for severity of dysmorphology.

* indicates a significantly different facial shape than control, based on the 95% control confidence intervals produced by bootstrapping the control sample.

^ indicates that E11.5 Procrustes distance values cannot be directly compared to E12.5-E14.5 values, because they are based on a different landmark set and separate Procrustes superimposition. However, the pattern of the ordering of Procrustes distance values within ages can be compared and show similar patterns of significance.

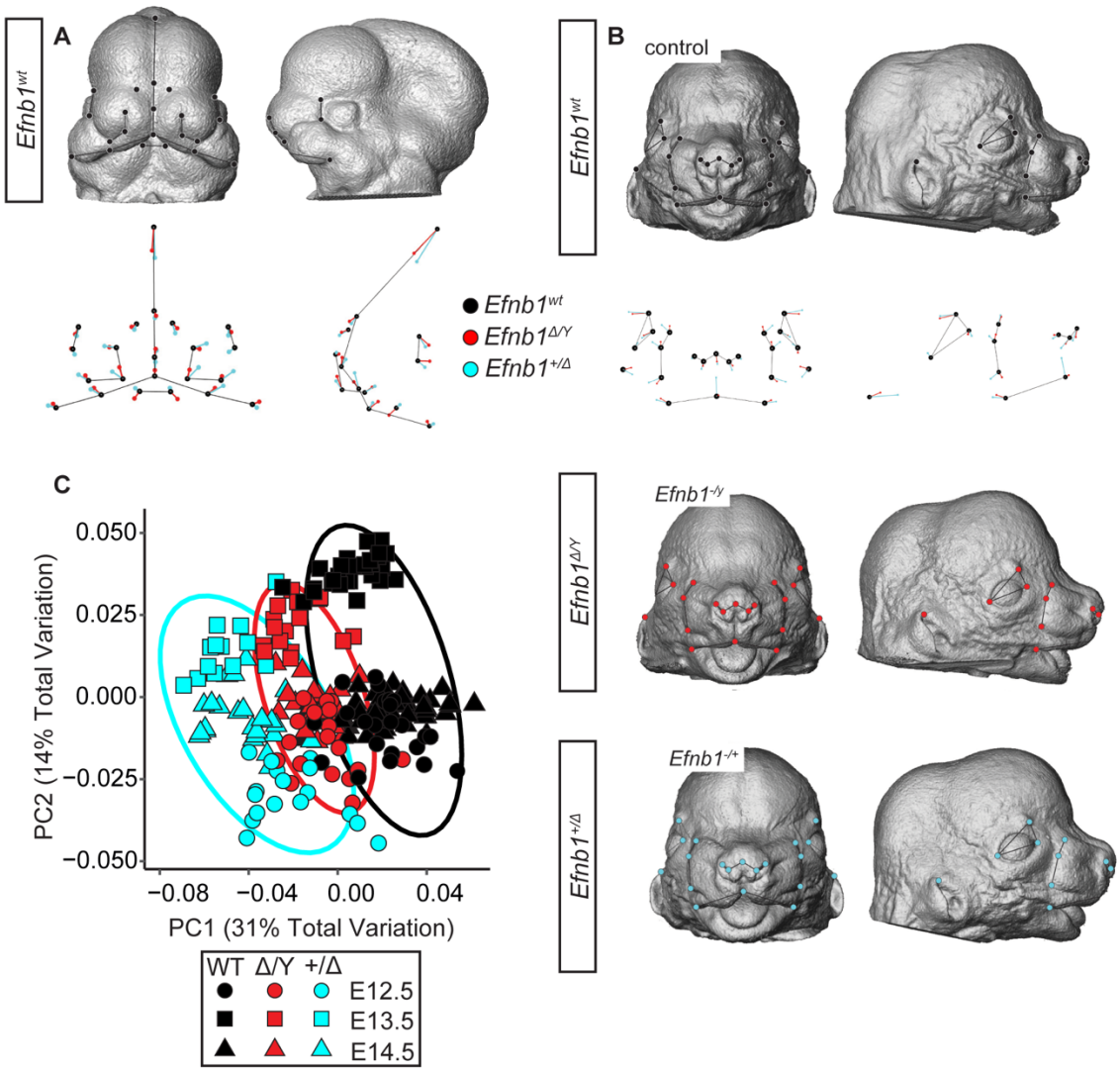

Figure 10. Ephrin-B1 has a significant effect on embryonic facial shape from E11.5 to E14.5 that mirrors CFNS. (A) A representative control E11.5 specimen surface from the anterior and lateral views, with landmarks identified. Plot of the predicted facial shape landmark positions for control (black points), *Efnb1*$^{\Delta/Y}$ (red points), and *Efnb1*$^{+/\Delta}$ (cyan points) from the anterior and lateral views. The lengths of these shape difference vectors are magnified three times to allow for easy comparison of directions of shape changes associated with the two affected genotypes. Thin black lines are placed for anatomical reference. **(B)** Specimens plotted along PC1 and PC2 of facial shape variation residuals of the multivariate regression of facial shape on size. These residuals can be interpreted as facial shape coordinates after accounting for a common allometric component associated with growth. Control, *Efnb1*$^{\Delta/Y}$, and *Efnb1*$^{+/\Delta}$ clusters are shown as black, red, and cyan symbols, respectively; circles indicate E12.5, squares indicate E13.5, and triangles indicate E14.5. **(C)** Representative control, *Efnb1*$^{\Delta/Y}$, and *Efnb1*$^{+/\Delta}$ E14.5 specimen surfaces from the anterior and lateral views, with landmarks superimposed on all three genotypes. Plots of the predicted facial shape landmark positions are also shown from the anterior and lateral views: control (black points), *Efnb1*$^{\Delta/Y}$ (red points), and *Efnb1*$^{+/\Delta}$ (blue points). The lengths of these shape difference vectors are magnified three times

to allow for easy comparison of directions of shape changes associated with the two affected genotypes. Thin black lines are placed for anatomical reference.

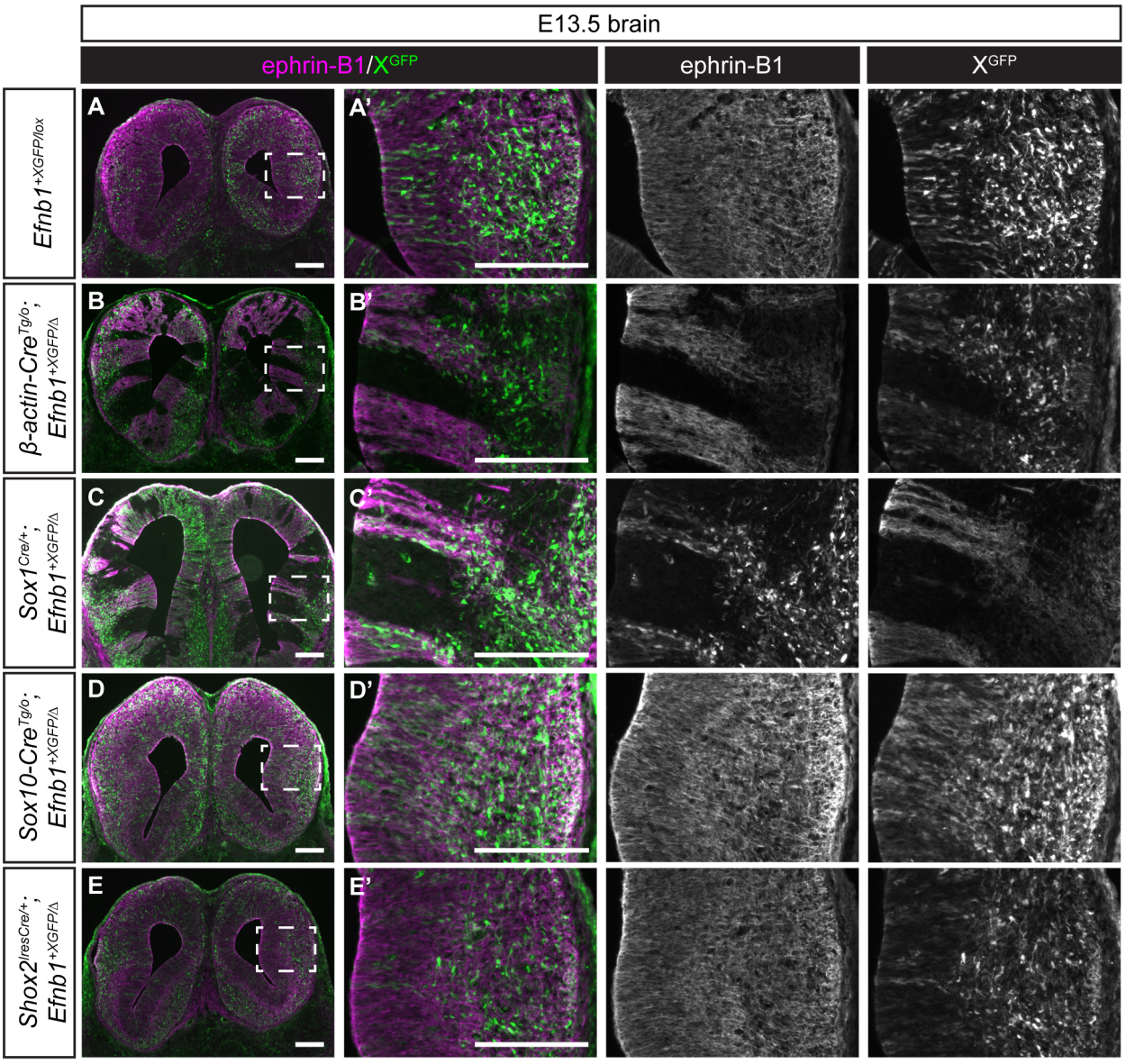

Figure 11. Ephrin-B1 mosaicism in neural progenitors produces cell segregation in the brain, whereas neural crest-specific mosaicism does not. (A, A') Control embryos demonstrate high ephrin-B1 expression in the brain, with no cell segregation as shown by a fine-grained mosaic pattern of XGFP expression. **(B, B')** In embryos with ubiquitous mosaicism for ephrin-B1 expression mediated by β-actin-Cre, cell segregation is evident throughout the brain as large patches of ephrin-B1 and GFP expression. **(C, C')** Generation of ephrin-B1 mosaicism specifically in neural progenitor cells using $Sox1^{Cre}$ results in dramatic segregation throughout the brain at E13.5, visible as large patches of ephrin-B1 and GFP expression. However, ephrin-B1 mosaicism generated in neural crest cells using Sox10-Cre **(D, D')** or in post-migratory neural crest cells of the palate mesenchyme using $Shox2^{IresCre}$ **(E, E')** does not lead to segregation in the brain, as demonstrated by an evenly distributed pattern of XGFP expression. *Scale bars, 200 μm*.

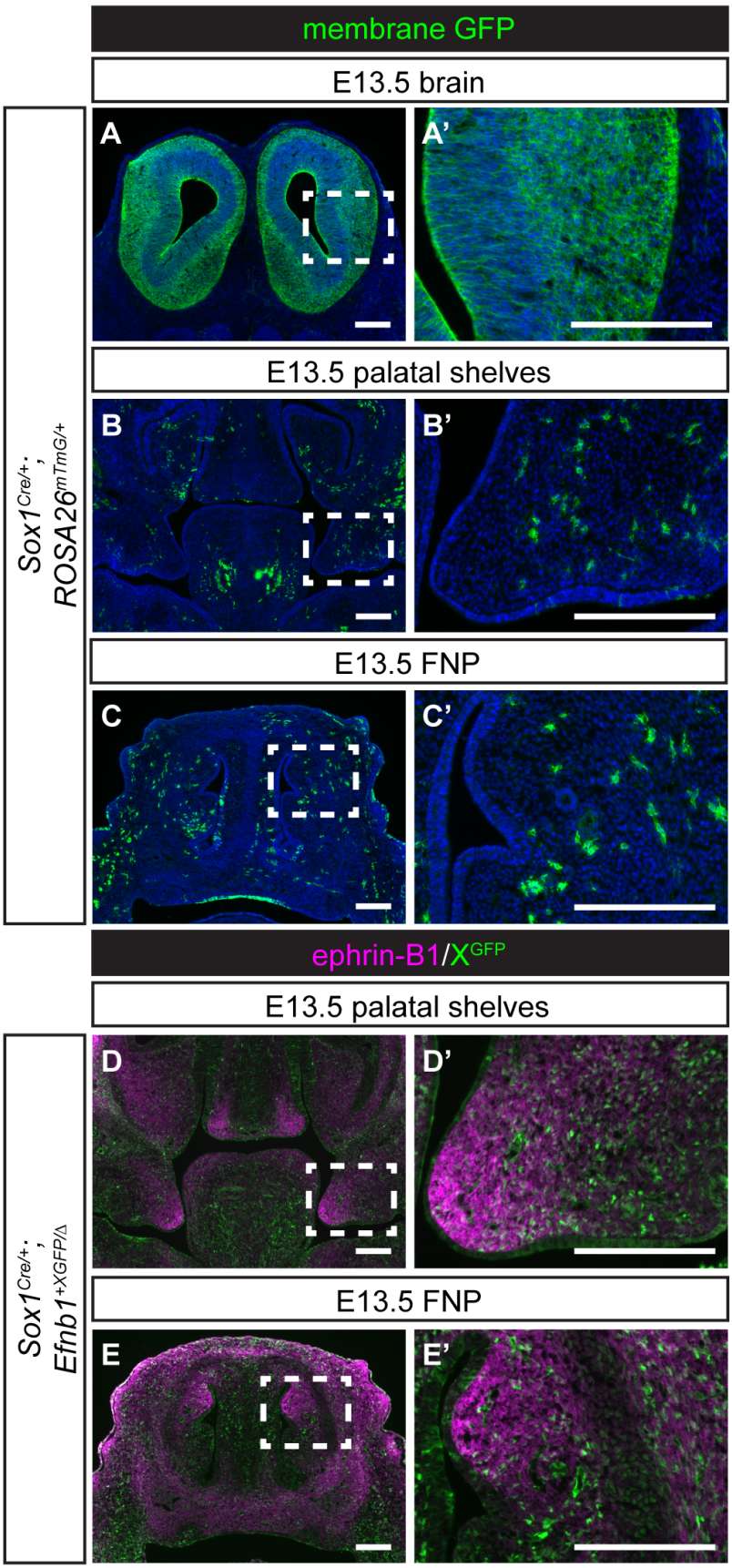
membrane GFP
E13.5 brain
A
A'
E13.5 palatal shelves
B
B'
E13.5 FNP
C
C'
Sox1Cre/+; ROSA26mTmG/+
ephrin-B1/XGFP
E13.5 palatal shelves
D
D'
E13.5 FNP
E
E'
Sox1Cre/+; Efnb1+XGFP/Δ

Figure 12. Ephrin-B1-mediated cell segregation in the brain does not affect development of craniofacial structures. (A, A') Recombination of the *ROSA26* locus in Sox1^{Cre}; *ROSA26*$^{mTmG/+}$ embryos leads to widespread membrane GFP expression throughout the brain at E13.5, but minimal membrane GFP expression in **(B, B')** anterior palatal shelves or **(C, C')** anterior frontonasal prominence (FNP). **(D, D')** Ephrin-B1 mosaicism in early neural progenitor cells mediated by Sox1^{Cre} does not drive segregation in neural crest-derived craniofacial structures such as the anterior palatal shelves or **(E, E')** FNP. Ephrin-B1 expression and craniofacial morphology appear normal in these embryos, indicating that neural progenitor cell segregation is an independent process. *Scale bars, 200 μm*.

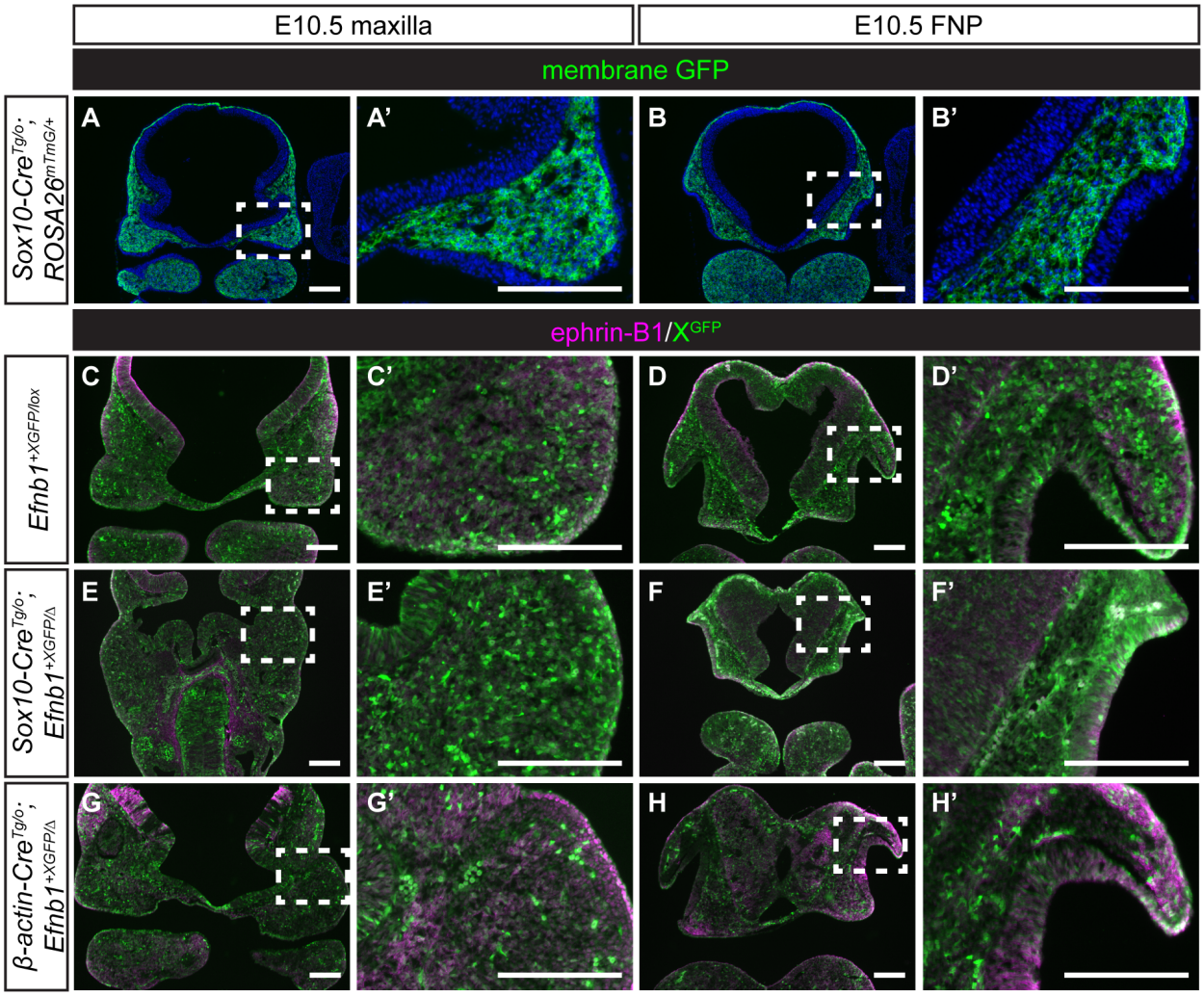

Figure 13. Craniofacial cell segregation first occurs in the post-migratory neural crest-derived mesenchyme, correlating with the onset of upregulation of ephrin-B1. (A, A') Sox10-Cre drives recombination in the maxillary prominences and **(B, B')** frontonasal prominence (FNP) of *Sox10-Cre*$^{Tg/o}$*; ROSA26*$^{mTmG/+}$ embryos at E10.5. **(C, C')** *Efnb1*$^{+XGFP/lox}$ control maxillary prominences and **(D, D')** FNP demonstrate a fine-grained mosaic pattern of XGFP expression at E10.5. Ephrin-B1 expression is not strong in the maxillae but has begun to be upregulated in the FNP at this stage. **(E, E')** Likewise, neural crest-specific *Sox10-Cre*$^{Tg/o}$*; Efnb1*$^{+XGFP/\Delta}$ heterozygous embryos demonstrate a fine-grained mosaic pattern of XGFP expression in the maxillary prominences at E10.5, indicating that segregation is not carried through from migratory NCCs. **(F, F')** The FNP of E10.5 *Sox10-Cre*$^{Tg/o}$*; Efnb1*$^{+XGFP/\Delta}$ heterozygous embryos show a small amount of segregation, visible as patches of ephrin-B1/GFP expression and non-expression, likely because ephrin-B1 has begun to be expressed in the FNP at this stage. **(G, G')** The maxillae of full ephrin-B1 heterozygotes (mediated by β-actin-Cre) are also not segregated at E10.5, but segregation can be seen in the neural tissues of these embryos. **(H, H')** Segregation is visible in the developing LNP and in neural tissues of full ephrin-B1 heterozygotes.

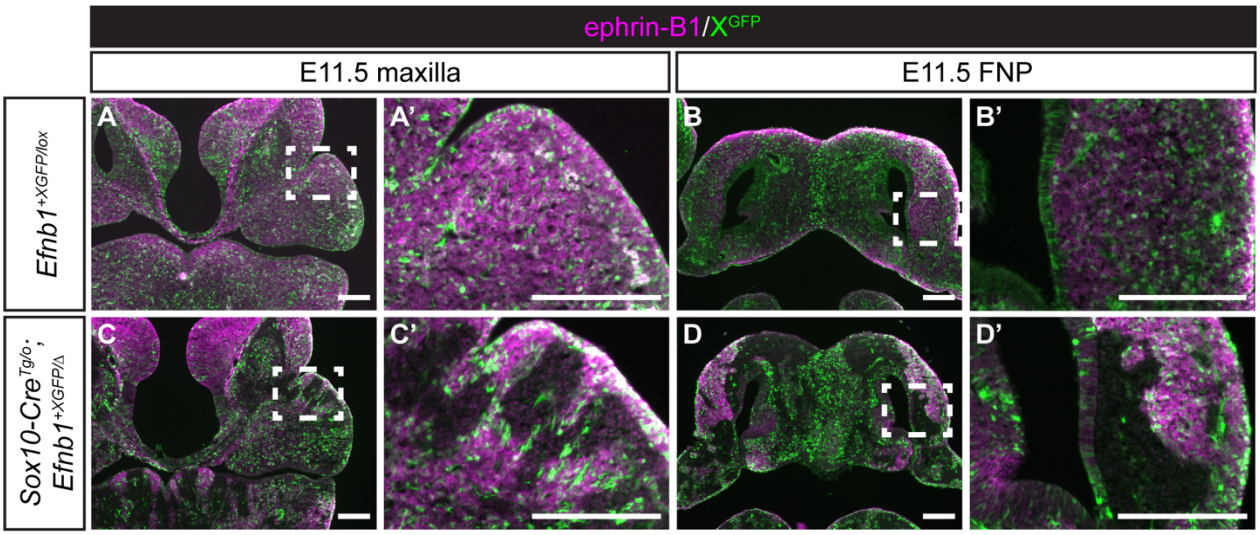

Figure 14. Neural crest cells mosaic for ephrin-B1 expression undergo cell segregation in craniofacial primordia. (A, A') At E11.5, *Efnb1*$^{+XGFP/lox}$ control embryos demonstrate a fine-grained mosaic pattern of XGFP expression, and ephrin-B1 expression is strong in both the maxillary prominences and **(B, B')** the lateral FNP. **(C, C')** *Sox10-Cre*$^{Tg/o}$*; Efnb1*$^{+XGFP/\Delta}$ embryos with ephrin-B1 mosaicism specifically in NCCs show dramatic cell segregation in the maxillary prominences and **(D, D')** the lateral FNP, indicating that NCCs are capable of undergoing ephrin-B1-mediated segregation resulting in aberrant ephrin-B1 expression patterns in craniofacial mesenchyme. *Scale bars, 200 μm*.

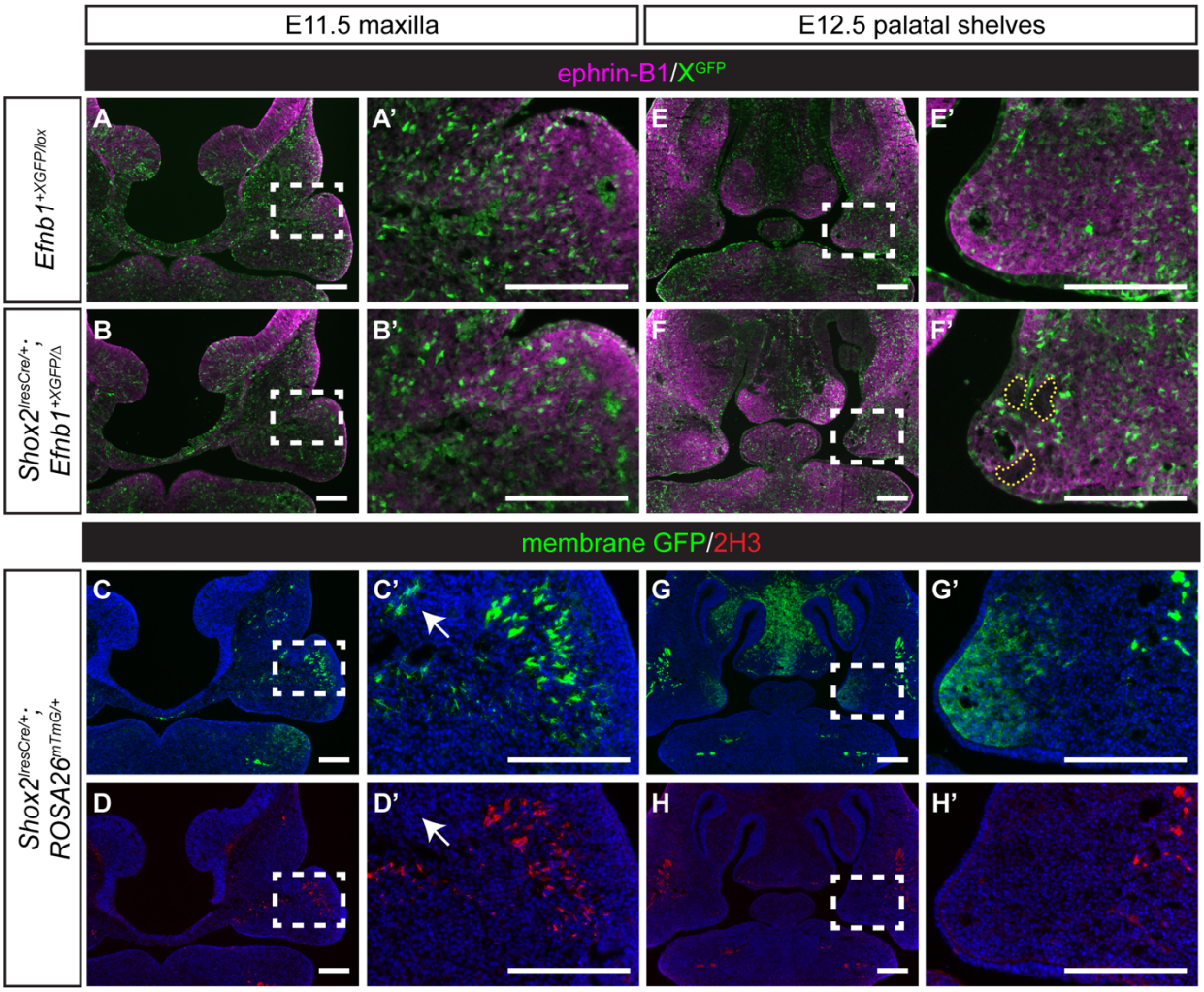

Figure 15. Palate-specific ephrin-B1 mosaicism results in cell segregation in the anterior palate mesenchyme after E11.5. (A, A') At E11.5, the maxillae of *Efnb1*$^{+XGFP/lox}$ control and **(B, B')** *Shox2*$^{IresCre/+}$*; Efnb1*$^{+XGFP/\Delta}$ heterozygous embryos are indistinguishable; both genotypes demonstrate a fine-grained mosaic pattern of XGFP expression in the maxillary prominences, indicating that no cell segregation has taken place. **(C, C')** Shox2^{IresCre} drives minimal recombination in the maxillary prominences of *Shox2*$^{IresCre/+}$*; ROSA26*$^{mTmG/+}$ embryos at E11.5. **(D, D')** Most membrane GFP-expressing cells also express neurofilament (2H3) and are likely nerve cells of the maxillary trigeminal ganglion; only a few mesenchymal cells have undergone recombination at this stage (white arrows). **(E, E')** At E12.5, control palatal shelves show a fine-grained mosaic pattern of XGFP expression. **(F, F')** Small patches of ephrin-B1/XGFP expressing and non-expressing cells are visible in the palatal shelves of *Shox2*$^{IresCre/+}$*; Efnb1*$^{+XGFP/\Delta}$ heterozygous embryos at E12.5, demonstrating that post-migratory neural crest cells are also subject to segregation mediated by ephrin-B1 mosaicism. **(G, G')** By E12.5, *Shox2*$^{IresCre/+}$*; ROSA26*$^{mTmG/+}$ embryos express membrane GFP in the palatal shelf mesenchyme as well as **(H, H')** in the nerve cells of the maxillary trigeminal ganglion. *Scale bars, 200 μm*.

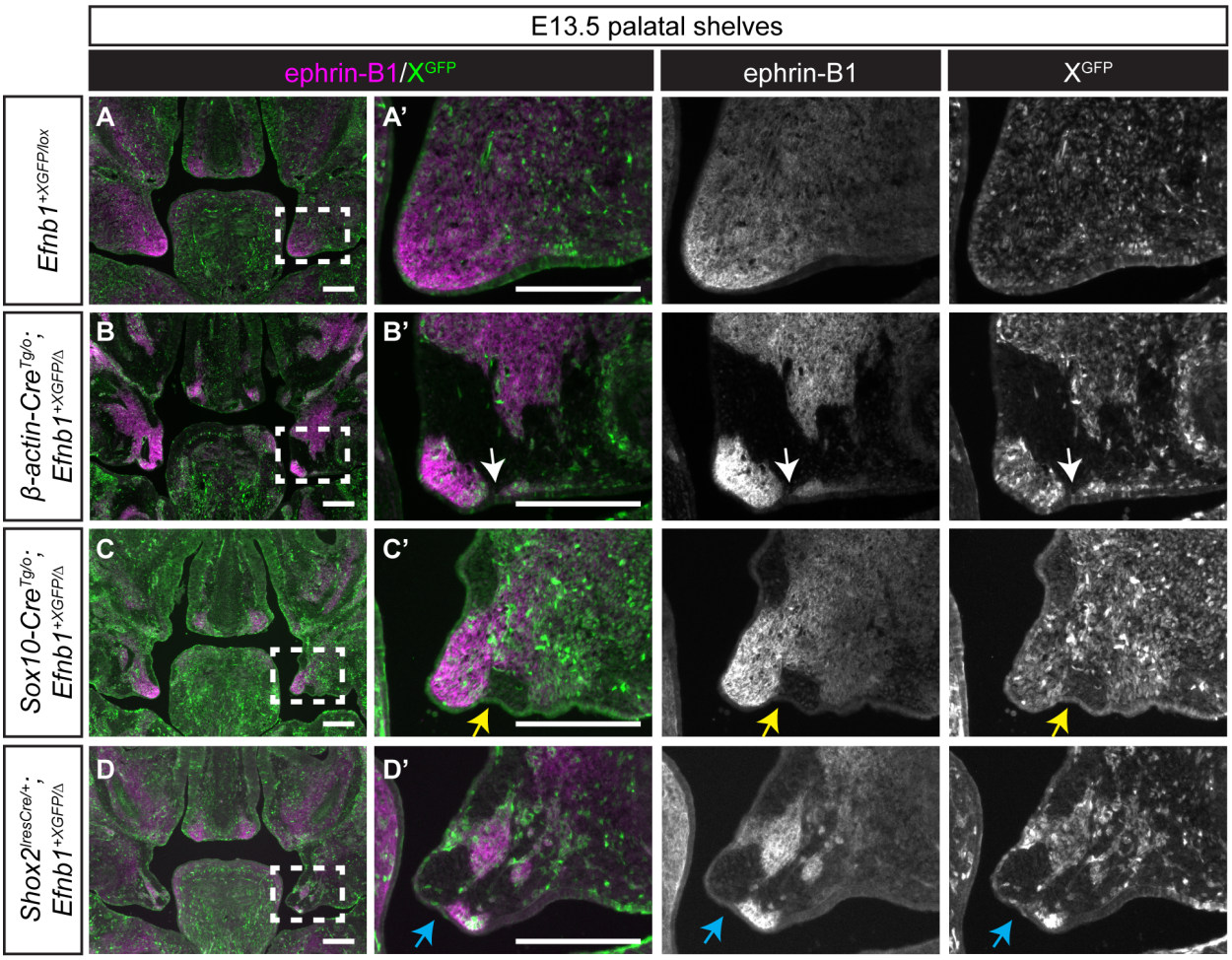

Figure 16. Post-migratory neural crest cell segregation correlates with local dysmorphology in the secondary palate. (A, A') Ephrin-B1 protein is strongly expressed in the anterior-middle palatal shelves. Evenly distributed XGFP expression in control *Efnb1*$^{+XGFP/lox}$ embryos indicates that no cell segregation has occurred. **(B, B')** Cell segregation is visible in the palatal shelves of full ephrin-B1 heterozygotes (mediated by β-actin-Cre) as large patches of ephrin-B1 and GFP expression in these structures. The palatal shelves are smaller and dysmorphic, with changes in shape occurring at boundaries between ephrin-B1 expressing and non-expressing domains (white arrow). **(C, C')** Generation of ephrin-B1 mosaicism specifically in neural crest cells using Sox10-Cre results in dramatic cell segregation in the palatal shelves, which are smaller and dysmorphic, with regions of dysmorphogenesis correlating with ephrin-B1 expression boundaries (yellow arrow). **(D, D')** Ephrin-B1 mosaicism in Shox2^{IresCre}-expressing cells results in cell segregation in the palatal shelves, which express both ephrin-B1 and Shox2. Areas of dysmorphogenesis are visible at the interface between ephrin-B1 expression and non-expression domains (blue arrow). *Scale bars, 200 μm*.

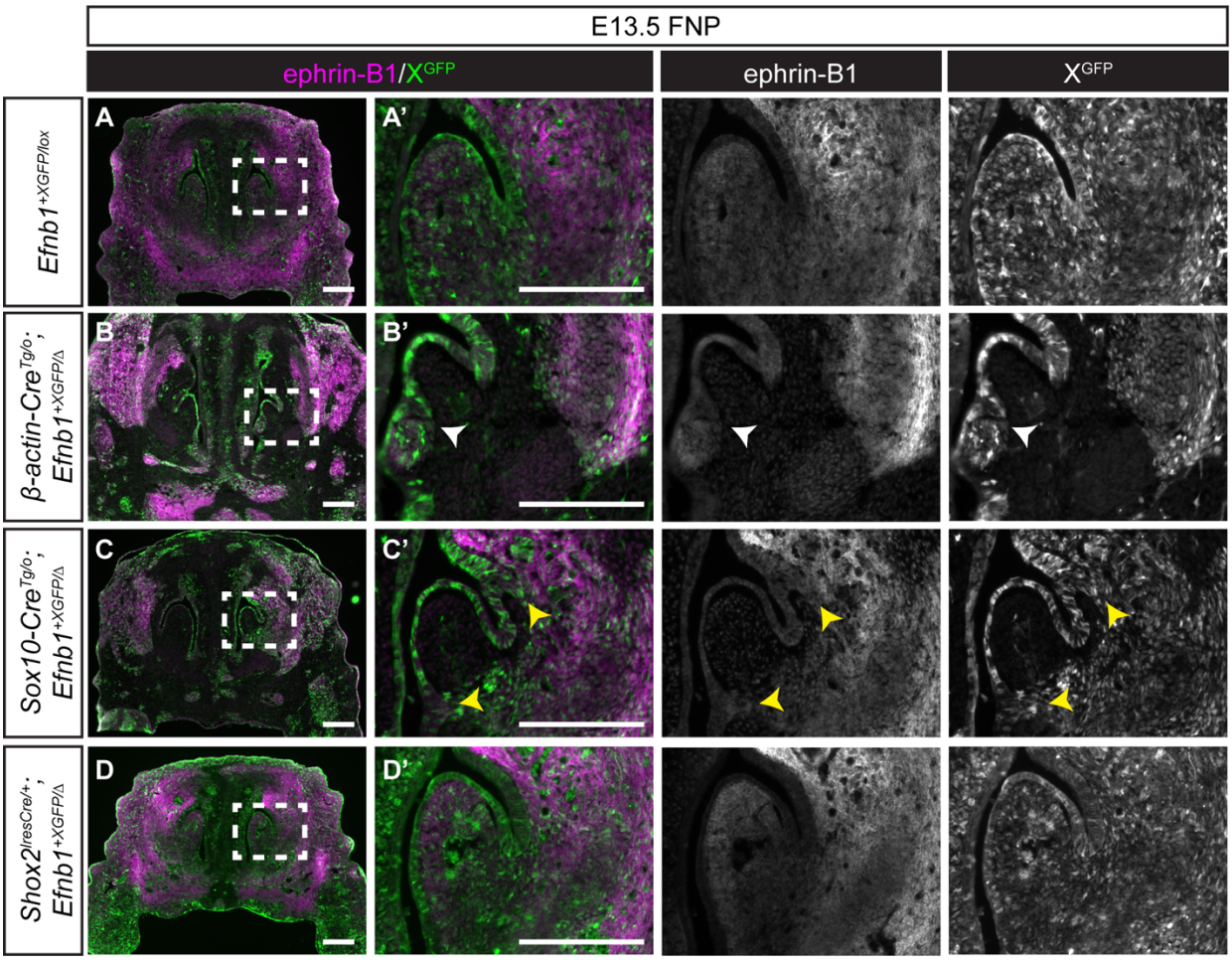

Figure 17. Post-migratory neural crest cell segregation correlates with dysmorphology in the nasal conchae of the frontonasal prominence. (A, A') In frontal sections of control *Efnb1*$^{+XGFP/lox}$ embryos at E13.5, ephrin-B1 protein expression is strong in the LNP lateral to the nasal concha of the anterior frontonasal prominence (FNP). XGFP expression is uniformly distributed in a mosaic pattern, indicating that random X inactivation has taken place, but no cell segregation is evident. **(B, B')** In embryos with ubiquitous mosaicism for ephrin-B1 expression mediated by β-actin-Cre, cell segregation is evident throughout the anterior FNP, and bifurcation of the nasal concha occurs at an aberrant ephrin-B1 expression boundary (white arrowhead). **(C, C')** Generation of ephrin-B1 mosaicism specifically in neural crest cells using Sox10-Cre results in cell segregation visible throughout the anterior FNP and bifurcation of the nasal concha visible at ephrin-B1 expression boundaries (yellow arrowhead). **(D, D')** Restriction of ephrin-B1 mosaicism to post-migratory neural crest cells using Shox2^{IresCre} does not cause cell segregation or dysmorphology in the nasal concha of the anterior FNP, as Shox2 is not expressed in this region. *Scale bars, 200 μm*.

CHAPTER 5. Mechanisms of ephrin-B1 *cis* regulation of EphB receptor signaling

Summary

Much of our perception of the mechanisms of Eph/ephrin signaling is based on the situation in which binding of an ephrin in one cell to an Eph receptor in an adjacent cell results in bidirectional signaling between the cells. Reciprocal expression patterns of Eph receptors and ephrins can be observed in some regions of the developing embryo, such as the brain and spinal cord, somites, and limb buds, reinforcing the concept that *trans* signaling occurs across Eph/ephrin expression boundaries to achieve downstream functions. However, ephrin-B1, a signaling pathway member important for maintenance of normal tissue boundaries and associated with pathogenic boundary formation in congenital craniofacial disease, is often coexpressed with its receptors EphB2 and EphB3 during craniofacial development. Generally, it remains mysterious how coexpression impacts signaling differently from complementary expression. During axon guidance, coexpression of ephrin-As and EphA receptors modulates EphA activation in response to external stimuli, a process known as *cis* inhibition. *Cis* inhibition has not been reported for B-type ephrins, and it is not known how *cis*-expression affects normal ephrin-B1-EphB signaling outcome or aberrant ephrin-B1 boundary formation in craniofacial disease. Here, we demonstrate that ephrin-B1 does not inhibit EphB receptors *in cis* as described for A-type ephrins. Rather, coexpression of ephrin-B1 with EphB receptors regulates signaling outcome through desensitization of EphB-expressing cells by receptor downregulation resulting from active signaling within a tissue. This finding expands our understanding of differences in signaling mechanisms utilized by A- and B-type ephrins and may shed light on the significance of reciprocal ephrin/EphB protein expression patterns during development.

Introduction

Defects in normal boundary formation during embryonic development result in malformations and congenital disease, and understanding the underlying mechanisms will improve our knowledge of these conditions. Congenital craniofacial diseases are among the

most common birth defects, and improved understanding at the cellular and molecular levels will be a key step toward developing new treatment strategies. Craniofrontonasal syndrome (CFNS) is an X-linked disorder caused by loss of function mutations in *EFNB1* that affect multiple aspects of craniofacial, neurological, and skeletal development (Twigg et al., 2004; Wieland et al., 2004). Unlike typical X-linked conditions, heterozygous females are severely affected, but hemizygous males are only mildly affected. Targeted mutagenesis of *Efnb1* in mice leads to some of the same phenotypes, including increased severity in heterozygous females (Bush and Soriano, 2010; Compagni et al., 2003; Davy et al., 2004). This unusual inheritance pattern is caused by mosaicism for ephrin-B1 expression after random X inactivation (Wieacker and Wieland, 2005), and mosaicism is key to increased severity: rare, severely affected male CFNS patients have somatic mosaic mutations in *EFNB1* (Twigg et al., 2013).

Ephrin-B1 is a member of the Eph/ephrin family of signaling molecules, which are the largest family of receptor tyrosine kinases in mammals (Kullander and Klein, 2002). Ephs and ephrins are separated into two classes: ephrin-As are membrane-bound through a GPI anchor, and ephrin-Bs are transmembrane molecules with a cytoplasmic tail. Although there is some overlap in binding affinity between the two classes (Himanen et al., 2004), ephrin-B1 solely uses EphBs as its signaling partners (Davis et al., 1994; Orioli et al., 1996). Ephrins activate forward signaling through Eph receptors in neighboring cells (signaling *in trans*) by binding to the ligand-binding domain of the receptor and initiating receptor oligomerization, tyrosine phosphorylation, and recruitment of downstream signaling partners. Eph/ephrin signaling plays an important role in developmental boundary formation and tissue self-organization, essential processes that require signaling between adjacent cells and often involve segregation between different cell types (Fagotto, 2014) (see **Chapter 2**). Complementary expression of Ephs and ephrins *in vivo* can restrict cell intermingling in the zebrafish hindbrain (Xu et al., 1999) and the mouse limb bud (Compagni et al., 2003; Davy et al., 2004). Expression of an Eph receptor in animal cap cells from one zebrafish embryo and an ephrin in animal cap cells from another restricts intermingling

of cells from the two animal caps (Mellitzer et al., 1999), and mixing a population of cells expressing an Eph with a population of cells expressing an ephrin results in segregation of the two populations in culture (Poliakov et al., 2008). Many of these processes have been attributed to bidirectional signaling across the boundary between populations of cells that reciprocally express Eph receptors and ephrins.

In *Efnb1*$^{+/-}$ mice, ephrin-B1 mosaicism leads to segregation of ephrin-B1 expressing and non-expressing cells in neural plate neuroepithelial cells (O'Neill et al., 2016) (see **Chapter 3**), neural crest cells, and neural crest-derived craniofacial mesenchyme (see **Chapter 4**). Ectopic boundaries between ephrin-B1 expression and non-expression domains generated by cell segregation correlate with craniofacial dysmorphology, providing an explanation for how mosaicism could have phenotypic consequences in CFNS (see **Chapter 4**). We hypothesize that defects in Eph/ephrin-mediated boundary formation underlie CFNS, but the mechanisms by which ephrin-B1-mediated cell segregation forms ectopic boundaries remain incompletely understood. In addition, a wide variety of mutations in ephrin-B1, including intronic mutations, have been discovered in different families (Twigg et al., 2004; Twigg et al., 2006); although these mutations are assumed to result in loss of protein function, not all mutations have been individually characterized. It is therefore possible that some CFNS-causing mutations could be hyper- or hypomorphic alleles that result in changes to ephrin-B1 expression, localization, or binding to the EphB receptor. This raises the question of whether differences in ephrin-B1 expression level, as opposed to presence and absence, may also result in cell segregation and phenotypic consequences. Ephrin-B1 expression levels have not been directly analyzed in human CFNS patients, but several individuals mosaic for genetic duplications of *EFNB1* with severe craniofacial phenotypes have been identified (Babbs et al., 2011; Baker et al., 2010; Evers et al., 2014), suggesting that mosaicism for differences in expression level of ephrin-B1 may cause craniofacial dysmorphology.

In addition to interacting with the canonical ligand-binding domain of the Eph receptor in an adjacent cell (signaling *in trans*), ephrins expressed *in cis* (in the same cell) with Eph receptors can repress their signaling, a process termed "*cis* inhibition." *Cis*-expression of ephrin-As with EphA receptors allows fine control of EphA receptor activation in migrating axons, and the resulting precise signaling response accurately defines the correct axon termination zone (Carvalho et al., 2006; Hornberger et al., 1999). Changing the *cis*-expression of ephrin-As disrupts the magnitude of the EphA signaling response and leads to changes in growth cone collapse (Carvalho et al., 2006; Hornberger et al., 1999), demonstrating that *cis* inhibition has functional significance in essential cellular processes. For example, expression of ephrin-A5 *in cis* with EphA3 in the growth cone of a retinal axon reduces the collapse response of the axon to exogenous ephrin-A5-Fc applied *in trans* (Carvalho et al., 2006). In cell culture models, coexpression of ephrin-A5 with EphA3 reduces EphA3 tyrosine phosphorylation, which is used as a measure of receptor activation (Carvalho et al., 2006). EphA receptors have been proposed to interact with ephrin-As *in cis* using their membrane-proximal fibronectin type III domain, a distinct domain from the ligand-binding domain used for *trans* interactions (Carvalho et al., 2006), but *cis* interactions have also been reported to require the canonical ligand-binding domain (Yin et al., 2004). In addition to the topographic mapping of retinal axons to the tectum, *cis* inhibition regulates other forms of axon guidance, such as that of spinal motor axons to the limb (Gatto et al., 2014; Kao and Kania, 2011; Kao et al., 2012). Binding of ephrins to Ephs *in cis* has also been demonstrated at the synapse (Antion et al., 2010) and in cancer cell lines (Falivelli et al., 2013), suggesting that *cis* inhibition could be an important general feature of Eph/ephrin signaling.

Although *cis* inhibition of EphA receptors by ephrin-As has been demonstrated in several contexts, it is not known whether ephrin-Bs participate in *cis* inhibition of EphB receptors. Furthermore, this alternative Eph/ephrin signaling mode has not been tested in the context of developmental boundary formation; it has been generally accepted that complementary

expression of Eph receptors and ephrins in adjacent compartments restricts signaling to the boundary between them (Gale et al., 1996; Kania and Klein, 2016; Kullander and Klein, 2002). However, EphB receptors and their ephrin-B counterparts are coexpressed during normal development of the germ layers, which require Eph/ephrin-mediated boundary formation (Rohani et al., 2011; Rohani et al., 2014). EphBs and ephrin-Bs are also coexpressed during the development of several tissues in which we see aberrant ephrin-B1-mediated cell segregation in the mouse model for CFNS, such as the neural plate neuroepithelium (O'Neill et al., 2016) (see **Chapter 3**) and the palatal shelves (Bush and Soriano, 2010) (see **Chapter 4**). These data suggest that *cis*-expression of ephrin-Bs may regulate EphB receptor expression and signaling to affect normal morphogenesis as well as ectopic boundary formation in congenital disease.

Here, we examine the consequences of *cis*-expression of ephrin-B1 and its receptors EphB2 and EphB3 on signaling outcomes and Eph/ephrin-mediated boundary formation in cellular and mouse model systems. Though we do not find evidence of *cis* inhibition by mechanisms similar to those employed by ephrin-A/EphA signaling, we instead find that coexpression of ephrin-B1 and EphB2 modulates signaling by a desensitization mechanism in which ephrin-B1 regulates expression levels of EphB receptors, leading to changes in the ability of these cells to segregate. Mosaic loss of ephrin-B1 in CFNS may therefore contribute to CFNS pathogenesis through loss of *cis*-regulation in ephrin-B1 negative tissue compartments, leading to increased EphB signaling sensitivity specifically in ephrin-B1 non-expressing cells.

Results

Individual mutations to the G-H loop of ephrin-B1 result in reduced EphB receptor binding but still permit activation of signaling

To investigate whether ephrin-B1 interacts with EphB receptors *in cis*, we reasoned that it would first be necessary to abrogate binding of ephrin-B1 to EphB receptors *in trans*. This allowed us to separate our consideration of potential *cis* interactions from *trans* interactions. In

studies of ephrin-A/EphA *cis* inhibition, single mutations to the ephrin-A5 G-H loop, the protein domain responsible for receptor-ephrin binding, were reported to abolish *trans* interactions while still permitting functional *cis* interactions to occur (Carvalho et al., 2006). We therefore generated three different ephrin-B1 expression vectors with single mutations to the G-H loop of ephrin-B1, each of which was predicted to disrupt ephrin-B1/EphB binding (**Figure 18A**). By making these mutations, we acknowledged that potential *cis* interactions requiring a functional receptor binding domain would not be under consideration. One of the mutations (c.G373A, p.E125K) was paralogous to the "*trans*-dead" mutation in ephrin-A5 (p.E129K) (Carvalho et al., 2006) and has been found in a CFNS patient (Apostolopoulou et al., 2012); the other two were CFNS patient mutations predicted to cause null loss of function of ephrin-B1 (c.A344C, p.Q115P; and c.C355A, p.P119T) (Twigg et al., 2004). To determine whether these single mutants had lost the ability to bind to the EphB receptor *in trans*, we first expressed each single G-H loop mutant in HEK293 cells, which do not express significant levels of endogenous ephrin-B1, EphB2, or EphB3, using the vector backbone pcDNA3.1 and transient transfection. Each single G-H loop mutant, as well as wild-type ephrin-B1, can be successfully transiently expressed in 293 cells (**Figure 18B**). To test the ability of these mutants to bind to the EphB2 receptor, we added unclustered EphB2-Fc, an Fc molecule attached to a soluble EphB2 receptor ectodomain that will bind wild-type ephrin-B1 at the cell surface, to the culture media of each population of ephrin-B1-transfected 293 cells. Pulldown of EphB2-Fc using protein A/G resin revealed that compared to ephrin-B1^{wt}, all three single G-H loop mutants (ephrin-B1^{Q115P}, ephrin-B1^{P119T}, and ephrin-B1^{E125K}) have dramatically reduced ability to bind to EphB2 *in trans* (**Figure 18B**, green box). To test the function of these mutants, therefore, we expressed ephrin-B1^{wt} and each single G-H loop mutant individually in 293 cells, then mixed each ephrin-B1-expressing cell population with 293 cells stably expressing EphB2 ("EphB2 cells"). EphB2 cells do not segregate appreciably from 293 cells alone (**Figure 19A**) but do segregate from 293 cells transiently expressing wild-type ephrin-B1 (**Figure 19B**). Surprisingly, EphB2 cells also

segregated significantly from 293 cells transiently expressing each ephrin-B1 single G-H loop mutant (**Figure 19C-E**). This indicates that although single mutations to the G-H loop reduce their binding to EphB2 *in trans*, they do not ablate the *trans* function of these G-H loop mutant ephrin-B1 proteins.

Combinatorial mutations to the G-H loop of ephrin-B1 abrogate EphB receptor binding and activation of signaling

It is possible that even in the absence of high levels of receptor ligation, overexpression of ephrin-B1 G-H loop mutants can still activate EphB signaling *in trans* or that low endogenous levels of another ephrin-B protein in HEK293 cells may hetero-oligomerize with ephrin-B1 G-H loop mutants to form functional complexes (Janes et al., 2011). To distinguish potential *cis* interactions from *trans* interactions, therefore, it was essential to completely abolish ephrin-B1 binding to EphB receptors *in trans*. We therefore generated an ephrin-B1 protein with three mutations in the G-H loop (ephrin-B1$^{Q115P/P119T/E125K}$, or ephrin-B1^{3xTD}). When expressed in 293 cells, ephrin-B1^{3xTD}, like its single mutant counterparts, demonstrated dramatically reduced binding to EphB2-Fc (**Figure 18B**, blue box). 293 cells transiently expressing ephrinB1^{3xTD} did not segregate from EphB2 cells (**Figure 19F**). Instead, they intermingled with EphB2 cells, behaving similarly to negative control 293 cells (compare to **Figure 19A**). The triple G-H loop mutant of ephrin-B1 has therefore lost the ability to bind to EphB2 *in trans* and activate signaling that results in cell segregation and can be used to determine whether *cis* interactions occur between ephrin-B1 and EphB receptors.

Coexpression of ephrin-B1 and EphB2 desensitizes cells to signals from ephrin-B1, a property which requires the G-H loop

Ephrin-A5 G-H loop mutants retain the ability to bind to EphA3 when coexpressed, and their coexpression results in functional differences in growth cone collapse (Carvalho et al.,

2006); we therefore sought to determine whether ephrin-B1 G-H loop mutants have similar properties with respect to EphB2. 293 cells stably expressing EphB2 and transiently coexpressing ephrin-B1^{wt} show a high amount of interaction between EphB2 and ephrin-B1 by immunoprecipitation of EphB2 and immunoblotting for ephrin-B1 (**Figure 20A**). This can be attributed to *trans* interactions in addition to any *cis* effects that may be occurring. Coexpression of EphB2 and single G-H loop mutants ephrin-B1^{Q115P}, ephrin-B1^{P119T}, or ephrin-B1^{E125K}, however, did not result in a similar level of interaction between EphB2 and any of these ephrin-B1 proteins (**Figure 20A**). Although it appeared that a small amount of interaction occurred (**Figure 20A**, green box and green bars), we cannot rule out the contribution of residual *trans* interactions, as these single mutants remain able to interact with EphB2 in a manner sufficient to induce cell segregation (**Figure 19C-E**).

To determine whether *cis* expression has a functional effect, therefore, we mixed 293 cells stably expressing wild-type ephrin-B1 ("ephrin-B1 cells") with EphB2 cells transiently coexpressing either pcDNA3.1, wild-type ephrin-B1, or mutant ephrin-B1. Ephrin-B1 cells were mixed with 293 cells alone as a control, which results in cell intermingling (**Figure 20B**) and EphB2 cells segregated dramatically from ephrin-B1 cells (**Figure 20C**), as did empty vector-transfected "EphB2 + pcDNA3.1" cells (**Figure 20D**), consistent with what has been demonstrated previously (Poliakov et al., 2008). However, EphB2 cells coexpressing wild-type ephrin-B1 or mutants that retain the ability to signal *in trans* (ephrin-B1^{Q115P}, ephrin-B1^{P119T}, or ephrin-B1^{E125K}) were "desensitized" or "blinded" from receiving ephrin-B1 signals *in trans* from the ephrin-B1 cells, resulting in reduced segregation (**Figure 20E-H**; quantified in **Figure 20J**). This desensitization requires functional signaling via the G-H loop, as coexpression of ephrin-B1^{3xTD} with EphB2 does not reduce the segregation of these cells from ephrin-B1 cells (**Figure 20I**). This indicates that ephrin-B1 does not participate in *cis* inhibition of EphB receptors in the same way that ephrin-A5 inhibits EphA3 signaling, as G-H loop mutants do not bind significantly to EphB2 when coexpressed. However, coexpression of ephrin-B1 does affect EphB2 signaling

response through a desensitization mechanism. This process requires some level of function of the G-H loop of ephrin-B1 and may therefore occur either through *cis* interactions between ephrin-B1 and EphB2 within an individual cell, or rather through active signaling *in trans* throughout a population of cells.

Desensitization of EphB2-expressing cells mediated by coexpression of ephrin-B1 occurs through modulation of EphB receptor levels

Since desensitization of EphB2-expressing cells by ephrin-B1 coexpression requires the G-H loop of ephrin-B1, we reasoned that it may take place by active signaling *in trans* throughout the population of cells *via* endocytosis and degradation of EphB2, a known mechanism for termination of Eph/ephrin signaling (Marston et al., 2003; Zimmer et al., 2003). Reduced surface expression of the receptor would "blind" these cells to receipt of a further signal from ephrin-B1 *in trans* during a cell mixing experiment. To test this possibility, we transfected EphB2 cells with wild-type, single G-H loop mutant, or triple G-H loop mutant ephrin-B1 and examined EphB2 expression levels by western blot at 48 hours after transfection, the time at which mixing experiments were conducted. Coexpression of EphB2 with ephrin-B1^{wt} resulted in dramatically decreased EphB2 expression (**Figure 21A**), as did coexpression of EphB2 with ephrin-B1 single G-H loop mutants retaining the ability to signal *in trans* (ephrin-B1^{Q115P}, ephrin-B1^{P119T}, or ephrin-B1^{E125K}) (**Figure 21A**, green box and green bars). This indicates that the desensitization we observed likely takes place through reduction in EphB2 protein levels. This effect requires the G-H loop of ephrin-B1, as coexpression of EphB2 and ephrin-B1^{3xTD} did not result in decreased EphB2 protein levels (**Figure 21A**, blue box and blue bar). Decreased EphB2 protein level was specific to coexpression of ephrin-B1, as EphB2 protein was not reduced upon coexpression of another transmembrane protein, CDO (**Figure 21B**). Decreases in EphB2 occurred at the protein level, not the transcript level, as *Ephb2* transcript levels were unchanged in EphB2/ephrin-B1 coexpressing cells (**Figure 21C**). It is

therefore likely that the desensitization of EphB2/ephrin-B1 coexpressing cells occurs through active signaling that results in internalization and degradation of the EphB2 receptor, preventing these cells from responding to further stimulation by ephrin-B1 presented *in trans*.

Ephrin-B1 regulates EphB receptor expression in vivo

293 cells serve as a useful model for Eph/ephrin signaling studies (Jorgensen et al., 2009; O'Neill et al., 2016; Poliakov et al., 2008), but we wondered whether the desensitization effect of ephrin-B1/EphB coexpression was relevant *in vivo* during embryonic development of the craniofacial primordia. We reasoned that mosaic loss of this effect could contribute to pathogenic cell segregation in *Efnb1*$^{+/-}$ mouse embryos, a model for CFNS, if regulation of EphB2 and EphB3 receptor levels were disrupted specifically in ephrin-B1 non-expressing cells in the head. We therefore investigated EphB2 and EphB3 expression level in embryo heads prior to palate fusion by western blotting of whole head lysates of E13.5 embryos mosaic for ephrin-B1 loss (*Efnb1*$^{+/-}$ embryos) or ephrin-B1 null (*Efnb1*$^{-/Y}$ embryos) (**Figure 21D**). Indeed, complete loss of ephrin-B1 (**Figure 21E**) resulted in significant increases in EphB2 (**Figure 21F**) and EphB3 (**Figure 21G**) levels in ephrin-B1 null heads. This effect was not detected in *Efnb1*$^{+/-}$ head lysates by western blot, but it has been shown by immunofluorescence analysis that in *Efnb1*$^{+/-}$ palatal shelves, patches of ephrin-B1 non-expressing cells have increased expression of EphB2 and EphB3 (Bush and Soriano, 2010). These observations indicate that loss of ephrin-B1 results in increased EphB2 and EphB3 accumulation within a population of cells *in vivo*. In hemizygous *Efnb1*$^{-/Y}$ embryos, increased expression of EphB2 and EphB3 could result in widespread increased signaling mediated by other ephrins expressed in the same tissue, but this may be a mild effect if few or no other ephrins that signal through EphB2 and EphB3 are expressed in this region. Additionally, it seems unlikely that other binding partners of EphB2 and EphB3 are present in this region, as their signaling *in trans* should also result in receptor internalization and downregulation. In *Efnb1*$^{+/-}$ embryos, however, increased EphB2 and EphB3

expression only in ephrin-B1 negative cells in a mosaic population could contribute to the increased signaling and actin accumulation seen in those cells (O'Neill et al., 2016), exacerbating the Eph/ephrin signaling differences already caused by mosaic loss of ephrin-B1.

Designing an Efnb1 *misexpression mouse to test the* in vivo *relevance of differences in ephrin-B1 expression within a mosaic cell population*

Based on the observations that several CFNS patient mutations in the G-H loop of ephrin-B1 allow retention of some signaling potential, and that EphB receptor levels are maintained at lower levels by broad ephrin-B1 expression, we wondered whether broad ectopic expression of ephrin-B1 would blunt mosaicism-driven segregation. To test this hypothesis *in vivo*, we designed two mouse lines in which misexpression of either ephrin-B1^{wt} or "*trans*-dead" ephrin-B1^{3xTD} is achieved by expression of Cre recombinase. We designed two constructs for gene targeting to the ubiquitously expressed *ROSA26* locus (Soriano, 1999) in mouse embryonic stem cells (mESCs). In the absence of Cre, ephrin-B1 should not be misexpressed due to a termination codon flanked by two loxP sites; in the presence of Cre, the termination codon will be spliced out, and ephrin-B1^{wt} or ephrin-B1^{3xTD} will be expressed under the control of the endogenous *ROSA26* promoter (**Figure 22A**). To identify cells in which ephrin-B1 is misexpressed, the constructs also contain an *mClover2* coding sequence in tandem with the *Efnb1* coding sequence, with an intervening P2A cleavage sequence.

When a *pcDNA3.1-Efnb1-P2A-mClover2* vector was transiently expressed in HEK293 cells, bicistronic expression of ephrin-B1 and mClover2 was achieved. P2A cleavage produced ephrin-B1 protein at the expected size by western blot, with only a very small amount of uncleaved product remaining (**Figure 22B**, black arrow). mClover2 was also strongly expressed and could be detected by fluorescence imaging (**Figure 22C**). Electroporation of the full linearized construct into 129S4 mESCs (Agouti coat color) for targeting to the *ROSA26* locus and selection using G418, followed by PCR across the 5' homology arm, revealed an overall

targeting efficiency of 9/135 clones (6.7%) for *Efnb1*^{wt} and 16/105 clones (15.2%) for *Efnb1*^{3xTD} (**Figure 22D**). A second round of targeting resulted in efficiencies of 12/155 clones (7.7%; combined efficiency 7.2%) for *Efnb1*^{wt} and 7/80 clones (8.8%; combined efficiency 12.4%) for *Efnb1*^{3xTD}. Quantitative PCR for *Neo* expression in each targeted clone confirmed that homologous recombination resulted in insertion of only one copy of the expression cassette per targeted mESC line, with the exception of *Efnb1*^{3xTD}-220, which was therefore not selected for injection (**Figure S6A**). To determine whether recombination occurs as expected when Cre is expressed in these mESCs, we transiently transfected targeted *Efnb1*^{wt} and *Efnb1*^{3xTD} mESC lines with a *PGK-Cre-bpA* expression vector, lysed transfected cells, and extracted DNA to perform PCR analysis for the recombined allele. In both lines, we detected the recombined allele by PCR only when Cre was present (**Figure 22E**). Based on this information, we selected three mESC lines from each construct for injection into C57BL6/J mouse blastocysts (black coat color).

Initial injection of mESC clones *Efnb1*^{wt}-66, *Efnb1*^{wt}-118, and *Efnb1*^{wt}-164 from the first round of targeting produced either no live pups (*Efnb1*^{wt}-66, *Efnb1*^{wt}-164) or no chimeric pups (*Efnb1*^{wt}-118). Injection of mESCs *Efnb1*^{3xTD}-236 and *Efnb1*^{3xTD}-240 from the first round of targeting resulted in the production of only one high-percentage chimera (~60%) from mESC line *Efnb1*^{3xTD}-240. When mated to C57BL6/J female mice, offspring of the *Efnb1*^{3xTD}-240 chimera were 31.8% Agouti coat color (**Figure S6B**), of which 52.9% carried the targeted allele (**Figure S6C**). These mice are currently being backcrossed to the C57BL/6J background. Preliminary observations of a breeding scheme between *β-Actin-Cre*$^{Tg/o}$ and *ROSA26-Efnb1*$^{3xTD/+}$ mice indicate that ubiquitous misexpression of *Efnb1*^{3xTD} in *β-Actin-Cre*$^{Tg/o}$*; ROSA26-Efnb1*$^{3xTD/+}$ pups is compatible with life and that these pups do not have any overt craniofacial phenotypes. After 10 generations of backcrossing to C57BL/6J, *ROSA26-Efnb1*$^{3xTD/+}$ mice will be crossed to *Efnb1*^{lox} mice to produce *ROSA26-Efnb1*$^{3xTD/+}$*; Efnb1*$^{lox/+}$ female mice, which will

be further crossed to a *β-Actin-Cre*$^{Tg/o}$ male mouse to test the efficacy of ubiquitous misexpression of ephrin-B1^{3xTD} and mClover2 *in vivo* in *β-Actin-Cre*$^{Tg/o}$*; Efnb1*$^{\Delta}$*/Y; ROSA26-Efnb1*$^{3xTD/+}$ embryos at E13.5, without the confounding presence of endogenous ephrin-B1 expression.

To obtain *ROSA26-Efnb1*^{wt} mice, a second set of injections is ongoing for clones *Efnb1*^{wt}-181, *Efnb1*^{wt}-329, and *Efnb1*^{wt}-332 from the second round of mESC targeting. High-percentage chimeras have been obtained from mESC clone *Efnb1*^{wt}-181; if they produce pups carrying the targeted allele, *ROSA26*$^{Efnb1\text{-}wt/+}$*; Efnb1*$^{lox/+}$ female mice will be crossed to a *β-Actin-Cre*$^{Tg/o}$ male stud to determine whether ephrin-B1^{wt} and mClover2 are successfully ubiquitously expressed *in vivo* in *β-Actin-Cre*$^{Tg/o}$*; Efnb1*$^{\Delta}$*/Y; ROSA26*$^{Efnb1\text{-}wt/+}$ embryos at E13.5. If both mouse lines perform as expected, we will proceed with further experiments. Because EphB receptor accumulation is reduced by expression of ephrin-B1, and both EphB2 and EphB3 forward signaling are required for ephrin-B1-mediated cell segregation (O'Neill et al., 2016), we will first determine whether ubiquitous expression of ephrin-B1^{wt} reduces segregation in *Efnb1*$^{+/-}$ embryos, using ubiquitous expression of ephrin-B1^{3xTD} as a control. We will cross *β-Actin-Cre*$^{Tg/o}$ studs with *Efnb1*$^{lox/lox}$*; ROSA26*$^{Efnb1\text{-}wt/+}$ and *Efnb1*$^{lox/lox}$*; ROSA26*$^{Efnb1\text{-}3xTD/+}$ females to generate *β-Actin-Cre*$^{Tg/o}$; *Efnb1*$^{\Delta/+}$*; ROSA26*$^{Efnb1\text{-}wt/+}$ experimental and *β-Actin-Cre*$^{Tg/o}$; *Efnb1*$^{\Delta/+}$*; ROSA26*$^{Efnb1\text{-}3xTD/+}$ control embryos. We will analyze these embryos for segregation in craniofacial structures such as the palatal shelves and frontonasal prominence at E13.5 and quantify segregation to determine whether EphB signaling resulting in cell segregation has been blunted by misexpression of ephrin-B1 that can actively signal to reduce surface expression of the receptors.

In addition, these mice can also be used to determine whether mosaicism for differing levels of ephrin-B1 expression results in segregation and craniofacial phenotypes. *ROSA26*$^{Efnb1\text{-}wt/+}$ and *ROSA26*$^{Efnb1\text{-}3xTD/+}$ female mice will be crossed to tamoxifen-inducible *ROSA26*^{CreERT2}

mice, with tamoxifen injections titrated to produce mosaic recombination in *Efnb1*$^{+/+}$; *ROSA26*$^{Efnb1\text{-}wt/CreERT2}$ and *Efnb1*$^{+/+}$; *ROSA26*$^{Efnb1\text{-}3xTD/CreERT2}$ embryos. *Efnb1*$^{+/+}$; *ROSA26*$^{Efnb1\text{-}wt/CreERT2}$ embryos treated with tamoxifen will be mosaic for differing levels of wild-type ephrin-B1 expression, while *Efnb1*$^{+/+}$; *ROSA26*$^{Efnb1\text{-}3xTD/CreERT2}$ embryos treated with tamoxifen will have mosaic misexpression of "*trans*-dead" ephrin-B1 and will serve as a control. These embryos will be analyzed for mClover2 expression at E13.5 by immunofluorescence analysis of frontal sections to determine whether or not segregation occurs between cell populations with differing ephrin-B1 expression levels. Embryos will also be examined at E14.5 for changes to craniofacial structures by histological analysis of frontal sections, and if pups are born, they will be analyzed by skeletal preparation at postnatal day 0 (P0) to determine whether mosaic misexpression of wild-type ephrin-B1 results in craniofacial and skeletal phenotypes. These results will shed light on the importance of ephrin-B1 expression level for regulating EphB receptor levels and signaling *in vivo* and improve our understanding of how mutations in ephrin-B1 contribute to cell segregation and craniofacial dysmorphology in CFNS by determining whether differences in expression level of ephrin-B1 can produce these phenotypes. Finally, these mice will serve as an important tool for *in vivo* signaling studies involving manipulation of ephrin-B1 and its receptor signaling partners.

Discussion

Although a simple bidirectional signaling model for Eph/ephrin signaling, with forward and reverse signaling occurring only at tissue boundaries, may be sufficient to describe some contexts in which Eph/ephrin signaling mediates boundary formation and maintenance during development, it is becoming increasingly evident that complementary expression of Ephs and ephrins is not the only situation in which this signaling pathway operates. Multiple Eph receptors and their specific ephrin signaling partners are coexpressed in many tissues in which their signaling is essential for normal boundary formation, including the germ layers during

gastrulation (Rohani et al., 2011; Rohani et al., 2014), the neural plate (O'Neill et al., 2016), the developing secondary palate (Bush and Soriano, 2010), and the axons of many pathfinding neurons, including spinal motor axons (Kao and Kania, 2011) and retinal axons (Hornberger et al., 1999). In addition to signaling at forming boundaries, therefore, intra-tissue Eph/ephrin signaling may be important to developmental processes in these structures. Signaling directionality is affected by more complex Eph/ephrin expression patterns, and it is now known that unidirectional signaling (O'Neill et al., 2016) and antiparallel signaling (Rohani et al., 2014) can contribute to boundary formation and tissue separation. (For a discussion of the evidence for reverse signaling mechanisms *in vivo*, please refer to **Chapter 2**.) Combinatorial expression of Eph receptors and ephrins, with some functional redundancy and some signaling specificity, can also contribute to increased Eph/ephrin signaling at a boundary relative to the baseline level of signaling within each tissue.

These developments have expanded our understanding of the possible modes of Eph/ephrin expression that aid in boundary formation and maintenance, but the purpose of intra-tissue Eph/ephrin signaling made possible by these more complex expression patterns remains essentially unexplored. It has been proposed that a baseline level of Eph/ephrin signaling within a tissue must be comparatively low to prevent dissolution of the tissue by active repulsion, and that this baseline signaling within a tissue may even directly oppose its dissolution by maintaining adhesion between cells of the same tissue, whereas higher levels of signaling at the boundary mediate segregation and boundary maintenance (Rohani et al., 2014). However, there is not yet any direct evidence for the regulation of adhesion by intra-tissue Eph/ephrin signaling. Instead, we hypothesize that broad Eph/ephrin signaling within a tissue acts to decrease adhesion enough to allow for essential cell movements within the tissue and does not result in repulsive migration that dissolves the tissue. It is also possible that intra-tissue Eph/ephrin signaling plays an as yet undiscovered role. Although EphAs and ephrin-As have been shown to interact physically when expressed in the same cell, and this interaction has

functional effects on axon guidance, coexpression of EphBs and ephrin-Bs had not been characterized at the protein level, and it was unknown how these molecules interact when coexpressed to change boundary formation and maintenance. To determine the function of Eph/ephrin coexpression in normal and aberrant boundary formation, we turned to cell culture and mouse models of CFNS, a disease which we hypothesize is caused by the formation of ectopic ephrin-B1 boundaries.

Although it has been long assumed that CFNS is caused by heterozygous loss of function of ephrin-B1 (Twigg et al., 2004), CFNS patient mutations are found abundantly throughout the coding sequence as well as the introns of *EFNB1*, making comprehensive analysis of each mutation difficult. Two missense mutations in ephrin-B1 have been shown to decrease its tyrosine phosphorylation after stimulation with preclustered EphB2-Fc (Makarov et al., 2010), but the effects of ephrin-B1 mutations on EphB2 signaling have not been examined in depth, and we have shown that ephrin-B1 reverse signaling is not required for most CFNS phenotypes (Bush and Soriano, 2009) or for cell segregation in the mouse (O'Neill et al., 2016). Relatively little is known about how individual ephrin-B1 mutations affect protein expression, localization, and function in forward signaling. In investigating possible *cis* interactions between ephrin-B1 and its receptors important for craniofacial development, EphB2 and EphB3, we discovered that three single missense mutations to the G-H loop, or receptor-binding domain, of ephrin-B1, each of which is found in CFNS patients, do not abolish all binding of ephrin-B1 to EphB2. Instead, we found that each single G-H loop mutant had reduced binding to EphB2 but maintained the ability to induce receptor signaling to drive cell segregation in an HEK293 cell model. This indicates that missense mutations may reduce Eph/ephrin binding rather than preventing it altogether; however, we cannot rule out the possibility that the levels of ephrin-B1 overexpression achieved by transfection allow these single mutants to produce a functional segregation effect that would not be seen at endogenous expression levels. As each of the single mutations we generated in ephrin-B1 occurs in CFNS patients, our data also raise the

possibility that differences in ephrin-B1 expression level or function between cell populations may be sufficient to drive segregation resulting in craniofacial phenotypes; this hypothesis will require further investigation that will be facilitated by our *Efnb1* misexpression mouse.

Reduction in the physical interaction of ephrin-B1 single G-H loop mutants with Eph-Fc fusion proteins does not prevent functional *trans* signaling, suggesting that even a small amount of residual *trans* binding due to incomplete disruption of receptor-ligand interactions can allow signaling between adjacent cells. On a practical experimental note, this finding indicates that reduced ephrin-Eph binding by Eph ectodomain-Fc fusion protein pulldown is not a good measure of complete disruption of signaling function. Rather, functional tests with a measurable outcome parameter for signaling (such as tyrosine phosphorylation, cell segregation, or growth cone collapse) are necessary to determine whether ephrin-to-Eph signaling has truly been ablated. Notably, the decreased ability of ephrin-A single G-H loop mutants to bind to EphA7-Fc was the only criterion used to determine whether or not *trans* interactions were abolished (Carvalho et al., 2006), and thus the reported ephrin-A mutants may also retain some functional *trans* signaling potential. With this knowledge, we can draw several possible conclusions about existing *cis* interaction studies, both ours and others'. (1) It is possible that the reported *cis* interactions between single G-H loop mutants of ephrin-A5 and EphA3 are not *cis* interactions at all, but rather residual *trans* interactions that are not strongly detected by EphA7-Fc immunofluorescence experiments when testing the binding ability of the single mutants, but are detected by western blot in coexpression experiments in 293 cells (Carvalho et al., 2006). A time course of EphA activation by tyrosine phosphorylation after coexpression, as well as a functional growth cone collapse assay to test the responsiveness of EphA3 to signaling from ephrin-A5^{E129K}, would aid in ruling out this possibility; although coexpression of ephrin-A5 and EphA3 results in decreased EphA3 tyrosine phosphorylation (Carvalho et al., 2006), this could also be caused by internalization and degradation of EphA3, depending on the timing of the assay. (2) Regardless of whether it is a *cis* or *trans* interaction, single mutant ephrin-A5^{E129K}

binds much more strongly to EphA3 (Carvalho et al., 2006) than single ephrin-B1 mutants bind to EphB2 (**Figure 18A**), suggesting that the ephrin-B subfamily does behave differently from the ephrin-As. Therefore, it is possible that ephrin-Bs do not participate in the same *cis* inhibitory mechanisms used by ephrin-As. This difference between subfamilies may spring from differences in expression context – perhaps coexpression in axons permits *cis* interactions, while coexpression in palate mesenchyme does not. It may also result from differences in protein structure and steric constraints, as ephrin-As are membrane-linked while ephrin-Bs are transmembrane proteins. It is also possible that the subcellular localization of ephrin-As is conducive to interaction with EphAs within the same cell; localization of ephrin-As within membrane microdomains has been shown to contribute to axon guidance by allowing discrimination of *cis* and *trans* interactions (Marquardt et al., 2005). Ephrin-B may be trafficked to different regions of the cell surface that are not permissive of *cis* interactions with EphB receptors. These possibilities and others merit further consideration in future work.

The study of *cis* interactions between Ephs and ephrins is confounded by the presence of *trans* interactions, a challenge that is difficult to address experimentally. It is important to consider that although *cis* interactions between EphA receptors and ephrin-As have been reported to require either the EphA3 membrane-proximal fibronectin type III domain (Carvalho et al., 2006) or the Eph receptor canonical ligand-binding domain (Yin et al., 2004), the residues of the ephrin important for these interactions have not yet been discovered. It is therefore possible that as yet unidentifiied ephrin-Eph *cis* interactions occur that require the G-H loop of the ephrin, a possibility that is not addressed by these studies. By creating three simultaneous mutations to the G-H loop of ephrin-B1 to ablate *trans* interactions in the ephrin-B1^{3xTD} mutant, we may have changed the architecture of the protein in a way that prevents *cis* interactions as well as *trans* interactions; we cannot rule out this possibility, but we would argue that it was necessary to remove all *trans* interactions resulting in a functional effect of signaling in order to convincingly study *cis* binding. In the triple mutant protein ephrin-B1^{3xTD}, *trans* signaling is fully

disrupted, with no binding by EphB2-Fc pulldown and no ability to induce cell segregation. This triple mutant ephrin-B1 protein has no effect on EphB2 signaling response when coexpressed, which leads us to the conclusion that coexpression effects of ephrin-B1 require the G-H loop. Whether these effects are mediated by *trans* signaling within the population or an as yet unknown *cis* interaction involving the G-H loop will require further study.

If ephrin-Bs do not bind to EphBs *in cis* to reduce their activation and tyrosine phosphorylation when presented with signals from ephrin-Bs *in trans*, what then is the effect of ephrin-B/EphB coexpression in tissue organization? We show that coexpression of wild-type or *trans*-competent single mutant ephrin-B1 results in active signaling within a tissue, leading to reduced EphB2 protein expression at the cell surface. This may occur by endocytosis and degradation of the EphB receptor, a known termination mechanism for Eph/ephrin signaling that allows cell detachment after the interaction necessary for producing the downstream signal (Marston et al., 2003; Zimmer et al., 2003). Whatever the mechanism, the functional impact of reduced EphB2 expression is striking: EphB2/ephrin-B1 coexpressing cells exhibit a significantly reduced ability to segregate from 293 cells stably expressing ephrin-B1. EphB/ephrin-B coexpression may therefore serve not as a physical or steric constraint on EphB reception of ephrin-B1 signals *in trans*, but rather as a desensitization mechanism that “blinds” the coexpressing cells to these signals through active signaling within a population. This desensitization mechanism may contribute to cell segregation by enhancing a differential in EphB signaling sensitivity.

Many of the contexts in which Eph/ephrin coexpression has been demonstrated have used *in situ* hybridization to look at mRNA expression levels; however, early studies of reciprocal or complementary expression of Ephs and ephrins used Eph and ephrin ectodomains fused to LacZ to determine expression patterns of these molecules (Gale et al., 1996), which would show surface protein localization as opposed to transcript expression. In our *in vivo* studies of embryo heads, loss of ephrin-B1 results in upregulation of EphB2 and EphB3 protein

expression. In addition, previously published data indicates that in ephrin-B1 mosaic secondary palate mesenchyme, ephrin-B1 non-expression domains have increased EphB2 and EphB3 expression by immunofluorescence (Bush and Soriano, 2010). These data raise the possibility that *cis*-expression of ephrin-B1 with EphB receptors may play a key role in morphogenesis during normal craniofacial development by establishing EphB-high and EphB-low compartments based on ephrin-B1 expression patterns. *Cis*-expression of ephrin-Bs with EphB receptors may thereby work alongside transcriptional regulation as an additional mechanism for enforcing complementary ligand and receptor activity domains during development.

These studies identify a new mechanism of regulation of EphB receptor levels and signaling and may also shed light on the signaling mechanisms of pathogenic cell segregation in CFNS. Although ephrin-B1 does not participate in *cis* inhibition as described for ephrin-As, these studies demonstrate that ephrin-B1 coexpression affects how EphB2-expressing cells respond to signals from adjacent cells by regulating surface accumulation of the receptor. In an *in vivo* wild-type situation, therefore, a baseline level of signaling between ephrin-B1/EphB-coexpressing cells may keep EphB receptor levels low through constant turnover. In an ephrin-B1 mosaic situation, however, wild-type cells with low EphB expression through this baseline signaling mechanism encounter ephrin-B1 non-expressing cells with increased EphB expression, resulting in an increased signaling response in these cells. This unidirectional signaling differential could provide an explanation for the increased actomyosin seen in these cells, which underlies cell segregation in the mouse model for CFNS (O'Neill et al., 2016). The downstream signaling partners of EphB receptors mediating changes to actomyosin contractility, as well as the mechanisms by which changes to actomyosin contractility result in cell segregation, are the subject of important future studies.

Materials and Methods

Mouse lines and maintenance. All animal experiments were performed in accordance with the protocols of the University of California, San Francisco Institutional Animal Care and Use Committee. Mice were socially housed under a twelve-hour light-dark cycle with food and water *ad libitum*. All alleles used for the experiments herein have been previously described. All mice were backcrossed and maintained on a congenic C57BL/6J genetic background. *Efnb1*^{lox}, MGI: 3039289 (Davy et al., 2004); *β-actin-Cre*, MGI: 2176050 (Lewandoski et al., 1997).

Construct design, cloning, and mESC targeting. Ephrin-B1 single and triple G-H loop mutant plasmids were designed using VectorNTI software. An existing *pcDNA3.1-efnb1*^{wt} construct (Davy et al., 2004) was first modified by site-directed mutagenesis to correct a signal peptide mutation (c.G52T) using the QuikChange Lightning Site-Directed Mutagenesis Kit (Agilent) according to the instructions provided by the manufacturer. Single G-H loop mutations to ephrin-B1 were made in the "corrected" plasmid using the same kit. The triple G-H loop mutant ephrin-B1 plasmid was made using the QuikChange Lightning Multi Site-Directed Mutagenesis Kit (Agilent) according to the instructions provided by the manufacturer. Ephrin-B1 wild-type and 3xTD mouse constructs (*pROSA26-LSL-efnb1-p2a-mClover2*) were built by first adding a P2A cleavage sequence to the end of ephrin-B1 in *pcDNA3.1-efnb1* (wt or 3xTD) using a synthetic nucleotide sequence and PCR cloning. The *mClover2* coding sequence, obtained from the UCSF Nikon Imaging Center, was then added to the end of the P2A cleavage sequence using PCR cloning and the multi-cloning site of *pcDNA3.1*, producing a 2 amino acid L-E linker between the *p2a* and *mClover2* sequences. The *efnb1-p2a-mClover2* sequence was then cloned into the *pBigT* plasmid (Srinivas et al., 2001) (Frank Costantini lab plasmids, Addgene #21270), which contains a *loxP-NeoR-3xPolyA-STOP-loxP* cassette, at the NheI restriction site. Finally, the *LSL-efnb1-p2a-mClover2* sequence was cloned into *pROSA26-PA* (Srinivas et al., 2001) (Frank Costantini lab plasmids, Addgene #21271), a modification of *pROSA26-1*

(Soriano, 1999) containing a PacI-AscI linker. Final constructs (wt and 3xTD) were linearized using AfeI and electroporated into AK-7 129S4 mESCs (a gift from Akira Imamoto). Electroporated mESCs were plated at clonal density and grown on irradiated Soriano ES cell feeder line SNL 76/7 STO feeder cells (a gift from Akira Imamoto) under G418 selection for 10-14 days, after which individual clones were picked for PCR screening and expansion. Primers for PCR screening spanned the 5' *ROSA26* homology arm of the construct (**Figure 22A**, red arrows) (**Table 7**). Positive clones were expanded and frozen back at low passage. Each positive mESC clone was tested for construct copy number using quantitative PCR for *Neo* expression compared to *Bambi* expression as a control (**Figure S6A**) (**Table 7**). mESC clones transfected with *PGK-Cre-bpA* to test for recombination were screened using a forward primer in the 5' *ROSA26* homology arm and a reverse primer in the first exon of Efnb1 (**Figure 22A**, blue arrows) (**Table 7**). C57BL/6J blastocyst injections were performed by the Gladstone mESC core (targeting 1) or the UC Davis Mouse Biology Program (targeting 2).

293 cell culture and transfection. HEK293 cells, HEK293 cells stably expressing EphB2 and membrane-targeted GFP ("EphB2 cells"), and HEK293 cells stably expressing ephrin-B1-HA ("ephrin-B1 cells") were obtained from A. Poliakov and D. Wilkinson (Medical Research Council National Institute for Medical Research, London, England, UK) (Jorgensen et al., 2009; Poliakov et al., 2008). Cells were cultured at 37°C with 5% CO_2 in DMEM high glucose (Gibco 11965-018) with 10% fetal bovine serum (Hyclone), 2 mM L-glutamine (Gibco), and 1X penicillin-streptomycin (UCSF Cell Culture Facility). Cells were transfected using Lipofectamine 2000 (Thermo Fisher Scientific) according to the instructions provided by the manufacturer.

293 cell segregation experiments and quantification of segregation. 24-well glass-bottom plates (MatTek) or 4-chamber glass-bottom dishes (Greiner Bio-One) were coated with 10 μg/mL

fibronectin (Sigma Aldrich) in D-PBS, calcium- and magnesium-free (Gibco), for 30 minutes at 37°C before removing excess PBS and adding 0.5 mL HEK293 cell media to each well. Cells to be mixed were lifted using 0.25% trypsin-EDTA (Gibco) and counted using a Countess cell counting system (Thermo Fisher Scientific). 100,000 cells per condition were added to each well and vigorously mixed to achieve a final concentration of 200,000 cells/well (~100,000 cells/cm^2). Cell mixtures were imaged at 24 hours after mixing using a Zeiss Cell Observer spinning disc confocal microscope and a 10X air Plan-Apochromat objective lens. Zen software was used to acquire images, adjust brightness and contrast, and export images as .tif files. Quantification of segregation was performed using a nearest-neighbor method (Mochizuki et al., 1998) as previously described (O'Neill et al., 2016).

Immunoprecipitation. Cells were lysed in NP-40 lysis buffer (20 mM Tris-HCl, 137 mM NaCl, 10% glycerol, 1% NP-40, 2 mM EDTA) supplemented with the following protease and phosphatase inhibitors: aprotinin, 2 µg/mL; leupeptin, 5 µg/mL; pepstatin, 1 µg/mL; PMSF, 1 mM; NaF, 10 mM; and $NaVO_4$, 1 mM. Lysates were cleared by centrifugation at 16,000 x g for 10 minutes at 4°C prior to use, and a 50 µL aliquot of lysate was transferred to a separate tube, flash frozen, and stored at -80°C. For EphB2-Fc pulldown, 50 µL Protein A/G UltraLink Resin slurry (Thermo Fisher Scientific) was added to the remainder of each lysate and rotated for 4 hours at 4°C, followed by 3 1-hour washes in NP-40 lysis buffer at 4°C with rotation. Complexes were eluted from the resin using 25 µL of 2X Laemmli buffer incubated with the resin for 5 minutes at 95°C. The resulting supernatant was flash frozen and stored at -80°C for immunoblotting. For EphB2 coimmunoprecipitation, 2 µg goat anti-EphB2 antibody (R&D systems; see **Table 6**) was added to the remainder of each lysate and rotated overnight at at 4°C, followed by the same pulldown protocol.

Immunoblotting. Cells or tissues were lysed in NP-40 lysis buffer (20 mM Tris-HCl, 137 mM NaCl, 10% glycerol, 1% NP-40, 2 mM EDTA) supplemented with 1 mM dithiothreitol (Sigma) and the following protease and phosphatase inhibitors: aprotinin, 2 µg/mL; leupeptin, 5 µg/mL; pepstatin, 1 µg/mL; PMSF, 1 mM; NaF, 10 mM; and $NaVO_4$, 1 mM. In the case of embryo head lysates, a probe sonicator was used for a 10 second pulse after addition of NP-40 to aid in breaking up the tissue. Lysates were cleared by centrifugation at 16,000 x g for 10 minutes at 4°C prior to use. Protein quantification was performed using the Pierce BCA Protein Assay Kit (Thermo Fisher Scientific). Immunoblotting was performed according to standard procedures using Odyssey® TBS blocking buffer (LI-COR) for blocking and dilution of antibodies (**Table 6**) and TBS with 0.1% Tween-20 for washing. Imaging of immunoblots was performed using an Odyssey® Infrared Imaging System (LI-COR), and analysis and quantification was carried out using Image Studio™ software (LI-COR).

qRT-PCR. Total RNA was extracted from cells using TRIzol (Thermo Fisher Scientific). RNA was reverse transcribed using a SuperScript™ II First-Strand Synthesis System for RT-PCR (Thermo Fisher Scientific). qRT-PCR was performed using iTaq Universal SYBR Green and a CFX96 Real Time System (Bio-Rad), with primer pairs that span exon-intron boundaries (**Table 7**). Analysis of relative gene expression was performed using the Pfaffl method (Bio-Rad Real-Time PCR Applications Guide, http://www.gene-quantification.com/real-time-pcr-guide-bio-rad.pdf).

Statistics. For analysis of immunoblotting and qRT-PCR data, GraphPad Prism 7.03 was used to plot mean expression ± standard deviation of biological and/or technical replicates, as indicated in figure legends. To pool data between immunoblots, signal data obtained from the Odyssey® Infrared Imaging System (LI-COR) and quantified using Image Studio™ software (LI-COR) for each blot were normalized to control, and the normalized values were averaged

across blots. To determine statistical significance, parametric measures (one-way ANOVA) were used if the data met the assumption of equality of group variances as calculated by the Brown-Forsythe test and homogeneity of variances across populations as calculated by Bartlett's test. For pairwise comparisons between groups, the Holm-Sidak correction for multiple comparisons was made. If these assumptions were not met, nonparametric measures (Kruskal-Wallace) were used, and for pairwise comparisons between groups, Dunn's test with correction for multiple comparisons was used.

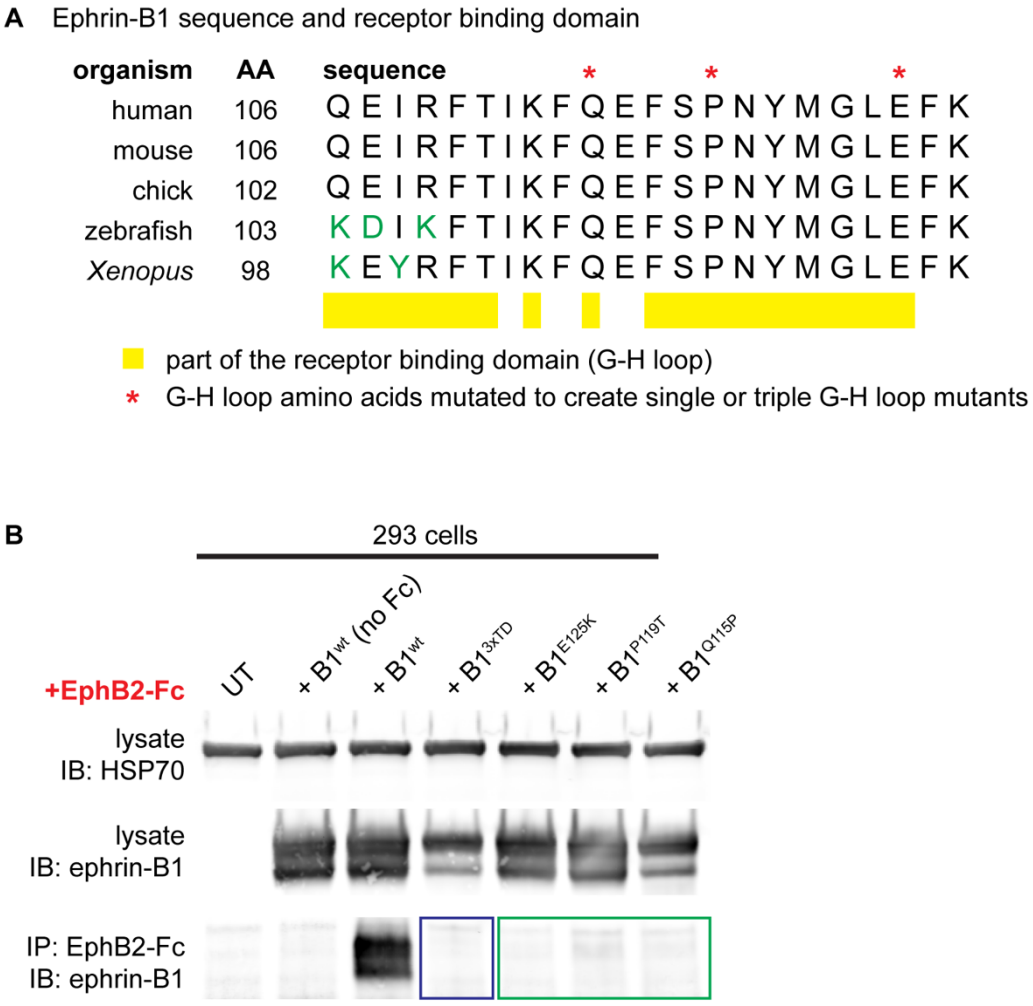

Figure 18. Individual and combinatorial mutations to the G-H loop of ephrin-B1 dramatically reduce EphB receptor binding. (A) Schematic showing the amino acid sequence of part of the G-H loop, or receptor-binding domain, of ephrin-B1, which is highly conserved across vertebrates. Red asterisks indicate amino acids mutated individually to create single G-H loop mutants Q115P, P119T, and E125K or in combination to create triple G-H loop mutant Q115P/P119T/E125K ("3xTD"). **(B)** 293 cells alone do not express high levels of endogenous ephrin-B1 (column 1), but transient transfection of wild-type ephrin-B1 (columns 2 and 3) or mutant ephrin-B1 (columns 4-7) results in robust expression of the protein. Addition of soluble EphB2-Fc to the culture media, followed by Fc pulldown, coprecipitates wild-type ephrin-B1. However, pulldown of single G-H loop mutant ephrin-B1 is dramatically reduced (green box), and triple G-H loop mutant ephrin-B1 is not pulled down (blue box). *UT, untransfected. B1, ephrin-B1.*

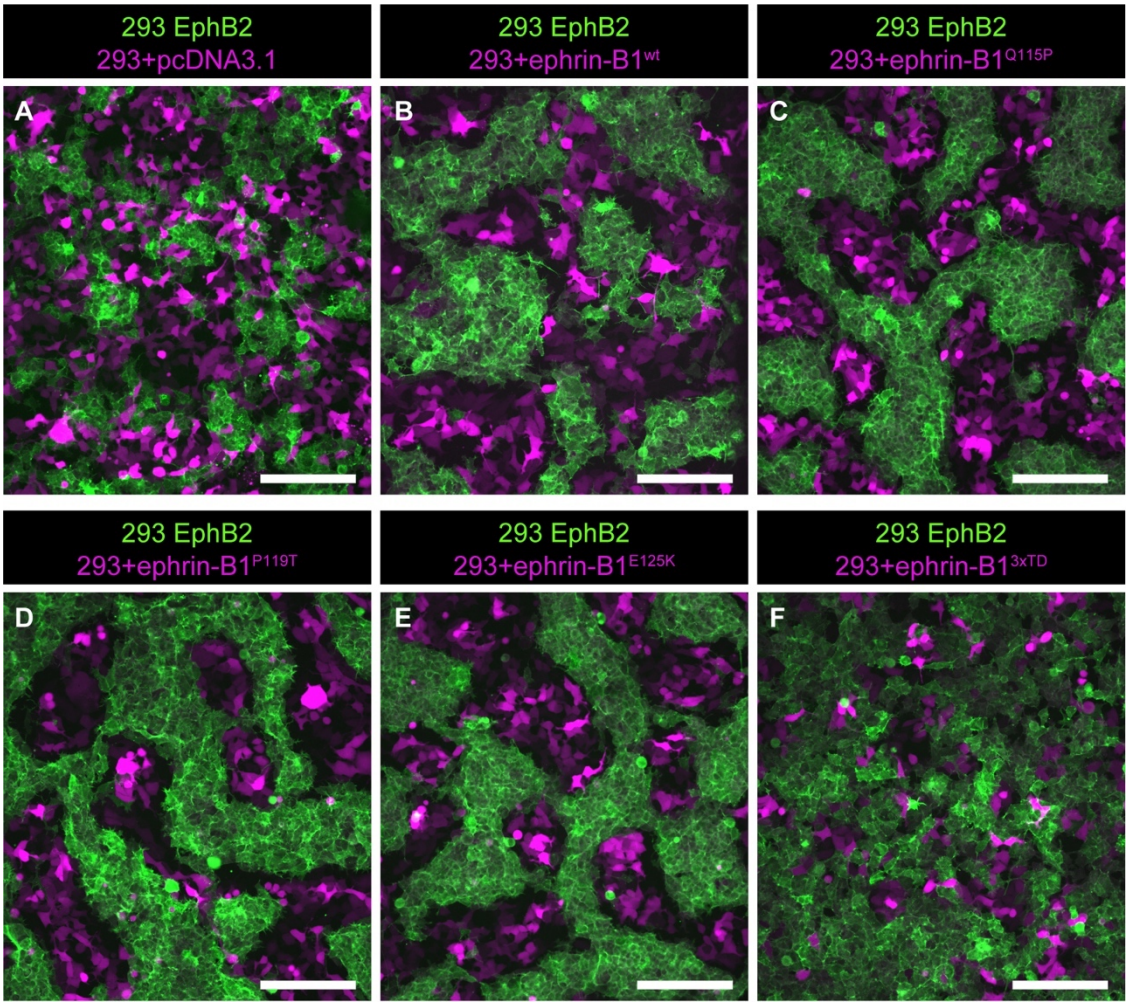

Figure 19. Single G-H loop mutants of ephrin-B1 retain the ability to activate EphB2, while a triple G-H loop mutant does not. (A) 293 cells transfected with empty vector pcDNA3.1 do not express high levels of ephrin-Bs or EphB receptors and intermingle with 293 cells stably expressing EphB2. **(B)** 293 cells transiently expressing ephrin-B1^{wt} segregate dramatically from EphB2 cells. **(C-E)** When transiently expressed in 293 cells, ephrin-B1 single G-H loop mutants Q115P, P119T, or E125K retain enough receptor binding capacity to initiate segregation from EphB2 cells. **(F)** Triple G-H loop mutant ephrin-B1^{3xTD} transiently expressed in 293 cells is not able to drive their segregation from EphB2 cells, indicating that this mutant is truly "*trans*-dead."

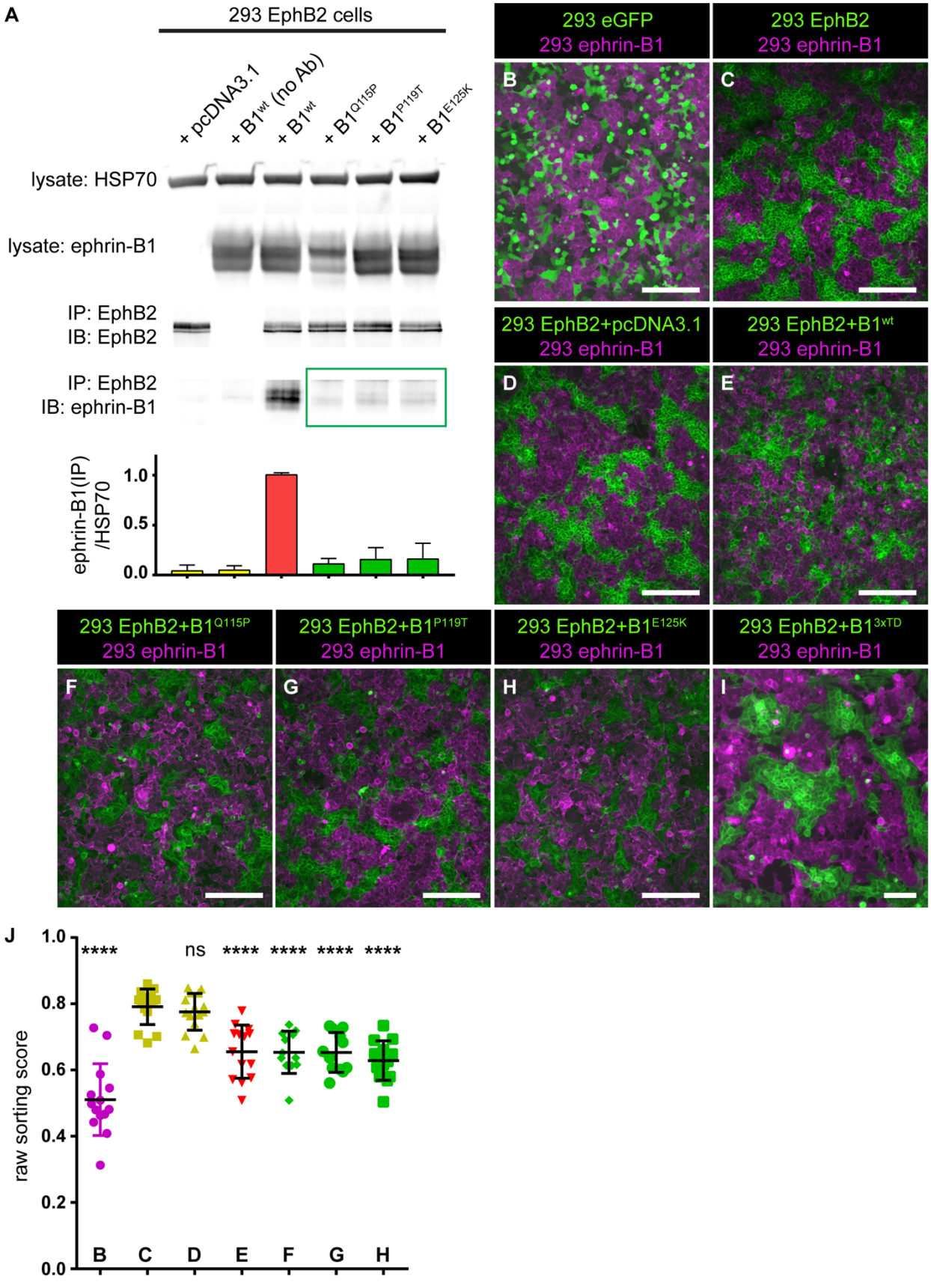
A
293 EphB2 cells
+ pcDNA3.1
+ B1wt (no Ab)
+ B1wt
+ B1Q115P
+ B1P119T
+ B1E125K
lysate: HSP70
lysate: ephrin-B1
IP: EphB2
IB: EphB2
IP: EphB2
IB: ephrin-B1
ephrin-B1(IP)
/HSP70
1.0
0.5
0.0
293 eGFP
293 ephrin-B1
B
293 EphB2
293 ephrin-B1
C
293 EphB2+pcDNA3.1
293 ephrin-B1
D
293 EphB2+B1wt
293 ephrin-B1
E
293 EphB2+B1Q115P
293 ephrin-B1
F
293 EphB2+B1P119T
293 ephrin-B1
G
293 EphB2+B1E125K
293 ephrin-B1
H
293 EphB2+B13xTD
293 ephrin-B1
I
J
raw sorting score
1.0
0.8
0.6
0.4
0.2
0.0
**** ns **** **** **** ****
B C D E F G H

Figure 20. Coexpression of EphB2 and *trans*-competent ephrin-B1 blinds cells to receipt of further signals from ephrin-B1 *in trans*. (A) Coexpression of ephrin-B1^{wt} in EphB2-expressing 293 cells results in coimmunoprecipitation of ephrin-B1 with EphB2 (red bar), but ephrin-B1 single G-H loop mutants do not coimmunoprecipitate significantly with EphB2 when coexpressed (green box, green bars). **(B)** HEK293 cells do not segregate from ephrin-B1 cells, but ephrin-B1 cells segregate dramatically from untransfected EphB2 cells **(C)** or EphB2 cells transiently expressing the empty vector pcDNA3.1. **(E-H)** EphB2 cells coexpressing ephrin-B1^{wt} or single G-H loop mutants are desensitized to signals from ephrin-B1 *in trans* and demonstrate reduced segregation from ephrin-B1 cells. **(I)** EphB2 cells coexpressing ephrin-B1^{3xTD} are not desensitized and still segregate dramatically from ephrin-B1 cells. **(J)** Quantification of segregation in panels **(B-H)** using a nearest-neighbor method. **** indicates $p<0.001$ in comparison with segregation of the positive control **(C)** by ANOVA followed by a Holm-Sidak correction for multiple comparisons. The graph displays the results of 2 biological replicates, each with 6-9 technical replicates per condition. *B1, ephrin-B1; UT, untransfected. Scale bars, 200 µm.*

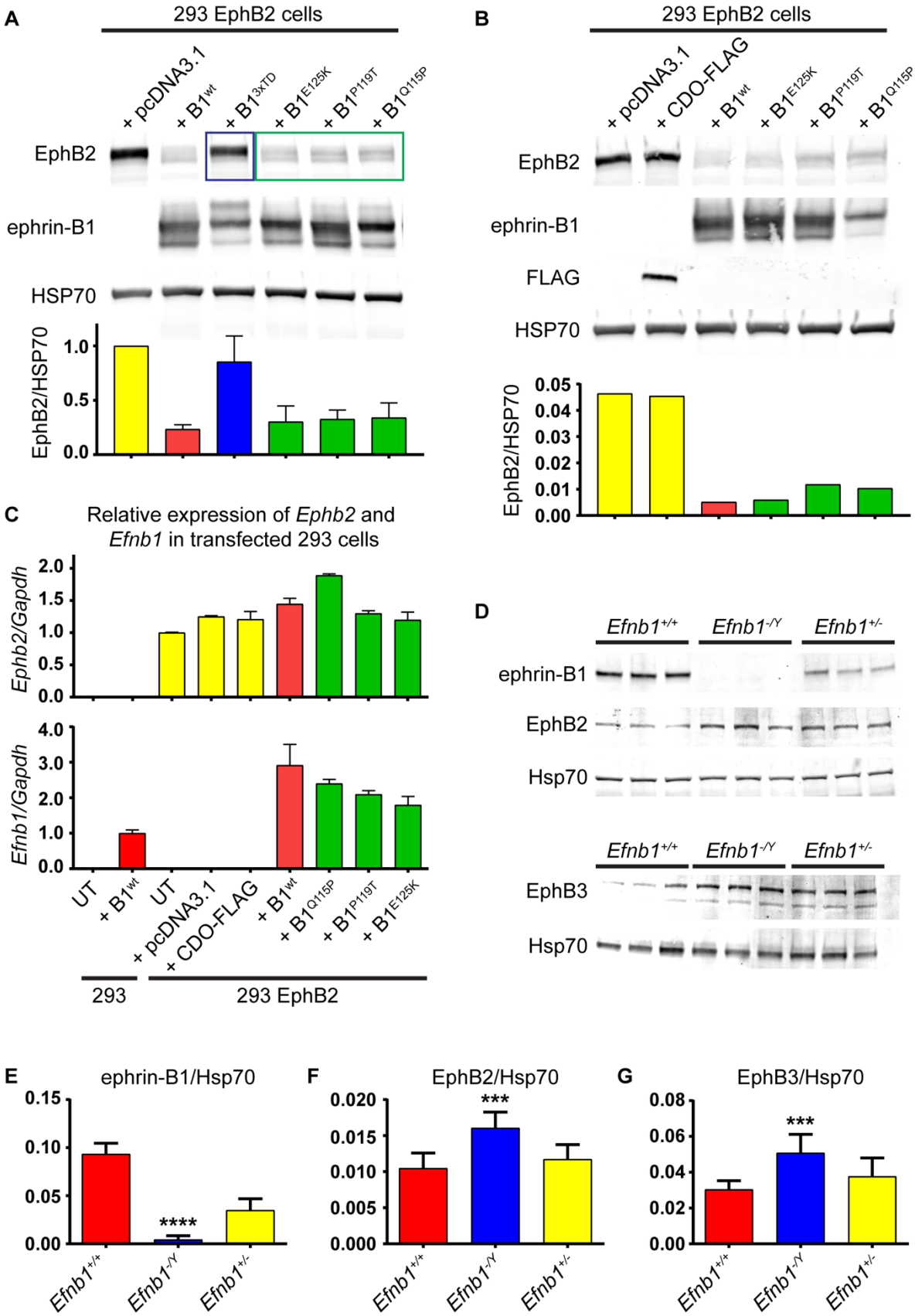
A
293 EphB2 cells
+ pcDNA3.1
+ B1wt
+ B13xTD
+ B1E125K
+ B1P119T
+ B1Q115P
EphB2
ephrin-B1
HSP70
EphB2/HSP70
1.0
0.5
0.0
B
293 EphB2 cells
+ pcDNA3.1
+ CDO-FLAG
+ B1wt
+ B1E125K
+ B1P119T
+ B1Q115P
EphB2
ephrin-B1
FLAG
HSP70
EphB2/HSP70
0.05
0.04
0.03
0.02
0.01
0.00
C
Relative expression of Ephb2 and Efnb1 in transfected 293 cells
Ephb2/Gapdh
2.0
1.5
1.0
0.5
0.0
Efnb1/Gapdh
4.0
3.0
2.0
1.0
0.0
UT
+ B1wt
UT
+ pcDNA3.1
+ CDO-FLAG
+ B1wt
+ B1Q115P
+ B1P119T
+ B1E125K
293
293 EphB2
D
Efnb1+/+
Efnb1-/Y
Efnb1+/-
ephrin-B1
EphB2
Hsp70
Efnb1+/+
Efnb1-/Y
Efnb1+/-
EphB3
Hsp70
E
ephrin-B1/Hsp70
0.15
0.10
0.05
0.00
****
Efnb1+/+
Efnb1-/Y
Efnb1+/-
F
EphB2/Hsp70
0.020
0.015
0.010
0.005
0.000
***
Efnb1+/+
Efnb1-/Y
Efnb1+/-
G
EphB3/Hsp70
0.08
0.06
0.04
0.02
0.00
***
Efnb1+/+
Efnb1-/Y
Efnb1+/-

Figure 21. *Cis*-expression of ephrin-B1 desensitizes EphB2-expressing cells through reduction of EphB2 protein levels. (A) Transient transfection of ephrin-B1^{wt} (red bar) or ephrin-B1 single G-H loop mutants (green box; green bars) into 293 cells stably expressing EphB2 results in decreased EphB2 expression after 48 hours compared with transient transfection of empty vector pcDNA3.1 (yellow bar). This process requires the G-H loop, as transient transfection of ephrin-B1^{3xTD} does not affect EphB2 expression (blue box; blue bar). Error bars represent standard deviation of n=3-7 biological replicates per condition; relative EphB2 expression (EphB2/HSP70) was normalized to 1 for empty vector-transfected cells. **(B)** Transient transfection of the transmembrane protein CDO does not decrease EphB2 expression, indicating that this phenomenon is not generally caused by increasing proteins at the cell surface. **(C)** 293 cells do not express significant levels of *Ephb2* or *Efnb1* compared to stably expressing or transfected cells. Decreases in EphB2 occur at the protein level; relative *Ephb2* expression is not changed in 293 cells expressing *Efnb1*. **(D-G)** E13.5 mouse embryo heads null for ephrin-B1 expression (*Efnb1*$^{-/Y}$) **(E)** have significant increases in EphB2 **(F)** and EphB3 **(G)** expression. Error bars represent standard deviation of n=7-8 biological replicates per condition. Stars indicate a statistically significant difference between *Efnb1*$^{+/+}$ and *Efnb1*$^{-/Y}$ embryos as follows: in **(E)**, **** indicates $p<0.0001$ by nonparametric Kruskal-Wallace test followed by a Dunn's correction for multiple comparisons; in **(F-G)**, *** indicates $p<0.001$ by ANOVA followed by a Holm-Sidak correction for multiple comparisons. *B1, ephrin-B1; UT, untransfected.*

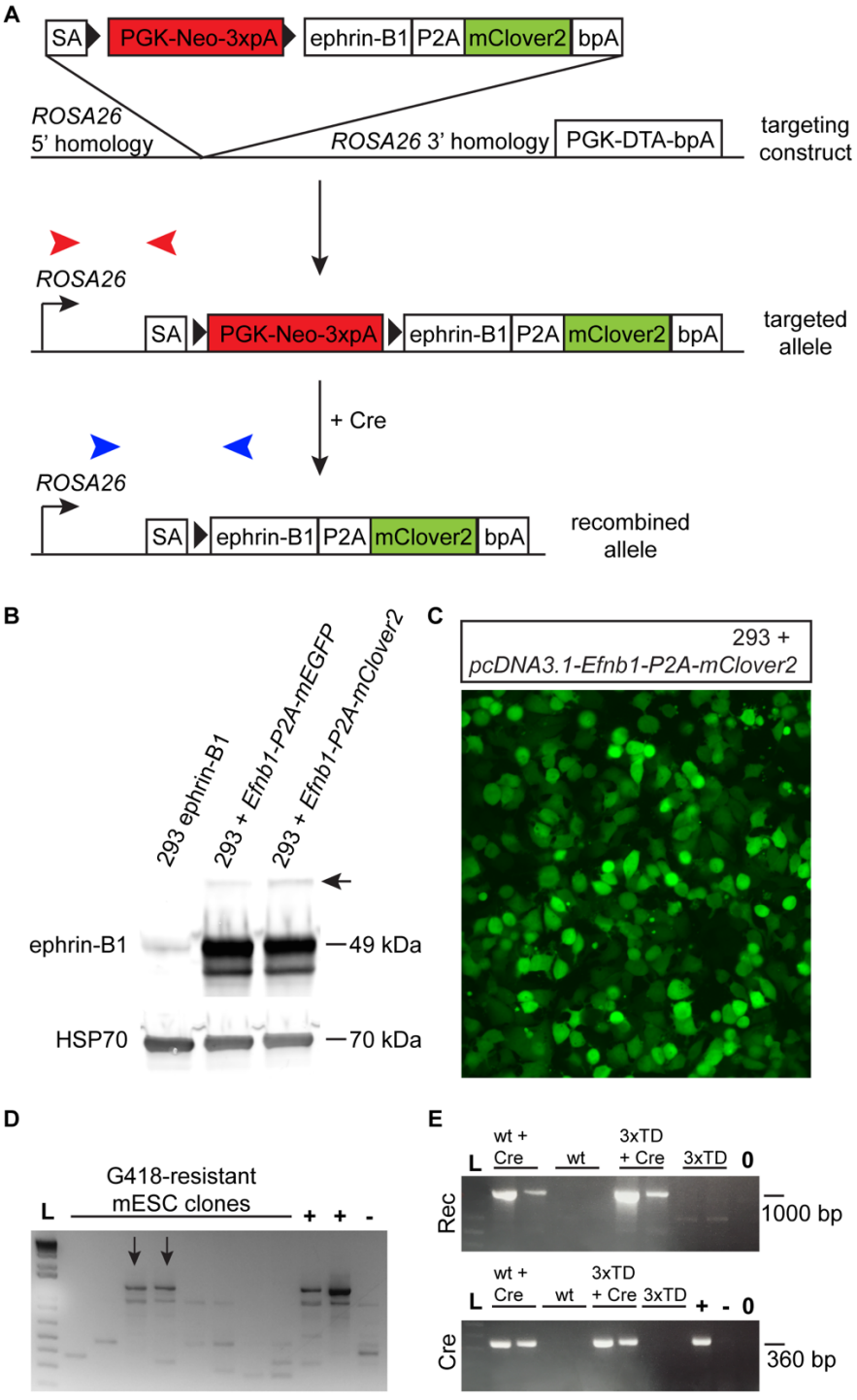

Figure 22. Ephrin-B1 misexpression mouse construct design, testing, and targeting. (A) Schematic diagram of targeting construct for conditional ephrin-B1 misexpression under the control of the *ROSA26* promoter, including depictions of the targeted allele and the recombined allele. **(B-C)** Transient transfection of the *Efnb1-P2A-mClover2* portion of the construct into 293 cells via the pcDNA3.1 plasmid results in P2A cleavage, ephrin-B1 expression at the expected size of 49 kDa, and mClover2 expression. Black arrow in **(B)** indicates a small amount of uncleaved protein remaining. **(D)** Representative gel image showing testing of G418-resistant

clones for correct targeting. PCR primers from *ROSA26*-flanking and splice acceptor DNA, indicated by red arrowheads in **(A)**, were used to amplify a fragment of approximately 1.3 kb. Black arrows indicate correctly targeted *Efnb1*^{wt} clones. +, positive control ROSA26 reporter mouse DNA; -, negative control mouse DNA; L, ladder. **(E)** Transient expression of PGK-Cre-bpA in targeted *Efnb1*^{wt} and *Efnb1*^{3xTD} mESCs results in the expected recombination event. PCR primers from Rosa26-flanking and Efnb1 coding sequence DNA, indicated by blue arrows in **(A)**, were used to amplify a 1-kb fragment of the recombined allele. Amplification occurred only in Cre-expressing wt and 3xTD mESCs, not in untransfected mESCs. +, Cre-positive control mouse DNA; -, Cre-negative control mouse DNA; 0, no DNA control; L, ladder.

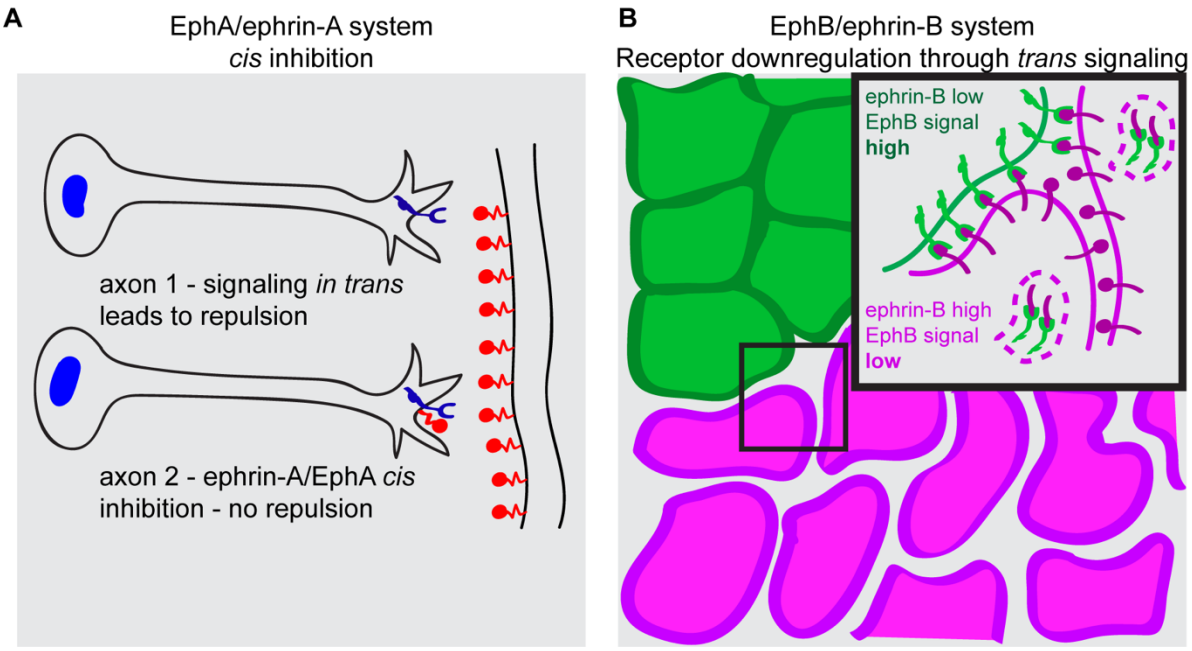

Figure 23. Differences in *cis* expression effects of ephrin-As and ephrin-Bs. (A) *Cis*-expression of ephrin-As with EphA receptors results in inhibition of EphA activation and signaling, with functional effects on axon growth cone collapse. This is thought to act as a method for fine-tuning signaling response to accurately define termination zones during axon guidance. **(B)** We have shown that ephrin-Bs do not bind directly to EphB receptors *in cis* in the same way that ephrin-As bind to EphA receptors. Instead, coexpression of ephrin-Bs and EphB receptors within a population of cells leads to signaling *in trans* that results in downregulation of EphB receptor expression, desensitizing these cells to receipt of further signals *in trans* from other cell populations.

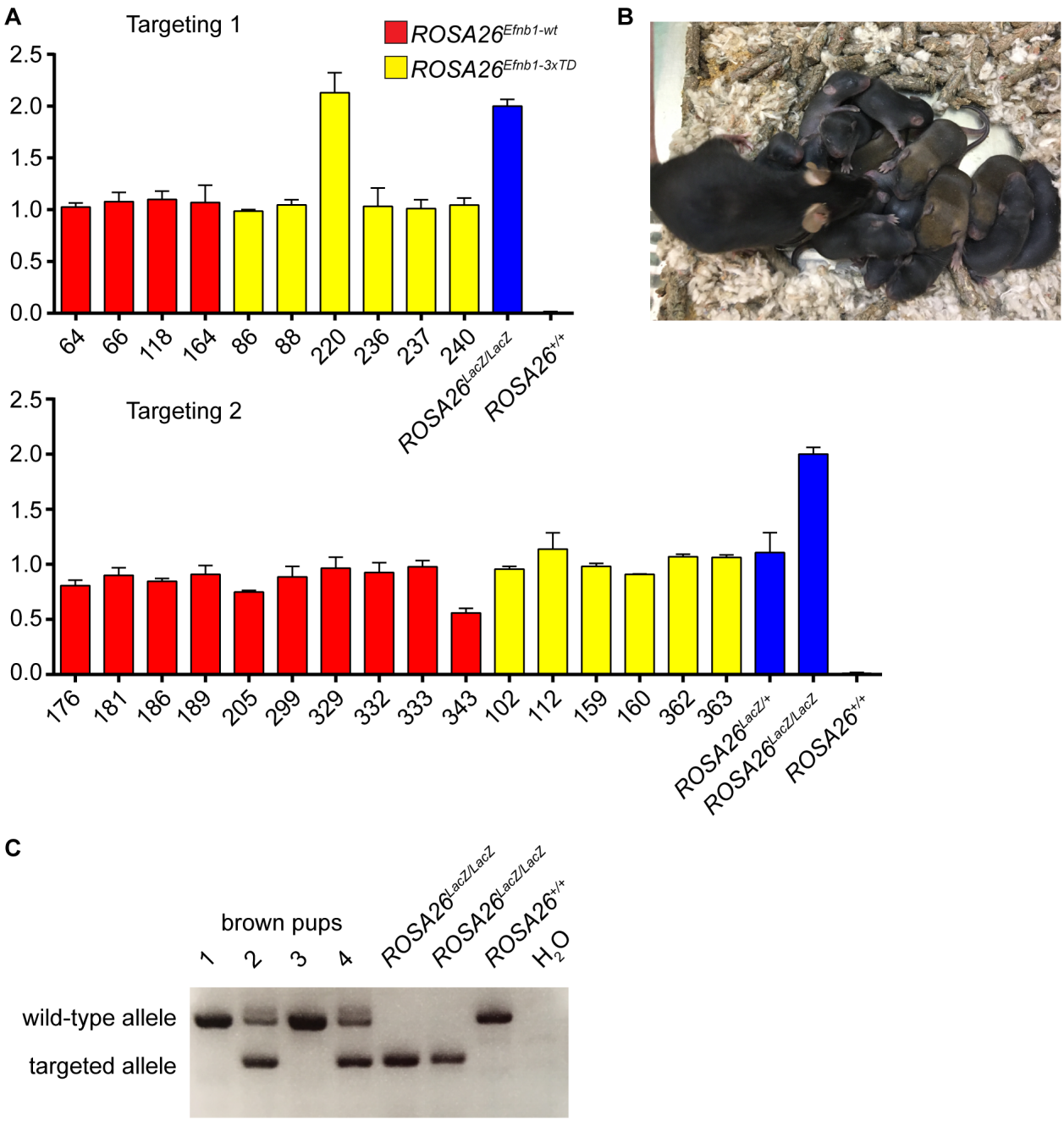

Figure S6. Preliminary characterization of *ROSA26*$^{Efnb1\text{-}3xTD}$ mouse ESCs. (A) qPCR to detect copy number of *Neo* insertion, normalized to the *Bambi* locus, was employed to test for construct integration number in each targeted mESC line compared to tail DNA from control ROSA26^{LacZ} reporter mice. All targeted lines had only one integration event except for *Efnb1*^{3xTD}-220, which had two copies of *Neo*. **(B)** Representative image showing a litter from the cross between the highest-percentage *Efnb1*^{3xTD}-240 chimera and a C57BL/6J female. Approximately 30% of the pups in each litter had the Agouti coat color. **(C)** Genotyping of four Agouti pups from the first litter from the cross between the highest-percentage *Efnb1*^{3xTD}-240 chimera and a C57BL/6J female. As expected, 50% of the Agouti pups carried the targeted allele.

CHAPTER 6. Conclusions and future work

This work explores the developmental etiology of the congenital craniofacial disease craniofrontonasal syndrome (CFNS), while also aiming to elucidate the general mechanisms of ephrin-B1 regulation of cell positioning and boundary formation in the developing craniofacial complex. It has been understood for some time that ephrin-B1 is a major player in the area of developmental boundary formation and maintenance, as its loss or mutation in humans results in defects such as agenesis of the corpus callosum, which results in axons failing to cross the midline boundary of the brain; syndactyly and polydactyly, in which boundaries are lost or gained in developing digits; coronal craniosynostosis, in which a major boundary between the frontal and parietal bones of the skull is lost; and cleft lip and palate, a failure of tissue fusion. This evidence and more suggest that ephrin-B1 has key developmental roles in many different structures, but the specific mechanisms of ephrin-B1 action during craniofacial development, as well as the ways in which ephrin-B1 loss and mosaicism in CFNS contribute to craniofacial dysmorphology, have remained incompletely understood. This work addresses three main questions that contribute to a greater body of work towards a better understanding of ephrin-B1-mediated cell segregation in craniofacial development and disease. The research contained herein represents a step towards better diagnostics and molecular therapies for CFNS, as well as towards a better understanding of the role of one important molecule and its function within a signaling pathway that is critical to the developing face.

Through the first hiPSC model of morphogenesis in a congenital craniofacial disorder, we have demonstrated that human CFNS patient iPSC-derived neuroepithelial cells mosaic for EPHRIN-B1 expression undergo cell segregation. This knowledge is essential because, although cell segregation in the neural plate neuroepithelium (O'Neill et al., 2016), palate mesenchyme (Bush and Soriano, 2010) and limb buds (Compagni et al., 2003) was proposed as a mechanism by which mosaicism in female heterozygous patients could lead to "cellular interference" between ephrin-B1 expressing and non-expressing cells, it was unclear whether or not cell segregation occurred in human cells. Our finding that ephrin-B1-mediated cell

segregation is conserved in humans suggests not only that its role applies across species, but also that this cellular behavior is likely key to human disease pathology. We have also provided proof of principle that hiPSC-derived cell types can be used to model morphogenesis in cell culture, a premise that will hopefully lead to additional human model systems for structural congenital craniofacial anomalies both in our group and elsewhere. In addition, the CFNS patient and family hiPSCs we have developed will be a key tool for further mechanistic studies of ephrin-B1-mediated cell segregation. These will include determining whether ephrin-B1-mediated cell segregation occurs in other human cell types relevant to CFNS, such as neural crest cells and their derivatives; these experiments will be particularly useful for investigation of human phenotypes not recapitulated in the mouse model for CFNS, such as craniosynostosis. The CFNS hiPSC model system will also be used to investigate whether differential cortical tension regulates segregation in human cells and to determine what downstream signaling partners of the EphB receptors mediate this process.

In addition to its role in mouse and human neural progenitor cells, we have shown that ephrin-B1 continues to drive cell segregation behavior in neural crest cells and their derivatives in the mouse as late as E12.5-E13.5 (~40 days gestation in humans), indicating that ephrin-B1 is a potent global regulator of cell segregation in the developing embryo. This finding has clear implications for understanding the developmental etiology of CFNS, as well as for the development of molecular therapies for this disorder; in order to treat pathogenic cell segregation, it is critical to know when and where it occurs. Our work indicates that segregation is an ongoing process through development, and it is possible that loss of ephrin-B1 allows inappropriate cell migration in even later-formed boundaries in the developing craniofacial complex, such as the sutures of the skull. This seems likely given the CFNS patient phenotype of craniosynostosis, but although mutations in *EFNB1* are responsible for 7% of craniosynostosis cases with a genetic diagnosis (Johnson and Wilkie, 2011), whether ectopic suture fusion occurs through a cell segregation mechanism or *via* some other effect of loss of

ephrin-B1 remains unknown. In the future, approaches using tissue-specific Cre recombinase mouse lines to generate ephrin-B1 mosaicism in the suture mesenchyme or osteoblast progenitors may shed light on this important question. More broadly, quantitative comparison of facial shapes in embryos with ephrin-B1 mosaicism in different tissues and cell types will allow pinpointing of the tissues in which craniofacial dysmorphology arises in CFNS, while similar studies in EphB receptor mutant embryos will aid in the determination of which EphB receptor signals contribute to craniofacial phenotypes. With the knowledge that segregation continues later into development, treatments that block or reverse this aberrant cell behavior have greater potential for success, and experiments to determine whether this is possible *in vivo* will be an important step towards the development of targeted molecular therapies for CFNS.

In an important discovery pertaining to the biochemistry of Eph/ephrin signaling, this work also identifies a mechanism by which *cis*-expression of ephrin-B1 with EphB receptors regulates their tissue-wide protein expression and signaling. The function of coexpression of Ephs and ephrins is just beginning to be explored, with ephrin-A coexpression repressing EphA signaling during axon guidance (Carvalho et al., 2006; Hornberger et al., 1999) and multiple Ephs and ephrins contributing to separation of the germ layers in Xenopus (Rohani et al., 2011; Rohani et al., 2014). These findings are not contained within the dogma of Eph/ephrin signaling in boundary formation, which maintains that reciprocal expression of Ephs and ephrins with bidirectional signaling at tissue interfaces forms and preserves tissue boundaries; although this can be shown in several different embryonic contexts, such as the rhombomeres (Xu et al., 1999) and somites (Durbin et al., 2000), we now know that it does not apply to all regions in which these molecules are expressed. Instead, we have demonstrated that coexpression of ephrin-B1 with EphB2 and EphB3 plays an essential role in the availability of the receptor to receive outside signals. Unlike ephrin-A *cis* inhibition of EphA receptors, ephrin-B1 does not bind directly to EphB receptors *in cis* or attenuate receptor phosphorylation using the same mechanisms. Instead, ephrin-B1/EphB coexpression throughout a tissue results in widespread

signaling *in trans* that leads to downregulation of receptor protein expression, thus effectively "blinding" or desensitizing these cells to receipt of further signals from other ephrin-expressing cells. Although many downstream signaling targets of Eph/ephrin signaling have been identified in different contexts, and the behavior of Ephs and ephrins at the cell surface has been described, this represents a novel regulatory mechanism that may apply in many situations in which Ephs and ephrins are coexpressed. Much remains unknown about the ways in which Ephs and ephrins interact, and future work will explore these mechanisms further. In addition, because we have shown that expression levels of ephrin-B1 regulate Eph receptor function, this work opens the door to studies that take advantage of ephrin-B1 misexpression to overcome the effects of mosaicism and aberrant segregation in CFNS by downregulating EphB receptor responses, a treatment that could be key to treating this congenital craniofacial disease.

Although it is a rare disease, craniofrontonasal syndrome is one of a large group of congenital disorders affecting the craniofacial complex that we are beginning to better understand. Future applications of this research will contribute to this improved understanding and aid in the work towards cellular and molecular therapies for this disorder and others, as we apply our knowledge of signaling mechanisms and human cell-based model systems to study defects in boundary formation in the developing embryo. Further, the ectopic boundary formation that occurs in CFNS provides us with an opportunity to delve into studies of cellular mechanisms of developmental boundaries, mechanisms which are not yet well understood in the development and function of mesenchymal structures. A more in-depth comprehension of the cellular behaviors that contribute to the intricate morphogenesis of the face will elucidate key cellular and molecular mechanisms that play important roles during normal development and disease.

Table 6. Antibody information for immunofluorescence (IF) and immunoblotting (IB)

IF - Conjugated Antibodies	Source	Catalog #	Dilution
TRA-1-60, Cy3 conjugate	Millipore	MAB4360C3	1:100
TRA-1-81, Cy3 conjugate	Millipore	MAB4381C3	1:100
NANOG, Alexa Fluor 488 conjugate	Millipore	MABD24A4	1:100
SOX2, Cy3 conjugate	Millipore	MAB4423C3	1:100
OCT4 (POU5FL), Alexa Fluor 488 conjugate	Millipore	MAB4419A4	1:100
IF - Primary Antibodies	**Source**	**Catalog #**	**Dilution**
βIII-tubulin (TUJ1)	Sigma	T8660	1:1000
α-fetoprotein (AFP)	Sigma	A8452	1:500
human muscle actin	DAKO	M0635	1:50
SOX1	R&D Systems	AF3369	1:150
PAX6	Covance	PRB-278P	1:200
OTX2	Millipore	AB9566	1:250
Ephrin-B1	R&D Systems	AF473	0.2 µg/mL
EphB2	R&D Systems	AF467	1:10
EphB3	R&D Systems	AF432	1:20
GFP	Abcam	ab13970	1:500
2H3 (neurofilament)	DSHB	2H3	2 µg/mL
IF - Secondary Antibodies	**Source**	**Catalog #**	**Dilution**
Donkey anti-rabbit Alexa Fluor 488	Jackson IR	711-165-152	1:400
Donkey anti-mouse Cy2	Jackson IR	715-225-150	1:400
Donkey anti-chicken Cy2	Jackson IR	703-225-155	1:400
Donkey anti-goat Cy3	Jackson IR	705-165-003	1:400
IB - Primary Antibodies	**Source**	**Catalog #**	**Dilution**
Ephrin-B1	R&D Systems	AF473	0.2 µg/mL
EphB2	R&D Systems	AF467	0.4 µg/mL
EphB3	R&D Systems	AF432	0.4 µg/mL
HSP70	BD Transduction	610607	1:1000
IB - Secondary Antibodies	**Source**	**Catalog #**	**Dilution**
Donkey anti-goat IRDye® 800CW	LI-COR Biosciences	926-32214	1:5000
Donkey anti-mouse IRDye® 680RD	LI-COR Biosciences	926-68072	1:5000

Table 7. Primer sequence information

qRT-PCR Primers		
Target	**Forward Primer Sequence (5' to 3')**	**Reverse Primer Sequence (5' to 3')**
hEFNB1	GTATCCTGGAGCTCCCTCAACC	GTAGTACTCATAGGGCCGCC
hPAX6	TCGGTGGTGTCTTTGTCAACG	ACTACCACCGATTGCCCTGG
hGAPDH	TCTTCACCACCATGGAGAAGG	CATGGATGACCTTGGCCAGG
hEFNB2	AATCCAGGTTCTAGCACAGACG	GTGCTTCCTGTGTCTCCTCC
hEPHB2	CCATCAAGCTCTACTGTAACGGG	GCTCTGTAGTAGCCATTGCG
hEPHB3	TGGGTAACATCTGAGTTGGC	CTTGAGCTCCACGTAGACCC
mEfnb1	CGTTGGCCAAGAACCTGGAGC	TCCAGCTTGTCTCCAATCTTCGG
mEphB2	TGCTGCTGCCGCTGCTAGC	TCGTAGCCGCTCACCTCTTCC
hiPSC screening: Plasmid PCR Primers		
Target	**Forward Primer Sequence (5' to 3')**	**Reverse Primer Sequence (5' to 3')**
EBNA-1	ATCAGGGCCAAGACATAGAGATG	GCCAATGCAACTTGGACGTT
GAPDH	ACCACAGTCCATGCCATCAC	TCCACCACCCTGTTGCTGTA
mESC screening: PCR and qPCR Primers		
Target	**Forward Primer Sequence (5' to 3')**	**Reverse Primer Sequence (5' to 3')**
ROSA26-adSA (screening)	GAGAGCCTCGGCTAGGTAGG	GATACCGTCGATCCCCACTG
ROSA26-Efnb1 (recombination)	GCACTTGCTCTCCCAAAGTC	CTTCATAGTGCGGGTGCG
ROSA26R (genotype)	AAAGTCGCTCTGAGTTGTTAT	GGAGCGGGAGAAATGGATATG and GCGAAGAGTTTGTCCTCAACC
Neo (qPCR)	AAGGCACTGGCTGCTATTGG	ATCCTGATCGACAAGACCG
mBambi (qPCR)	GGGTTCACGCGATGTTTATGT	TTGCAAGTGAGTCCAGGCAGC

Table 8. Genetic crosses and sample sizes for mouse embryo experiments

Morphometrics	***β-actin-Cre$^{Tg/o}$ x Efnb1$^{lox/lox}$* or *C57BL/6J***			
	E11.5	**E12.5**	**E13.5**	**E14.5**
control (*Efnb1$^{lox/Y}$*; *Efnb1$^{lox/+}$*; wt)	28	23	29	45
β-actin-Cre$^{Tg/o}$; Efnb1$^{Δ/Y}$ (*Efnb1$^{Δ/Y}$*)	21	19	17	25
β-actin-Cre$^{Tg/o}$; Efnb1$^{+/Δ}$ (*Efnb1$^{+/Δ}$*)	26	17	13	29
Immunofluorescence	***β-actin-Cre$^{Tg/o}$; X^{GFP}/Y x Efnb1$^{lox/lox}$***			
	E10.5	**E11.5**	**E12.5**	**E13.5**
control *Efnb1$^{+XGFP/lox}$*	2	--	--	1
β-actin-Cre$^{Tg/o}$; Efnb1$^{+XGFP/Δ}$ (*Efnb1$^{+XGFP/Δ}$*)	3	--	--	2
	Sox10-Cre$^{Tg/o}$; X^{GFP}/Y x Efnb1$^{lox/lox}$			
	E10.5	**E11.5**	**E12.5**	**E13.5**
control *Efnb1$^{+XGFP/lox}$*	4	4	--	4
Sox10-Cre$^{Tg/o}$; Efnb1$^{+XGFP/Δ}$	6	2	--	5
	ROSA26$^{mTmG/mTmG}$ x Sox10-Cre$^{Tg/o}$			
	E10.5	**E11.5**	**E12.5**	**E13.5**
Sox10-Cre$^{Tg/o}$; ROSA26$^{mTmG/+}$	1	--	--	--
	Sox1$^{Cre/+}$; X^{GFP}/Y x Efnb1$^{lox/lox}$			
	E10.5	**E11.5**	**E12.5**	**E13.5**
control *Efnb1$^{+XGFP/lox}$*	--	--	--	--
Sox1$^{Cre/+}$; Efnb1$^{+XGFP/Δ}$	--	--	--	2
	ROSA26$^{mTmG/mTmG}$ x Sox1$^{Cre/+}$			
	E10.5	**E11.5**	**E12.5**	**E13.5**
Sox1$^{Cre/+}$; ROSA26$^{mTmG/+}$	--	--	--	3
	Shox2$^{IresCre/+}$; X^{GFP}/Y x Efnb1$^{lox/lox}$			
	E10.5	**E11.5**	**E12.5**	**E13.5**
control *Efnb1$^{+XGFP/lox}$*	--	3	3	3
Shox2$^{IresCre/+}$; Efnb1$^{+XGFP/Δ}$	--	3	4	4
	ROSA26$^{mTmG/mTmG}$ x Shox2$^{IresCre/+}$			
	E10.5	**E11.5**	**E12.5**	**E13.5**
Shox2$^{IresCre/+}$; ROSA26$^{mTmG/+}$	--	2	2	2

References

Adams, D. C. and Otárola-Castillo, E. (2013). geomorph: an R package for the collection and analysis of geometric morphometric shape data. *Methods Ecol. Evol.* **4**, 393–399.

Aldridge, K., Kane, A. A., Marsh, J. L., Yan, P., Govier, D. and Richtsmeier, J. T. (2005). Relationship of brain and skull in pre- and postoperative sagittal synostosis. *J. Anat.* **206**, 373–385.

Aliee, M., Röper, J.-C., Landsberg, K. P., Pentzold, C., Widmann, T. J., Jülicher, F. and Dahmann, C. (2012). Physical mechanisms shaping the Drosophila dorsoventral compartment boundary. *Curr. Biol. CB* **22**, 967–976.

Antion, M. D., Christie, L. A., Bond, A. M., Dalva, M. B. and Contractor, A. (2010). Ephrin-B3 regulates glutamate receptor signaling at hippocampal synapses. *Mol. Cell. Neurosci.* **45**, 378–388.

Apostolopoulou, D., Stratoudakis, A., Hatzaki, A., Kaxira, O. S., Panagopoulos, K. P., Kollia, P. and Aleporou, V. (2012). A Novel de Novo Mutation Within EFNB1 Gene in a Young Girl with Craniofrontonasal Syndrome. *Cleft Palate. Craniofac. J.* **49**, 109–113.

Arvanitis, D. N., Béhar, A., Tryoen-Tóth, P., Bush, J. O., Jungas, T., Vitale, N. and Davy, A. (2013). Ephrin B1 maintains apical adhesion of neural progenitors. *Dev. Camb. Engl.* **140**, 2082–2092.

Astin, J. W., Batson, J., Kadir, S., Charlet, J., Persad, R. A., Gillatt, D., Oxley, J. D. and Nobes, C. D. (2010). Competition amongst Eph receptors regulates contact inhibition of locomotion and invasiveness in prostate cancer cells. *Nat. Cell Biol.* **12**, 1194–1204.

Babbs, C., Stewart, H. S., Williams, L. J., Connell, L., Goriely, A., Twigg, S. R. F., Smith, K., Lester, T. and Wilkie, A. O. M. (2011). Duplication of the EFNB1 gene in familial hypertelorism: imbalance in ephrin-B1 expression and abnormal phenotypes in humans and mice. *Hum. Mutat.* **32**, 930–938.

Baker, P. R., Tsai, A. C.-H., Springer, M., Swisshelm, K., March, J., Brown, K. and Bellus, G. (2010). Male with mosaicism for supernumerary ring X chromosome: analysis of phenotype and characterization of genotype using array comparative genome hybridization. *J. Craniofac. Surg.* **21**, 1369–1375.

Barrios, A., Poole, R. J., Durbin, L., Brennan, C., Holder, N. and Wilson, S. W. (2003). Eph/Ephrin signaling regulates the mesenchymal-to-epithelial transition of the paraxial mesoderm during somite morphogenesis. *Curr. Biol. CB* **13**, 1571–1582.

Batlle, E. and Wilkinson, D. G. (2012). Molecular mechanisms of cell segregation and boundary formation in development and tumorigenesis. *Cold Spring Harb. Perspect. Biol.* **4**, a008227.

Bénazéraf, B. and Pourquié, O. (2013). Formation and segmentation of the vertebrate body axis. *Annu. Rev. Cell Dev. Biol.* **29**, 1–26.

Bershteyn, M., Hayashi, Y., Desachy, G., Hsiao, E. C., Sami, S., Tsang, K. M., Weiss, L. A., Kriegstein, A. R., Yamanaka, S. and Wynshaw-Boris, A. (2014). Cell-autonomous correction of ring chromosomes in human induced pluripotent stem cells. *Nature* **507**, 99–103.

Betancur, P., Bronner-Fraser, M. and Sauka-Spengler, T. (2010). Assembling neural crest regulatory circuits into a gene regulatory network. *Annu. Rev. Cell Dev. Biol.* **26**, 581–603.

Bhatt, S., Diaz, R. and Trainor, P. A. (2013). Signals and switches in Mammalian neural crest cell differentiation. *Cold Spring Harb. Perspect. Biol.* **5**,.

Bouché, E., Romero-Ortega, M. I., Henkemeyer, M., Catchpole, T., Leemhuis, J., Frotscher, M., May, P., Herz, J. and Bock, H. H. (2013). Reelin induces EphB activation. *Cell Res.* **23**, 473–490.

Boughner, J. C., Wat, S., Diewert, V. M., Young, N. M., Browder, L. W. and Hallgrímsson, B. (2008). Short-faced mice and developmental interactions between the brain and the face. *J. Anat.* **213**, 646–662.

Brodland, G. W. (2002). The Differential Interfacial Tension Hypothesis (DITH): a comprehensive theory for the self-rearrangement of embryonic cells and tissues. *J. Biomech. Eng.* **124**, 188–197.

Brückner, K., Pasquale, E. B. and Klein, R. (1997). Tyrosine phosphorylation of transmembrane ligands for Eph receptors. *Science* **275**, 1640–1643.

Bush, J. O. and Jiang, R. (2012). Palatogenesis: morphogenetic and molecular mechanisms of secondary palate development. *Development* **139**, 828–828.

Bush, J. O. and Soriano, P. (2009). Ephrin-B1 regulates axon guidance by reverse signaling through a PDZ-dependent mechanism. *Genes Dev.* **23**, 1586–1599.

Bush, J. O. and Soriano, P. (2010). Ephrin-B1 forward signaling regulates craniofacial morphogenesis by controlling cell proliferation across Eph–ephrin boundaries. *Genes Dev.* **24**, 2068–2080.

Bush, J. O. and Soriano, P. (2012). Eph/ephrin signaling: genetic, phosphoproteomic, and transcriptomic approaches. *Semin. Cell Dev. Biol.* **23**, 26–34.

Byrne, J. A., Nguyen, H. N. and Reijo Pera, R. A. (2009). Enhanced Generation of Induced Pluripotent Stem Cells from a Subpopulation of Human Fibroblasts. *PLoS ONE* **4**, e7118.

Calzolari, S., Terriente, J. and Pujades, C. (2014). Cell segregation in the vertebrate hindbrain relies on actomyosin cables located at the interhombomeric boundaries. *EMBO J.* **33**, 686–701.

Canty, L., Zarour, E., Kashkooli, L., François, P. and Fagotto, F. (2017). Sorting at embryonic boundaries requires high heterotypic interfacial tension. *Nat. Commun.* **8**, 157.

Carvalho, R. F., Beutler, M., Marler, K. J. M., Knöll, B., Becker-Barroso, E., Heintzmann, R., Ng, T. and Drescher, U. (2006). Silencing of EphA3 through a *cis* interaction with ephrinA5. *Nat. Neurosci.* **9**, 322–330.

Catchpole, T. and Henkemeyer, M. (2011). EphB2 tyrosine kinase-dependent forward signaling in migration of neuronal progenitors that populate and form a distinct region of the dentate niche. *J. Neurosci. Off. J. Soc. Neurosci.* **31**, 11472–11483.

Cavodeassi, F., Ivanovitch, K. and Wilson, S. W. (2013). Eph/Ephrin signalling maintains eye field segregation from adjacent neural plate territories during forebrain morphogenesis. *Dev. Camb. Engl.* **140**, 4193–4202.

Cayuso, J., Xu, Q. and Wilkinson, D. G. (2015). Mechanisms of boundary formation by Eph receptor and ephrin signaling. *Dev. Biol.* **401**, 122–131.

Cayuso, J., Dzementsei, A., Fischer, J. C., Karemore, G., Caviglia, S., Bartholdson, J., Wright, G. J. and Ober, E. A. (2016). EphrinB1/EphB3b Coordinate Bidirectional

Epithelial-Mesenchymal Interactions Controlling Liver Morphogenesis and Laterality. *Dev. Cell* **39**, 316–328.

Chai, Y. and Maxson, R. E. (2006). Recent advances in craniofacial morphogenesis. *Dev. Dyn.* **235**, 2353–2375.

Chambers, S. M., Fasano, C. A., Papapetrou, E. P., Tomishima, M., Sadelain, M. and Studer, L. (2009). Highly efficient neural conversion of human ES and iPS cells by dual inhibition of SMAD signaling. *Nat. Biotechnol.* **27**, 275–280.

Chenaux, G. and Henkemeyer, M. (2011). Forward signaling by EphB1/EphB2 interacting with ephrin-B ligands at the optic chiasm is required to form the ipsilateral projection. *Eur. J. Neurosci.* **34**, 1620–1633.

Cohen, M. M., Jr. (1979). Craniofrontonasal dysplasia. *Birth Defects Orig. Artic. Ser.* **15**, 85–9.

Compagni, A., Logan, M., Klein, R. and Adams, R. H. (2003). Control of skeletal patterning by ephrinB1-EphB interactions. *Dev. Cell* **5**, 217–230.

Cooke, J., Moens, C., Roth, L., Durbin, L., Shiomi, K., Brennan, C., Kimmel, C., Wilson, S. and Holder, N. (2001). Eph signalling functions downstream of Val to regulate cell sorting and boundary formation in the caudal hindbrain. *Dev. Camb. Engl.* **128**, 571–580.

Cooke, J. E., Kemp, H. A. and Moens, C. B. (2005). EphA4 is required for cell adhesion and rhombomere-boundary formation in the zebrafish. *Curr. Biol. CB* **15**, 536–542.

Cortina, C., Palomo-Ponce, S., Iglesias, M., Fernández-Masip, J. L., Vivancos, A., Whissell, G., Humà, M., Peiró, N., Gallego, L., Jonkheer, S., et al. (2007). EphB-ephrin-B interactions suppress colorectal cancer progression by compartmentalizing tumor cells. *Nat. Genet.* **39**, 1376–1383.

Cowan, C. A., Yokoyama, N., Saxena, A., Chumley, M. J., Silvany, R. E., Baker, L. A., Srivastava, D. and Henkemeyer, M. (2004). Ephrin-B2 reverse signaling is required for axon pathfinding and cardiac valve formation but not early vascular development. *Dev. Biol.* **271**, 263–271.

Cox, T. C. (2004). Taking it to the max: the genetic and developmental mechanisms coordinating midfacial morphogenesis and dysmorphology. *Clin. Genet.* **65**, 163–176.

Daar, I. O. (2012). Non-SH2/PDZ reverse signaling by ephrins. *Semin. Cell Dev. Biol.* **23**, 65–74.

D'Arcangelo, G., Homayouni, R., Keshvara, L., Rice, D. S., Sheldon, M. and Curran, T. (1999). Reelin is a ligand for lipoprotein receptors. *Neuron* **24**, 471–479.

Davis, S., Gale, N. W., Aldrich, T. H., Maisonpierre, P. C., Lhotak, V., Pawson, T., Goldfarb, M. and Yancopoulos, G. D. (1994). Ligands for EPH-related receptor tyrosine kinases that require membrane attachment or clustering for activity. *Science* **266**, 816–819.

Davy, A. and Robbins, S. M. (2000). Ephrin-A5 modulates cell adhesion and morphology in an integrin-dependent manner. *EMBO J.* **19**, 5396–5405.

Davy, A. and Soriano, P. (2007). Ephrin-B2 forward signaling regulates somite patterning and neural crest cell development. *Dev. Biol.* **304**, 182–193.

Davy, A., Gale, N. W., Murray, E. W., Klinghoffer, R. A., Soriano, P., Feuerstein, C. and Robbins, S. M. (1999). Compartmentalized signaling by GPI-anchored ephrin-A5 requires the Fyn tyrosine kinase to regulate cellular adhesion. *Genes Dev.* **13**, 3125–3135.

Davy, A., Aubin, J. and Soriano, P. (2004). Ephrin-B1 forward and reverse signaling are required during mouse development. *Genes Dev.* **18**, 572–583.

Davy, A., Bush, J. O. and Soriano, P. (2006). Inhibition of gap junction communication at ectopic Eph/ephrin boundaries underlies craniofrontonasal syndrome. *PLoS Biol.* **4**, e315.

Depew, M. J. and Compagnucci, C. Tweaking the hinge and caps: testing a model of the organization of jaws. *J. Exp. Zoolog. B Mol. Dev. Evol.* **310B**, 315–335.

Diewert, V. M. (1985). Growth movements during prenatal development of human facial morphology. *Prog. Clin. Biol. Res.* **187**, 57–66.

Dixon, M. J., Marazita, M. L., Beaty, T. H. and Murray, J. C. (2011). Cleft lip and palate: understanding genetic and environmental influences. *Nat. Rev. Genet.* **12**, 167–178.

Dougherty, K. J., Zagoraiou, L., Satoh, D., Rozani, I., Doobar, S., Arber, S., Jessell, T. M. and Kiehn, O. (2013). Locomotor rhythm generation linked to the output of spinal shox2 excitatory interneurons. *Neuron* **80**, 920–933.

Dravis, C. and Henkemeyer, M. (2011). Ephrin-B reverse signaling controls septation events at the embryonic midline through separate tyrosine phosphorylation-independent signaling avenues. *Dev. Biol.* **355**, 138–151.

Dravis, C., Yokoyama, N., Chumley, M. J., Cowan, C. A., Silvany, R. E., Shay, J., Baker, L. A. and Henkemeyer, M. (2004). Bidirectional signaling mediated by ephrin-B2 and EphB2 controls urorectal development. *Dev. Biol.* **271**, 272–290.

Dudanova, I., Kao, T.-J., Herrmann, J. E., Zheng, B., Kania, A. and Klein, R. (2012). Genetic evidence for a contribution of EphA:ephrinA reverse signaling to motor axon guidance. *J. Neurosci. Off. J. Soc. Neurosci.* **32**, 5209–5215.

Durbin, L., Brennan, C., Shiomi, K., Cooke, J., Barrios, A., Shanmugalingam, S., Guthrie, B., Lindberg, R. and Holder, N. (1998). Eph signaling is required for segmentation and differentiation of the somites. *Genes Dev.* **12**, 3096–3109.

Durbin, L., Sordino, P., Barrios, A., Gering, M., Thisse, C., Thisse, B., Brennan, C., Green, A., Wilson, S. and Holder, N. (2000). Anteroposterior patterning is required within segments for somite boundary formation in developing zebrafish. *Dev. Camb. Engl.* **127**, 1703–1713.

Egea, J. and Klein, R. (2007). Bidirectional Eph-ephrin signaling during axon guidance. *Trends Cell Biol.* **17**, 230–238.

Etchevers, H. C., Amiel, J. and Lyonnet, S. (2006). Molecular Bases of Human Neurocristopathies. In *Neural Crest Induction and Differentiation* (ed. Saint-Jeannet, J.-P.), pp. 213–234. Springer US.

Evers, C., Jungwirth, M. S., Morgenthaler, J., Hinderhofer, K., Maas, B., Janssen, J. W. G., Jauch, A., Hehr, U., Steinbeisser, H. and Moog, U. (2014). Craniofrontonasal syndrome in a male due to chromosomal mosaicism involving EFNB1: further insights into a genetic paradox. *Clin. Genet.* **85**, 347–353.

Fagotto, F. (2014). The cellular basis of tissue separation. *Dev. Camb. Engl.* **141**, 3303–3318.

Fagotto, F., Rohani, N., Touret, A.-S. and Li, R. (2013). A Molecular Base for Cell Sorting at Embryonic Boundaries: Contact Inhibition of Cadherin Adhesion by Ephrin/Eph-Dependent Contractility. *Dev. Cell* **27**, 72–87.

Fagotto, F., Winklbauer, R. and Rohani, N. (2014). Ephrin-Eph signaling in embryonic tissue separation. *Cell Adhes. Migr.* **8**, 308–326.

Falivelli, G., Lisabeth, E. M., Rubio de la Torre, E., Perez-Tenorio, G., Tosato, G., Salvucci, O. and Pasquale, E. B. (2013). Attenuation of eph receptor kinase activation in cancer cells by coexpressed ephrin ligands. *PloS One* **8**, e81445.

Freywald, A., Sharfe, N. and Roifman, C. M. (2002). The Kinase-null EphB6 Receptor Undergoes Transphosphorylation in a Complex with EphB1. *J. Biol. Chem.* **277**, 3823–3828.

Gale, N. W., Holland, S. J., Valenzuela, D. M., Flenniken, A., Pan, L., Ryan, T. E., Henkemeyer, M., Strebhardt, K., Hirai, H., Wilkinson, D. G., et al. (1996). Eph receptors and ligands comprise two major specificity subclasses and are reciprocally compartmentalized during embryogenesis. *Neuron* **17**, 9–19.

Gatto, G., Morales, D., Kania, A. and Klein, R. (2014). EphA4 receptor shedding regulates spinal motor axon guidance. *Curr. Biol. CB* **24**, 2355–2365.

Georgakopoulos, A., Litterst, C., Ghersi, E., Baki, L., Xu, C., Serban, G. and Robakis, N. K. (2006). Metalloproteinase/Presenilin1 processing of ephrinB regulates EphB-induced Src phosphorylation and signaling. *EMBO J.* **25**, 1242–1252.

Global strategies to reduce the health care burden of craniofacial anomalies: report of WHO meetings on international collaborative research on craniofacial anomalies

(2004). *Cleft Palate-Craniofacial J. Off. Publ. Am. Cleft Palate-Craniofacial Assoc.* **41**, 238–243.

Gong, J., Körner, R., Gaitanos, L. and Klein, R. (2016). Exosomes mediate cell contact-independent ephrin-Eph signaling during axon guidance. *J. Cell Biol.* **214**, 35–44.

Hadjantonakis, A. K., Gertsenstein, M., Ikawa, M., Okabe, M. and Nagy, A. (1998). Non-invasive sexing of preimplantation stage mammalian embryos. *Nat. Genet.* **19**, 220–222.

Hadjantonakis, A.-K., Cox, L. L., Tam, P. P. L. and Nagy, A. (2001). An X-linked GFP transgene reveals unexpected paternal X-chromosome activity in trophoblastic giant cells of the mouse placenta. *genesis* **29**, 133–140.

Hattori, M., Osterfield, M. and Flanagan, J. G. (2000). Regulated Cleavage of a Contact-Mediated Axon Repellent. *Science* **289**, 1360–1365.

Helms, J. A., Cordero, D. and Tapadia, M. D. (2005). New insights into craniofacial morphogenesis. *Development* **132**, 851–861.

Henkemeyer, M., Marengere, L. E., McGlade, J., Olivier, J. P., Conlon, R. A., Holmyard, D. P., Letwin, K. and Pawson, T. (1994). Immunolocalization of the Nuk receptor tyrosine kinase suggests roles in segmental patterning of the brain and axonogenesis. *Oncogene* **9**, 1001–1014.

Henkemeyer, M., Orioli, D., Henderson, J. T., Saxton, T. M., Roder, J., Pawson, T. and Klein, R. (1996). Nuk controls pathfinding of commissural axons in the mammalian central nervous system. *Cell* **86**, 35–46.

Himanen, J.-P., Chumley, M. J., Lackmann, M., Li, C., Barton, W. A., Jeffrey, P. D., Vearing, C., Geleick, D., Feldheim, D. A., Boyd, A. W., et al. (2004). Repelling class

discrimination: ephrin-A5 binds to and activates EphB2 receptor signaling. *Nat. Neurosci.* **7**, 501–509.

Himanen, J. P., Yermekbayeva, L., Janes, P. W., Walker, J. R., Xu, K., Atapattu, L., Rajashankar, K. R., Mensinga, A., Lackmann, M., Nikolov, D. B., et al. (2010). Architecture of Eph receptor clusters. *Proc. Natl. Acad. Sci. U. S. A.* **107**, 10860–10865.

Hirai, H., Maru, Y., Hagiwara, K., Nishida, J. and Takaku, F. (1987). A novel putative tyrosine kinase receptor encoded by the eph gene. *Science* **238**, 1717–1720.

Hogue, J., Shankar, S., Perry, H., Patel, R., Vargervik, K. and Slavotinek, A. (2010). A novel EFNB1 mutation (c.712delG) in a family with craniofrontonasal syndrome and diaphragmatic hernia. *Am. J. Med. Genet. A.* **152A**, 2574–2577.

Holland, S. J., Gale, N. W., Mbamalu, G., Yancopoulos, G. D., Henkemeyer, M. and Pawson, T. (1996). Bidirectional signalling through the EPH-family receptor Nuk and its transmembrane ligands. *Nature* **383**, 722–725.

Holmberg, J., Genander, M., Halford, M. M., Annerén, C., Sondell, M., Chumley, M. J., Silvany, R. E., Henkemeyer, M. and Frisén, J. (2006). EphB receptors coordinate migration and proliferation in the intestinal stem cell niche. *Cell* **125**, 1151–1163.

Hornberger, M. R., Dütting, D., Ciossek, T., Yamada, T., Handwerker, C., Lang, S., Weth, F., Huf, J., Wessel, R., Logan, C., et al. (1999). Modulation of EphA receptor function by coexpressed ephrinA ligands on retinal ganglion cell axons. *Neuron* **22**, 731–742.

Howell, B. W., Herrick, T. M. and Cooper, J. A. (1999). Reelin-induced tyrosine [corrected] phosphorylation of disabled 1 during neuronal positioning. *Genes Dev.* **13**, 643–648.

Huai, J. and Drescher, U. (2001). An ephrin-A-dependent signaling pathway controls integrin function and is linked to the tyrosine phosphorylation of a 120-kDa protein. *J. Biol. Chem.* **276**, 6689–6694.

Hwang, Y.-S., Lee, H.-S., Kamata, T., Mood, K., Cho, H. J., Winterbottom, E., Ji, Y. J., Singh, A. and Daar, I. O. (2013). The Smurf ubiquitin ligases regulate tissue separation via antagonistic interactions with ephrinB1. *Genes Dev.* **27**, 491–503.

Janes, P. W., Saha, N., Barton, W. A., Kolev, M. V., Wimmer-Kleikamp, S. H., Nievergall, E., Blobel, C. P., Himanen, J.-P., Lackmann, M. and Nikolov, D. B. (2005). Adam Meets Eph: An ADAM Substrate Recognition Module Acts as a Molecular Switch for Ephrin Cleavage In trans. *Cell* **123**, 291–304.

Janes, P. W., Griesshaber, B., Atapattu, L., Nievergall, E., Hii, L. L., Mensinga, A., Chheang, C., Day, B. W., Boyd, A. W., Bastiaens, P. I., et al. (2011). Eph receptor function is modulated by heterooligomerization of A and B type Eph receptors. *J. Cell Biol.* **195**, 1033–1045.

Jiang, R., Bush, J. O. and Lidral, A. C. (2006). Development of the upper lip: morphogenetic and molecular mechanisms. *Dev. Dyn. Off. Publ. Am. Assoc. Anat.* **235**, 1152–1166.

Johnson, D. and Wilkie, A. O. M. (2011). Craniosynostosis. *Eur. J. Hum. Genet.* **19**, 369–376.

Jones, N. C., Lynn, M. L., Gaudenz, K., Sakai, D., Aoto, K., Rey, J.-P., Glynn, E. F., Ellington, L., Du, C., Dixon, J., et al. (2008). Prevention of the neurocristopathy Treacher Collins syndrome through inhibition of p53 function. *Nat. Med.* **14**, 125–133.

Jorgensen, C., Sherman, A., Chen, G. I., Pasculescu, A., Poliakov, A., Hsiung, M., Larsen, B., Wilkinson, D. G., Linding, R. and Pawson, T. (2009). Cell-Specific Information

Processing in Segregating Populations of Eph Receptor Ephrin-Expressing Cells. *Science* **326**, 1502–1509.

Jülich, D., Mould, A. P., Koper, E. and Holley, S. A. (2009). Control of extracellular matrix assembly along tissue boundaries via Integrin and Eph/Ephrin signaling. *Dev. Camb. Engl.* **136**, 2913–2921.

Kania, A. and Klein, R. (2016). Mechanisms of ephrin-Eph signalling in development, physiology and disease. *Nat. Rev. Mol. Cell Biol.* **17**, 240–256.

Kao, T.-J. and Kania, A. (2011). Ephrin-mediated cis-attenuation of Eph receptor signaling is essential for spinal motor axon guidance. *Neuron* **71**, 76–91.

Kao, T.-J., Law, C. and Kania, A. (2012). Eph and ephrin signaling: Lessons learned from spinal motor neurons. *Semin. Cell Dev. Biol.* **23**, 83–91.

Kasemeier-Kulesa, J. C., Kulesa, P. M. and Lefcort, F. (2005). Imaging neural crest cell dynamics during formation of dorsal root ganglia and sympathetic ganglia. *Development* **132**, 235–245.

Kasemeier-Kulesa, J. C., Bradley, R., Pasquale, E. B., Lefcort, F. and Kulesa, P. M. (2006). Eph/ephrins and N-cadherin coordinate to control the pattern of sympathetic ganglia. *Development* **133**, 4839–4847.

Kemp, H. A., Cooke, J. E. and Moens, C. B. (2009). EphA4 and EfnB2a maintain rhombomere coherence by independently regulating intercalation of progenitor cells in the zebrafish neural keel. *Dev. Biol.* **327**, 313–326.

Kiedrowski, L. A., Raca, G., Laffin, J. J., Nisler, B. S., Leonhard, K., McIntire, E. and Mongomery, K. D. (2011). DNA Methylation Assay for X-Chromosome Inactivation in Female Human iPS Cells. *Stem Cell Rev. Rep.* **7**, 969–975.

Kim, S., Lewis, A. E., Singh, V., Ma, X., Adelstein, R. and Bush, J. O. (2015). Convergence and extrusion are required for normal fusion of the mammalian secondary palate. *PLoS Biol.* **13**, e1002122.

Klein, R. and Kania, A. (2014). Ephrin signalling in the developing nervous system. *Curr. Opin. Neurobiol.* **27**, 16–24.

Koshida, S., Kishimoto, Y., Ustumi, H., Shimizu, T., Furutani-Seiki, M., Kondoh, H. and Takada, S. (2005). Integrinalpha5-dependent fibronectin accumulation for maintenance of somite boundaries in zebrafish embryos. *Dev. Cell* **8**, 587–598.

Krieg, M., Arboleda-Estudillo, Y., Puech, P.-H., Käfer, J., Graner, F., Müller, D. J. and Heisenberg, C.-P. (2008). Tensile forces govern germ-layer organization in zebrafish. *Nat. Cell Biol.* **10**, 429–436.

Krull, C. E., Lansford, R., Gale, N. W., Collazo, A., Marcelle, C., Yancopoulos, G. D., Fraser, S. E. and Bronner-Fraser, M. (1997). Interactions of Eph-related receptors and ligands confer rostrocaudal pattern to trunk neural crest migration. *Curr. Biol. CB* **7**, 571–580.

Kullander, K. and Klein, R. (2002). Mechanisms and functions of Eph and ephrin signalling. *Nat. Rev. Mol. Cell Biol.* **3**, 475–486.

Kullander, K., Croll, S. D., Zimmer, M., Pan, L., McClain, J., Hughes, V., Zabski, S., DeChiara, T. M., Klein, R., Yancopoulos, G. D., et al. (2001). Ephrin-B3 is the midline

barrier that prevents corticospinal tract axons from recrossing, allowing for unilateral motor control. *Genes Dev.* **15**, 877–888.

LaBonne, C. and Bronner-Fraser, M. (1998). Induction and patterning of the neural crest, a stem cell-like precursor population. *J. Neurobiol.* **36**, 175–189.

Lackmann, M., Oates, A. C., Dottori, M., Smith, F. M., Do, C., Power, M., Kravets, L. and Boyd, A. W. (1998). Distinct subdomains of the EphA3 receptor mediate ligand binding and receptor dimerization. *J. Biol. Chem.* **273**, 20228–20237.

Laussu, J., Khuong, A., Gautrais, J. and Davy, A. (2014). Beyond boundaries--Eph:ephrin signaling in neurogenesis. *Cell Adhes. Migr.* **8**, 349–359.

Le Douarin, N. M. and Dupin, E. (2003). Multipotentiality of the neural crest. *Curr. Opin. Genet. Dev.* **13**, 529–536.

Lessing, D. and Lee, J. T. (2013). X Chromosome Inactivation and Epigenetic Responses to Cellular Reprogramming. *Annu. Rev. Genomics Hum. Genet.* **14**, 85–110.

Lewandoski, M., Meyers, E. N. and Martin, G. R. (1997). Analysis of Fgf8 gene function in vertebrate development. *Cold Spring Harb. Symp. Quant. Biol.* **62**, 159–168.

Lewis, A. E., Hwa, J., Wang, R., Soriano, P. and Bush, J. O. (2015). Neural crest defects in ephrin-B2 mutant mice are non-autonomous and originate from defects in the vasculature. *Dev. Biol.* **406**, 186–195.

Lin, D., Gish, G. D., Songyang, Z. and Pawson, T. (1999). The carboxyl terminus of B class ephrins constitutes a PDZ domain binding motif. *J. Biol. Chem.* **274**, 3726–3733.

Losa, M., Risolino, M., Li, B., Hart, J., Quintana, L., Grishina, I., Yang, H., Choi, I. F., Lewicki, P., Khan, S., et al. (2018). Face morphogenesis is promoted by Pbx-dependent EMT via regulation of Snail1 during frontonasal prominence fusion. *Development* **145**, dev157628.

Lu, Q., Sun, E. E., Klein, R. S. and Flanagan, J. G. (2001). Ephrin-B reverse signaling is mediated by a novel PDZ-RGS protein and selectively inhibits G protein-coupled chemoattraction. *Cell* **105**, 69–79.

Makarov, R., Steiner, B., Gucev, Z., Tasic, V., Wieacker, P. and Wieland, I. (2010). The impact of CFNS-causing EFNB1 mutations on ephrin-B1 function. *BMC Med. Genet.* **11**, 98.

Makinen, T. (2005). PDZ interaction site in ephrinB2 is required for the remodeling of lymphatic vasculature. *Genes Dev.* **19**, 397–410.

Marcucio, R. S., Young, N. M., Hu, D. and Hallgrimsson, B. (2011). Mechanisms that underlie co-variation of the brain and face. *Genes. N. Y. N 2000* **49**, 177–189.

Marcucio, R., Hallgrimsson, B. and Young, N. M. (2015). Facial Morphogenesis: Physical and Molecular Interactions Between the Brain and the Face. *Curr. Top. Dev. Biol.* **115**, 299–320.

Marquardt, T., Shirasaki, R., Ghosh, S., Andrews, S. E., Carter, N., Hunter, T. and Pfaff, S. L. (2005). Coexpressed EphA receptors and ephrin-A ligands mediate opposing actions on growth cone navigation from distinct membrane domains. *Cell* **121**, 127–139.

Marston, D. J., Dickinson, S. and Nobes, C. D. (2003). Rac-dependent trans-endocytosis of ephrinBs regulates Eph-ephrin contact repulsion. *Nat. Cell Biol.* **5**, 879–888.

Marulanda, J. and Murshed, M. (2018). Role of Matrix Gla protein in midface development: Recent advances. *Oral Dis.* **24**, 78–83.

Marulanda, J., Eimar, H., McKee, M. D., Berkvens, M., Nelea, V., Roman, H., Borrás, T., Tamimi, F., Ferron, M. and Murshed, M. (2017). Matrix Gla protein deficiency impairs nasal septum growth, causing midface hypoplasia. *J. Biol. Chem.* **292**, 11400–11412.

Matsuoka, T., Ahlberg, P. E., Kessaris, N., Iannarelli, P., Dennehy, U., Richardson, W. D., McMahon, A. P. and Koentges, G. (2005). Neural crest origins of the neck and shoulder. *Nature* **436**, 347–355.

Mellitzer, G., Xu, Q. and Wilkinson, D. G. (1999). Eph receptors and ephrins restrict cell intermingling and communication. *Nature* **400**, 77–81.

Mendes, S. W. (2006). Multiple Eph Receptors and B-Class Ephrins Regulate Midline Crossing of Corpus Callosum Fibers in the Developing Mouse Forebrain. *J. Neurosci.* **26**, 882–892.

Merlos-Suárez, A. and Batlle, E. (2008). Eph-ephrin signalling in adult tissues and cancer. *Curr. Opin. Cell Biol.* **20**, 194–200.

Merrill, A. E., Bochukova, E. G., Brugger, S. M., Ishii, M., Pilz, D. T., Wall, S. A., Lyons, K. M., Wilkie, A. O. M. and Maxson, R. E. (2006). Cell mixing at a neural crest-mesoderm boundary and deficient ephrin-Eph signaling in the pathogenesis of craniosynostosis. *Hum. Mol. Genet.* **15**, 1319–1328.

Mochizuki, A., Wada, N., Ide, H. and Iwasa, Y. (1998). Cell-cell adhesion in limb-formation, estimated from photographs of cell sorting experiments based on a spatial stochastic model. *Dev. Dyn. Off. Publ. Am. Assoc. Anat.* **211**, 204–214.

Moens, C. B. and Prince, V. E. (2002). Constructing the hindbrain: insights from the zebrafish. *Dev. Dyn. Off. Publ. Am. Assoc. Anat.* **224**, 1–17.

Monier, B., Pélissier-Monier, A., Brand, A. H. and Sanson, B. (2010). An actomyosin-based barrier inhibits cell mixing at compartmental boundaries in Drosophila embryos. *Nat. Cell Biol.* **12**, 60–69.

Moore, K. L., Persaud, T. V. N. and Torchia, M. G. (2007). *The Developing Human: Clinically Oriented Embryology*. 8th edition. Saunders.

Muzumdar, M. D., Tasic, B., Miyamichi, K., Li, L. and Luo, L. (2007). A global double-fluorescent Cre reporter mouse. *Genes. N. Y. N 2000* **45**, 593–605.

Neely, M. D., Litt, M. J., Tidball, A. M., Li, G. G., Aboud, A. A., Hopkins, C. R., Chamberlin, R., Hong, C. C., Ess, K. C. and Bowman, A. B. (2012). DMH1, a Highly Selective Small Molecule BMP Inhibitor Promotes Neurogenesis of hiPSCs: Comparison of PAX6 and SOX1 Expression during Neural Induction. *ACS Chem. Neurosci.* **3**, 482–491.

Nguyen, T. M., Arthur, A., Paton, S., Hemming, S., Panagopoulos, R., Codrington, J., Walkley, C. R., Zannettino, A. C. W. and Gronthos, S. (2016). Loss of ephrinB1 in osteogenic progenitor cells impedes endochondral ossification and compromises bone strength integrity during skeletal development. *Bone* **93**, 12–21.

Noh, H., Park, E. and Park, S. (2014). In vivo expression of ephrinA5-Fc in mice results in cephalic neural crest agenesis and craniofacial abnormalities. *Mol. Cells* **37**, 59–65.

Nose, A., Nagafuchi, A. and Takeichi, M. (1988). Expressed recombinant cadherins mediate cell sorting in model systems. *Cell* **54**, 993–1001.

Okita, K., Matsumura, Y., Sato, Y., Okada, A., Morizane, A., Okamoto, S., Hong, H., Nakagawa, M., Tanabe, K., Tezuka, K., et al. (2011). A more efficient method to generate integration-free human iPS cells. *Nat. Methods* **8**, 409–412.

O'Neill, A. K., Kindberg, A. A., Niethamer, T. K., Larson, A. R., Ho, H.-Y. H., Greenberg, M. E. and Bush, J. O. (2016). Unidirectional Eph/ephrin signaling creates a cortical actomyosin differential to drive cell segregation. *J. Cell Biol.* **215**, 217–229.

Orioli, D., Henkemeyer, M., Lemke, G., Klein, R. and Pawson, T. (1996). Sek4 and Nuk receptors cooperate in guidance of commissural axons and in palate formation. *EMBO J.* **15**, 6035.

Parsons, T. E., Schmidt, E. J., Boughner, J. C., Jamniczky, H. A., Marcucio, R. S. and Hallgrímsson, B. (2011). Epigenetic integration of the developing brain and face. *Dev. Dyn. Off. Publ. Am. Assoc. Anat.* **240**, 2233–2244.

Pasquale, E. B. (2005). Eph receptor signalling casts a wide net on cell behaviour. *Nat. Rev. Mol. Cell Biol.* **6**, 462–475.

Pasquale, E. B. (2008). Eph-ephrin bidirectional signaling in physiology and disease. *Cell* **133**, 38–52.

Pegg, C. L., Cooper, L. T., Zhao, J., Gerometta, M., Smith, F. M., Yeh, M., Bartlett, P. F., Gorman, J. J. and Boyd, A. W. (2017). Glycoengineering of EphA4 Fc leads to a unique, long-acting and broad spectrum, Eph receptor therapeutic antagonist. *Sci. Rep.* **7**, 6519.

Percival, C. J., Green, R., Marcucio, R. and Hallgrímsson, B. (2014). Surface landmark quantification of embryonic mouse craniofacial morphogenesis. *BMC Dev. Biol.* **14**,.

Pohlkamp, T., Xiao, L., Sultana, R., Bepari, A., Bock, H. H., Henkemeyer, M. and Herz, J. (2016). Ephrin Bs and canonical Reelin signalling. *Nature* **539**, E4–E6.

Poliakov, A., Cotrina, M. and Wilkinson, D. G. (2004). Diverse roles of eph receptors and ephrins in the regulation of cell migration and tissue assembly. *Dev. Cell* **7**, 465–480.

Poliakov, A., Cotrina, M. L., Pasini, A. and Wilkinson, D. G. (2008). Regulation of EphB2 activation and cell repulsion by feedback control of the MAPK pathway. *J. Cell Biol.* **183**, 933–947.

Prin, F., Serpente, P., Itasaki, N. and Gould, A. P. (2014). Hox proteins drive cell segregation and non-autonomous apical remodelling during hindbrain segmentation. *Dev. Camb. Engl.* **141**, 1492–1502.

R Developmental Core Team (2008). *R: A language and environment for statistical computing.* Vienna, Austria: R Foundation for Statistical Computing.

Richtsmeier, J. T., Aldridge, K., DeLeon, V. B., Panchal, J., Kane, A. A., Marsh, J. L., Yan, P. and Cole, T. M. (2006). Phenotypic integration of neurocranium and brain. *J. Exp. Zoolog. B Mol. Dev. Evol.* **306B**, 360–378.

Risley, M., Garrod, D., Henkemeyer, M. and McLean, W. (2009). EphB2 and EphB3 forward signalling are required for palate development. *Mech. Dev.* **126**, 230–239.

Robichaux, M. A., Chenaux, G., Ho, H.-Y. H., Soskis, M. J., Dravis, C., Kwan, K. Y., Šestan, N., Greenberg, M. E., Henkemeyer, M. and Cowan, C. W. (2014). EphB receptor forward signaling regulates area-specific reciprocal thalamic and cortical axon pathfinding. *Proc. Natl. Acad. Sci. U. S. A.* **111**, 2188–2193.

Robichaux, M. A., Chenaux, G., Ho, H.-Y. H., Soskis, M. J., Greenberg, M. E., Henkemeyer, M. and Cowan, C. W. (2016). EphB1 and EphB2 intracellular domains regulate the formation of the corpus callosum and anterior commissure. *Dev. Neurobiol.* **76**, 405–420.

Rohani, N., Canty, L., Luu, O., Fagotto, F. and Winklbauer, R. (2011). EphrinB/EphB Signaling Controls Embryonic Germ Layer Separation by Contact-Induced Cell Detachment. *PLoS Biol.* **9**, e1000597.

Rohani, N., Parmeggiani, A., Winklbauer, R. and Fagotto, F. (2014). Variable combinations of specific ephrin ligand/Eph receptor pairs control embryonic tissue separation. *PLoS Biol.* **12**, e1001955.

Sakai, D., Dixon, J., Achilleos, A., Dixon, M. and Trainor, P. A. (2016). Prevention of Treacher Collins syndrome craniofacial anomalies in mouse models via maternal antioxidant supplementation. *Nat. Commun.* **7**, 10328.

Santiago, A. and Erickson, C. A. (2002). Ephrin-B ligands play a dual role in the control of neural crest cell migration. *Dev. Camb. Engl.* **129**, 3621–3632.

Schaupp, A., Sabet, O., Dudanova, I., Ponserre, M., Bastiaens, P. and Klein, R. (2014). The composition of EphB2 clusters determines the strength in the cellular repulsion response. *J. Cell Biol.* **204**, 409–422.

Seiradake, E., Harlos, K., Sutton, G., Aricescu, A. R. and Jones, E. Y. (2010). An extracellular steric seeding mechanism for Eph-ephrin signaling platform assembly. *Nat. Struct. Mol. Biol.* **17**, 398–402.

Sentürk, A., Pfennig, S., Weiss, A., Burk, K. and Acker-Palmer, A. (2011). Ephrin Bs are essential components of the Reelin pathway to regulate neuronal migration. *Nature* **472**, 356–360.

Smith, A., Robinson, V., Patel, K. and Wilkinson, D. G. (1997). The EphA4 and EphB1 receptor tyrosine kinases and ephrin-B2 ligand regulate targeted migration of branchial neural crest cells. *Curr. Biol. CB* **7**, 561–570.

Solanas, G., Cortina, C., Sevillano, M. and Batlle, E. (2011). Cleavage of E-cadherin by ADAM10 mediates epithelial cell sorting downstream of EphB signalling. *Nat. Cell Biol.* **13**, 1100–1107.

Soriano, P. (1999). Generalized lacZ expression with the ROSA26 Cre reporter strain. *Nat. Genet.* **21**, 70–71.

Soskis, M. J., Ho, H.-Y. H., Bloodgood, B. L., Robichaux, M. A., Malik, A. N., Ataman, B., Rubin, A. A., Zieg, J., Zhang, C., Shokat, K. M., et al. (2012). A Chemical Genetic Approach Reveals Distinct Mechanisms of EphB Signaling During Brain Development. *Nat. Neurosci.* **15**, 1645–1654.

Srinivas, S., Watanabe, T., Lin, C. S., William, C. M., Tanabe, Y., Jessell, T. M. and Costantini, F. (2001). Cre reporter strains produced by targeted insertion of EYFP and ECFP into the ROSA26 locus. *BMC Dev. Biol.* **1**, 4.

Steinberg, M. S. (1970). Does differential adhesion govern self-assembly processes in histogenesis? Equilibrium configurations and the emergence of a hierarchy among populations of embryonic cells. *J. Exp. Zool.* **173**, 395–433.

Suzuki, A., Sangani, D. R., Ansari, A. and Iwata, J. (2016). Molecular mechanisms of midfacial developmental defects. *Dev. Dyn. Off. Publ. Am. Assoc. Anat.* **245**, 276–293.

Takahashi, K. and Yamanaka, S. (2006). Induction of pluripotent stem cells from mouse embryonic and adult fibroblast cultures by defined factors. *Cell* **126**, 663–676.

Takahashi, K., Tanabe, K., Ohnuki, M., Narita, M., Ichisaka, T., Tomoda, K. and Yamanaka, S. (2007). Induction of pluripotent stem cells from adult human fibroblasts by defined factors. *Cell* **131**, 861–872.

Takashima, Y., Era, T., Nakao, K., Kondo, S., Kasuga, M., Smith, A. G. and Nishikawa, S.-I. (2007). Neuroepithelial cells supply an initial transient wave of MSC differentiation. *Cell* **129**, 1377–1388.

Taylor, H. B., Khuong, A., Wu, Z., Xu, Q., Morley, R., Gregory, L., Poliakov, A., Taylor, W. R. and Wilkinson, D. G. (2017). Cell segregation and border sharpening by Eph receptor–ephrin-mediated heterotypic repulsion. *J. R. Soc. Interface* **14**, 20170338.

Tchieu, J., Kuoy, E., Chin, M. H., Trinh, H., Patterson, M., Sherman, S. P., Aimiuwu, O., Lindgren, A., Hakimian, S., Zack, J. A., et al. (2010). Female Human iPSCs Retain an Inactive X Chromosome. *Cell Stem Cell* **7**, 329–342.

Theil, T., Frain, M., Gilardi-Hebenstreit, P., Flenniken, A., Charnay, P. and Wilkinson, D. G. (1998). Segmental expression of the EphA4 (Sek-1) receptor tyrosine kinase in the hindbrain is under direct transcriptional control of Krox-20. *Dev. Camb. Engl.* **125**, 443–452.

Ting, M.-C., Wu, N. L., Roybal, P. G., Sun, J., Liu, L., Yen, Y. and Maxson, R. E. (2009). EphA4 as an effector of Twist1 in the guidance of osteogenic precursor cells during calvarial bone growth and in craniosynostosis. *Development* **136**, 855–864.

Tiscornia, G., Vivas, E. L. and Izpisúa Belmonte, J. C. (2011). Diseases in a dish: modeling human genetic disorders using induced pluripotent cells. *Nat. Med.* **17**, 1570–1576.

Tomoda, K., Takahashi, K., Leung, K., Okada, A., Narita, M., Yamada, N. A., Eilertson, K. E., Tsang, P., Baba, S., White, M. P., et al. (2012). Derivation conditions impact X-inactivation status in female human induced pluripotent stem cells. *Cell Stem Cell* **11**, 91–99.

Torres, R., Firestein, B. L., Dong, H., Staudinger, J., Olson, E. N., Huganir, R. L., Bredt, D. S., Gale, N. W. and Yancopoulos, G. D. (1998). PDZ proteins bind, cluster, and synaptically colocalize with Eph receptors and their ephrin ligands. *Neuron* **21**, 1453–1463.

Townes, P. L. and Holtfreter, J. (1955). Directed movements and selective adhesion of embryonic amphibian cells. *J. Exp. Zool.* **128**, 53–120.

Twigg, S. R. F. and Wilkie, A. O. M. (2015). New insights into craniofacial malformations. *Hum. Mol. Genet.* **24**, R50-59.

Twigg, S. R., Kan, R., Babbs, C., Bochukova, E. G., Robertson, S. P., Wall, S. A., Morriss-Kay, G. M. and Wilkie, A. O. (2004). Mutations of ephrin-B1 (EFNB1), a marker of tissue boundary formation, cause craniofrontonasal syndrome. *Proc. Natl. Acad. Sci. U. S. A.* **101**, 8652–8657.

Twigg, S. R. F., Matsumoto, K., Kidd, A. M. J., Goriely, A., Taylor, I. B., Fisher, R. B., Hoogeboom, A. J. M., Mathijssen, I. M. J., Lourenço, M. T., Morton, J. E. V., et al. (2006). The Origin of EFNB1 Mutations in Craniofrontonasal Syndrome: Frequent Somatic Mosaicism and Explanation of the Paucity of Carrier Males. *Am. J. Hum. Genet.* **78**, 999–1010.

Twigg, S. R. F., Babbs, C., Elzen, M. E. P. van den, Goriely, A., Taylor, S., McGowan, S. J., Giannoulatou, E., Lonie, L., Ragoussis, J., Akha, E. S., et al. (2013). Cellular interference in craniofrontonasal syndrome: males mosaic for mutations in the X-linked EFNB1 gene are more severely affected than true hemizygotes. *Hum. Mol. Genet.* **22**, 1654–1662.

Umetsu, D., Dunst, S. and Dahmann, C. (2014). An RNA interference screen for genes required to shape the anteroposterior compartment boundary in Drosophila identifies the Eph receptor. *PloS One* **9**, e114340.

van den Elzen, M. E. P., Twigg, S. R. F., Goos, J. a. C., Hoogeboom, A. J. M., van den Ouweland, A. M. W., Wilkie, A. O. M. and Mathijssen, I. M. J. (2014). Phenotypes of craniofrontonasal syndrome in patients with a pathogenic mutation in EFNB1. *Eur. J. Hum. Genet.* **22**, 995–1001.

Wang, H. U. and Anderson, D. J. (1997). Eph family transmembrane ligands can mediate repulsive guidance of trunk neural crest migration and motor axon outgrowth. *Neuron* **18**, 383–396.

Watanabe, K., Ueno, M., Kamiya, D., Nishiyama, A., Matsumura, M., Wataya, T., Takahashi, J. B., Nishikawa, S., Nishikawa, S., Muguruma, K., et al. (2007). A ROCK

inhibitor permits survival of dissociated human embryonic stem cells. *Nat. Biotechnol.* **25**, 681–686.

Watanabe, T., Sato, Y., Saito, D., Tadokoro, R. and Takahashi, Y. (2009). EphrinB2 coordinates the formation of a morphological boundary and cell epithelialization during somite segmentation. *Proc. Natl. Acad. Sci. U. S. A.* **106**, 7467–7472.

Wehby, G. L. and Cassell, C. H. (2010). The impact of orofacial clefts on quality of life and healthcare use and costs. *Oral Dis.* **16**, 3–10.

Wei, S., Xu, G., Bridges, L. C., Williams, P., White, J. M. and DeSimone, D. W. (2010). ADAM13 induces cranial neural crest by cleaving class B Ephrins and regulating Wnt signaling. *Dev. Cell* **19**, 345–352.

Wieacker, P. and Wieland, I. (2005). Clinical and genetic aspects of craniofrontonasal syndrome: Towards resolving a genetic paradox. *Mol. Genet. Metab.* **86**, 110–116.

Wieland, I., Jakubiczka, S., Muschke, P., Cohen, M., Thiele, H., Gerlach, K. L., Adams, R. H. and Wieacker, P. (2004). Mutations of the Ephrin-B1 Gene Cause Craniofrontonasal Syndrome. *Am. J. Hum. Genet.* **74**, 1209–1215.

Wieland, I., Makarov, R., Reardon, W., Tinschert, S., Goldenberg, A., Thierry, P. and Wieacker, P. (2007). Dissecting the molecular mechanisms in craniofrontonasal syndrome: differential mRNA expression of mutant EFNB1 and the cellular mosaic. *Eur. J. Hum. Genet.* **16**, 184–191.

Wieland, I., Makarov, R., Reardon, W., Tinschert, S., Goldenberg, A., Thierry, P. and Wieacker, P. (2008). Dissecting the molecular mechanisms in craniofrontonasal

syndrome: differential mRNA expression of mutant EFNB1 and the cellular mosaic. *Eur. J. Hum. Genet.* **16**, 184–191.

Wilkinson, D. G. (2001). Multiple roles of eph receptors and ephrins in neural development. *Nat. Rev. Neurosci.* **2**, 155–164.

Wimmer-Kleikamp, S. H., Janes, P. W., Squire, A., Bastiaens, P. I. H. and Lackmann, M. (2004). Recruitment of Eph receptors into signaling clusters does not require ephrin contact. *J. Cell Biol.* **164**, 661–666.

Wutz, A. (2012). Epigenetic alterations in human pluripotent stem cells: a tale of two cultures. *Cell Stem Cell* **11**, 9–15.

Xu, N.-J. and Henkemeyer, M. (2009). Ephrin-B3 reverse signaling through Grb4 and cytoskeletal regulators mediates axon pruning. *Nat. Neurosci.* **12**, 268–276.

Xu, N.-J. and Henkemeyer, M. (2012). Ephrin reverse signaling in axon guidance and synaptogenesis. *Semin. Cell Dev. Biol.* **23**, 58–64.

Xu, Q., Mellitzer, G., Robinson, V. and Wilkinson, D. G. (1999). In vivo cell sorting in complementary segmental domains mediated by Eph receptors and ephrins. *Nature* **399**, 267–271.

Xu, N.-J., Sun, S., Gibson, J. R. and Henkemeyer, M. (2011). A dual shaping mechanism for postsynaptic ephrin-B3 as a receptor that sculpts dendrites and synapses. *Nat. Neurosci.* **14**, 1421–1429.

Yin, Y., Yamashita, Y., Noda, H., Okafuji, T., Go, M. J. and Tanaka, H. (2004). EphA receptor tyrosine kinases interact with co-expressed ephrin-A ligands in cis. *Neurosci. Res.* **48**, 285–296.

Yokoyama, N., Romero, M. I., Cowan, C. A., Galvan, P., Helmbacher, F., Charnay, P., Parada, L. F. and Henkemeyer, M. (2001). Forward signaling mediated by ephrin-B3 prevents contralateral corticospinal axons from recrossing the spinal cord midline. *Neuron* **29**, 85–97.

Young, N. M., Wat, S., Diewert, V. M., Browder, L. W. and Hallgrímsson, B. (2007). Comparative morphometrics of embryonic facial morphogenesis: Implications for cleft-lip etiology. *Anat. Rec. Adv. Integr. Anat. Evol. Biol.* **290**, 123–139.

Young, N. M., Chong, H. J., Hu, D., Hallgrímsson, B. and Marcucio, R. S. (2010). Quantitative analyses link modulation of sonic hedgehog signaling to continuous variation in facial growth and shape. *Dev. Camb. Engl.* **137**, 3405–3409.

Young, N. M., Hu, D., Lainoff, A. J., Smith, F. J., Diaz, R., Tucker, A. S., Trainor, P. A., Schneider, R. A., Hallgrímsson, B. and Marcucio, R. S. (2014). Embryonic bauplans and the developmental origins of facial diversity and constraint. *Development* **141**, 1059–1063.

Yu, J., Vodyanik, M. A., Smuga-Otto, K., Antosiewicz-Bourget, J., Frane, J. L., Tian, S., Nie, J., Jonsdottir, G. A., Ruotti, V., Stewart, R., et al. (2007). Induced pluripotent stem cell lines derived from human somatic cells. *Science* **318**, 1917–1920.

Zhang, G., Brady, J., Liang, W.-C., Wu, Y., Henkemeyer, M. and Yan, M. (2015). EphB4 forward signalling regulates lymphatic valve development. *Nat. Commun.* **6**, 6625.

Zhang, J., Jiang, Z., Liu, X. and Meng, A. (2016). Eph/ephrin signaling maintains the boundary of dorsal forerunner cell cluster during morphogenesis of the zebrafish embryonic left-right organizer. *Dev. Camb. Engl.* **143**, 2603–2615.

Zimmer, M., Palmer, A., Köhler, J. and Klein, R. (2003). EphB-ephrinB bi-directional endocytosis terminates adhesion allowing contact mediated repulsion. *Nat. Cell Biol.* **5**, 869–878.

Publishing Agreement

It is the policy of the University to encourage the distribution of all theses, dissertations, and manuscripts. Copies of all UCSF theses, dissertations, and manuscripts will be routed to the library via the Graduate Division. The library will make all theses, dissertations, and manuscripts accessible to the public and will preserve these to the best of their abilities, in perpetuity.

Please sign the following statement:

I hereby grant permission to the Graduate Division of the University of California, San Francisco to release copies of my thesis, dissertation, or manuscript to the Campus Library to provide access and preservation, in whole or in part, in perpetuity.

Teresa Kathryn Nitthamm
Author Signature

25 September 2018
Date